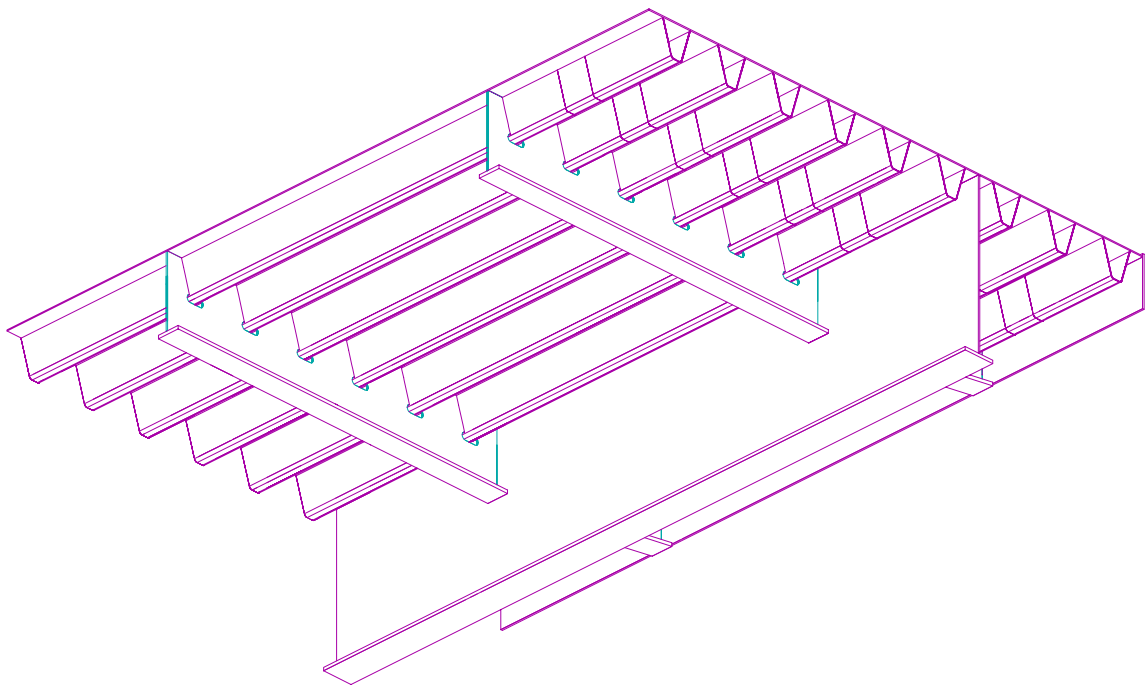


Fatigue Behaviour of Closed Stiffener to Crossbeam Connections in Orthotropic Steel Bridge Decks



J.S. Leendertz

Fatigue Behaviour of Closed Stiffener to Crossbeam Connections in Orthotropic Steel Bridge Decks

Proefschrift

ter verkrijging van de graad van doctor
aan de Technische Universiteit Delft,
op gezag van de Rector Magnificus prof. dr.ir.J.T.Fokkema,
voorzitter van het College voor Promoties,
in het openbaar te verdedigen op donderdag 6 maart 2008 om 12.30 uur

door

Johan Sebastiaan LEENDERTZ

HBO-ingenieur (weg- en waterbouwkunde)

Geboren te Amersfoort

Dit proefschrift is goedgekeurd door de promotor:

Prof. ir. F.S.K. Bijlaard

Samenstelling promotiecommissie:

Rector Magnificus

Prof. ir. F.S.K. Bijlaard

Prof. dr.ir. J. Wardenier

Prof. ir. A.W.C.M. Vrouwenvelder

Prof. ir. H.H. Snijder

Prof. Dr.-Ing. G. Sedlacek

Prof. ir. J. Raoul

Ir. H. van der Weijde

Voorzitter

Technische Universiteit Delft, promotor

Technische Universiteit Delft

Technische Universiteit Delft

Technische Universiteit Eindhoven

Rheinisch-Westfälische Technische Hochschule Aachen

École Nationale des Ponts et Chaussées Paris

Ministry of Transport, Public Works and Water Management

Utrecht

Published and distributed by:

J.S. Leendertz

Email: hanleendertz@gmail.com

ISBN 978-90-9022798-6

Copyright © 2008 by J.S.Leendertz

All right reserved. No part of this material protected by this copyright notice may be reproduced or utilized in any form or by any means, electronic or mechanical, including photocopying, recording or by any information storage or retrieval system, without written permission of the author.

SUMMARY

Fatigue Behaviour of Closed Stiffener to Crossbeam Connections in Orthotropic Steel Bridge Decks

This study concerns the behaviour of the closed stiffener (trough) to crossbeam connection in orthotropic steel bridge decks and in particular, the connection where a continuous closed stiffener passes through the crossbeam. For this connection, the crossbeam in-plane and out-of-plane behaviour is analysed. The nominal stresses for unit loads on the crossbeam, unit rotations of the connection and the deck bending are determined for locations that are relevant for fatigue. For these locations, the geometrical stress concentration factors are also determined.

Traffic loads for fatigue from ENV 1991-3 (EN 1991-2) are simulated by maximum crossbeam load, connection rotation and deck bending moment intervals with equivalent numbers of cycles.

By applying geometrical stress concentration factors to the nominal stresses the geometrical stresses are obtained. By scaling these geometrical stresses of the unit loads, rotations and deck bending moments, the resulting geometrical stress intervals are used for a fatigue assessment of an example crossbeam with three different types of connections:

- Closed stiffener through a cut-out with a cope hole,
- Closed stiffener through a close fitting cut-out,
- Closed stiffener fitted between the crossbeams.

The restraints generated by local bending in the deck and torsion in the closed stiffeners are analysed separately.

The results of the calculations obtained by analytical models and FE models, are compared with measurements.

Conclusions are drawn about the analytical models and the sensitivity of the analysed locations to fatigue cracks:

- The analytical models show a good compliance with FE models and measurements, although the analytical in-plane Vierendeel model should be extended with a rotational restraint at the top of the tooth caused by the bending stiffness of the deck.
- The welded connections of continuous troughs through crossbeams are generally only susceptible to fatigue at the cope hole location of the crossbeam and the bottom location of the continuous trough with a close fit. In calculations realistic fatigue lives for these locations are only obtained if the deck restraint is included in the model for the in-plane behaviour, an “average” fatigue classification is used and measured traffic loads are used.
- The welded connections of closed stiffeners fitted between the crossbeams are very sensitive to fatigue but provide a good solution for shallow crossbeams in combination with a low lorry density.

SAMENVATTING

Vermoeingsgedrag van verbindingen van gesloten verstijvingen met dwarsdragers in orthotrope stalen brugdekken

Deze studie betreft het gedrag van de verbindingen van de gesloten verstijvers (troggen) met de dwarsdragers in orthotrope stalen brugdekken en meer in het bijzonder de verbinding waarbij de gesloten verstijvers zijn doorgevoerd door de dwarsdragers. Het gedrag van deze verbinding is geanalyseerd voor de werking in het vlak van de dwarsdrager (in-plane) en het gedrag uit het vlak van de dwarsdrager. De nominale spanningen voor de plaatsen van deze verbinding die relevant zijn voor vermoeiing zijn bepaald voor belastingen, rotaties en buiging in het dek. Tevens zijn voor deze verbindingen de geometrische spanningsconcentratiefactoren bepaald.

De verkeersbelastingen van ENV 1991-3 (EN 1991-2) die gebruikt dienen te worden voor vermoeingsanalyses zijn geschematiseerd als maximum intervallen in relatie tot dwarsdragerbelastingen, verdraaiingen van de trog- dwarsdragerverbinding en buigende momenten in de dekconstructie in samenhang met equivalente aantallen.

Door het toepassen van de geometrische spanningsconcentratiefactoren op de nominale spanningen en vervolgens deze geometrische spanningen die behoren bij de eenheidsbelastingen rotaties en momenten te schalen, ontstaan intervallen van geometrische spanningen. Deze factoren worden gebruikt voor een vermoeingsanalyse van een voorbeelddwarsdrager. Deze is voorzien van drie verschillende typen verbindingen:

- Gesloten verstijver door een uitsparing met een z.g. muizegat “mouse hole”
- Gesloten verstijver door een uitsparing geheel afgelast
- Gesloten verstijver passend tussen de dwarsdragers

Het effect van de locale buigingweerstand in het dek in dwarsrichting en torsie in de gesloten verstijvers is separaat geanalyseerd.

De resultaten van de berekeningen met analytische modellen en eindige elementen modellen zijn vergeleken met metingen. Er zijn conclusies getrokken met betrekking tot de analytische modellen en de gevoeligheid van de geanalyseerde plaatsen voor vermoeiing:

- De analytische modellen vertonen een goede overeenkomst met de eindige elementen modellen en metingen. Het analytische “in-plane” “Vierendeel” model behoort aan het bovineind van de tand uitgebreid te worden met een rotatieveer die de weerstand tegen verdraaiing door het dek in rekening brengt.
- Over het algemeen zijn van de gelaste verbindingen met doorgestoken troggen slechts de vrije rand van het muizegat op de smalste locatie van de tand en de bodem van de geheel afgelaste trog gevoelig voor vermoeiing. Met berekeningen worden alleen realistische vermoeiingslevensduren gevonden wanneer de buigstijfheid van het dek wordt meebeschoofd in het “in-plane”model en een gemiddelde vermoeiingssterkte wordt gebruikt in combinatie met gemeten verkeersbelastingen.
- De verbindingen van gesloten verstijvers, gelast tussen de dwarsdragers zijn erg gevoelig voor vermoeiing maar bieden een goede oplossing voor lage dwarsdragers in combinatie met een klein volume aan vrachtauto's.

ACKNOWLEDGEMENTS

The research reported in this thesis has been carried out at the Faculty of Civil Engineering and Geosciences of Delft University of Technology.

I thank the Ministry of Transport Civil Engineering Division and more specifically the former head of its Steel and Mechanical department Henk van der Weijde for giving me the opportunity and strongly supporting me in carrying out this research, the various colleagues that supported me with FE calculations and drawings and their fruitful cooperation.

Further, I thank Henk Kolstein of Delft University of Technology for his fruitful collaboration and particularly Prof. J. Wardenier (who was my supervisor until the end of 2007), for his critical appraisals, proposals for improvements and all our detailed discussions. Without these critical discussions, this thesis would not have been realised.

I also thank Prof. F.S.K. Bijlaard who took over the position of supervisor for his comments and giving me the opportunity to finish this work.

Further, I thank John Baker for correcting the English language and his contribution in achieving consistency and in making this thesis accessible.

Finally, I thank my wife Liesbeth de Jonge for her patience during this long period of work.

KEYWORDS

Steel bridges, orthotropic steel decks, stiffener to crossbeam connection, mechanical behaviour, stress concentrations, transfer functions, fatigue design

Table of Contents

0	DEFINITIONS, SYMBOLS AND ABBREVIATIONS.....	10
0.1	Definitions	10
0.2	Symbols and Abbreviations	11
1	INTRODUCTION	17
1.1	History and development of orthotropic steel bridge decks	18
1.2	Orthotropic steel bridge decks in The Netherlands.....	19
1.2.1	Bridge decks with open stiffeners	20
1.2.2	Crossbeams in decks with open stiffeners	20
1.2.3	Bridge decks with closed stiffeners.....	21
1.2.4	Crossbeams in decks with closed stiffeners	23
1.2.5	Main girders	23
1.2.6	Orthotropic steel bridge decks in The Netherlands today	24
1.3	Mechanical behaviour of orthotropic steel bridge decks	24
1.3.1	Global crossbeam behaviour	24
1.3.2	Local crossbeam behaviour.....	25
1.4	Fatigue of orthotropic steel bridge decks	27
1.4.1	General	27
1.4.2	Details, locations, cracks.....	28
1.5	Objective of this research.....	29
1.6	Need for this research.....	30
1.7	Overview of the investigated aspects.....	30
2	LITERATURE REVIEW	32
2.1	Investigated aspects	32
2.2	Orthotropic steel bridge deck types and their behaviour	32
2.2.1	Review	32
2.2.2	Aspects not sufficiently covered in literature.....	36
2.3	Loads and load transfer	37
2.3.1	Review	37
2.3.2	Aspects not sufficiently covered in literature.....	38
2.4	Strength	38
2.4.1	Review	38

2.4.2	Aspects not sufficiently covered in literature.....	41
2.5	Geometrical stress concentration factors	41
2.5.1	Review	41
2.5.2	Aspects not sufficiently covered in literature.....	43
2.6	Fatigue assessment procedures.....	43
2.6.1	Review	43
2.6.2	Aspects not sufficiently covered in literature.....	44
2.7	Concluding remarks.....	44
3	DESIGN PHILOSOPHY, CRACK LOCATIONS AND FATIGUE ASSESSMENT PROCEDURE.....	45
3.1	Design Philosophy.....	45
3.1.1	General considerations.....	45
3.1.2	Crack growth categories.....	46
3.1.3	Design philosophy	47
3.2	Design methods for fatigue	48
3.2.1	Simplified design methods.....	48
3.2.2	Detailed design methods	48
3.2.3	Methods developed in this research.....	48
3.3	Typical fatigue crack locations in the closed stiffener to crossbeam connection	49
3.4	Load models	52
3.5	Function of the structural parts	53
3.5.1	The deck plate	53
3.5.2	Deck with stiffener assembly	54
3.5.3	The crossbeam.....	54
3.5.4	Stiffener to crossbeam connection	56
3.6	Fatigue assessment procedure	58
3.7	Concluding remarks.....	59
4	CONVENTIONAL CROSSBEAMS.....	60
4.1	General	60
4.1.1	Introduction to the conventional crossbeam	60
4.1.2	Analysed dimensions and parameters	60
4.1.3	In-plane loads and out-of-plane rotations	63
4.1.4	Introduction to the crossbeam in-plane behaviour	64
4.1.5	Introduction to the crossbeam out-of-plane behaviour	65
4.2	Crossbeam in-plane analyses.....	66
4.2.1	Models.....	66
4.2.2	Global model for the crossbeam in-plane analysis.....	76
4.2.3	Local cut-out behaviour	79

4.2.4	Local in-plane behaviour of the crossbeam web with cut-outs	93
4.3	Crossbeam out-of-plane analyses	99
4.3.1	Out-of-plane model	99
4.3.2	Global model for the out-of-plane analysis	102
4.3.3	Local load transfer analysis	102
4.3.4	Local stresses	103
4.4	Concluding remarks	105
4.4.1	Models	105
4.4.2	Results of the analyses	106
5	GEOMETRICAL STRESS CONCENTRATION FACTORS	107
5.1	Introduction	107
5.2	Models	108
5.2.1	Connection with a cope hole - trough web	108
5.2.2	Connection with a cope hole - crossbeam web	115
5.2.3	Crossbeam - cope hole location	117
5.2.4	Model for the connection with a close fit	117
5.3	Analyses	117
5.3.1	Connection with a cope hole - trough web	117
5.3.2	Connection with a cope hole - crossbeam web	122
5.3.3	Crossbeam - cope hole location	124
5.3.4	Connection with a close fit - crossbeam web	125
5.4	Boundary condition effects	126
5.4.1	In-plane support conditions	126
5.4.2	Out-of-plane support conditions	126
5.5	Summary of concentration factors	127
5.6	Concluding remarks	129
6	TRANSFER FUNCTIONS	130
6.1	Introduction	130
6.2	Structural dimensions and properties investigated	131
6.3	Modelling of the deck with the crossbeams	133
6.3.1	Equivalent vertical spring properties for the fully loaded crossbeam	133
6.3.2	Equivalent vertical spring properties for the deck	134
6.3.3	Equivalent rotational spring properties for the deck	136
6.4	Crossbeam and deck spring constants	137
6.4.1	Fully loaded crossbeam	137
6.4.2	Partially loaded crossbeams	139
6.5	Influence Lines	141

6.5.1	Influence lines for crossbeam loads	142
6.5.2	Influence lines for trough to crossbeam connection rotations.....	145
6.5.3	Influence lines for deck bending moments at crossbeam 3.....	149
6.6	Crossbeam load, rotation and deck bending moment histories due to unit loads and vehicle loads	150
6.6.1	Crossbeam in-plane load histories	151
6.6.2	Trough to crossbeam connection; out-of-plane rotation histories.....	157
6.6.3	Deck bending moment histories.....	163
6.7	Partially loaded crossbeams	168
6.7.1	Crossbeam load intervals	168
6.7.2	Crossbeam rotation intervals.....	168
6.7.3	Deck bending moments.....	168
6.8	Concluding remarks	168
7	VALIDATION OF ANALYTICAL CALCULATION METHODS WITH FE CALCULATIONS AND MEASUREMENTS	170
7.1	Introduction and objective.....	170
7.2	Single trough specimens.....	170
7.2.1	Test specimen.....	170
7.2.2	Measurements and Models.....	170
7.3	Full scale crossbeam test specimen	172
7.3.1	Introduction.....	172
7.3.2	Dimensions and materials	172
7.3.3	Calculation models.....	174
7.3.4	Stresses at a cope hole for Test load 1A (in-plane).....	178
7.3.5	Stresses in the trough web for a connection with a cope hole for Test load 1A (in-plane)	180
7.3.6	Stresses at a cope hole for Test load 3 (out-of-plane)	183
7.3.7	Stresses in a close fit connection for Test load 1A (in-plane).....	184
7.3.8	Stresses in a close fit connection for Test load 3 (out-of-plane).....	189
7.3.9	Conclusions for the full-scale test specimen.....	191
7.4	Concluding remarks	193
8	ASSESSMENT PROCEDURES.....	194
8.1	Introduction and objective.....	194
8.2	Assessment procedure overview.....	195
8.3	Fatigue damage calculation procedure.....	198
8.4	Combination of load effects	201
8.4.1	Multi-lane effects	201
8.4.2	Combination of crossbeam in-plane loads and out-of-plane rotations of the trough to crossbeam connection.....	201

8.4.3	Combined numbers of cycles	202
8.5	Recommended detail classifications and partial factors	203
8.5.1	Closed stiffener fitted between crossbeams, detail "a"	205
8.5.2	Continuous closed stiffener through crossbeam with close fit, detail "b1"	205
8.5.3	Continuous closed stiffener through a cut out in the Crossbeam with an oval cope hole or with a "Haibach" cope hole, detail "b2" and "b3"	206
8.6	Concluding remarks	207
9	CALCULATION EXAMPLE FOR A TROUGH TO CROSSBEAM CONNECTION IN THREE TYPES OF CROSSBEAMS	208
9.1	Introduction	208
9.2	General	208
9.3	Dimensions	209
9.4	Material	210
9.5	Loads.....	210
9.6	Section properties	210
9.6.1	Deck plate	210
9.6.2	Trough stiffener with deck plate	211
9.6.3	Lane deck stiffness.....	211
9.6.4	Full deck stiffness	211
9.6.5	Crossbeam properties.....	211
9.7	Equivalent crossbeam properties	212
9.7.1	In-plane bending	212
9.7.2	In-plane shear.....	213
9.7.3	Equivalent crossbeam properties.....	215
9.7.4	Equivalent crossbeam spring stiffness in-plane	215
9.8	Equivalent deck spring stiffness properties	216
9.9	Stiffness ratios.....	216
9.10	Influence lines and load/rotation/moment intervals.....	217
9.11	Crossbeam and traffic lane in-plane section force, out-of-plane rotation and deck bending moment intervals at trough 8.....	218
9.12	Detailed analyses for Crossbeam type "AA"	219
9.12.1	Stresses due to crossbeam in-plane behaviour	219
9.12.2	Stresses due to crossbeam out-of plane behaviour.....	222
9.12.3	Stresses in deck stiffeners due to deck bending	224
9.12.4	Combination of stresses	224
9.12.5	Fatigue assessments	225
9.12.6	Additional analyses for the fatigue location C.4.5.s.	228

9.12.7	Conclusions and observations for Crossbeam type “AA”	229
9.13	Detail analyses for Crossbeam type "BB"	230
9.13.1	Stresses due to crossbeam in-plane behaviour	230
9.13.2	Stresses due to crossbeam out-of plane behaviour.....	231
9.13.3	Bending of the deck	232
9.13.4	Combination of stresses	232
9.13.5	Fatigue assessment.....	233
9.13.6	Additional analyses for the fatigue location C.4.1.w	235
9.13.7	Conclusions and observations for Crossbeam type “BB”	237
9.14	Detail analyses for Crossbeam type "CC"	237
9.14.1	Stresses due to crossbeam in-plane behaviour	237
9.14.2	Stresses due to crossbeam out-of plane behaviour.....	238
9.14.3	Bending of the deck	238
9.14.4	Combination of stresses	238
9.14.5	Fatigue assessment.....	239
9.15	Summary of fatigue life results and concluding remarks	242
10	CONCLUSIONS, REMARKS AND RECOMMENDATIONS.....	245
10.1	Introduction	245
10.2	Objectives	245
10.3	Comparison of the results to the objectives.....	245
10.4	Conclusions	248
10.5	Recommendations.....	251
10.6	Aspects proposed for further study.....	251
	REFERENCES.....	252
	APPENDIX 1 MORE DETAILED ANALYSES LOCATIONS C.4.5.S AND C.4.1.W.	257
	APPENDIX 2 LOAD AND ROTATION INTERVALS FROM FE CALCULATIONS.....	287
	CURRICULUM VITAE.....	291

0 DEFINITIONS, SYMBOLS AND ABBREVIATIONS

0.1 Definitions

Closed stiffeners	Elements in the longitudinal direction of the bridge connected to the deck plate; e.g. V-shaped, U-shaped or trapezoidal cross sections rolled or pressed from plate material
Conventional crossbeam	Structural beam element, consisting of an “effective” part of the deck plate, a web plate and a bottom flange.
Cope hole	Extension of a cut-out, for easy fitting of the stiffeners facilitating the passing of continuous stiffeners through the crossbeam
Crack (fatigue)	A separation of material, propagating through the thickness of the material
Cut-out	An area where material has been removed from the crossbeam web generally in the shape of the cross section of the stiffener
Deck plate	Steel plate, which carries the wearing course and the traffic loads
Deck restraint effect	The restraining effect against the rotation of the top of the tooth, caused by the deck resistance against bending
Detail	The assembly of steel plates and welds in a connection
Equivalent bending stiffness ratio	The moment of inertia of a crossbeam with cut-outs, divided by the moment of inertia of a crossbeam without cut-outs
Equivalent shear stiffness ratio	The effective shear area of a crossbeam with cut-outs, divided by that of a crossbeam without cut-outs
Floating deck structure	Bridge deck structure where the lever system of the deck plate and the crossbeam provide a rotational spring with respect to crossbeam bending
Location (fatigue)	The place in the assembly where fatigue cracks may occur
Modified in-plane stress interval	The in-plane stress interval increased by 50% of the out-of-plane stress interval
Open stiffeners	Elements in the longitudinal direction of the bridge connected to the deck plate; e.g. strips, bulb flats and angles.
Stress quotient	The maximum stress interval divided by the stress interval for a fatigue life of 2 million cycles
T-beam	Remaining part of the conventional crossbeam below a trough stiffener to crossbeam connection with a cut-out (and cope hole)
T-frame	Structural part of the crossbeam, comprising of the T-beams and the part of the tooth that is considered to be rigid
Tooth	Remaining part of the web between the cut-outs of a conventional crossbeam web
Trough	Closed stiffener with trough shape
Vierendeel girder	Beam, consisting of horizontal and vertical elements, transferring the in-plane shear forces by secondary bending and shear in the horizontal and vertical elements

0.2 Symbols and Abbreviations

Latin upper case letters

A	<ol style="list-style-type: none">1. Cross section area2. Axle type3. Analytical procedure4. Amplitude
A^1	Equivalent crossbeam web area of crossbeam with the cut-outs
A_{webplate}	Cross section area of web plate of the tooth
A_{fl}	Cross section area of flange
A_{full}	Cross section area of crossbeam without cut-outs
$A_{\text{T-beam}}$	Cross section area of T-beam
A_{tooth}	Cross section area of tooth
A_1	Cross section area at narrowest section of tooth
A_2	Cross section area at bottom of tooth
B	<ol style="list-style-type: none">1. Axle type2. Amplitude
BFL	Bottom flange
Bn	Fictitious beam “n” in beam for model out-of-plane bending
B1	Fictitious horizontal beam between troughs
B2	Fictitious vertical beam between deck plate and bottom flange of crossbeam
B3	Fictitious vertical beam between trough bottom and bottom flange of crossbeam
C	<ol style="list-style-type: none">1. Axle type2. Amplitude
CBW	Crossbeam web
D	<ol style="list-style-type: none">1. Amplitude2. Fatigue damage
DPL	Deck plate
D_i	Fatigue damage for number of cycles for stress interval $\Delta\sigma_i$
D_{L1}	Fatigue damage due to traffic on Lane 1
D_{L1+L2}	Fatigue damage due to traffic on Lane 1 and Lane 2
D_{rel}	Relative fatigue damage
D1	Horizontal deflection of Beam1 (B1) by a Unit Force (P_{unity1}) at the lower end of Beam 2 (B2).
D2	Horizontal deflection (as cantilever) at top of Beam2 by equilibrium force of P_{unity1}
D3	Horizontal deflection (as cantilever) at bottom of Beam2 by P_{unity}
D4	Horizontal deflection of Beam3 by P_{unity}
E	Modulus of Elasticity
F	<ol style="list-style-type: none">1. Force2. Fatigue life in years3. Enclosed area for torsion of a trough stiffener
F_L	Force due to a lane load
FE	Finite Elements
FE-G	FE beam grid model
FE-S	FE shell model
FESh	FE shell elements model
FESh_//	Stress determined with the shell model, parallel to the weld toe
FESh_per	Stress determined with the shell model, perpendicular to the weld toe
p	
A_1	Stress determined with the analytical model, parallel to the weld toe
A_2	Stress determined with the analytical model, perpendicular to the weld toe
FESo	FE solid elements model
F_{hA}	Horizontal normal force in T-beam at the left side of T-frame
F_{hE}	Horizontal normal force in T-beam at the right side of T-frame
FLMn	Fatigue load model “n” in relation to EN 1991-2 “Traffic loads on bridges”

Fi	Relative force in out-of-plane model
G	1. Global behaviour 2. Shear modulus
H	Depth of crossbeam web, indicating a crossbeam type
H _{Ms}	Bending moment history in the deck (lane) for a stiffener span of 4000 mm
H _{Pr}	Vertical reaction history for a stiffener span of 3500 mm
H _{Ps}	Vertical reaction history for a stiffener span of 4000 mm
H _{Pt}	Vertical reaction history for a stiffener span of 4500 mm
H _{Rr}	Rotation history for a stiffener span of 3500 mm
H _{Rs}	Rotation history for a stiffener span of 4000 mm
H _{Rt}	Rotation history for a stiffener span of 4500 mm
I	Moment of inertia
I _n	Interval “n”
I ¹	Equivalent moment of inertia of crossbeam with the cut-outs
I ₁	Moment of inertia at narrowest section of tooth
I ₂	Moment of inertia at bottom of tooth
I _{cb}	Moment of inertia of crossbeam without cut-outs
I _D	Moment of inertia for the complete deck
I _{D,13}	Moment of inertia for a deck with a thick wearing course, carrying one traffic lane (effectively three stiffeners are carrying one axle)
I _{D,15}	Moment of inertia for a deck with a thin wearing course, carrying one traffic lane (effectively five stiffeners are carrying one axle)
I _{deckplate}	Moment of inertia of the deck plate
I _S	Moment of inertia for one stiffener
I _t	Polar moment of inertia
I _{full}	Moment of inertia of crossbeam without cut-outs
I _{imax}	Maximum (load, rotation of bending moment) interval for lorry type “i”
I _{Mds}	Influence line for the bending moment in the deck
I _{frame}	Moment of inertia of trough bottom modelled as a frame
I _{tooth}	The moment of inertia of a tooth
I _{T-beam}	Moment of Inertia of T-beam
I _{Ps}	Influence line for vertical reaction for a deck with stiffener spans of 4000 mm
I _{Rs}	Influence line for trough to crossbeam connection rotation for a deck with stiffener spans of 4000 mm
I _S	Moment of inertia for a stiffener with deck plate $b_{eff} = 600$ mm
I _{webplate}	Moment of inertia derived from the web plate of the tooth
K	Spring constant (P/δ)
K _{B1B2}	Spring constant, substituting the Beam1 with Beam2 system
K _{B3}	Spring constant, substituting Beam3
K ¹ _C	Spring stiffness of crossbeam with equivalent properties
K ¹ _{C3}	Spring stiffness of crossbeam 3 with equivalent properties
K ¹ _D	Spring stiffness of deck, supported by crossbeams with equivalent properties
K ¹ _{D3}	Spring stiffness of deck at crossbeam 3, supported by crossbeams with equivalent properties
L	1. Local behaviour 2. Left-hand side
Li	Traffic lane number “i”
M	1. Moment 2. Measured stress
M _A	Clamping moment at Edge A
M _{D3}	Bending moment in deck at the location of crossbeam 3
M _E	Bending moment in section E
M _G	Eccentricity moment in base of tooth
M _{cb}	Clamping moment at centre of radial beams due to bending of radial beams
M _{cb}	Clamping moment in closed stiffener bottom due to out-of-plane behaviour
M _{cw}	Clamping moment in closed stiffener web due to out-of-plane behaviour
M _d	Moment introduced into the deck

M_{Ct}	Clamping moment at centre of radial beams due to torsion of radial beams
M_{lever}	Part of the crossbeam in-plane bending moment distributed to the lever system
$M_{midspan}$	In-plane mid-span bending moment in the crossbeam
M_n	Bending moment of crossbeam type “n”
M_T	Part of the crossbeam section bending moment distributed to the T-beam
M_{res}	Resulting moment at tooth-deck connection
M_{Sb}	Clamping moment at centre of radial beams due to bending of trough web
M_{sum}	The bending moment in the tooth at cut-out level due to the shear force at the top minus the effect of the restraining moment at the top
M_t	Moment applied on top of tooth
$M_{torsion}$	Torsion moment
M_{unity}	Unity bending moment
M_1	Bending moment in crossbeam type “1”
M_3	Moment at crossbeam 3
N	1. Normal force 2. Fatigue capacity as number of cycles 3. Nominal stress at edge of parent material
NWR	Nominal stress at weld root location in accordance with EN 1993-1-9
NWS	Geometric stress at edge of parent material
NWT	Nominal stress at weld toe location
N_C	Number of 2.0×10^6 cycles associated with the fatigue category
N_a	Fatigue capacity as number of axles
N_l	Fatigue capacity as number of lorries
N_i	Design number of cycles for stress interval $\Delta\sigma_i$
P	Force
P_A	Load on radial beam at Edge A
P_{C3V}	Vertical force on crossbeam 3
P_{D3V}	Vertical force on the deck at the location of crossbeam 3
P_h	Horizontal force
P_t	Reaction force at the deck plate
P_v	Vertical force
P_{unity1}	Unit force on out-of-plane model, system B1B2
P_{unity2}	Unit Force on out-of-plane model, system B3
R	Right hand side
R_{C3V}	Vertical reaction at crossbeam 3
R_{C3Vx}	Vertical reaction at crossbeam 3 due to a load at location x
R_l	Lever system ratio, portion of lever system
R_T	Lever system ratio, portion of T-beam
Q_A	Distributed load along Edge A
S	Shear force
S_1, S_2, S_3	Principal stresses 1, 2 and 3
SCF	Stress concentration factor
SQ_a	Stress quotient for axles
SQ_l	Stress quotient for lorries
S_h	Horizontal shear force
S_v	Vertical shear force
S_{vn}	Vertical shear force of crossbeam type “n”
S_{vl}	Vertical shear force left-hand side
S_{vr}	Vertical shear force right-hand side
TSn	Tandem system on lane “n”
V_i	Lorry volume on traffic lane “i”
W	1. Section modulus for elastic behaviour 2. Width of cut-out (including cope hole)
W_B	Section modulus of trough web at Edge B

W_1	Section modulus elastic behaviour of Beam Type 1, H=600, without cut-outs
W_n	Section modulus for elastic behaviour of crossbeam type "n"
W_{Su}	Upper part section modulus of stiffener with deck plate
W_{Sl}	Lower part section modulus of stiffener with deck plate
W_{tooth}	Section modulus for elastic behaviour of tooth
R	Right hand side
R_l	Lever system ratio, portion of lever system
R_T	Lever system ratio, portion of T-beam
X	Distance from lane centre to crossbeam support
Z	Selected value for a spring stiffness

Latin lower case letters

A	<ol style="list-style-type: none"> 1. Dimension "a" 2. Boundary configuration for closed stiffener bottom model 3. Equivalent crossbeam load cycles per vehicle for $m = 3$
a_l	Lever arm between deck plate and T-beam
a_{cz}	Distance from neutral axis of the crossbeam cross section to the bottom of the cope hole
a_z	Distance from neutral axis of the crossbeam cross section to the centre of the deck plate
B	<ol style="list-style-type: none"> 1. Width of section 2. Length of two times the horizontal leg in half frame model of closed stiffener bottom 3. Dimension "b" 4. Boundary configuration for closed stiffener bottom model 5. Equivalent number of load cycles per vehicle for $m = 5$
b_A	Effective width of radial beam at Edge A
b_{eff}	Effective width of the deck plate acting as the flange of the crossbeam or stiffener (shear lag)
$b_{eff,b}$	Effective width of the deck plate for the deck restraint effect (local deck plate bending)
b_l	Width of a traffic lane
b^l	Effective width of radial beam of analytical trough web model at Edge A, projected in direction of radial beam on Edge A
C	<ol style="list-style-type: none"> 1. Centre-to-centre distance of closed stiffeners 2. Boundary configuration for closed stiffener bottom model 3. Equivalent number of load cycles for long distance traffic for $m = 3$
c_b	Equivalent bending stiffness ratio of crossbeam
c_c	Correction factor for tooth length
c_d	<ol style="list-style-type: none"> 1. Correction factor for the rotation interval for a traffic lane 2. Stiffness coefficient of the deck against rotation
c_s	Equivalent shear stiffness ratio of crossbeam
c_t	Stiffness coefficient against rotation of the tooth
D	<ol style="list-style-type: none"> 1. Equivalent number of load cycles for long distance traffic for $m = 5$ 2. Number of working days per year
d_c	<ol style="list-style-type: none"> 1. Twice the radius of the cope hole in crossbeam web 2. Depth of cope hole in crossbeam web
E	<ol style="list-style-type: none"> 1. Eccentricity 2. Equivalent number of rotation cycles per vehicle for $m = 3$
e_{un}	Distance from centre of gravity of T-beam to the centre of its bottom flange
F	<ol style="list-style-type: none"> 1. Horizontal projection of leg in trapezoidal Frame model of closed stiffener 2. Equivalent number of rotation cycles per vehicle for $m = 5$ 3. fraction of lorries 4. fraction of axles
f_l	Fatigue life extension factor in case of Moerdijk 1998 traffic instead of FLM4
G	<ol style="list-style-type: none"> 1. Vertical projection of leg in trapezoidal frame model of closed stiffener 2. Equivalent number of rotation cycles for long distance traffic for $m = 3$
H	Equivalent number of rotation cycles for long distance traffic for $m = 5$

J	Equivalent deck bending moment cycles per vehicle for $m = 3$
K	Equivalent deck bending moment cycles per vehicle for $m = 5$
L	1. Span length 2. Length of radial beam in geometrical stress concentration models 3. Equivalent number of deck bending moment cycles for long distance traffic for $m = 3$
l_C	Span length of crossbeam
l_n	Span length of crossbeam type “n”
l_S	Stiffener span length
L_1	Length of upper part of tooth
L_2	Length of lower part of tooth over depth of cope hole and extension
$l_I, l_{II}, l_{III}, l_{IV}$	Lengths of parts I, II, III, IV, respectively in reversed T-frame of Vierendeel model
M	1. Inverse log – log slope of S – N line 2. Equivalent number of deck bending moment cycles for long distance traffic for $m = 5$
N	Leg length of trapezoidal frame model of closed stiffener
n_d	Number of lorries per working day
n_{eq}	Equivalent number of cycles
$n_{eq,i}$	Equivalent number of cycles for lorry type “i”
$n_{eq,C}$	Equivalent number of cycles with respect to $\Delta\sigma_C$
n_i	Number of occurring cycles for stress interval $\Delta\sigma_i$
P	Span length of B1 in out-of-plane model
p_i	Fraction of vehicle type “i”
Q	1. Uniformly distributed line load 2. Distance B1 to bottom flange in out-of-plane model
R	Distance of B1 to deck plate in out-of-plane model
r_t	Radius of transition between trough web and trough bottom at trough plate centre
r_c	Outer radius of transition between trough web and trough bottom
S	Distance between trough bottom and bottom flange
t_d	Deck plate thickness
t_t	Thickness of trough
t_w	Thickness of crossbeam web plate
Y	Fatigue life in years

Greek upper case letters

ΣD	Accumulated fatigue damage
ΣP	Total vehicle load
ΣP_T	Total load interval caused by a lorry
ΔR	Crossbeam load interval
ΔM	Bending moment interval
$\Delta\varphi$	Trough to crossbeam connection rotation interval
$\Delta\sigma$	Stress interval
$\Delta\sigma_C$	Stress interval in relation to a design life of 2.0×10^6 cycles
$\Delta\sigma_{Cr}$	Stress interval in relation to a design life of 2.0×10^6 cycles reduced with partial factor for fatigue
$\Delta\sigma_{Dr}$	Constant amplitude limit reduced with partial factor for fatigue
$\Delta\sigma_L$	Cut-off limit
$\Delta\sigma_{Lr}$	Cut-off limit reduced with partial factor for fatigue
$\Delta\sigma_{max}$	Maximum stress interval caused by a lorry

Greek lower case letters

α	Angle between radial beam and Edge A
α_{Q1}	Adaptation factor for traffic loads in ENV 1991-3 and EN 1991-2
δ_A	Displacement at Edge A
δ_h	Horizontal displacement

δ_{hB1}	D1
δ_{hB1B2}	Horizontal displacement of system B1B2 due to a unit force
δ_{hB3}	D4
$\delta_{h-tooth}$	Horizontal displacement of tooth
δ_M	Deflection due to a bending moment
δ_{rel}	Relative displacement
δ_S	Deflection due to shear forces
δ_{total}	Total deflection of crossbeam due to bending and shear
δ_v	Vertical displacement
$\delta_{v-total}$	Deflection due to bending and shear
δ_{vl}	Vertical displacement location at location "L", left-hand side
δ_{vr}	Vertical displacement location at location "R", right-hand side
δ_{vP}	Vertical displacement due to external vertical load P
δ_x	Deflection at "x"
δ_{v-add}	Additional vertical displacement caused by horizontal deflections of tooth
δ_{v-full}	Vertical displacement of crossbeam with full web due to shear force
δ_3	Deflection at crossbeam 3
ϕ	Rotation
ϕ_A	1. Rotation of section A 2. Rotation at Edge A
$\phi_{A-cutout}$	Rotation of section A in crossbeam with cut-outs
ϕ_{A-full}	Rotation of Section A in crossbeam without cut-outs
ϕ_B	1. Rotation due to crossbeam bending 2. Rotation of section B
ϕ_d	Rotation of deck due to M_d
$\phi_{res-total}$	Resulting rotation of top of tooth due to crossbeam bending and Vierendeel behaviour
$\phi_{T-frame}$	Rotation of the T-frame
ϕ_t	Rotation of the trough
$\phi_{t-local}$	Local tooth rotation of tooth due to S_h
ϕ_{t-add}	Additional rotation of tooth due to T-beam deformation
ϕ_{t-Mt}	Rotation of the tooth due to M_t
$\phi_{torsion}$	Rotation due to torsion
ϕ_{t-Sh}	Resultant tooth rotation of tooth due to S_h without deck restraint effect
ϕ_s	Rotation of stiffener
ϕ_1	Rotation in Part I of crossbeam
ϕ_2	Rotation in Part II of crossbeam
γ_{Mf}	Partial factor applied on fatigue detail category
ϕ_3	Rotation at crossbeam 3
σ	Normal stress
σ_b	1. Bending stress 2. Stress in closed stiffener web due to crossbeam bending
σ_{bh}	Stress in closed stiffener web due to horizontal translations caused by crossbeam bending
σ_{bp}	Stress in closed stiffener web due to section rotations caused by crossbeam Bending
σ_e	Equivalent stress
σ_{HS}	Stress in including the effect of geometrical stress concentration
σ_{Nom}	Nominal stress
σ_{pn}	Stress in closed stiffener web due to contraction of closed stiffener by stiffener bending
σ_s	Stress in closed stiffener web due to crossbeam shear
σ_{wr}	Resulting stress including geometrical concentration effect in crossbeam web cause by continuous closed stiffener in close fit
γ_{Mf}	Partial factor for fatigue

1 INTRODUCTION

This study concerns the behaviour of orthotropic steel bridge decks and in particular the behaviour and the fatigue strength of the closed stiffener to crossbeam connection. For this connection, the behaviour is analysed and simple calculation methods for fatigue are derived. The design life and the mean life expectation for fatigue are shown with example calculations.

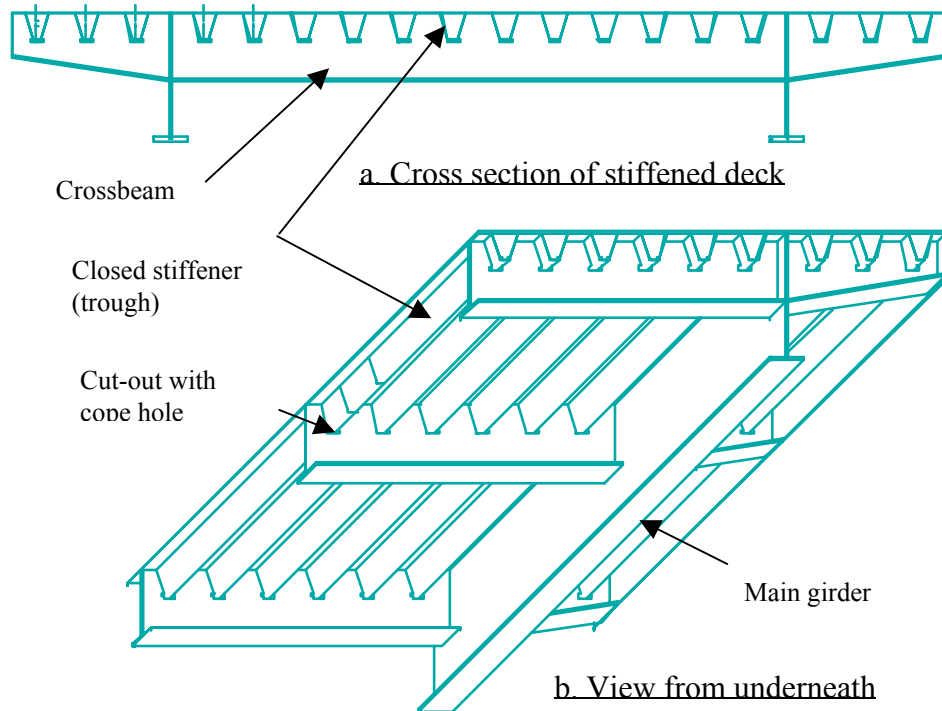


Fig. 1.1 Orthotropic steel deck with crossbeams and main girder

Fig. 1.1 shows part of an orthotropic steel bridge deck with closed stiffeners in the longitudinal direction passing through cut-outs with cope holes in the crossbeams.

Fig. 1.1a shows a cross section of the stiffened deck with the crossbeam in elevation. Fig. 1.1b shows an isometric view from underneath.

1.1 History and development of orthotropic steel bridge decks

In the third decade of the twentieth century, engineers in Germany and the USA were searching for an alternative to wooden decks and concrete decks supported by stringers and crossbeams and they considered steel decks to be a promising development. Pelikan et al. (1957), AISC Design Manual (1963) and Troitsky (1967), give a more elaborate description of this search. The objective to be met was cost savings by a reduction of the steel weight - as labour was more expensive -, which affects the support structures such as piers, abutments etc. The first generation of steel decks in the USA, called "Battle decks", consisted of steel deck plates welded to stringers. The deck plate was assumed to carry the applied traffic loads and to act as an additional top flange reducing the stresses in the stringers.

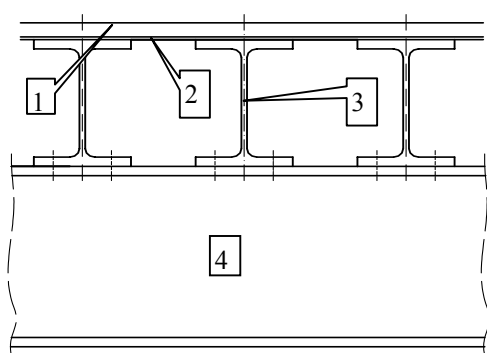


Fig. 1.2 Cross section of a bridge with a battle deck

Fig.1.2 shows a cross section of a "Battle deck". The deck consists of a steel plate 10 to 20 mm thick (2) with longitudinal I-beams (stringers) (3) welded to its underside along each edge of their top flange. The I-beams have a centre-to-centre distance of 250 to 850 mm and are supported on crossbeams (4) spaced between 4.5 to 7.5 m apart. An asphalt wearing course (1) is applied to the top surface of the deck plate.

Through testing, a good insight was obtained into the behaviour of a steel deck plate with welded-on beams. This insight led to proposals for higher allowable stresses. However, the

savings obtained were disappointing.

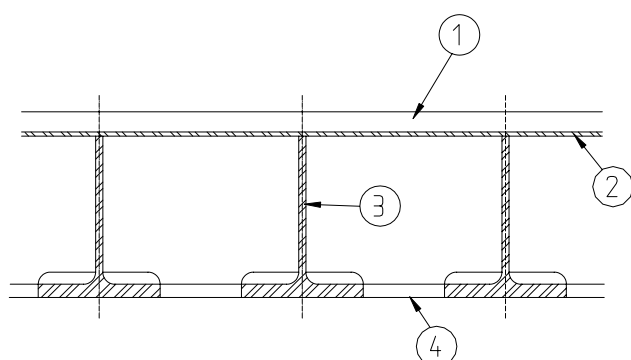


Fig. 1.3 Deck plate stiffened by a beam grid

At the same time, German engineers had begun experiments with deck plates (2), stiffened by T-beams (3) in longitudinal and transverse direction (4) as shown in Fig.1.3.

The T-beam flange acted as the bottom flange and the webs were welded to the deck plate.

An asphalt wearing (1) course was applied to the deck plate.

However, this type of structure was not economical, as it comprised too

many connections. Without additional components, such as deck plate stiffeners between the beam grid, it was not possible to increase the crossbeam and longitudinal stiffeners distances substantially.

Search for a more economical use of materials and a reduction in the labour for fabrication and assembly led, after the 2nd World War, to orthotropic steel bridge decks with open stiffeners as shown in Fig.1.4a. In this type of structure, the functions of deck plate, stringer, crossbeam and main girder are combined.

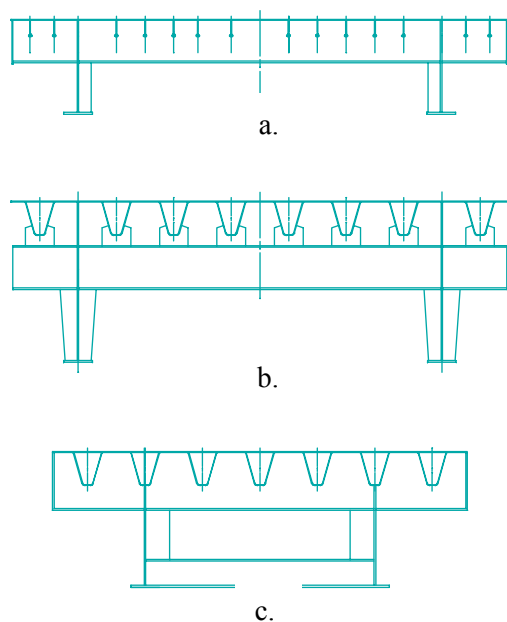


Fig. 1.4 Cross sections of steel bridges with orthotropic decks (not to scale)

The use of these decks resulted in a reduction in the structure height of the structures and gave savings in the approaches. The AISC Design Manual (1963) states that, compared to bridges erected before the 2nd World War, the steel weight savings per m^2 are: 55% for plate girder bridges, 25% for cable-stayed bridges and 44% for suspension bridges. The AISC Design Manual (1963) and Troitsky (1967) give a wider description of the history of these structures in Germany, the USA and Canada.

The structural characteristics are different in the longitudinal and transverse directions or: "Orthogonal anisotropic". Abbreviated to: "Orthotropic" decks.

Fig.1.4 shows typical cross sections of bridge decks (a) with open stiffeners, (b) with closed stiffeners on plate supports, called "Floating deck" and (c) with trapezoidal closed stiffeners through conventional crossbeams in a box girder bridge.

1.2 Orthotropic steel bridge decks in The Netherlands

The development of orthotropic steel bridge decks in The Netherlands started after the 2nd World War and was initiated by the engineering office of the Ministry of Transport, the erstwhile "Directie Bruggen", which merged into the Rijkswaterstaat Civil Engineering Division (Bouwdienst).

Later, others joined in this development and the engineering office of the City of Rotterdam played an important role.

V.d.Eb (1962) showed the state of the art of the application of these decks in the Netherlands. Kingma (1964) showed an overview of the calculation methods for orthotropic steel decks. Various reports from research at that time by the Netherlands Organisation for Applied Scientific Research (TNO) and by Delft University of Technology show the interest in this type of structure.

The first generation of orthotropic steel deck bridges in The Netherlands was built between 1955 and 1965.

1.2.1 Bridge decks with open stiffeners

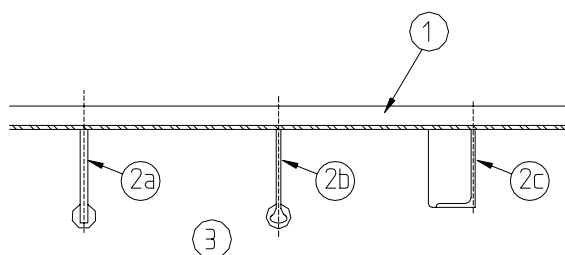


Fig. 1.5, Typical sections of open stiffeners

Fig. 1.5 shows details of "open" stiffeners under a deck plate with a thick wearing course (1). The stiffeners shown are: (2a) strip, (2b) bulb and (2c) angle. The crossbeam web is indicated as (3). Originally, these types of stiffener were used in the ship building industry.

In most bridges, these stiffeners have a maximum depth of 200 mm and a thickness of 12 mm. The stiffener webs are connected to the deck plate with a fillet weld along both sides and in bridges they are usually aligned in the longitudinal direction. In this way, their cross sectional area contributes to the top flange area of the main girder. Their centre distance is approximately 300 mm, which was mainly determined from the static strength of the 10 – 12 mm thick deck plate but it also permitted good accessibility for welding leading to a good quality of work and easier maintenance.

The strength of the deck plate assembly with open stiffeners allows structures with stiffener spans of approximately 2.0 m. In many structures, this necessitates secondary crossbeams and secondary main girders.

The number of structural elements, i.e. stiffeners, secondary crossbeams, primary crossbeams etc. leads to many connections, resulting in a high labour content. This is a disadvantage of these structures. Some of these bridges have been discussed by V.d.Eb (1962) and Weitz (1975).

Examples of fixed bridges with open stiffeners in The Netherlands, together with their steel weight per m^2 and year of erection are shown in Table 1.1.

Table 1.1 Examples of bridges with open stiffeners

Bridge	Year	Type	Main span (m)	Steel weight (kg/m^2)
Bridge near Rhenen over the river Rhine	1957	Continuous plate girder	143	418
Bridge near Rotterdam on A16 over the river Nieuwe Maas (East bridge)	1961	Arch	287	494
Bridge near Numansdorp on A29 over the Haringvliet	1964	Continuous box girder	100	265
Bridge near Rheden on A12 over the river IJssel	1964	Continuous plate girder	105	356

1.2.2 Crossbeams in decks with open stiffeners

The crossbeams in decks with open stiffeners are inverted T-beams. Usually, the stiffeners are continuous and pass through the crossbeams. Flats and bulbs pass through a slot with a "cope hole" and angle stiffeners pass the crossbeam through a "cut-out". Stiffeners fitted between the crossbeams could suffer from misalignment, which would make them more susceptible to fatigue.

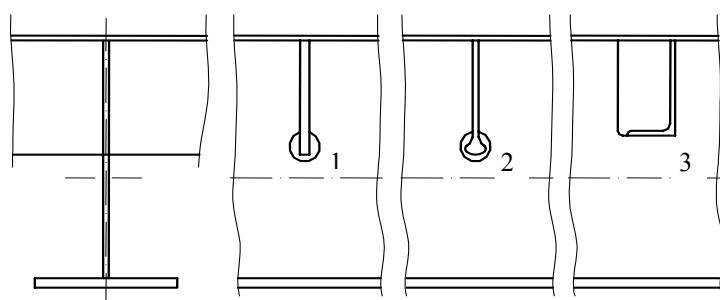


Fig. 1.6 Crossbeam connections with continuous open stiffeners

Fig. 1.6 shows the connections for continuous open stiffeners. Type (1) is a strip stiffener through a slot with a cope hole, Type (2) is a bulb stiffener through a slot with a cope hole and Type (3) is an angle stiffener through a cut-out.

These types of deck structures do not differ much from the structures used in other countries. Pelikan et al. (1957), V.d.Eb (1962), the AISC Design Manual (1963) and Troitsky (1967) discussed these extensively.

1.2.3 Bridge decks with closed stiffeners

As in other countries, designers in The Netherlands searched for a way of increasing the stiffener span length in order to reduce the number of crossbeams needed and thus reduce the number of structural elements and connections.

The solution was found to be the closed stiffener with one (fillet) weld along each side. Large cost savings resulted from the reduced amount of welded connections. First a weld length reduction of up to 50% was achieved by the one sided longitudinal welds connecting the stiffeners to the deck plate compared with the longitudinal fillet welds on both sides connecting the open stiffeners.

The closed stiffeners that were developed had various cross sections. In The Netherlands, only the V, U and Trapezoidal shapes were used. These were made from cold pressed plates and were also known as "Trough" stiffeners.

Initially the V-shape was used, with a depth of 200 mm and a plate thickness of 6 mm, but due to the small cross sectional area of the bottom of the stiffener, the increase in bending capacity and thus the increase in the possible stiffener spans compared to the open stiffeners was limited. The extension of the V-stiffener beam depth by means of a T-section, resulting in the "wine-glass" shape, was sometimes used in Germany, but was never used in The Netherlands.

An improvement was the U-shaped stiffener, with a height of 300 mm and a plate thickness of 6 mm, which was used in several bridges. Tromp (1969) reported tests on U-shaped stiffeners for crossbeams in "Floating Decks" and Ypeij (1972) showed the application of these decks. The bottom of these stiffeners acts like a true bottom flange and the maximum spans are approximately 3.5 m.

Later on, the German steel manufacturers (e.g. Krupp and Hoesch) developed various cold rolled trapezoidal sections. These sections, manufactured by Krupp, with a depth of 325 mm and a thickness from 6 - 10 mm allowed stiffener spans of 4.0 to 5.0 m.

	V-shaped stiffener	U-shaped stiffener	Trapezoidal stiffener	
Stiffener fitted between crossbeams				
Continuous stiffener on supports				
Continuous stiffener through crossbeam				

Fig. 1.7 Overview of closed stiffener types used in The Netherlands

These spans reduced the number of crossbeams by 40%, compared to the original decks with open stiffeners. The leg-to-leg distance of the closed stiffeners adjacent to the deck is approximately 300 mm, when used in combination with a deck plate thickness of 10 – 12 mm, which is the same as the centre-to-centre distance used for open stiffeners in the original decks.

Fig.1.7 gives an overview of the types of stiffeners used to date in The Netherlands. In all fixed bridges and a large number of movable bridges built in The Netherlands after 1975, the trapezoidal closed sections ("troughs") were used. Nowadays the trough shapes are no longer rolled by the steel manufacturers, but are again cold pressed.

Examples of fixed bridges with closed stiffeners in The Netherlands with their steel weight per m² are shown in Table 1.2.

Table 1.2 Examples of bridges with closed stiffeners

Bridge	Year	Type	Main span (m)	Steel weight (kg/m ²)
Twin bridge on A12 over the Amsterdam - Rhine canal near Utrecht (Galecopper bridge)	Bridge 1: 1971 Bridge 2: 1976	Cable-stayed plate girder Cable-stayed plate girder	180	330
Bridge near Muiden on A1 over the Amsterdam Rhine canal	1971	Continuous box girder	162	333
Bridge near Ewijk on A 50 over the river Waal	1973	Cable-stayed single cell box girder	270	346
Bridge near Moerdijk on A16 over the Hollands Diep	1978	Twin cell box girder with 10 simply supported spans	100	226

1.2.4 Crossbeams in decks with closed stiffeners

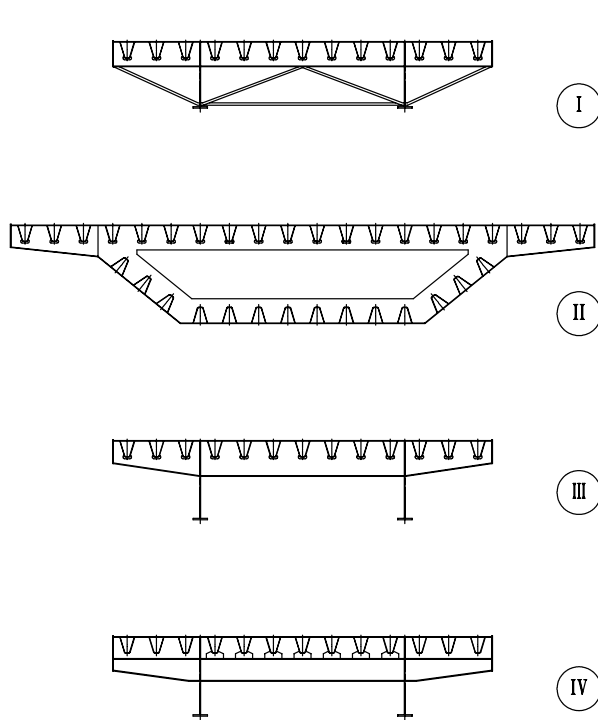


Fig. 1.8 Structural types of main girders (not to scale)

Where possible, the stiffeners are continuous, passing through cut-outs. Additional cope holes, also called "mouse holes", are often used near the bottom of the trough to allow easy fitting of the stiffeners in the workshop. In decks with shallow crossbeams, which is often the case in movable bridges, the closed stiffeners are usually fitted between the crossbeams.

These structures are discussed by Pelikan et al. (1957), by the AISC Design Manual (1963), by Troitsky (1967), by Drost (1965) and by Bercum et al. (1971).

Fig. 1.8 shows some typical crossbeams in relation to the main girder system. The crossbeam design has a strong relationship to the main girder system and the assembly and erection of the bridge. In general, the crossbeams are reversed T-beams.

Fig.1.8-I shows a crossbeam, which acts as the upper chord of a truss. Plate girder

bridges with the bottom flanges of the main girders connected by a bracing system are called "open box girder bridges". When the bottom flanges are connected by a continuous plate, the main girder system becomes a "closed box girder".

Fig. 1.8.-II shows a box girder with cantilevers, where the diaphragms act as crossbeams. The cantilevers are featured as "conventional" crossbeams.

In Fig.1.8-III, a "conventional" crossbeam is shown, supported by plate girders.

Fig.1.8-IV shows a crossbeam in a "floating deck" structure. Each individual closed stiffener is welded to a supporting plate and the plate is welded to an I-shaped crossbeam. The cantilever parts of the I-beam are connected to the deck plate by plates, which give a full connection. This type of deck was developed for its ease of assembly, and is discussed more extensively by Ypey (1972). Tromp (1969, 1974) presented test results for this type of connection with U-shaped and trapezoidal stiffeners.

1.2.5 Main girders

The main girders for the first orthotropic steel bridges in The Netherlands, were plate girders as in the Bridge on the motorway A12 over the river IJssel and the Bridge on the highway N 320 over the river Rhine, discussed by V.d.Eb (1962), or rectangular box girders like those in the Bridge on the motorway A29 over the Haringvliet near Numansdorp.

At the seventies of the twentieth century, larger spans (over 120 m) were bridged by arch structures, like the Van Brienoord Bridge on the motorway A16 over the river Nieuwe Maas near Rotterdam (East bridge) with a span of 287 m, V.d.Eb (1962). The lower chord of this arch bridge is a narrow box girder. It can be concluded that initially plate girders and box girders were the most common main girder types.

Later, for spans over 160 m, the plate girders were combined with cable stays, such as in the Twin Bridges on the motorway A12 over the Amsterdam - Rhine canal (Galecopper bridge). Typical cross sections of plate girders are shown in Fig.1.8-III and Fig.1.8-IV. An open rectangular box girder is shown in Fig.1.8-I.

Bridges using box girders with inclined webs similar to those in other countries, e.g. the Erskine and Severn bridges in the U.K., have also been used in the Netherlands. The Bridge on the motorway A75 over the river Waal near Ewijk is a single cell box girder in combination with cable stays. The Bridge on the motorway A16 over the Haringvliet near Moerdijk is featured as a twin cell box girder. The total bridge consists of 10 simply supported spans.

1.2.6 Orthotropic steel bridge decks in The Netherlands today

Developments in concrete bridge design nowadays result in economic solutions for spans of fixed bridges in concrete where steel decks were more favourable in the past (>120 m). However, where a small structural height is required with a low weight per square metre, such as with movable bridges, the orthotropic steel deck is still the most favourable solution. Open stiffeners are still used if a low torsional rigidity is required, e.g. for "roll on roll off" bridges.

Existing older fixed steel bridges with concrete decks (without composite action) can be upgraded by replacing the old concrete deck with a lightweight orthotropic steel deck. If the area for the traffic loads is restricted, due to the main girder system such as cable-stays, trusses or arches, higher traffic loads can be allowed or if the area for traffic loads is not limited, these lightweight deck structures allow a larger area to be used for traffic loads.

1.3 Mechanical behaviour of orthotropic steel bridge decks

1.3.1 Global crossbeam behaviour

Vertical traffic loads are applied to the wearing course of the steel deck and thence transferred to the steel deck plate. In the transverse direction the deck plate is supported by open or closed stiffeners between the crossbeams. Shear and bending is generated in the transverse direction of the deck plate in the same way as in a continuous beam on spring supports.

In the longitudinal direction, the stiffeners act together with a part of the deck plate and transfer the applied traffic loads to the crossbeams. Shear forces and bending moments are present in the stiffeners. The stiffener supports (stiffener to crossbeam connections) transfer the applied loads to the crossbeams and due to the deflection of the stiffeners between the crossbeams; the supports are subjected to a rotation.

Near the crossbeams, the traffic loads are directly introduced into the crossbeams through the deck plate. The crossbeams, with a part of the deck plate acting as the upper flange, transfer the loads to the main girders. The load transfer in the crossbeam generates shear forces and bending moments, under the in-plane crossbeam behaviour.

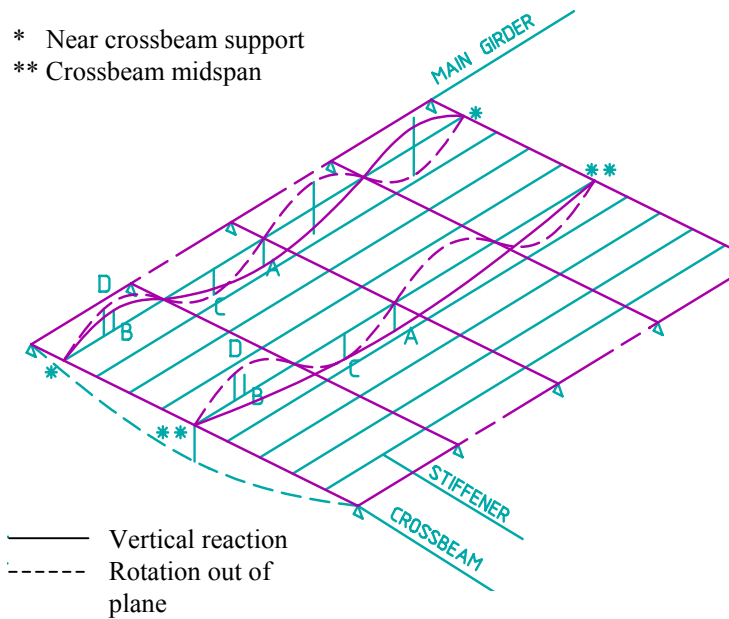


Fig. 1.9 Influence lines for stiffener reactions and rotations at the locations "A" of the middle crossbeam

influence lines depend on the crossbeam stiffness. Near the main girder (crossbeam support), the crossbeams act as rigid supports.

Beales (1979) and Dowling (1971) showed influence lines for a wide variety of locations and details.

The bridge main girders may be the chord of an arch bridge or the chord of a truss bridge. The bridge can also be supported by a cable-stay system (cable-stayed bridge) or by hangers (suspension bridge). In all cases part of the deck plate with a number of longitudinal stiffeners, depending on the "effective width", acts as the upper flange of the main girder.

Pelikan et al. (1957), V.d. Eb (1962), the AISC Design Manual (1963), Troitsky (1967) and Weitz (1975) give more elaborate descriptions of the structural behaviour.

1.3.2 Local crossbeam behaviour

1.3.2.1 Decks with open stiffeners

Fig. 1.6 shows stiffener to crossbeam connections with open stiffeners. The slot with the cope hole or "mouse hole" in the crossbeam web, used for the strip (1) and bulb (2) stiffeners when passing through the crossbeam web, will hardly affect the response of the crossbeam for the in-plane or the out-of-plane behaviour. At the "cope hole" location, stress concentrations will occur for the in-plane and the out-of-plane behaviour.

Furthermore, the crossbeams will deform by the applied rotations of the stiffeners caused by bending under traffic loads, which causes local bending and torsion, the so-called out-of-plane crossbeam behaviour.

For a better understanding, Fig.1.9 shows the influence lines for the crossbeam in-plane support reactions of the deck (continuous lines) with the extreme amplitudes A and B. It further shows the out-of-plane rotations of the deck to crossbeam connections (dotted lines) with the extreme amplitudes C and D.

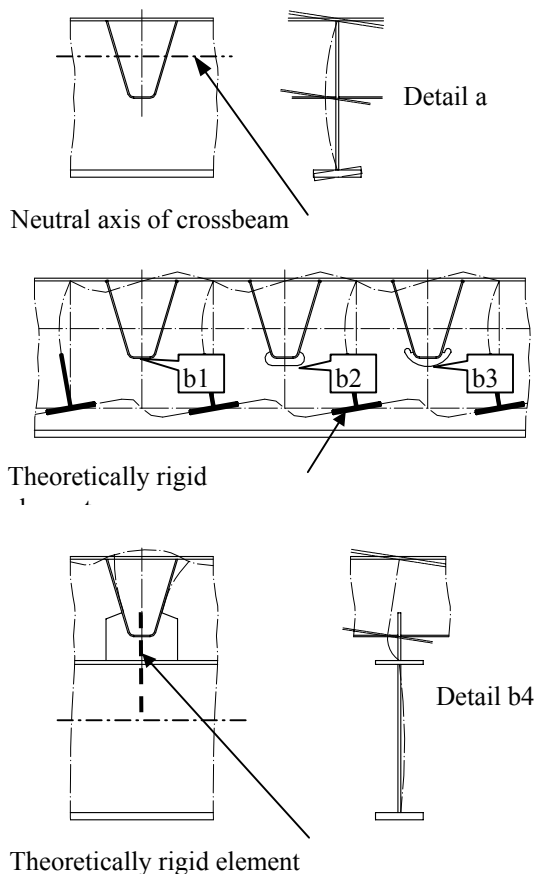
Here, the crossbeams act as spring supports for the stiffeners and deck plate assembly. The

The angle stiffener (3) passes through a cut-out and if the dimensions of this cut-out become large with respect to the remaining web the crossbeam will act in-plane increasingly like a Vierendeel system.

The out-of-plane rotations will cause bending in the crossbeam web and the stresses will be increased due to stress concentrations at the cut-outs.

1.3.2.2 Decks with closed stiffeners

The load transfer in the crossbeam is affected by its type and the details of the stiffener to crossbeam connection. Fig.1.10 shows the behaviour of the crossbeams and the stiffener to crossbeam connections for the in-plane load transfer and the imposed out-of-plane rotations for various closed stiffener to crossbeam connections. The detail types are classified as "a" when the stiffeners are fitted between the crossbeams and "b" when the stiffeners are continuous.



Detail "a" is used for structures with shallow crossbeams, where cut-outs would reduce the shear capacity of the crossbeam too much. The crossbeam remains a full I-section for the in-plane shear and bending behaviour but is distorted out-of-plane by the rotation of the connection.

Detail "b" is used for deeper conventional crossbeams, crossbeams of floating deck structures and for diaphragms of box girder bridges. It is subdivided into four types: "b1", "b2", "b3" and "b4".

Detail "b1" refers to a trough welded all round, detail "b2" to a trough with a conventional cope hole or mouse hole and detail "b3" to a trough with a so called "Haibach" cope hole.

The crossbeam with cut-outs acts in-plane like a Vierendeel girder, generating secondary shear forces and bending moments. The out-of-plane behaviour is nearly similar to detail "a".

In some countries, the connection to the deck plate comprises an additional cope hole in the crossbeam web. This detail has never been used in The Netherlands.

Fig. 1.10 In-plane and out-of-plane closed stiffener to crossbeam connection behaviour

In a "Floating deck" structure as shown in detail "b4" the crossbeam in-plane shear and bending cause horizontal displacements of the deck plate with respect to the I-beam, which results in imposed deformations in the closed stiffeners and in the deck plate. Under out-of-plane rotations, the top flange of the I-beam acts more or less like a rigid support, resulting in bending in the support plate.

From the above it can be concluded that a distinction has to be made between the crossbeam local behaviour for the transfer of traffic loads from the deck plate to the crossbeam and the global load transfer through the crossbeam to the main girders. For the local load transfer by bending and shear the load transfer and stresses have to be determined by a detailed model. For the global behaviour, the crossbeam is considered to be a beam with equivalent properties.

1.4 Fatigue of orthotropic steel bridge decks

1.4.1 General

At the time when the orthotropic steel decks were developed, it was known that steel structures with fluctuating stresses might suffer from fatigue. Since the stresses in the orthotropic steel decks generated by the traffic loads are high, it was recognised that fatigue could play a role.

The AISC Design Manual (1963) refers to research in Germany carried out by Klöppel et al. (1960) and states that for most of the details fatigue is not considered to be a limiting factor. Troitsky (1967) stated that fatigue might be a limiting factor, however, insufficient information was available.

V.d.Eb (1962) discussed the fatigue tests carried out by Drost (1965) on open stiffener to deck connections. Ypeij (1972) presented the results of fatigue tests carried out by Tromp (1969) on closed stiffener to crossbeam connections. The results presented in the literature show that, although no failures were known, fatigue was a matter of interest from the beginning.

Part 10 of BS 5400 (1980), deals with traffic loads and fatigue, but at that time the knowledge about the fatigue strength of orthotropic steel bridge decks did not allow the inclusion of these structures in a standard. The Dutch code NEN 1008 (VOSB 1963), "recommendations for the design of steel bridges", addresses fatigue, but does not specifically cover orthotropic steel decks.

In the period 1970 - 1990, there was a growing concern about the fatigue strength of orthotropic steel decks. Defects observed during inspections resulted in several publications which indicated that more information about the resistance of the details, the design strength, manufacture and repair was needed in the field of fatigue.

Research was started in the UK by Dowling (1971) and Beales (1979) who reported influence lines as one of the elements needed. In the USA, Fisher (1977) published the Bridge Fatigue Guide, which gives a few advisory notes on closed stiffener to deck connections, stiffener splices and stiffener to crossbeam connections.

In Europe, most of the research was sponsored by the ECSC and started with measurements of the traffic loads and tests of construction details as reported by Kolstein et al. (1989) and Bruls et al. (1997).

1.4.2 Details, locations, cracks

For the purpose of this thesis the following definitions apply:

- **Detail**
The assembly of steel plates and welds in a connection
- **Location**
The place in the assembly where fatigue cracks may occur.
- **Crack**
A separation of material, propagating through the thickness of the material

Figs. 1.5 to 1.7 and 1.10 show the details that are common practice in The Netherlands. Fig.1.11 gives a selection of the locations susceptible to fatigue in orthotropic steel bridge decks.

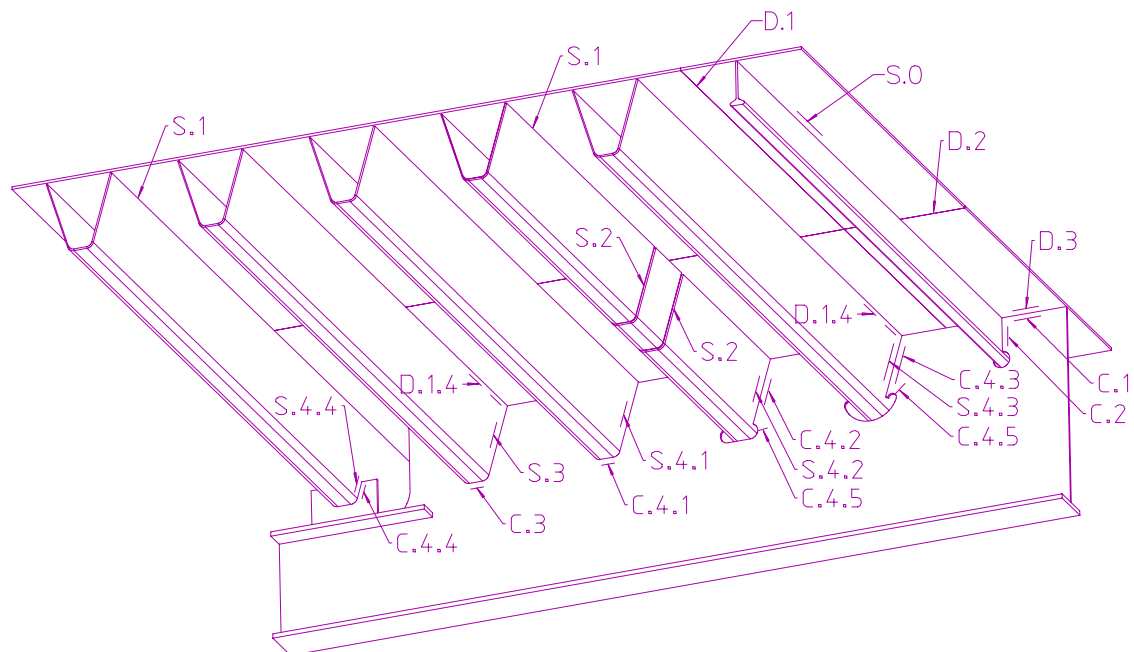


Fig. 1.11 Susceptible locations for fatigue in orthotropic steel bridge decks

The locations susceptible to fatigue, indicated in Fig.1.11 are explained in more detail in Table 1.3.

The selection of locations shown, is limited to those in the deck plate, the open and the closed stiffener and the crossbeam. Usually cracks are initiated at the toe of the weld, but sometimes at the root. For each location, whether cracks were observed in real bridges in The Netherlands (P) or in tests (T) is indicated.

For the locations in closed stiffener to crossbeam connections the detail types are indicated in accordance with Fig.1.10: a, b1, b2, b3 or b4.

At a specific location of a detail (for example b1), generally the crack will occur either in the stiffener or in the crossbeam.

Table 1.3 Locations susceptible to fatigue, explanation to Fig.1.11,

	Type	Observation	Location
Deck plate			
Longitudinal weld		No cracks	D.1
Transverse weld		No cracks	D.2
Deck plate to crossbeam		No cracks	D.3
Continuous closed stiffener to deck plate		Cracks, predominantly in bridges with a thin wearing course and in some heavily trafficked bridges with a thick wearing course (P),(T)	D.1.4
Open stiffener			
Stiffener to deck plate weld		No cracks	S.0
Closed stiffener			
Stiffener to deck plate weld		Numerous cracks in heavily trafficked bridges (P),(T)	S.1
Stiffener splice		Cracks in various bridges (P),(T)	S.2
Closed stiffener fitted between crossbeams	a	Cracks in various bridges (P),(T)	S.3
Continuous stiffener at crossbeam connection:			
1) Welded around	b1	Cracks in test specimens (T)	S.4.1
2) With cope hole	b2	Cracks in test specimens (T)	S.4.2
3) With Haibach cope hole	b3	Cracks in test specimens (T)	S.4.3
4) With plate support	b4	Cracks in test specimens (T)	S.4.4
On plate support			
Crossbeam			
Crossbeam web to deck plate weld		No cracks	C.1
Crossbeam to open stiffener		Cracks in crossbeam web near stiffener (P)	C.2
Crossbeam to closed stiffener between crossbeams	a	Cracks from stiffener and weld into crossbeam (P), (T)	C.3
Crossbeam to continuous closed stiffener:			
1) Welded around	b1		C.4.1
2) With cope hole	b2	Cracks in test specimens (T)	C.4.2
3) With Haibach cope hole	b3	Cracks in web near stiffener and at cope hole edge (P), (T)	C.4.3
4) With plate support	b4	Cracks in test specimens (T)	C.4.4
Crossbeam web, free edge of cope hole	b2,b3	No cracks	C.4.5
		Cracks in real crossbeams (P) and test specimens (T)	

(P) Practice

(T) Test

1.5 Objective of this research

The closed stiffener to crossbeam connection is a detail that shows a complicated mechanical behaviour. It was selected for this study with the following objectives:

1. To obtain insight into the mechanical behaviour and interaction effects of closed stiffener to crossbeam connections in orthotropic steel bridge decks
2. To gain insight into past design errors
3. To derive simple methods for fatigue design of closed stiffener to crossbeam connections in orthotropic steel bridge decks

4. To devise a basis for the improvement of the fatigue behaviour of closed stiffener to crossbeam connections in orthotropic steel deck design
5. To develop knowledge to be applied to inspection, repair and modifications of existing bridges

1.6 Need for this research

The following aspects justify the need for this research:

- A large number of existing bridges are suffering from cracks due to increasing traffic intensities and past design shortcomings.
- Design criteria and procedures are not available for all details but are required because:
 - Orthotropic steel decks are still a favourable solution for new fixed bridges in some cases
 - Orthotropic decks provide an efficient solution for replacing concrete decks in older bridges.
 - Orthotropic steel decks are the most favourable solution for larger movable bridges.
- A basis for the development of inspection and repair philosophy is required.

1.7 Overview of the investigated aspects

Chapter 2 gives a literature review of the relevant design aspects of orthotropic steel decks in relation to the aspects mentioned in 1.5 and 1.6 and particularly in relation to the fatigue design of closed stiffener to crossbeam connections. Whether particular aspects need more analysis or whether available data can be used is identified.

Chapter 3 shows a design philosophy with a closer observation of the details "a", "b1", "b2", "b3" and "b4" as shown in Fig.1.10 together with the behaviour and the available procedures for the fatigue assessment of the closed stiffener to crossbeam connections.

Chapter 4 presents a more detailed investigation into the behaviour of the conventional crossbeams and the continuous closed stiffener to crossbeam connections with cut-outs and cope holes. The behaviour is investigated with simple line models, loaded with unit loads and unit rotations. The results from analytical models are compared to 2D and 3D FE-models.

Chapter 5 gives the geometrical force/stress concentrations, sometimes including the local relations, in the trough to crossbeam web connections and the cope holes, which can be used for the nominal stresses calculated from the local forces and moments in chapter 4. The results from the analytical models are compared to 3D FE-models.

Chapter 6 deals with the analysis of the deck behaviour in conjunction with the global crossbeam behaviour as presented in chapter 4. Transfer functions are obtained, which results can be used to define the load and rotation histories of the crossbeams. The results from analytical models are compared to 2D and 3D FE-models.

Chapter 7 shows a comparison of the results obtained by analytical models, FE-models and measurements from test specimens.

Chapter 8 deals with the combination effects of loads on traffic lanes and the in-plane and the out-of-plane behaviour. The fatigue resistance of the details according to standards, literature and research is shown.

Chapter 9 gives procedures for the fatigue assessment with simplifications and gives an example of a fatigue assessment procedure.

Chapter 10 gives a summary and conclusions on the results of this research, and deals with the need for further work.

Appendix 1 describes additional analyses with respect to crossbeam in-plane behaviour, the influence of the fatigue detail classifications and the difference between the lorry loads in EN 1991-2 and those observed at measurements.

Appendix 2 shows tables with load and rotation intervals determined with FE models in relation to chapter 7.

2 Literature review

2.1 Investigated aspects

This research concentrates on the fatigue behaviour of stiffener to crossbeam connections and in particular on the connections with closed stiffeners. The literature related to this research subject, has been divided into 5 groups which cover the following aspects:

- * **Orthotropic steel bridge deck types and their behaviour**
Decks, open and closed stiffener types, crossbeams and details
In-plane and out-of-plane behaviour
- * **Loads and load transfer**
Traffic loads, load models, load distribution, load transfer from deck to crossbeam and influence lines, dynamic amplification factors
- * **Strength**
Static and fatigue strength of orthotropic steel deck details
- * **Stress concentration factors**
Geometrical stress concentration and relation factors
- * **Fatigue assessment procedures**
Damage calculations, crack growth calculations

Literature written by or with contributions from the author is, where relevant, included in this thesis.

An overview of the above aspects is given in the following paragraphs. Aspects that are not covered or only partially covered are described in a separate paragraph and are summarised in 2.7.

2.2 Orthotropic steel bridge deck types and their behaviour

2.2.1 Review

The behaviour of all elements in orthotropic decks is discussed by Pelikan et al. (1957). They show the basic behaviour of orthotropic steel decks with open and closed stiffeners supported by crossbeams made from reversed T-beams (see Figs. 1.4, 1.5, 1.6 and 1.7). Design formulae are derived based on the literature published between 1923 and 1956 and secondary effects such as support deflections are taken into account. Criteria for the design of orthotropic decks are presented. The design method given is suitable for decks with open and closed stiffeners fitted between the crossbeams. Orthotropic steel decks can be designed using the derived formulae and the charts given. A complete design calculation and the resulting structure of the Save Bridge in Belgrade is shown with its details as an example.

In a series of articles V.d.Eb, (1962), shows the "state of the art" for orthotropic steel deck bridges with open stiffeners. Several bridges built at that time are described as examples. V.d.Eb considered the closed trough stiffeners to be unsuitable because their torsional rigidity might cause assembly problems.

The AISC Design Manual (1963) gives a brief overview of the development of orthotropic steel decks and their application from about 1930 until 1963, with references to Pelikan et al. (1957). In addition the development of the "Battledeck" (see Fig.1.2), a predecessor of the orthotropic steel deck in the USA, is described. The theoretical background to the behaviour of the orthotropic deck and the economic considerations in the USA at the time of publication of the manual are discussed at length. The construction details for decks with open and closed stiffeners are discussed. Fabrication, erection and corrosion protection is considered and special attention is paid to the wearing course, the design criteria for the deck structure and the computational procedures for practical design. A number of calculation examples are given.

Troitsky (1967), in his guide, gives an introduction explaining the background that led to the development of orthotropic steel decks; "Battledecks" are discussed as a predecessor. The theory of orthotropic plates is presented together with the 3-dimensional bridge analysis, the deck plate analysis and the methods of deck analysis.

The method given by Pelikan et al. (1957) is dealt with and the design of decks with open stiffeners and closed stiffeners on rigid and elastic supports is given. A large number of bridges are presented with special attention to the structural details. Further, numerical examples of orthotropic deck designs are shown.

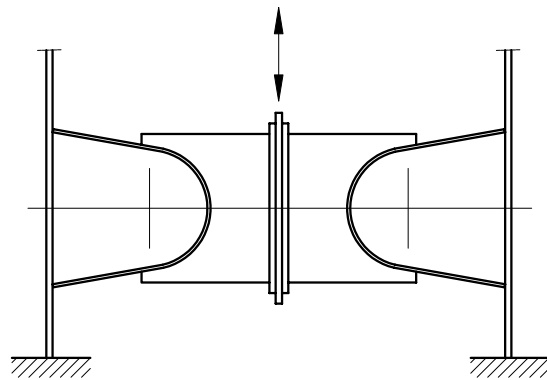


Fig. 2.1 Test specimen for floating deck stiffener to crossbeam connection

Tromp (1969) investigated the in-plane crossbeam behaviour of U-shaped continuous trough to crossbeam connections with support plates for bridges with Floating decks (see Fig.1.8-IV). The testing arrangement is shown in Fig.2.1. The design of bridges with these decks is presented by Ypeij (1972). This system was developed for the ease of fabrication and erection of the deck.

For re-decking projects where wooden or concrete decks were to be replaced with orthotropic steel decks, Tromp (1974) investigated two types of trough stiffener to crossbeam connections where the stiffeners were fitted between the crossbeams. One type of connection had a full penetration weld and the second had an additional end plate welded to the stiffeners and the deck. The end plate was bolted to the crossbeam web. The latter solution was designed for the ease of erection.

In his thesis, Weitz (1975) also describes the development of bridges with orthotropic steel decks. The characteristics of many bridges are described and given in tables, together with the types and details of orthotropic decks. Much attention is paid to the fabrication and the erection methods.

In the search for a better understanding of the behaviour of orthotropic steel decks, Beales (1979) describes tests on a full-scale test panel, a model of the Wye Bridge deck, with four spans of trapezoidal stiffeners fitted between the crossbeams. Wheel loads and the results of measurements are included.

In his thesis, Falke (1983) gives an elaborate description of the in-plane behaviour of crossbeams with cut-outs for continuous closed stiffeners. Various models describing the crossbeam behaviour are presented. FE-models with a fine mesh of vertical line elements are used to present a more accurate analysis and a model where the crossbeam web with cut-outs is represented by a system with a large number of vertical elements as shown in Fig.2.2.

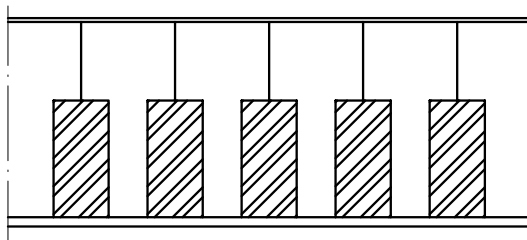


Fig. 2.2 Model of crossbeam with vertical posts consisting of a rigid and a flexible part

The vertical elements in Falke's model consist of a flexible part between the level of the deck and the bottom of the cut-out and a part with an infinite bending rigidity between the bottom of the cut-out and the bottom flange. These elements are positioned close together, with a much smaller centre-to-centre distance than that of the closed stiffeners. Together they represent the average bending and shear stiffness of the crossbeam web.

In this way, an appropriate simulation of the global behaviour of the crossbeam is obtained. No secondary bending due to shear transfer in the bottom part of the crossbeam is generated by the model, however, Falke states that the model is simple and gives more accurate results than those obtained with the analytical models in which the cut-outs with cope holes are neglected or those obtained by the Vierendeel model. The crossbeam stiffness in his method includes the shear deformation and in some cases, this may result in a contribution up to 30% of the total deformation. The stress effects due to the primary and secondary load transfer by bending and shear is investigated.

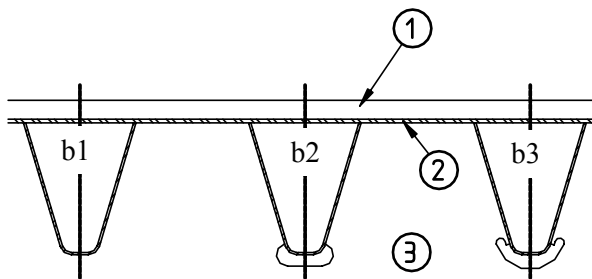


Fig. 2.3 Various cut-outs with cope holes

As a result, of the search for improved detailing of cope holes, Haibach et al. (1983) compared the details of crossbeams with continuous closed stiffeners for the in-plane behaviour of the crossbeams.

Fig.2.3 shows the cope holes investigated i.e. trapezoidal cut-out "b1", cut-out with oval cope hole "b2" and the cut-out with the "Haibach" cope hole "b3".

The trough to deck connection, splice joints in the closed stiffeners and the effect of contraction in the trough are discussed.

Lehrke (1990) discusses the in-plane behaviour of the crossbeam and the results of the FE calculation of the crossbeams with "Haibach" cope holes (see Fig. 2.3, type "b3"). He compares the results with those from crossbeams with traditional cut-outs with cope holes (see Fig. 2.3 type "b2").

De Jong (1981) presents an analytical method for the calculation of the in-plane and the out-of-plane behaviour of the crossbeam. The shear deformation of the crossbeam is ignored but the method allows for the interaction between the stiffeners and the crossbeams. The deck is modelled with two spans of stiffeners over three crossbeams.

In his design guide for the designers of the department for movable bridges within the Civil Engineering Division of the Ministry of Transport (The Netherlands), Stroosma (1982) describes the behaviour of crossbeams and decks with open and closed stiffeners. The mechanical behaviour is analysed based on the method of Pelikan et al. (1957) and formulae and tables are derived for a deck system including four crossbeams.

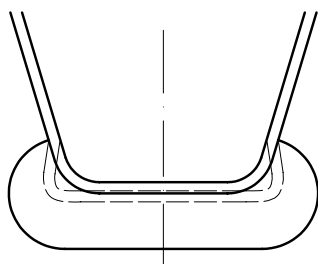


Fig. 2.4 Deformation of closed stiffener bottom due to contraction

Wolchuk et al. (1992) draw attention to secondary stresses in continuous closed stiffeners caused by deformations due to contraction effects as shown in Fig. 2.4. These stresses become more important when troughs with wider bottoms intersect the crossbeams through shallow cope holes.

Mang et al. (1995) show, for a railway bridge, the stress distributions due to shear forces under in-plane loading in crossbeams with "Haibach" cope holes. It is concluded that manual calculation methods give results that differ from the calculations with FE-analysis. At midspan both methods gave results that deviated from the measurements. The crossbeam in-plane load transfer from the deck to the main girder is analysed by FE models. It is concluded that the stresses around the cut-out with cope hole are mainly caused by the shear transfer of the crossbeam.

The crossbeam details used in The Netherlands and their behaviour are shown in various publications e.g.: Kolstein et al. (1995a), related to the tests for the ECSC and Leendertz et al. (1995a) showing the numerical analyses of crossbeams and closed stiffener to crossbeam connections.

Leendertz et al. (1995b) and Kolstein et al. (1995b) give analytical models for the crossbeam in-plane shear behaviour, together with the stress distributions around two types of cut-outs with cope holes. Leendertz et al. (1995c) give a more extensive analysis of the crossbeam behaviour.

Further, Leendertz et al. (1996b) show a comparison of closed stiffener to crossbeam connections in “conventional” crossbeams with the connections in “Floating decks”.

Bruls et al. (1997) deal with structural details of orthotropic steel bridge decks used in the EU and investigated in the ECSC research Phase 4 and describe their behaviour qualitatively. A large part of this work was carried out at the University of Pisa and included measurements of full-scale specimens and FE analyses of the in-plane behaviour of the crossbeams with eight types of stiffeners with various cut-outs.

Kolstein et al. (1998) show typical details in orthotropic steel bridge decks and give a summary of the ECSC Phase 4 work.

2.2.2 Aspects not sufficiently covered in literature

The behaviour of the crossbeams is discussed in many publications. The earlier publications date from the period when continuous open stiffeners and closed stiffeners fitted between the crossbeams were most common. In this case, the shear stiffness of the crossbeams is not affected and the deformations of the crossbeams are mainly due to bending moments. However, the in-plane shear behaviour of crossbeams with continuous stiffeners is generally not sufficiently addressed in the publications.

The publications dealing with continuous closed stiffeners discuss the shear force deformations (Vierendeel effect) as far as they cause additional stresses in the crossbeam web. Only Falke (1983) discussed the contribution of the shear deformations to the crossbeam deflection in such a way that it can be used for the calculation of the equivalent beam properties. The determination of local stresses in the closed stiffener is not described.

This means that the in-plane behaviour of the crossbeam and the effects on the closed stiffeners have to be investigated in more detail in order to find the relevant mechanisms and stresses.

In most publications, the crossbeam out-of-plane behaviour is not addressed. However, there are indications in the test results of the ECSC Phase 3 fatigue tests, that it might be a critical phenomenon, and worthy of a more detailed analysis.

Interaction between the in-plane and the out-of-plane behaviour is not addressed in any literature, although the stresses occur at the same locations and this also needs further analysis.

Chapter 4 gives a full description of the in-plane and out-of-plane behaviour of conventional crossbeams.

2.3 Loads and load transfer

2.3.1 Review

The approach to load transfer described in the literature is related to the static resistance or the fatigue resistance.

Initially, most attention was paid to the static behaviour. The main objective was to find the combination of loadings, producing the highest internal forces and stresses.

With respect to fatigue, initially, determination of the maximum and minimum stresses was considered essential. The calculation of these stresses was a logical extension of the static calculations taking into account the positions of traffic loads. The introduction of the stress range concept and using the Palmgren-Miner rule as the basis for damage calculations required a spectrum of load intervals and the associated numbers of cycles which can be derived from the influence lines. Typical influence lines for the load transfer from the stiffener to the crossbeam and for the rotation of the connection are shown in Fig.1.9.

V.d.Eb (1962) presented simplified methods based on the theory shown by Pelikan et al. (1957). Bats et al. (1962) show influence lines for decks with open stiffeners, with and without wearing courses.

Based on Pelikan (1957), The AISC Design Manual (1963) gives a full explanation of the load transfer through the elements of the orthotropic decks with open and closed stiffeners. The composite action of the asphalt with the deck plate is discussed and dynamic amplification factors are addressed.

Troitsky (1967), referring to Pelikan et al (1957), gives an extensive explanation of the load transfer through the orthotropic deck and discussed wheel load distribution and the load transfer from deck plate to the main girders. Dowling (1971) showed various influence lines for orthotropic steel decks, which give information about the relevant positions of the vehicles, axles and wheels.

Ypeij (1972) explained the load transfer in floating decks. Particular attention was paid to the transverse shift of the deck with respect to the crossbeam under live load.

Beales (1979) showed influence lines for stresses in a large number of locations in a deck panel. They were based on measurements for a typical wheel travelling over a test panel with four spans, representing a part of the Wye Bridge.

BS 5400 (1980) gives influence lines to be used for fatigue assessment procedures.

Stroosma (1982) discussed the load transfer from the deck to the stiffeners and the stiffeners to the crossbeams for a deck geometry comprising three stiffener spans.

Yamada (1990) showed the measured influence lines for two details and Yamada et al. (1997) give, for two types of truck, the measured strains and the influence lines for the reaction of the crossbeam. in a bridge deck with open stiffeners They showed a comparison between the measured and the calculated stress distribution in the deck. The paper also deals with axle spectra and gives a histogram of transverse wheel load positions.

Kolstein (1997) showed the contribution of the wearing course to the stiffness of the deck plate. The mechanism was explained and distinction was made between the static and the dynamic modulus of elasticity of asphalt.

2.3.2 Aspects not sufficiently covered in literature

The effect of the crossbeam shear stiffness on the in-plane behaviour is included in the measurements but not always separately investigated. The crossbeam out-of-plane behaviour and the effects of imposed deformations are hardly addressed.

These phenomena are investigated in chapter 6 for a variety of crossbeams. The results obtained from the analyses for the in-plane and the out-of-plane behaviour can be combined and used for fatigue assessment procedures.

2.4 Strength

2.4.1 Review

From the early stage of the development of orthotropic steel bridge decks, designers were aware that in addition to the static strength, the fatigue strength plays a role. In Germany, it was discussed by Pelikan et al. (1957) and was regarded as a subject for further research.

V.d.Eb (1962) showed results of the static and the fatigue strength observed in tests. Based on these test results, it was concluded that sufficient static strength automatically endowed sufficient fatigue strength.

For a specific detail with open stiffeners passing through a crossbeam with cope holes, Drost et al. (1965) presented fatigue test results for various open stiffener to crossbeam connections.

The loading conditions of the specimen were such that the detail was only tested for shear forces. Some of the conclusions are already included in the work by V.d.Eb (1962).

The AISC Design Manual (1963) discusses the static strength of the deck with crossbeams extensively. For the fatigue strength reference was made to research of Klöppel et al. (1960) whose tests on a deck plate supported by open stiffeners and loaded by stress cycles up to 80% of the yield strength showed a fatigue strength up to 7 million cycles. Based on these results the strength of the stiffeners was considered sufficient, because in practice the stress amplitudes were considered low.

Troitsky (1967) discussed the static strength of orthotropic steel bridge decks in relation to the bridges designed in Germany. Design criteria for the main structural parts and optimal deck design criteria for static strength were given. For the fatigue resistance he refers to tests carried out in Halle (Germany) but the fatigue strength is not described and considered a subject for further study.

Tromp (1969) presented the test results for “floating decks” with U-shaped trough to crossbeam connections by means of plate supports as shown in Fig. 1.8-IV). He tested the static strength and the fatigue strength under cyclic loading to a maximum of 4 million cycles. The fatigue tests consist of a cyclic deck displacement of 0.9 mm with respect to the crossbeam, parallel to the crossbeam axis. These tests do not include the influence from loads directly applied to the deck. The testing arrangement is shown in Fig. 2.1. After 2 million cycles, no cracks were found and the displacement range was increased from 0.9 to 1.4 mm. The first cracks in the trough web occurred after the next 500.000 cycles.

Test results for the stiffener to crossbeam connection for decks with closed stiffeners fitted between the crossbeams were presented by Van Bercum et al. (1971). The tests were carried out on several types of closed stiffeners with deck plates. These panels were connected in longitudinal direction by means of a full penetration weld between the stiffener and the end plate, simulating the crossbeam web. Additionally, a connection with axially loaded prestressed high strength bolts was tested. The crossbeam webs had a thickness of 10 and 16 mm. These types of connection are still in use for re-decking projects to replace concrete decks with orthotropic steel decks. For the welded connection, the static strength was determined and the fatigue strength for a nominal stress range of 50 N/mm^2 , was 1.6 million cycles.

Ypey (1972) showed how the results from Tromp (1969) were integrated in the design of steel bridges with "Floating decks". As a further development of the floating deck, Tromp (1974) describes tests on trapezoidal shaped stiffener to crossbeam connections in floating deck structures. For the plate supports two depths were used. Both had the same distance between the stiffener and the crossbeam flange, but the distance from the upper boundary of the support plate to the deck was different. The type with the largest distance between deck and support plate showed the most favourable behaviour, with the first cracks in the trough web occurring at 500.000 cycles for an imposed displacement amplitude of 1.7 mm.

Fisher (1977) gave an overview of details susceptible to fatigue, which are still very common today, not only in all existing older bridges but also in newer steel bridges. For the behaviour and the fatigue strength of the trough to crossbeam connection, reference is made to UK research. In this research, the connection with the stiffener fitted between the crossbeams showed many cracks, and it was concluded that the connection with a continuous closed stiffener is the more favourable solution. All common closed stiffener splices of that time were also discussed. The AASHTO and the AREA fatigue specifications were presented together with the fatigue strength detail classes. Attention was drawn to the fact that the stress ratio approach (Max. vs. Min. Stress), which was used at that time, might have to be replaced by the stress range approach. The "Palmgren-Miner" summation rule was presented for the fatigue damage calculation.

Falke (1983) discusses the static strength of crossbeams with cut-outs and cope holes. The fatigue strength is only mentioned in relation to deformations caused by the crossbeam in-plane behaviour.

Haibach et al. (1983) showed the fatigue strength of a crossbeam with trough to crossbeam connections incorporating several types of cope holes. The crossbeam in-plane fatigue strength of the web was higher for specimens with a special cope hole (the later so called "Haibach" cope hole) than for specimens with the conventional cope holes. An attempt was made to test the fatigue strength in relation to the contraction effect in the trapezoidal stiffener.

Kolstein (1989) reported results of the fatigue testing of orthotropic steel deck details in the ECSC Phase 3 research. Various shapes of continuous trough to crossbeam connections with and without cope holes were tested and reported. The locations where fatigue cracks were observed were affected by several phenomena acting together, such as, support reaction transfer, out-of-plane bending of the crossbeam web and contraction of the trough bottom.

Lehrke (1990) showed the results of fatigue tests in the ECSC Phase 3 research on the in-plane behaviour of full-scale crossbeams with continuous closed stiffeners. The crossbeam with the "Haibach" cope holes (Fig. 2.3.b3) did not show a better fatigue behaviour than the beam with the oval cope holes (Fig. 2.3.b2). Once a crack in the stiffener web had reached a certain length it did not grow further.

Mang et al. (1995) showed the results of full-scale fatigue tests on a crossbeam specimen for railway bridges with "Haibach" cope holes. The fatigue strength of the crossbeam web with Haibach cope holes was found to be higher than the fatigue strength of the crossbeam web with the conventional cope hole. Nevertheless it was concluded that the fatigue classifications in DS 804 overestimated the fatigue strength of the structure.

The above observations regarding the crossbeam in-plane behaviour with Haibach cope holes shows contradictory conclusions. However, these conclusions are drawn for slightly different cope hole geometries, e.g. the radii are different.

In Kolstein et al. (1995a and 1995b) fatigue strength results of tests on closed stiffener field splices and trough stiffener to deck connections are given. Kolstein et al. (1996 and 1998) showed fatigue detail class proposals based on the ECSC Phase 3 and ECSC Phase 4 research.

Bruls et al. (1997) report a complete overview of all results of Phase 4 and where possible, linked to the results of the ECSC research Phase 3. The fatigue test results included tests carried out at the Laboratorium für Betriebsfestigkeit in Darmstadt, the University of Pisa, the Laboratoire des Ponts et Chaussées in Paris and Delft University of Technology.

Yamada et al. (1997) discuss the fatigue strength of details of orthotropic steel decks tested in Japan and compared the results with those from the ECSC Phase 3 and 4 research. The details considered are the closed stiffener splice connection, stiffener to deck connection, stiffener to crossbeam connection for stiffeners fitted between the crossbeams and continuous stiffeners and for the crossbeam web and the main girder web to deck plate connection.

De Jong (2007) carried out research, mainly concentrating on the details D.1.4 and S.1. He studied traffic loads and the composite action of the wearing course and the deck plate. He reports the derived models for fatigue assessment of these details taking into account the probabilistic aspects and studied repair methods as well as renovation and improvement measures for these details. He also gives a brief description of inspection methods.

Kolstein (2007) gives an exhaustive overview of the ECSC fatigue research concerning orthotropic steel decks, carried out between 1976 and 1994 and additional work carried out worldwide until 2006.

2.4.2 Aspects not sufficiently covered in literature

The static strength of the decks with open and closed stiffeners is extensively discussed in literature. The same applies to the fatigue strength of the details. However, the fatigue strength of details with local bending, which is the case for several locations e.g. the closed stiffener to crossbeam connection, has not been extensively investigated and the test results sometimes seem to be contradictory.

The detail classes resulting from IIW Recommendation for Fatigue design of Welded Joints and Components by Hobbacher et al (2005) and the fatigue design classifications given in EN 1993-1-9 are given in chapter 8, where they are adapted, as necessary, to facilitate design calculations.

2.5 Geometrical stress concentration factors

2.5.1 Review

In many reports and documents the fatigue strength of a detail is linked to the nominal stress in the detail under a certain loading condition, which means that the detail fatigue class includes the geometrical stress concentration factor. This is the case in the following literature: AISC Design manual (1963), Drost (1965), Tromp (1969), Van Bercum (1971), Ypeij (1972), Tromp (1974), Fisher (1977) and Bruls et al. (1997).

In those cases where the fatigue strength is related to the geometrical stress, also called “Hot-spot Stress”, measured at, or extrapolated to a particular location, this geometrical stress can be related to the nominal stress by a geometrical stress concentration factor.

However, the definition of the stress concentration factors is not always consistent with the location of the measured stress and the extrapolation method.

BS 5400 (1980) gives geometrical stress concentration factors for typical apertures and re-entrant corners.

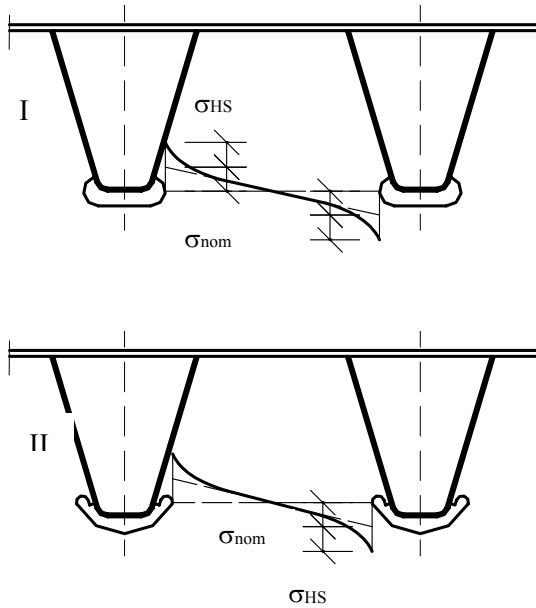


Fig. 2.5 Stress concentration effect in crossbeam web cope holes

Haibach et al. (1983) determined the stress concentration factor ($SCF = \sigma_{HS}/\sigma_{nom}$) for the narrowest cross section between the cope holes, the “tooth”, for the so-called "Haibach" cope holes shown in Fig.2.5-II under crossbeam in-plane loading.

The geometrical stress concentration factors were derived from measurements on a prototype beam. The SCF was approximately 1.6 for a cope hole with a radius of 20 mm near the connection to the stiffener.

Falke (1983) in his thesis shows stress concentration factors for various shapes of cope holes at the narrowest section of the tooth. An oval cope hole as shown in Fig. 2.5-I with $r = 15$ mm results in a geometrical $SCF = 3.3$ and with an $r = 25$ mm in a $SCF = 2.5$.

Roark et al. (1986) give tables and formulae for stress concentration factors for a large variety of details, holes etc.

Lehrke (1990) showed geometrical stress concentration factors for the oval cope holes (see Fig. 2.5-I) and the "Haibach" cope hole (see Fig. 2.5-II) for the in-plane behaviour of the crossbeam. The "Haibach" cope hole used, resulted in a geometrical stress concentration factor of 2.8 for the narrowest horizontal section of the tooth, which differs from the values found by Haibach et al. (1983) and by Falke (1983).

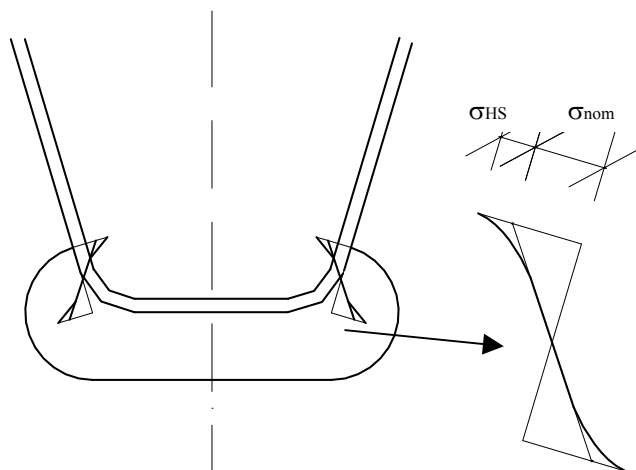
Mang et al. (1995) describe the stress concentrations around the "Haibach" cope hole for crossbeam in-plane behaviour. The locations of the stress concentrations coincide with the locations of the observed fatigue cracks.

Kolstein et al. (1996 and 1998b) discuss the relationship between the concentrated stresses considered in the test results for the measured locations and the concentrated stresses to be considered for design purposes at these locations. The importance of the extrapolation method and the measured location is addressed.

Yamada et al. (1997) gave stress concentration factors in the crossbeam web for the crossbeam in-plane behaviour.

2.5.2 Aspects not sufficiently covered in literature

The geometrical stress concentration factors occurring at the free edges of the cope holes of the crossbeam webs were discussed in several publications. The SCF's given in 2.5.1 vary from 1.6 to 3.3, and are strongly influenced by the shape of the cope holes.



The stress concentration effects in the crossbeam web at the connection with the closed stiffener web have not yet been investigated.

In chapter 5 analytical and FE models are developed, through which a better insight into the stress distribution in the closed stiffener near the crossbeam can be obtained, see Fig.2.6.

Fig. 2.6 Concentrated stresses in crossbeam web near trough

The stress concentration factors for the cope holes are determined using the formulae given by Roark et al. (1986) and compared to the factors found by Lehrke (1990), Mang (1995) and Yamada (1997).

Where possible, in chapter 7, the stress concentration effects are compared with those observed in the test specimen of the ECSC Phase 4 conducted at the Stevin Laboratory.

The geometrical stress concentration factors related to plate bending effects as occur in the stiffener web (see Fig.2.6) under in-plane shear deformations of the crossbeam web and the contraction effects in the closed stiffener bottom are not addressed separately.

2.6 Fatigue assessment procedures

2.6.1 Review

BS 5400 (1980) gives a fatigue assessment procedure including loads and details, however this does not cover the fatigue classification of details of orthotropic steel decks, which means that additional analyses are needed.

Yamada (1990) showed a fatigue assessment procedure for several details. In this publication, the damage for a known vehicle spectrum was calculated with the detail classifications from EN 1993-1-9 (1995). A parameter study was carried out for the effect of different trucks.

Maddox (1991) gave a fatigue assessment procedure using the "Palmgren-Miner" rule and presented in addition a method using fracture mechanics.

NEN 6788 gives a vehicle spectrum and rules for the fatigue design of bridges, but not specifically for orthotropic steel bridge decks.

Kolstein et al. (1995b) show generalised axle and vehicle spectra. The contribution of typical vehicles to fatigue damage is clarified with reference to ENV 1991-3 (1995) "Traffic loads on bridges".

2.6.2 Aspects not sufficiently covered in literature

Standards, fatigue assessment procedures and crack growth procedures are given in various publications. However, the fatigue strength of the closed stiffener to crossbeam connection is not addressed in detail. This is due to the lack of information on geometrical hot spot stresses and the interaction of the crossbeam in-plane and the crossbeam out-of-plane behaviour.

In chapter 8 and in the case study presented in chapter 9 and Appendix 1, these effects are combined.

2.7 Concluding remarks

The following aspects need further study:

- Mechanical in-plane and out-of-plane behaviour of the continuous closed stiffener to crossbeam connections.
- Geometrical stress concentration factors for the closed stiffener to crossbeam connection
- Stress and rotation histories for the closed stiffener to crossbeam connections due to traffic loads (influence lines)
- Combinations of stress histories and components for specific location

3 DESIGN PHILOSOPHY, CRACK LOCATIONS AND FATIGUE ASSESSMENT PROCEDURE

3.1 Design Philosophy

3.1.1 General considerations

An orthotropic steel bridge deck shall be designed in such a way that:

- (1) It resists the design loads during its design life,
- (2) The deformations which occur cause no hazard to the users.

The first requirement can be related to the "Ultimate Limit State" (ULS), which represents the behaviour at collapse of the structure and its component parts. The second requirement relates to the "Serviceability Limit State" (SLS) beyond which the structure as a whole and its component parts are subjected to a degree of deformation inappropriate to their intended function.

Both requirements are laid down in the Construction Products Directive of the European Union CPD (1988) with Amendment (1993), as:

1. Essential Requirement No.1: Mechanical Resistance and Stability
2. Essential Requirement No.4: Safety in Use.

The design philosophy can be considered as the synthesis of the multiple considerations that are the basis of the design of a structure. These include technical considerations, such as design life, design loads, static strength, fatigue strength, inspectability, maintainability, and possibilities for repair, durability, and reliability. It takes into account restraining boundary conditions such as economic aspects and the specific wishes of the future owner. (Often the design loads or use conditions are changing during the service life of a structure.)

Moving vehicles may cause fatigue damage, which results in the structure reaching one of the limit states mentioned above. Crack growth in a detail may cause a redistribution of loads leading to excessive deformations and/or collapse.

Clearly, the accessibility of the crack location plays an important role. It influences the inspection method and inspection interval to be used, and allows an assessment to be made of whether a crack has reached a critical stage (length and depth) and whether intervention is needed.

It is necessary that an observed crack can be repaired before it exceeds the critical length and/or depth or reaches a critical location. Further crack growth would then lead to collapse of the structure or a part of it.

It is essential that analyses predict the development of cracks, i.e. the moment when they are expected to become detectable, the direction and the expected crack growth.

Repair options are influenced by the accessibility and the possibilities for welding. The repair method may require that, during the execution of the repair work, only small relative movements occur at the cracked location. This requirement may lead to the need for one or more traffic lanes to be closed during repair work.

When a crack occurs in a location where it can be observed, inspected and repaired, the "as built" quality can be (partially) restored or improved. This procedure is commonly designated as the "fail safe" approach.

This "unlimited fatigue life design" implies that the component is designed such that under all stress cycles there is no fatigue damage. However, if the vehicle loads and/or the axle loads increase during service life the "infinite life" assumption may not longer be valid.

3.1.2 Crack growth categories

In most cases, fatigue cracks do not pose an immediate threat to the integrity of the structure as a whole. A distinction can be made between cracks that are caused in a load-carrying element or in a connection for load transfer, and cracks that are generated by imposed deformations. The latter will stop growing, once the stresses resulting from the imposed deformations are relieved, although when these cracks grow into areas where the load carrying stresses govern, they may also become threatening to the structural integrity.

Locations susceptible to fatigue can be assigned to one of the following categories:

- Cat. A. - Locations subject to direct load transfer will show a progressive crack growth as the crack reduces the cross section available for load transfer, causing increased stresses. Progressive growth can make the locations critical within a short period of time.
- Cat. B. - Locations subject to imposed deformations will show diminishing crack growth as the cross sectional rigidity is reduced by the propagating crack. These cracks are not critical with respect to the load transfer through the structure.
- Cat. C. - Locations, initially subjected to imposed deformations (category B), but where the crack may grow into an area, which is subject to direct load transfer (category A) (sequence effect) and may become critical if the crack exceeds a certain length.

EN 1993-1-9 Table 3.1 (see also Table 3.1) gives partial factors γ_{Mf} for the fatigue strength, which are related to the importance of the detail for the structure as a whole, the inspection possibilities and accessibility for repair.

Table 3.1 EN 1993-1-9 Table 3.1 Recommended values for partial factors for fatigue strength

Assessment method	Consequence of failure	
	Low consequence	High consequence
Damage tolerant	1,00	1,15
Safe life	1,15	1,35

They do not include the distinction between load transfer and imposed deformations.

The inspectability of the crack locations plays an important role as it determines the inspection method and inspection interval to be used, and to determine whether cracks have reached a critical stage (length and depth) and whether intervention is needed. It is essential that analyses predict the development of cracks, i.e. the moment when they are expected to become detectable, the direction and the expected crack growth.

It is necessary that an observed crack can be repaired before it exceeds the critical length or reaches a critical location. Further crack growth would then lead to collapse of the structure or a part of it. Depending on the repair quality that can be achieved a repaired crack may have a lower or an equivalent fatigue classification than originally.

3.1.3 Design philosophy

The design can be based on a “limited fatigue life design” with a “fail safe” approach considering regular inspections at indicated locations. The time intervals depend on the traffic volume and shall be adjusted when the numbers of vehicles, traffic type, axle spacings and axle loads are changing. In this case, repairs will be needed and it is important that details are easily repairable.

When inspection is only carried out at fixed time intervals and the inspection results are interpreted with an "ad hoc" re-analysis of the structure resulting in repair proposals, it can be considered as a special procedure within the "fail safe" approach.

Details at inaccessible locations that cannot be inspected or repaired should be designed for an “unlimited fatigue life”. When this approach is used, no inspection or repair of fatigue damage will be needed, provided that the traffic loads and boundary conditions remain unchanged.

For the “limited fatigue life design” and the “unlimited fatigue life design” the fatigue detail classifications should be modified with the values given in EN 1993-1-9 Table 3.1. In addition to the “Damage tolerant” and “Safe life” categories with their consequences of failure, the choice of the factor γ_{Mf} , consideration can also be given to cracks in a detail growing due to the load transfer (A), the imposed deformations (B) or start due to imposed deformations and continue into a region where they further grow due to the load transfer (C).

For a structure or detail which is considered to be damage tolerant and with a low consequence of failure the $\gamma_{Mf} = 1.0$. Cracks in the crossbeam due to imposed deformations and with a good accessibility for inspection, which do not grow into areas relevant to the load transfer fall into this category (B). The $\gamma_{Mf} = 1.0$ also applies for cracks in the crossbeam, initially caused by imposed deformations but growing into critical areas subjected to direct load transfer (C), in relation to less inspections, it is recommended to use $\gamma_{Mf} = 1.15$.

For a safe life concept with a high consequence of failure and with a poor accessibility the $\gamma_{Mf} = 1.15$. This is the case for cracks in the crossbeam, growing due to direct load transfer (A). Cracks in the stiffener do not immediately threaten the overall bearing capacity and therefore $\gamma_{Mf} = 1.0$.

3.2 Design methods for fatigue

3.2.1 Simplified design methods

Instead of a full analysis, the required fatigue resistance for new bridges can be achieved by the use of a "Standard Deck". In such a design, the dimensions are e.g. determined in advance through a method with relative stiffnesses, taking account of reference traffic load spectra, the detail fatigue strength classifications and the combinations of in-plane and out-of-plane effects

The "fail safe" approach requires the availability of specific design documents dealing with the "built in" design resistance, with the locations for inspection and the estimated inspection intervals.

When no inspection and repair specifications are available, the design life for fatigue in the above-mentioned methods must be unlimited, requiring the number of critical stress cycles to be below the level where any fatigue crack can be generated. When the critical stress cycles in the design are below the fatigue limit and the actual traffic does not cause higher stresses, the number of vehicles does not play a role.

When the traffic type and volume deviates from the reference traffic, a re-analysis has to be carried out.

3.2.2 Detailed design methods

The detailed design methods use a load spectrum, dynamic impact factors, transfer functions for the loads on the deck to the stress location, and where needed, stress concentration factors and a fatigue strength classification of the detail. When a designer uses this method, all locations susceptible to fatigue cracks have to be assessed by means of fatigue life calculations with a Palmgren-Miner summation or with crack growth calculations.

These methods can be used for the design of new decks and for evaluation and upgrading of existing decks.

3.2.3 Methods developed in this research

As mentioned in 1.5, one of the objectives of this research is the development of a simple, but sufficiently detailed, design method, including all aspects from vehicle loads to fatigue classifications.

The insight obtained, can be used for the development of standard decks, improved details and simplified methods considering relative stiffnesses.

3.3 Typical fatigue crack locations in the closed stiffener to crossbeam connection

Typical fatigue cracks in the stiffener to crossbeam connections (not the stiffener to deck plate connection in this area) are shown in Figs. 3.1 - 3.6 and classified in accordance with the crack growth category A, B or C together with brief background information about the consequences for the structural strength of the detail.

The fatigue crack locations and the cracks are evaluated with respect to the following aspects:

- Crack growth category
- Consequences
- Inspectability
- Repairability.

In general, all the cracks identified in this section show a good accessibility for visual inspection and repair work, but when a crack originates from the weld root, it is not visible until it reaches the surface. NDT-techniques may provide reliable indications before the crack has reached the surface.

Repaired welds may have a fatigue class different from the original weld, depending on the accessibility of the weld root, the weld position, the conditions and the shape of the weld. A repaired weld toe can be upgraded by post weld heat treatments or mechanical treatments.

Open stiffener to crossbeam connection

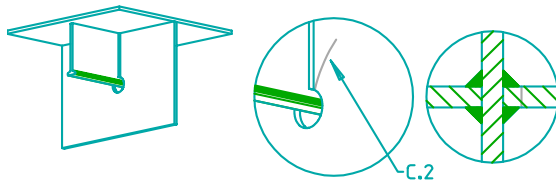


Fig. 3.1 Open stiffener to crossbeam connection with a cope hole

Crack C.2, Crossbeam web (Fig. 3.1)

Crack growth cat.: C. Imposed stiffener rotations out-of-plane with fluctuating in-plane load transfer to the crossbeam.

Consequences: Reduced strength of the crossbeam.

Inspectability: Good

Repairability: Good

Conclusion: Good inspectability and low consequence, $\gamma_{Mf} = 1.0$

Closed stiffener fitted between crossbeams, detail "a"

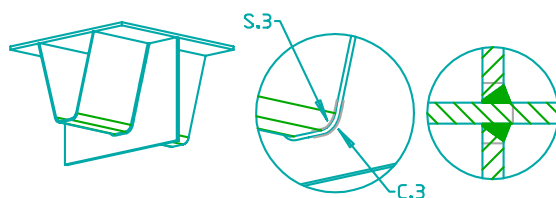


Fig. 3.2 Closed stiffener fitted between crossbeams

Crack S.3, Closed stiffener (Fig. 3.2)

Crack growth cat.: A. Fluctuating in-plane load transfer from the stiffener to the crossbeam with contraction of the stiffener bottom.

Consequences: Reduced strength of the stiffener, the crack could grow through the weld into the crossbeam.

Inspectability: Good

Repairability: Good

Conclusion: Good inspectability and low consequence, $\gamma_{Mf} = 1.0$

Crack C.3, Crossbeam web

Crack growth cat.: C. Fluctuating in-plane load transfer to the crossbeam with imposed rotations out-of-plane.

Consequences: Reduced strength of the crossbeam, the crack may grow into the weld and the stiffener.

Inspectability: Good

Repairability: Good

Conclusion: Good inspectability and low consequence, $\gamma_{Mf} = 1.0$ or 1.15 (with larger inspection intervals)

Continuous closed stiffener through crossbeam with close fit, detail "b1"

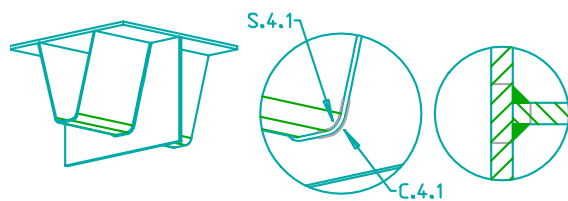


Fig. 3.3 Continuous closed stiffener through crossbeam with close fit

Crack S.4.1, Closed stiffener (Fig. 3.3)

Crack growth cat.: A. Fluctuating in-plane load transfer to the stiffener with contraction.

Consequences: Reduced strength of the stiffener, the crack may grow into the weld and the crossbeam.

Inspectability: Good

Repairability: Good

Conclusion: Good inspectability and low consequence, $\gamma_{Mf} = 1.0$

Crack C.4.1, Crossbeam web near connection (Fig. 3.3)

Crack growth cat.: C, Fluctuating in-plane load transfer to the crossbeam with imposed rotations out-of-plane.

Consequences: Reduced crossbeam strength, the crack may grow into the weld and the stiffener.

Inspectability: Good

Repairability: Good

Conclusion: Good inspectability and high consequence, $\gamma_{Mf} = 1.15$

Continuous closed stiffener through a cut-out in the Crossbeam with an oval cope hole or with a "Haibach" cope hole, detail "b2" and "b3"

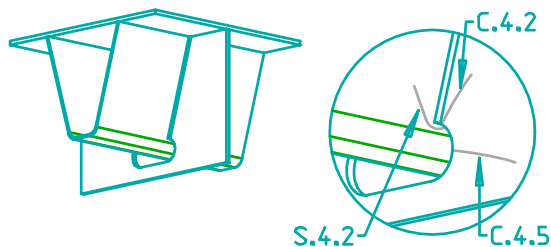


Fig. 3.4 Closed stiffener through crossbeam with oval cope hole

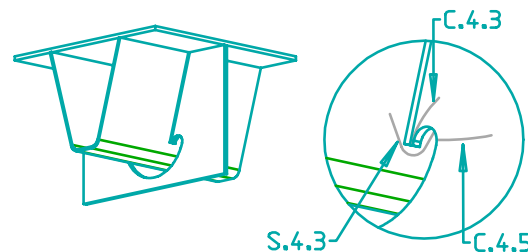


Fig. 3.5 Closed stiffener through crossbeam with "Haibach" cope hole

Cracks S.4.2 and S.4.3, Closed stiffener (Figs. 3.4 and 3.5)

Crack growth cat.: C. Fluctuating in-plane load transfer to the crossbeam with imposed rotations out-of-plane.

Consequences: Reduced strength of the stiffener.

Inspectability: Good

Repairability: Good

Conclusion: Good inspectability and low consequence, $\gamma_{Mf} = 1.0$

Cracks C.4.2 and C.4.3, Crossbeam web near connection (Figs. 3.4 and 3.5)

Crack growth cat.: C. Fluctuating in-plane load transfer to the crossbeam with imposed rotations out-of-plane.

Consequences: Reduced strength of the crossbeam.

Inspectability: Good

Repairability: Good

Conclusion: Good inspectability and low consequence, $\gamma_{Mf} = 1.0$ or 1.15 (with larger inspection intervals)

Crack C.4.5, Crossbeam web cope hole (Figs. 3.4 and 3.5)

Crack growth cat.: A. Fluctuating in-plane load transfer to the crossbeam together with imposed rotations out-of-plane.

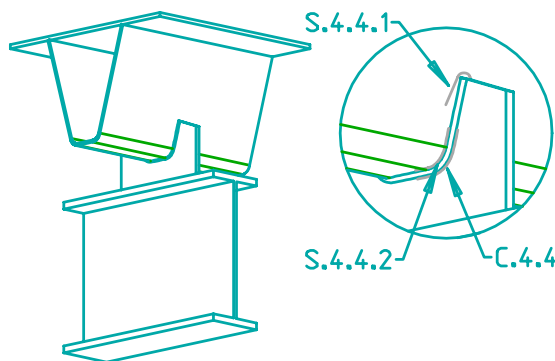
Consequences: Reduced strength of the crossbeam.

Inspectability: Good

Repairability: Good

Conclusion: Good inspectability and high consequence, $\gamma_{Mf} = 1.15$

Continuous closed stiffener on a plate support ("Floating Deck"), detail "b4"



Crack S.4.4.1, Closed stiffener web (Fig.3.6)

Crack growth cat.: C. Fluctuating in-plane load transfer to the stiffener with imposed in-plane deformations of the crossbeam.

Consequences: Reduced strength of the stiffener

Inspectability: Good

Repairability: Good

Conclusion: Good inspectability and low consequence, $\gamma_{Mf} = 1.0$

Fig. 3.6 Continuous closed stiffener on plate support

Crack S.4.4.2, Closed stiffener bottom (Fig.3.6)

Crack growth cat.: A. Fluctuating in-plane load transfer to the stiffener.

Consequences: Reduced strength of the stiffener.

Inspectability: Good

Repairability: Good

Conclusion: Good inspectability and low consequence, $\gamma_{Mf} = 1.0$

Crack C.4.4, Plate support (Fig.3.6)

Crack growth cat.: B. Fluctuating out-of-plane load transfer due to imposed rotations caused by crossbeam out-of-plane behaviour.

Consequences: Reduced strength of the plate support.

Inspectability: Good

Repairability: Good

Conclusion: Good inspectability and low consequence, $\gamma_{Mf} = 1.0$

3.4 Load models

The governing stresses for fatigue are caused by lorries. For some structural details, the lorry loads as a whole are relevant, for others the axle loads and sometimes the individual wheel loads are the most relevant. Contract documents may specify the bridge loading derived from measurements or from standards.

In this study, the fatigue load models from ENV 1991-3, the predecessor of EN 1991-2, are used. Fatigue Load Model 2 (FLM2) is a set of frequent lorries (see ENV 1991-3, Table 4.6) and Fatigue Load Model 4 (FLM4) is a set of lorries with equivalent loads given in ENV 1991-3, Table 4.7.

Table 3.1 gives the axle arrangements and loads of the lorries for the frequent loads and the axle types for the “frequent lorries” and the “equivalent lorries”. Further, the total vehicle load is given. In this study, the lorry percentages for the long distance traffic type are taken from ENV 1991-3:1995, which is superseded by EN 1991-2 (values in brackets).

Table 3.1 Fatigue load models 2 and 4

Lorry	Axle type	Frequent loads FLM2 (kN)		Equivalent loads FLM4 (kN)			Axle spacing (m)
		Axle load	Vehicle load	Axle load	Vehicle load	Lorry percentage Long distance	
1 2 axles ↓↓	A	90	280	70	200	20 (20)	4.50
	B	190		130			
2 3 axles ↓↓↓	A	80	360	70	310	5 (5)	4.20 1.30
	B	140		120			
	B	140		120			
3 Semi-trailer 2 axles, 3 axles ↓↓↓↓↓	A	90	630	70	490	40 (50)	3.20 5.20 1.30 1.30
	B	180		150			
	C	120		90			
	C	120		90			
4 Semi-trailer 2 axles, 2 axles ↓↓↓↓↓	A	90	560	70	390	25 (15)	3.40 6.00 1.80
	B	190		140			
	B	140		90			
	B	140		90			
5 Trailer combination 2 axles, 3 axles ↓↓↓↓↓	A	70	590	70	450	10 (10)	4.80 3.60 4.40 1.30
	B	180		130			
	C	120		90			
	C	110		80			
	C	110		80			

Note: The values in brackets () are currently given in EN 1991-2.

Fatigue Load Model 3 (FLM3), i.e. a single vehicle with four axles, each 120 kN and Fatigue Load Model 5 (FLM5), based on recorded traffic, are not used in this study.

The load models used in this study ignore the modifications in the National Application Document. If the stress amplitudes caused by FLM2 are below the constant amplitude limit, the fatigue life is considered to be unlimited. However, if the stress amplitudes caused by FLM2 are above the constant amplitude limit, a damage calculation with FLM4 should be carried out.

Table 3.2 Axle types and wheel print configuration

Axle type	Nr. of wheels	Wheel centre distance (mm)	Wheel print b x l (-mm,mm)	Designation
A	2	2.000	220x320	Single
B	4	320/1.680/320	220x320	Dual
C	2	2.000	270x320	Super single

The axle types used, are shown in Table 3.2, which gives the axle and wheel print geometries as given in (ENV 1991-3 Table 4.8). The vehicle loads and the axle configurations comply with observed axle loads including dynamic effects from the pavement, vehicle suspension and wheel unroundness.

3.5 Function of the structural parts

In 1.3, the mechanical behaviour of the orthotropic decks was introduced. In the following paragraphs, the function of the structural parts for the load transfer is discussed.

3.5.1 The deck plate

The wheel loads are applied on the wearing course, which is supported by the deck plate. Thus, the deck plate supported by the stiffeners carries the wheel loads. Fig.3.7 shows the wheels of axle types A, B and C from Table 3.2, together with a cross section of the deck plate stiffened with trapezoidal stiffeners. The applied loading on the deck plate and the distribution of loads to the stiffeners is affected by the stiffness of the deck plate and the load spreading capability of the wearing course.

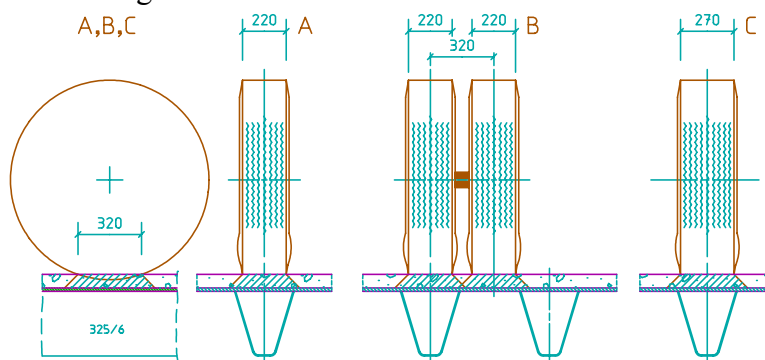


Fig. 3.7 Wheels on deck plate with trapezoidal stiffeners

The load spreading capability of the wearing course depends on its composition, thickness, loading period and the temperature. For example, a thick wearing course gives a larger dispersal than a thin one. The dispersal effect is addressed in ENV 1991-3, clause 4.3.6.

The composite action of the wearing course with the deck plate in combination with its dynamic modulus of elasticity was more extensively studied by Kolstein (1997) and De Jong (2007), but the composite action is not yet commonly used for fatigue assessment.

It is affected by the composition of the wearing course and its mechanical properties, which vary with the loading period and the temperature. In practice, this means that in some cases for modelling purposes, the stiffness of a fictitious thicker deck plate can be used.

These phenomena influence the deck plate and the deck plate to trough connection behaviour at locations D.1, D.2 and S.1, shown in Fig. 1.11. The wearing course effect is small as far as the crossbeam in-plane behaviour is concerned. However, the support rotation of the stiffeners and thus the crossbeam out-of-plane behaviour is directly affected by the distribution of the axle loads to the stiffeners. This means that the composite action between the wearing course and the deck plate and the dynamic modulus of elasticity of the wearing course should be taken into account.

3.5.2 Deck with stiffener assembly

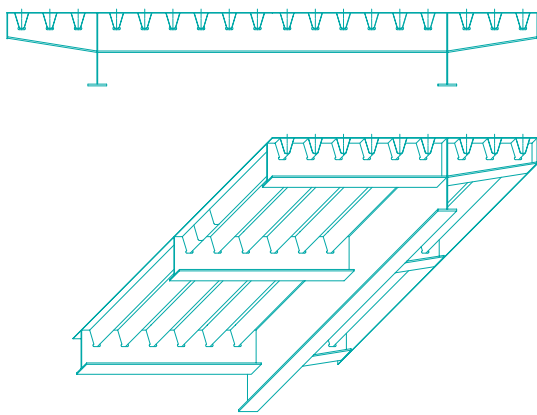


Fig. 3.8 Isometric view on an orthotropic steel deck

The traffic loads that are introduced through the deck plate are transferred by the stiffener / deck - plate assembly to the crossbeam. They cause bending and shear in the deck plate / stiffener assembly. In most cases, the stiffeners are positioned in the longitudinal direction of the bridge deck.

Fig. 3.8 (equal to Fig. 1.1) shows an isometric view of an orthotropic steel deck from underneath.

When the stiffeners with deck plate are considered as isolated beams, their top flange, being a part of the deck plate, may not be fully effective due to "shear lag", however in practice this is normally ignored.

The loads that do not act on the centre line of the stiffener cause a rotation of the stiffener / deck plate assembly about the longitudinal axis causing torsion and warping.

The geometry of the axles and wheels and the geometry and type of the wearing course affect the way in which loads are distributed over the stiffeners and will have to be assessed separately.

3.5.3 The crossbeam

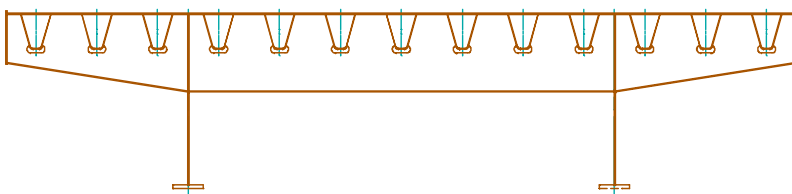


Fig. 3.9 Conventional crossbeam

The crossbeam receives the loads from the stiffeners and transfers these to the main girders or other elements that belong to the main load carrying system, such as the box girder or the hangers of a suspension bridge.

Sometimes, the crossbeams support the main girders and have to transfer these loads to the bearings situated under the crossbeams. These crossbeams are a part of the main load carrying system.

In The Netherlands two types of crossbeams can be identified: "conventional" crossbeams (see Fig. 3.9) and crossbeams in "Floating deck structures" (see Fig. 3.11). The "conventional" crossbeam consists of a bottom flange, a web plate and a part of the deck.

In the decks where the stiffeners are fitted between the crossbeams, the crossbeams act in-plane as asymmetric I-beams. The top flange is the part of the deck that is characterised by the effective width. When the stiffeners are not fitted between the crossbeams, they pass through cut-outs, often enlarged with cope holes.

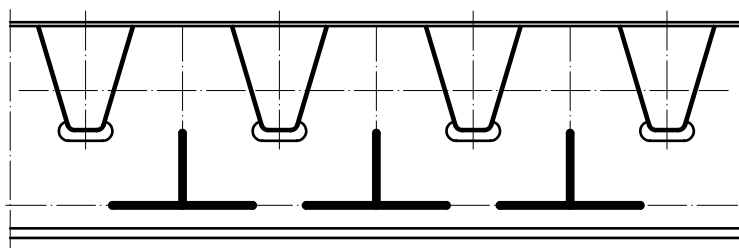


Fig. 3.10 Conventional crossbeam model (Vierendeel system)

Fig. 3.10 shows a conventional crossbeam with continuous stiffeners through cut-outs with cope holes in the crossbeam web. In this case, the crossbeam can be considered as an asymmetrical I-beam with

modified properties for bending and shear and with an upper flange represented by the effective width of the deck plate.

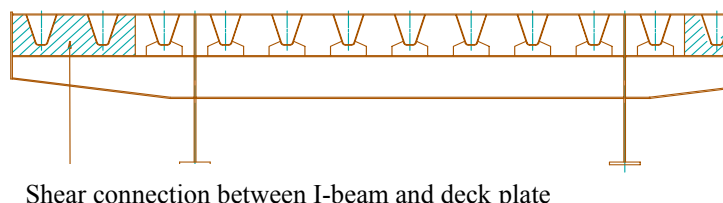
The shear force transfer takes place through a "Vierendeel" system, as shown in Figs. 3.10 and 3.12. It includes horizontal elements under the cut-outs and vertical elements between the cut-outs. Below the level of the cut-out and in longitudinal direction between the cut-outs, the parts of the Vierendeel system are considered rigid.

The shear force transfer causes local shear and local bending in the remaining part of the crossbeam web under the cut-out and in the T-shaped horizontal elements, and shear forces and bending moments in the part of the crossbeam web between the cut-outs, often called "tooth".

The deformations of these elements cause relative horizontal and vertical displacements in the trough to crossbeam connection.

The relative horizontal displacements depend on their position with respect to the neutral axis of a crossbeam with equivalent bending properties. When they are above the neutral axis, a decrease of the horizontal distance will occur under positive bending, when they are below, an increase will occur. Relative vertical displacements and rotations are caused by the local bending and shear deformations of the "Vierendeel" system elements due to the shear transfer in the crossbeam.

Considering the crossbeam "out-of-plane" behaviour, the rotation of the stiffeners causes bending of the crossbeam web plate and horizontal bending of the crossbeam bottom flange.



Shear connection between I-beam and deck plate

Fig. 3.11 Crossbeam in floating deck

In Fig. 3.11 the "Floating deck" structure is shown, where the crossbeam in-plane loads are transferred to the main girders by an I-beam. At the ends, the I-beam is connected to the deck plate with plates acting as shear connectors. This assembly generates a lever system comprising the deck and the I-beam, which acts as a

rotational spring for the I-beam and therefore reduces its midspan bending moment.

The in-plane bending of the stiffeners causes out-of-plane bending of the plate supports, horizontal bending of the top and probably the bottom flange of the I-beam and out-of-plane bending of the I-beam web.

3.5.4 Stiffener to crossbeam connection

The forces from the stiffeners are transmitted to the crossbeam. For connections of open and closed stiffeners to the crossbeam a large variety of details exist. (See Figs. 3.1 - 3.6.)

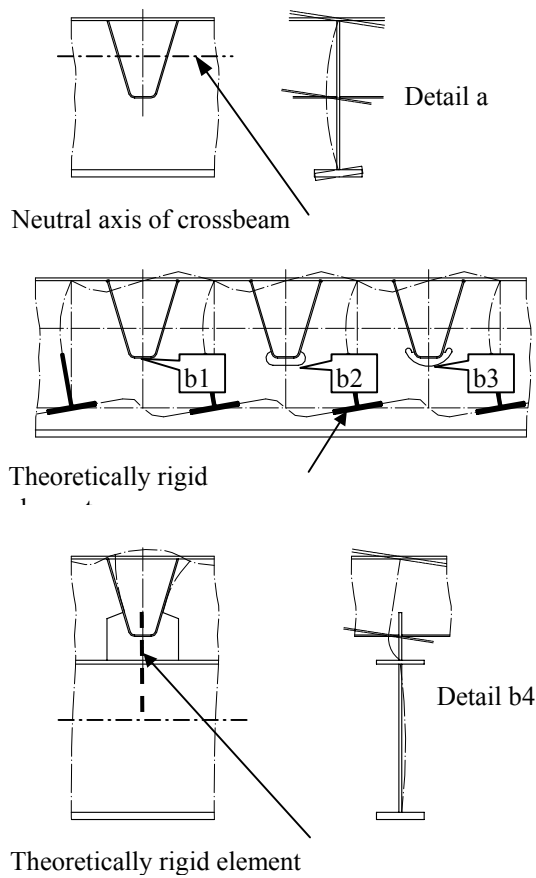
The connection of the open stiffener to the crossbeam shown in Fig.3.1 is made by vertical welds. Due to the cope hole in the crossbeam, the stresses generated by the crossbeam in-plane behaviour and the bending stresses caused by the crossbeam out-of-plane behaviour are enlarged by stress concentration factors. When the cut-outs are larger and the open stiffeners are only welded to one side of the cut-out, the crossbeam tends to act like a Vierendeel system similar to the connections of the continuous closed stiffeners.

Fig. 3.12 (which is identical to Fig. 1.10) shows again the closed stiffener to crossbeam connections and their behaviour. The trough stiffener to crossbeam connection consists of welds that transfer the loads from the stiffeners with deck plate into the crossbeams or transfer the section forces and bending moments from the stiffener through the crossbeam web to the adjacent stiffener.

In Fig. 3.12, the neutral axis of the crossbeam for the in-plane behaviour is indicated.

The rotation of the stiffener causes out-of-plane bending of the crossbeam web plate, which gives bending stress concentrations near the connection.

When a welded continuous trough to crossbeam connection with a close fit "Detail b1" (see Figs. 3.3 and 3.12) is used, the crossbeam in-plane shear behaviour causes stress concentrations in the crossbeam web plate especially near the bottom of the stiffener. The stiffener will further be deformed by imposed deformations from the crossbeam web.



In addition, the out-of-plane stiffener support rotation causes a comparable behaviour to that mentioned for "Detail a".

Where a cope hole is added, see "Detail b2" and "Detail b3" in Figs. 3.4, 3.5 and 3.12, the closed stiffener web is subjected to imposed deformations caused by the displacements at the lower part of the connection by the crossbeam in-plane shear behaviour. The crossbeam out-of-plane effects are of lesser importance compared to "Detail a" and "Detail b1" as the connection becomes more flexible.

The closed stiffener to crossbeam connection in the floating deck "Detail b4" (see Figs.3.6 and 3.12) is subjected to a vertical load introduction and to imposed deformations of the trough. At the critical locations in the trough to plate connection, a similar behaviour is observed as in the trough to crossbeam web connections "Detail b2" and "Detail b3".

The load transfer through the connections causes stresses in and near the welds, which are increased by geometrical stress concentration effects.

Fig. 3.12 In-plane and out-of-plane closed stiffener to crossbeam connection behaviour

3.6 Fatigue assessment procedure

A complete overview of the relationship of the models that can be used for the fatigue life assessment procedure and the aspects to be dealt with, are given in Table 3.3:

Table 3.3 Relationship between items in **steps 1-5** in a fatigue assessment procedure

Step nr.	Aspect	Method	Requirement
1. General	Fatigue life	(Not applicable)	<ul style="list-style-type: none"> • Standards • Contract
2. Loads	<ul style="list-style-type: none"> • Lorry loads • Axle loads • Wheel prints • Axle and wheel distances 	(Not applicable)	<ul style="list-style-type: none"> • Standards • Contract
3. Determination of stresses	<ul style="list-style-type: none"> • Crossbeam load transfer • Global and local behaviour • Nominal stresses • Geometrical stresses 	<ul style="list-style-type: none"> • Analytical method with geometrical stress concentration factors • Beam grid FE-model with geometrical stress concentration factors • FE shell element model • FE solid element model 	-
4. Fatigue damage assessment	<ul style="list-style-type: none"> • Transfer functions • Stress histories • Fatigue detail classes • Interaction effects for loads and mechanical behaviour • Damage assessment 	<ul style="list-style-type: none"> • Analytical model • Simulation 	<ul style="list-style-type: none"> • Standards • Contract
5. Inspection and repair	<ul style="list-style-type: none"> • Inspection • Repair 	<ul style="list-style-type: none"> • Non-destructive inspection method • Welding 	Contract

The requirements in **step 1** depend on the performance required from the structure and do not depend on the assessment approach. The required **design life** is given in contract specifications or standards e.g. EN 1991-1.

Step 2 items comprise the **loads** (Spectrum of vehicle loads, Axle spectrum, Wheel load and Wheel print configuration, Dynamic impact factors) obtained from standards e.g. ENV 1991-3 (1995) or from project specifications.

The loads are applied on the models of the structure. The way they are applied depends on the type of **modelling** selected in step 3.

Step 3 includes load dispersal, load introduction, load transfer, determination of the section forces, nominal stresses, Hot Spot stresses and combined stress effects.

If an analytical model is used, which includes the global crossbeam model, the loads are applied paying due attention to load dispersal, composite action of the wearing course and deck plate, the distribution of the loads over the stiffeners and the transfer functions.

The global crossbeam model section gives forces and section moments, which are used in the local crossbeam model and from which local section forces and moments and nominal stresses can be calculated.

In a beam grid model, the loads are applied with due attention to the wearing course effects and the distribution effect over the stiffeners. The result will be nominal section forces and bending moments from which nominal stresses can be calculated.

The loads for the shell element model can be applied directly on the modelled deck plate with due attention to the wearing course effects, or on a modelled wearing course, which may consist of shell elements of a fictitious thickness. The result is a stress distribution.

Depending on the model used, the stresses may have to be increased using stress concentration factors.

In **step 4**, the **fatigue damage assessment calculation** combines the derived stress with the load variation effect in time, which results in stress histories. From the histories stress spectra are derived, e.g. with a "Rainflow" counting method. The stress spectra and the fatigue classes of the details are used in a "Palmgren-Miner" damage calculation, which results in an expected fatigue life. Alternatively, fracture mechanics methods may give the expected crack dimensions and the crack growth.

In **step 5**, the damage can be related to the **design life** and the **inspection intervals** and the need for **repair** can be estimated.

3.7 Concluding remarks

This chapter shows that fatigue cracks may not always directly endanger the resistance of the structure. The origin of the cracks for the relevant locations is explained together with the function of the structural parts of the deck in the load transfer. Several procedures for the fatigue assessment of the closed stiffener to crossbeam connections are shown.

4 CONVENTIONAL CROSSBEAMS

4.1 General

4.1.1 Introduction to the conventional crossbeam

A "conventional" crossbeam in orthotropic steel bridge decks comprises a web plate, a bottom flange and an effective part of the deck plate acting as the upper flange. When closed stiffeners are used, they can be fitted between the crossbeams or they can be continuous, passing through cut-outs in the crossbeams. Often the cut-outs are enlarged with cope holes.

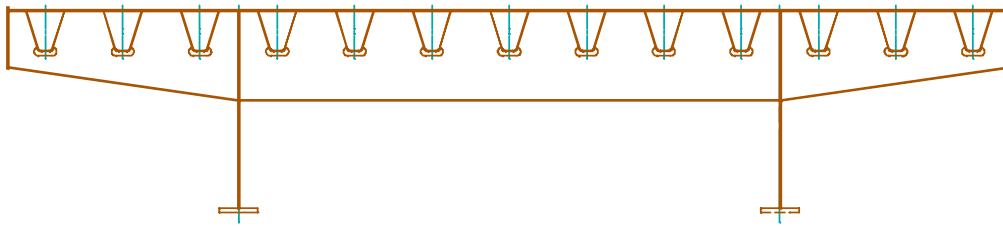


Fig. 4.1 Conventional crossbeam

This chapter deals with the behaviour of conventional crossbeams with continuous closed stiffeners passing through cut-outs with cope holes as shown in Fig. 4.1. and crossbeams where stiffeners are passing through a close fit.

Some of the models that are derived for the structural behaviour of these crossbeams, are applicable to decks with continuous open stiffeners and to those with closed stiffeners fitted between the crossbeams.

In this chapter, common crossbeam dimensions are initially chosen and the in-plane load capacity for bending of a reference beam is derived. The influence of the web depth and the cut-out is analysed with respect to the load transfer and stresses in the stiffener and crossbeam web and equivalent crossbeam properties are determined. The same effective width of the upper flange has been chosen for all the crossbeams analysed. For the same range of crossbeam dimensions, the out-of-plane behaviour is analysed for a unit rotation.

4.1.2 Analysed dimensions and parameters

The analysed crossbeams are assumed to be part of a plate girder bridge with crossbeams at centre-to-centre distances of 3.5 - 4.5 m.

For a range of crossbeam depths and cope hole widths, the influence of the depth of the crossbeam and the width of the cope hole is analysed. The calculation results are shown for in-plane loading and applied deformations. Fig. 4.2 shows two typical cross-sections of the analysed crossbeams. Section A is on the longitudinal centre line of the closed stiffener where it passes through the crossbeam, section C is away from the stiffener through the full crossbeam web (see also Fig. 4.3). The crossbeam is assumed to consist of a top flange 1400 x 12 mm, with a bottom flange 200 x 16 mm and a web with a thickness of 10 mm. The web depth is varied from 600 – 2200 mm.

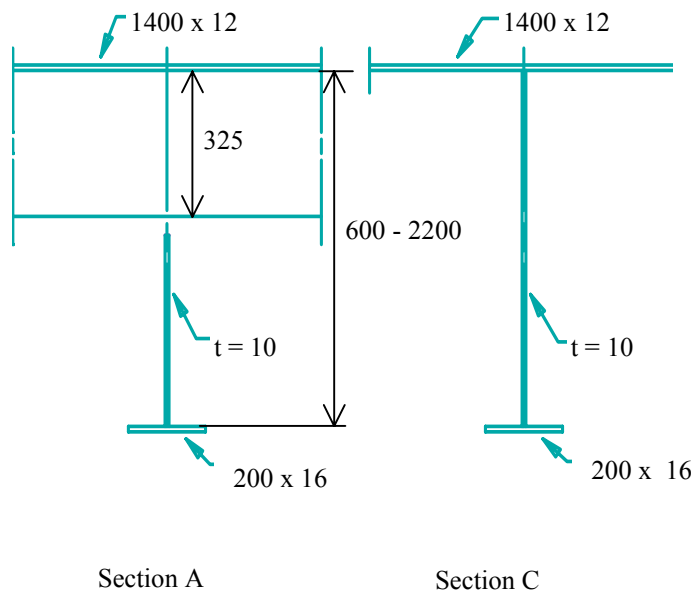


Fig. 4.2 Cross sections of investigated crossbeams (Dimensions in mm)

The assumed top flange is a part of the deck plate for which the effective width due to shear lag depends on the crossbeam centre to centre distances and the crossbeam span length. In addition, it is influenced by the support conditions (simply supported, continuous or “built in”) and the type of loading, (uniformly distributed or concentrated).

When the crossbeam is considered to be a simply supported span, loaded with a uniformly distributed load, the effective width $b_{\text{eff}} = 2400$ mm in accordance with the former DIN 1073 and with EN 1993-1-5 (1997) $b_{\text{eff}} = 2600$ mm.

When the crossbeam is considered to be an interior span of a continuous beam, loaded by a uniformly distributed load, the effective width $b_{\text{eff}} = 1450$ mm in accordance with the former DIN 1073 and 1600 – 1950 mm in accordance with EN 1993-1-5 (1997).

NEN 6788 (1996) gives an effective width $b_{\text{eff}} = 2400$ mm for simply supported spans and 1500 - 1650 mm for interior parts of continuous beams.

The analyses in this study were carried out for simple span crossbeams, although the selected effective width b_{eff} corresponds to the value for interior parts of continuous beams according to the former DIN 1073. The influence of other effective widths on the results of the analysis is discussed in 4.2.3.3.

The former FKH (Friedrich Krupp Hüttenwerke) profile 2/325/6, which is often used in practice with an oval cope hole 175 mm wide, is also used in the analysis. The depth of the trough is 325 mm and the thickness is 6 mm. The troughs to deck plate connections are 300 mm apart, the bottom width is 105 mm and the centre-to-centre distance of the stiffeners is 600 mm.

For the parameter studies the width of the cope hole is considered to vary between 75 and 275 mm and the trough stiffener bottom width is considered to vary as a function of the cope hole width. The depth of the cut-out with the cope hole is 350 mm, see Fig. 4.3.

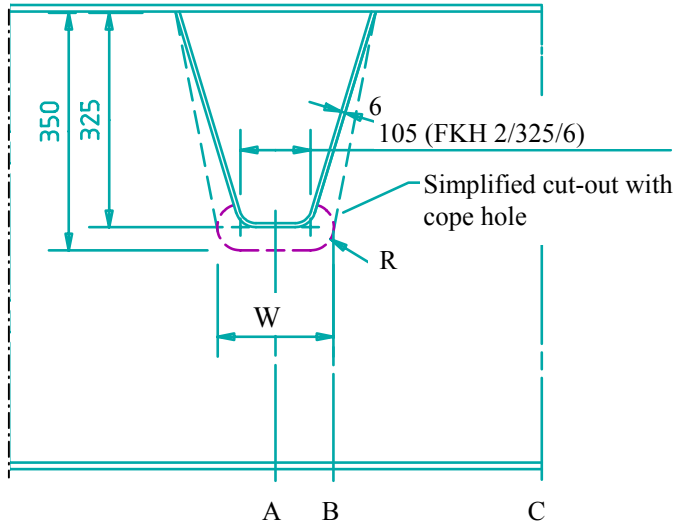


Fig. 4.3 Simplified cut-out with cope hole (Dimensions in mm)

The position of the crossbeam cross section A shown in Fig. 4.2, is also indicated in Fig. 4.3, together with the position of a transition cross section B, which is considered to be identical to cross section, C shown in Fig. 4.2.

In addition, Fig. 4.3 shows the geometrical simplification used for the modelling of the cut-outs with cope holes (dashed lines). The width of the cope hole (W) is variable. For the analytical model, straight edges are assumed, using the outer boundaries of the cope hole width (W) as a reference.

Most beams are analysed for a reference span length l_1 of 7200 mm. In addition, four deeper crossbeams are analysed, based on the maximum bending stresses. For these deeper crossbeams the spans l_n are analysed, based on the following procedure:

Equation [4.1] gives the bending moment for a simply supported beam with a span length l_n with a uniformly distributed load:

$$M = \frac{1}{8} q l_n^2 \quad [4.1]$$

With eq. [4.2] the bending stress in the bottom flange is calculated for beam "n".

$$\sigma_b = \frac{q \cdot l_n^2}{8 \cdot W_n} \quad [4.2]$$

Using the crossbeam ($n = 1$) as a reference with a span of $l_1 = 7200$ mm and a web depth $h_1 = 600$ mm with an elastic section modulus W_1 and a fixed bending stress σ_b , the span length l_n for a crossbeam type "n", with web depth h_n and an elastic section modulus of W_n can be found with eq. [4.3].

$$l_n = l_1 \sqrt{\frac{W_n}{W_1}} \quad [4.3]$$

For crossbeam type "n" the bending moment M_n can be calculated with eq. [4.4].

$$M_n = M_1 \cdot \frac{W_n}{W_1} \quad [4.4]$$

The associated shear force S_{vn} for a beam with M_n is given by eq. [4.5]:

$$S_{vn} = S_{v1} \cdot \sqrt{\frac{W_n}{W_1}} \quad [4.5]$$

Table 4.1 gives an overview of the dimensions that are varied in the analyses.

Table 4.1 Analysed crossbeam dimensions

Beam type NR.	Web depth H (mm)	Cope hole width W (mm)	Span l_1 (mm)	Span l_n (mm)
1	600	75, 125, 175, 225, 275	7200	7200
2	800	75, 125, 175, 225, 275	7200	8750
3	1000	75, 125, 175, 225, 275	7200	10225
4	1200	75, 125, 175, 225, 275	7200	11635
5	1400	75, 125, 175, 225, 275	7200	13030
7	1800	175	7200	-
9	2200	175	7200	-

The dimensions of the crossbeams are realistic for plate girder twin bridges with a two lane carriageway and an emergency lane, requiring a total distance between the safety barriers of approximately 12 m. Beams with $H = 600$ mm are considered to be shallow beams, beams with $H = 1000 - 1400$ mm are more practical.

4.1.3 In-plane loads and out-of-plane rotations

4.1.3.1 In-plane

The uniformly distributed load q is calculated with the elastic section modulus W_1 , based on a working bending stress of 240 N/mm^2 at midspan in the bottom flange of the crossbeam with a web depth $H = 600$ mm.

The calculated uniformly distributed load q is 108 kN/m^1 , which is henceforth used in the analyses as a fixed reference load. It corresponds to a total load on the crossbeam of 780 kN , a shear force of 390 kN at the end supports and a midspan bending moment of 700 kNm .

Determination of the crossbeam loads in accordance with ENV 1991-3, without load factors and with a simple procedure, for the Tandem System (TS1) given in clause 4.3.2 using $\alpha_{Q1} = 1.0$, would result in 150 kN/m^1 for the Static Load Model 1.

Using the tridem system of the semi-trailer of the Fatigue Load Model 2 (FLM2), clause 4.6.3, Table 4.6, the result would be: 100 kN/m^1 .

The Dutch code NEN 6788 class 60 (60 tons design lorry) gives 133 kN/m^1 , without dynamic amplification factor.

Therefore, it may be concluded that the reference load used for the analysis can be considered as a realistic working load.

4.1.3.2 Out-of-plane

For the out-of-plane loading, a unit rotation of the closed stiffener connections of 0.01 rad is used.

The effects for the realistic traffic loads can be obtained by extrapolating the results obtained in the analysis with the unit rotations. The values resulting from a simple analysis with the load models mentioned for the in-plane loads give rotations of 0.005 - 0.018 rad.

4.1.4 Introduction to the crossbeam in-plane behaviour

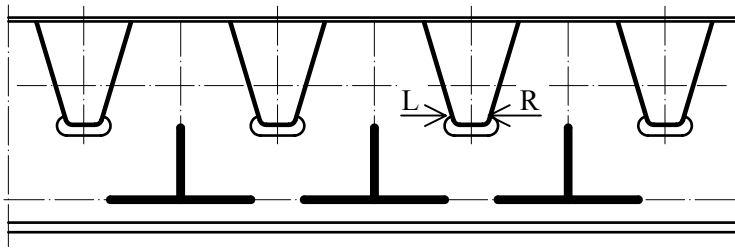


Fig. 4.4 Vierendeel system

In crossbeams with connections "b1", "b2" and "b3", shown in Fig. 3.12, where the stiffeners pass through the crossbeam, a significant part of the crossbeam web is removed. As discussed in 1.3.1, 1.3.2, and 3.5.3, the applied loads are transferred to the main girders by an in-plane Vierendeel system, shown in Fig. 4.4. The parts of the Vierendeel system below the column (tooth) and between the cut-outs, shown in bold, are considered to have infinite bending and shear stiffness.

Depending on the position of the neutral axis of the system, deflection of the crossbeam causes an increase or a decrease in the distance between "L" and "R" and relative rotations are generated at "L" and "R". The shear forces cause secondary bending and shear in the remaining vertical (tooth) and horizontal (inverted T-beam) parts of the crossbeam web which result in relative vertical displacements and rotations at "L" and "R".

These relative displacements and rotations cause a local deformation at the bottom of the trough. The nominal stresses arising from this deformation can be calculated with a local frame analysis of the lower part of the closed stiffener cross section.

With geometrical stress concentration factors (SCF), the geometrical "Hot Spot Stresses" can be obtained. For other locations around the cut-out, with and without a cope hole, the stresses can be calculated from the section forces and moments in the Vierendeel system and appropriate stress concentration factors.

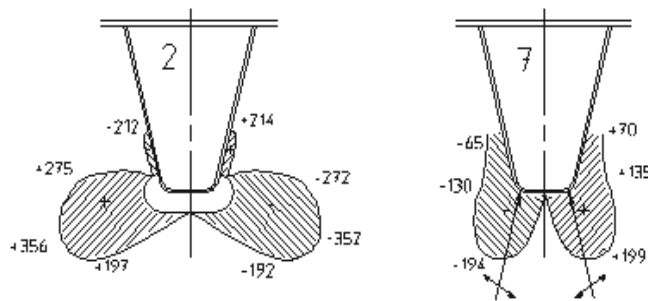


Fig. 4.5 Typical principal stress distributions around cope hole "b2" and continuous weld "b1" due to in-plane load

Fig.4.5 shows an example of the principal stresses obtained from the FE-analyses for the ECSC 4th Phase test specimens with closed stiffeners (discussed in detail in chapter 7).

The magnitude of the stresses is indicated as a graph, perpendicular to the cope hole edge (2) or the weld toe (7). In the figure on the left (2), the locations of the principal stresses are situated along the cope hole and the direction of the stresses is parallel to the edge of the cope hole.

In the figure, on the right (7) the principal stresses with the highest values are approximately in the direction of the double arrows.

Several authors have described this model. Falke (1983) describes the Vierendeel phenomenon extensively in his thesis. In the discussion of the analyses, the consequences of this behaviour are not only explained for the local behaviour of the crossbeam web, but also for the global behaviour of the crossbeam.

The effects of the relative displacements and rotations in the closed stiffener to crossbeam connections (locations "L" and "R" in Fig.4.4) on the closed stiffeners are not presented in any literature.

In this study, these relative displacements and rotations are determined in order to obtain the imposed deformations and the resulting stresses in the crossbeam web and the closed stiffener, because they are also relevant for fatigue.

4.1.5 Introduction to the crossbeam out-of-plane behaviour

Moving vehicles generate bending and shear in the stiffeners, which cause deflections and rotations of the stiffener to crossbeam connections (see also Figs. 1.9 and 1.10). The rotation of this connection causes out-of-plane displacements and bending in parts of the crossbeam web.

This phenomenon affects crossbeams with all types of stiffeners. The connections "b1", "b2" and "b3" as discussed in 3.3.1 and shown in Fig. 1.10 were tested in the ECSC research programme Phases 3 and 4, described by Kolstein et al. (1989) and Bruls et al. (1997). In this research, the fatigue strength of the details was investigated under vertical loads with simultaneous out-of-plane bending in the crossbeam web.

Fig. 4.6 shows, for the details "b1", "b2" and "b3", the stresses along the edge of the cut-out and the weld toe obtained from the FE analyses for the three test specimens of the ECSC Phase 3 programme under the same vertical loads and out-of-plane rotations. The figure shows that for this loading case, the detail "b1" has the highest and the detail "b3" has the lowest bending stresses.

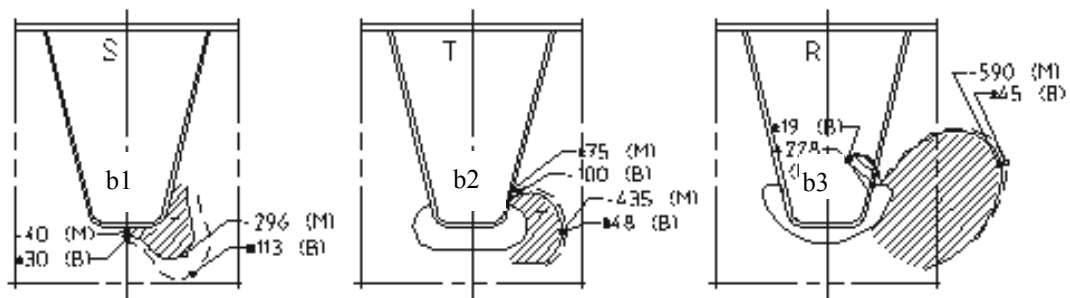


Fig. 4.6 Stress distributions parallel to weld toe and cope hole edge under vertical load in combination with out-of-plane bending

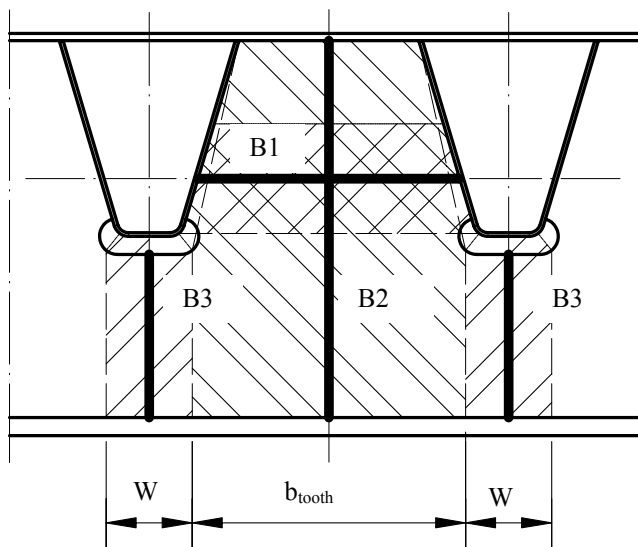


Fig. 4.7 Out-of-plane model

In the analyses in this study, the crossbeam out-of-plane behaviour is modelled with beams as shown in Fig. 4.7. Beam system B1B2 simulates the remaining full-depth crossbeam web and the “tooth” with B1 representing the web between the troughs and B2 the connection of the deck plate to the bottom flange, which is also connected to B1. Beam B3 represents the crossbeam web below the closed stiffener, in order to make the model suitable for connections with and without cope holes.

From the deformations under unit loads and unit displacements, the section forces and nominal stresses in the relevant locations are calculated.

The nominal stresses obtained from these unit loads and rotations can be scaled to the actual loads and rotation levels. The geometrical Hot Spot stresses, required for fatigue analysis, can be calculated by applying geometrical stress concentration factors.

The nominal stresses obtained from

4.2 Crossbeam in-plane analyses

The "global" behaviour of the crossbeam describes its behaviour as a beam in its environment, i.e. stiffened deck and main girders.

The "local" behaviour is analysed considering bending and shear in the crossbeam parts and the effect of the introduction of external loads into the stiffener to crossbeam connection. The results of the analyses presented here show nominal stresses, except for some locations, where the hot spot stresses are calculated considering the associated stress concentration factors.

4.2.1 Models

The calculations are carried out with analytical models and the results are verified with 2-D FE models.

4.2.1.1 Analytical model for bending in-plane

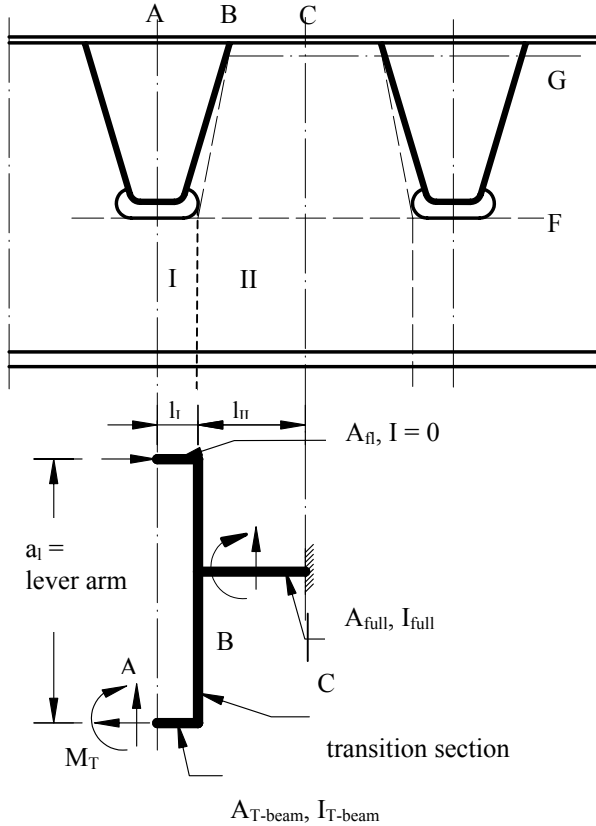


Fig.4.8 Analytical model in-plane bending

Fig.4.8 shows a relevant part of the crossbeam. Due to the absence of web material at the cut-outs (with cope holes), the crossbeam consists of sections with a top flange and a T-beam, but without a direct connection (Part I, between sections A and B). The crossbeam consists of sections where an upper flange, a web and a bottom flange are present, which act like a complete I-beam (Part II, between sections B and C).

In Part I the bending moment is taken by a lever system, with a lever arm a_1 and secondary bending in the T-beam, as the bending stiffness of the deck plate is generally negligible.

In Part II the beam acts as a full I-beam. In the model a transition section B is assumed, connecting Part I and Part II.

When a Moment M_1 is applied on the lever system of cross section A, the rotation angle (ϕ_1) with respect to cross section B can be computed from the compression of the flange and the elongation of the T-beam.

The T-beam is forced to have the same rotation angle. This causes an additional bending moment M_T in the T-beam, the secondary bending moment. The Moment M_1 with the added secondary bending moment M_T can be applied on Part II, causing a rotation (ϕ_2) of cross section B with respect to cross section C and causing an additional rotation in cross section A. The sum of M_1 and M_T is defined as the unity moment M_{unity} .

The rotation of cross section A (ϕ_A) can also be computed for the case that both Part I and Part II have the full I-section. Based on the comparison of these results for Section A, the effect of the cut-out with cope hole can be computed.

The stiffness ratio c_b between a crossbeam with cut-outs and a crossbeam without cut-outs is called: "Equivalent bending stiffness ratio".

The following procedure can be used to find the bending moment contributions from each section of the crossbeam:

The rotation ϕ_1 due to the unity moment is found by considering the deformations of the flange and the T-beam and the lever arm a_1 .

$$\phi_1 = \left(\frac{1}{a_1}\right) \cdot \left(\frac{M_1 \cdot l_I}{a_1 \cdot E}\right) \cdot \left(\frac{1}{A_{fl}} + \frac{1}{A_{T-beam}}\right) \quad [4.6]$$

Applying the rotation from eq. [4.6], the secondary bending moment in the T-beam can be determined with eq. [4.7].

$$M_T = \frac{E \cdot I_{T-beam} \cdot \phi_1}{l_I} \quad [4.7]$$

The rotation over Part II with length l_{II} can be determined with eq. [4.8].

$$\phi_2 = \frac{(M_I + M_T) \cdot l_{II}}{E \cdot I_{full}} \quad [4.8]$$

This means that the rotation in cross section A with respect to cross-section C can be found with eq. [4.9].

$$\phi_{A-cutout} = \phi_1 + \phi_2 \quad [4.9]$$

Where a full web is present over Part I and Part II, the rotation in Section A can be determined with equation [4.10].

$$\phi_{A-full} = \frac{(M_I + M_T) \cdot (l_I + l_{II})}{E \cdot I_{full}} \quad [4.10]$$

with: $M_{unity} = M_I + M_T$.

The rotations in cross section A for a crossbeam with a full web and a crossbeam with cut-outs can be related to each other by the "Equivalent bending stiffness ratio" c_b in equation [4.11]. The result shows the effect of the cut-outs on the general bending stiffness of the crossbeam.

$$c_b = \frac{\phi_{A-full}}{\phi_{A-cutout}} \quad [4.11]$$

The contribution of the lever system in the total bending moment in the crossbeam is given by the "Lever system ratio" R_l in eq. [4.12].

$$R_l = \frac{M_I}{M_{unity}} \quad [4.12]$$

The contribution from the T-beam in the total bending moment is given by equation [4.13].

$$R_T = \frac{M_T}{M_{unity}} \quad [4.13]$$

Fig. 4.9 shows the T-beam ratio R_T calculated with the analytical procedure (dotted line) and with a 2-D FE model with line elements for the top and bottom flange and shell elements for the crossbeam web (continuous lines).

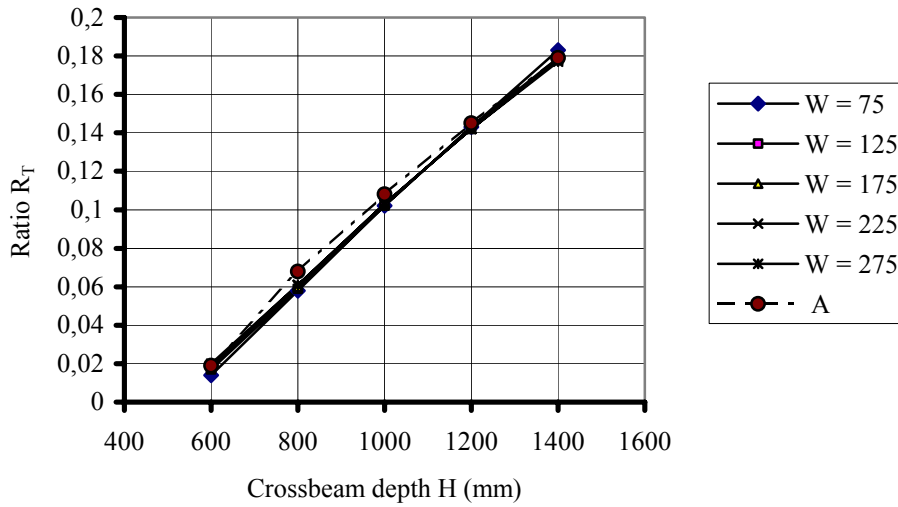


Fig.4.9 T-beam ratio R_T

Based on equation [4.13], the analytical model shows values for the contribution of the T-beam R_T varying from 0.019 for $H = 600$ mm to 0.179 for $H = 1400$ mm. The width of the cut-out does not play a role. In the FE analyses the effect of the cut-out is found to be 0.014 for $H = 600$ mm and $W = 75$ mm and 0.020 for $W = 275$ mm. For $H = 1400$ mm the ratio for $W = 75$ mm is 0.180 and for $W = 275$ mm the ratio is 0.177. Thus, a good agreement exists between the analytical results and those from FE analyses.

The method with eqs [4.6] – [4.10] gives a good insight into the distribution of the crossbeam bending moment over the lever system and the T-beam. However, this is not needed for the determination of the equivalent bending stiffness. Here, the following alternative method for the determination of c_b can be used.

Over Part I, the $I_{cut-out}$ can be calculated assuming the assembly of top flange and T-beam acting together in a beam, where the cross section remains straight.

Then, the calculation procedure for c_b is as follows:

The rotation over the length $l_I + l_{II}$ caused by M_{unity} for the beam with a cut-out is calculated with equation [4.14].

$$\phi_{A-cutout} = \frac{M_{unity}}{E} \cdot \left(\frac{l_I}{I_{cutout}} + \frac{l_{II}}{I_{full}} \right) \quad [4.14]$$

For a beam without cut-outs loaded by M_{unity} the rotation is found with equation [4.15].

$$\phi_{A-full} = \frac{M_{unity}}{E} \cdot \frac{l_I + l_{II}}{I_{full}} \quad [4.15]$$

As before, c_b is calculated with equation [4.11]. The rotations obtained are, compared to the results of eqs. [4.9] and [4.10] somewhat smaller than before, because here only the M_{unity} is used in the crossbeam section.

4.2.1.2 Numerical model for bending

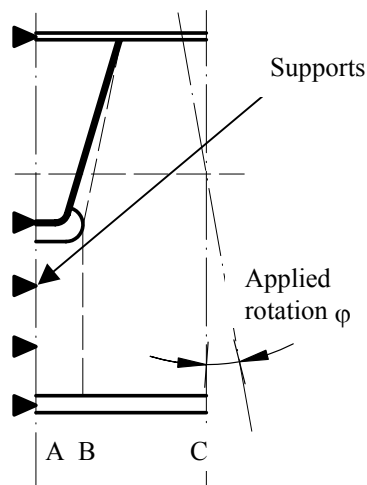


Fig. 4.10 Numerical model in-plane bending

Fig. 4.10 shows the numerical bending verification model, mentioned in 4.2.1.1.

The deck plate and the bottom flange are modelled with line elements. The crossbeam web is modelled with shell elements. In one version, the full web is present and in another version, a cut-out and a cope hole are included.

The mid-section of the trough (cross section A) is clamped and the centre line of the tooth (cross section C) is subjected to a unit rotation. The reactions in cross section A can be related to the rotation of cross section C. The results can be compared to the results obtained from the analytical model, as shown in Fig. 4.9.

This model is only used for the verification of the equivalent bending stiffness.

4.2.1.3 Analytical model for in-plane shear (“Vierendeel” system)

The cut-outs with cope holes in the crossbeams may have substantial dimensions compared to the remaining parts of the web plate between the cut-outs; the teeth, and below the cut-outs; the T-beams. The absence of material affects the shear force transfer in the crossbeam considerably.

The effect of the cut-outs on the shear transfer was investigated by Falke (1983), using a Vierendeel model as a basis. In the Vierendeel model, the shear forces in the beam cause local shear and bending in the remaining vertical and horizontal structural elements.

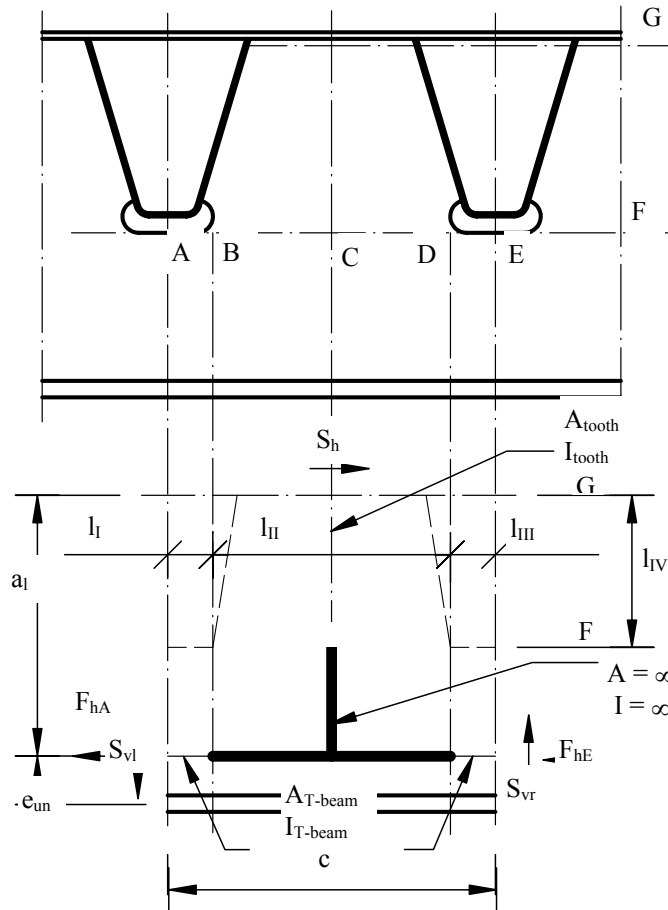
Fig. 4.11 shows a part of the crossbeam with two-cut-outs including cope holes and the line element model used for the analyses in this study. It consists of a horizontal rigid part between the cross sections B and D, and a vertical rigid part below the horizontal cross section F. These parts are assumed to remain undeformed. The remaining parts are assumed to deform under bending and shear. Between the cross sections A and B the cross section is a T-beam, upside down, with a length l_I . The same applies between the cross sections D and E with the length l_{III} . Between the horizontal cross sections F and G the tooth can be considered as a column with a length l_{IV} .

For a connection with continuous trough stiffeners in a cut-out with a close fit (detail "b1"), the effective width b_{eff} of the trough web can be considered to act as a flange for the tooth.

At the location of the corner of the trough bottom, the effective width for the flange of the tooth can be calculated with equation [4.16], see Roark and Young (1986).

$$b_{eff} = 1.56 \cdot \sqrt{r \cdot t} \quad [4.16]$$

For a trough bottom radius $r = 28$ mm and a trough thickness $t = 6$ mm, the effective width $b_{\text{eff}} = 20$ mm. The effect of this small flange on the tooth stiffness is not substantial. In cases where a cope hole is used (detail "b2" or detail "b3"), there is no "flange" at the base of the tooth, the location with the highest bending moment.



The behaviour of the line element model, shown in Fig. 4.11, which looks like an inverted T-shaped frame, is as follows:

The vertical shear forces caused by the self-weight of the structure and the traffic loads are introduced by the adjacent systems as S_{vl} and S_{vr} . If the tooth does not introduce an additional vertical load, they have an opposite sign of the same magnitude. The vertical shear forces generate a moment, which is stabilised by S_h and the forces F_{hA} and F_{hE} .

The horizontal bending stresses at the edge of the cut-out, are caused by S_{vl} and S_{vr} . At the edge of the cut-out they interact with the vertical bending stresses caused by S_h . The two perpendicular stress effects have the same sign, but a different magnitude. These perpendicular stresses cause a certain "locked in" effect resulting in a behaviour like a rigid body for the parts of the bottom chord between the cross sections B and D. The same is assumed for the tooth below the horizontal cross section F.

Fig. 4.11 Analytical model in-plane shear

Fig. 4.12 shows the line model with its deformations. The centres of the cut-outs with cope holes are at a distance "c" and the distance from the neutral axis of the T-beam under the cut-outs with cope holes to the centre of the top flange is a_l .

The shear forces S_{vl} and S_{vr} cause the shear and bending deformations of the T-beam δ_{vl} and δ_{vr} .

The shear force S_h causes a shear and bending deformation of the tooth δ_h . The effect of δ_h can be transferred (by rotating) into additional vertical deformations $0.5\delta_{v-add}$ at both sides of the system.

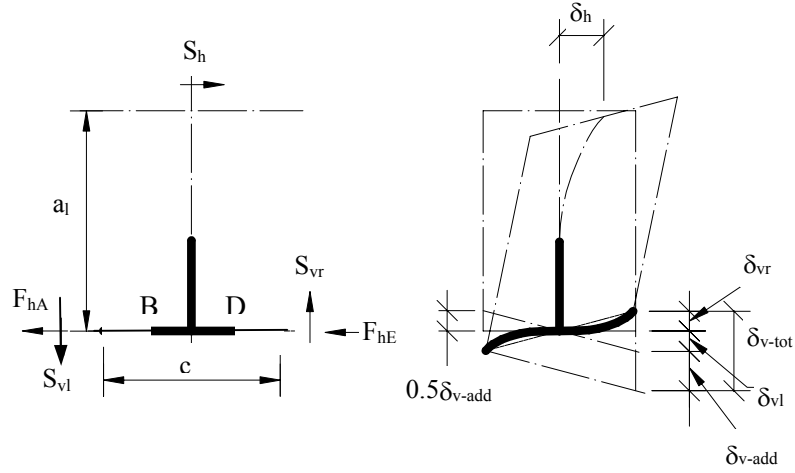


Fig. 4.12 Forces, deformations and displacements due to shear

The Vierendeel system is now analysed as follows:

S_h is calculated from the equilibrium of moments of the vertical shear forces S_{vl} and S_{vr} . with equation [4.17].

$$S_h = \frac{S_{vl} \cdot 0.5c + S_{vr} \cdot 0.5c}{a_l} \quad [4.17]$$

The deformations of the tooth due to shear and bending are calculated with equation [4.18], in which:

$$I_{tooth} = I_{webplate} \text{ and } A_{tooth} = A_{webplate} \text{ (over cross section F of Fig. 4.11),}$$

The correction factor c_c is determined in conjunction with the FE analyses.

$$\delta_h = \frac{S_h \cdot c_c \cdot l_{IV}^3}{3 \cdot E \cdot I_{tooth}} + \frac{S_h \cdot C_c \cdot l_{IV}}{G \cdot A_{tooth}} \quad [4.18]$$

The vertical displacement due to bending and shear at the left hand side of the T-beam is calculated with equation [4.19], in which:

$$I_T = \text{moment of inertia of the full T-section}$$

$$A_T = \text{cross sectional area of the web of the T-beam}$$

$$\delta_{vl} = \frac{S_{vl} \cdot l_I^3}{3 \cdot E \cdot I_{T-beam}} + \frac{S_{vl} \cdot l_I}{G \cdot A_{T-beam}} \quad [4.19]$$

The vertical displacement due to bending and shear at the right hand side of the T-beam is calculated with equation [4.20].

$$\delta_{vr} = \frac{S_{vr} \cdot l_{III}^3}{3 \cdot E \cdot I_{T-beam}} + \frac{S_{vr} \cdot l_{III}}{G \cdot A_{T-beam}} \quad [4.20]$$

Fig 4.13 shows the relative deformation contributions due to bending in the tooth in relation to total deformation, calculated with equation [4.18].

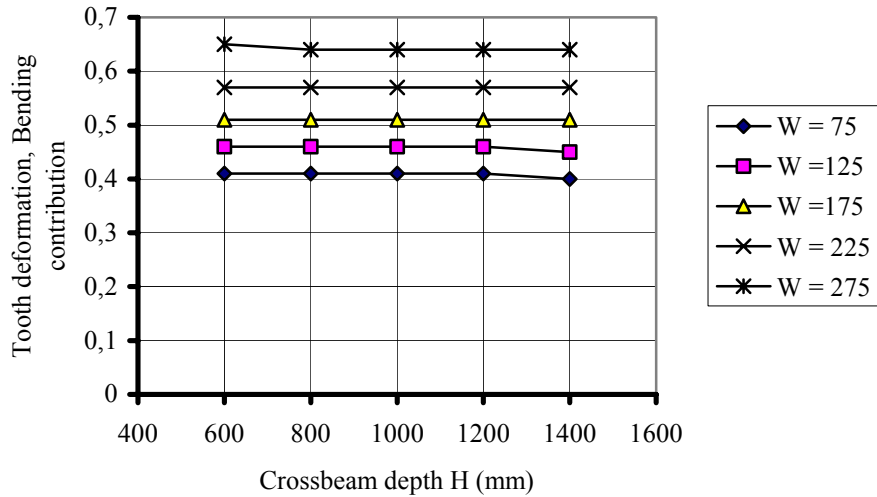


Fig.4.13 Relative deformation contributions due to bending in the tooth

For bending (B) the deformation contributions vary from 0.41 (W = 75 B) to 0.64 (W = 275 B), thus for shear (S) they vary from 0.59 (W = 75 S) to 0.36 (W = 275 S).

The same analyses are carried out for the T-beams with eqs. [4.19] and [4.20] and are shown in Fig. 4.14.

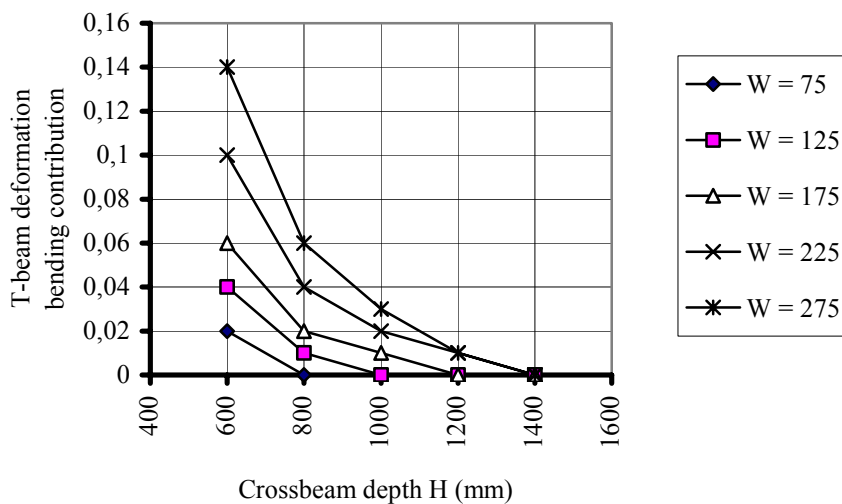


Fig.4.14 Relative Deformation contributions due to bending in the T-beam

The relative deformation contributions due to the bending moment transfer vary from 0.14 to zero and thus the contributions due to shear vary from 0.86 to 1.00. The highest contribution due to bending is found in the crossbeams with the widest cut-outs.

In most of the investigated crossbeams, the shear deformation is the most important contribution.

In order to obtain equivalent beam properties the tooth deformations have to be transformed into additional vertical deformations of the "T" frame model (shown in Fig. 4.11) between cross sections A and E.

$$0.5\delta_{v-add} = \frac{\delta_h}{a_l} \cdot 0.5c \quad [4.21]$$

The horizontal deformation of the tooth results in a vertical displacement $0.5\delta_{v-add}$ at both sides of a T frame model: Thus, the displacement between the cross sections A and E in Fig. 4.11 due to the tooth deformations is equal to δ_{v-add} .

The total vertical deformation over the length "c" is calculated with equation [4.22]. This is a summation of the vertical deformations of the T-beams and the transferred horizontal deformation of the tooth.

$$\delta_{v-total} = \delta_{vl} + \delta_{vr} + \delta_{v-add} \quad [4.22]$$

Fig. 4.15 shows the contributions to the total vertical deformation ($\delta_{v-add}/\delta_{v-total}$) between cross sections A and E from the horizontal tooth deformations (H).

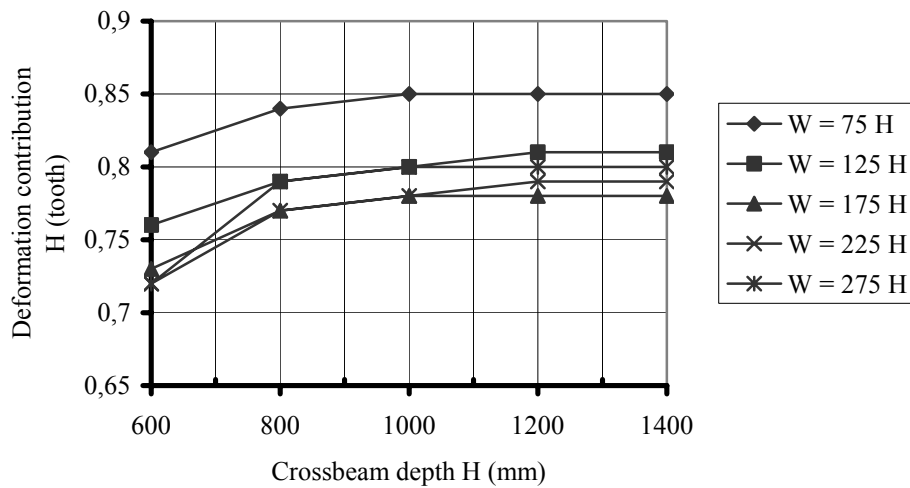


Fig.4.15 Contributions from tooth deformation H

The contribution from the tooth (H) to the total vertical deformation $\delta_{v-total}$ varies from 0.85 to 0.72, which means that the contribution from the T-beams below the cut-out (V) to the total vertical deformation $\delta_{v-total}$ varies from 0.15 to 0.28.

The above-mentioned contributions (H) show some sensitivity to the width of the cut-out and the crossbeam web depth has a small influence.

In all cases, the horizontal deflection of the tooth gives the largest contribution to the deformation $\delta_{v-total}$.

As shown in Fig. 4.13, both contributions from bending and shear are relevant for δ_h of the tooth. Further, Fig. 4.14 shows that the bending deformations play a minor role for the T-beam.

Based on Figs. 4.14 and 4.15 it can be concluded that the bending contribution of the T-beam in relation to the total deformation of the T-frame model between cross sections A and E is less than 4% for wider cope holes. For the more practical narrower cope holes, the effect is approximately 2%, which can be ignored.

The equivalent shear stiffness ratio (c_s) modifies the crossbeam web plate thickness for the effect of the cut-outs with cope holes for calculation purposes. It can be derived by using the vertical deformation between the sections A and E of the T frame model, as the deformation of a beam with a full web with equivalent properties.

The factor c_s is determined as follows:

Where: $S_v = S_{vI} = -S_{vE}$, the vertical displacement between Section A and E for a beam with a web without cut-outs is calculated with equation [4.23].

$$\delta_{v-full} = \frac{S_v \cdot c}{G \cdot A_{web}} \quad [4.23]$$

The Equivalent Shear Stiffness Ratio (c_s) can be found with equation [4.24].

$$c_s = \frac{\delta_{v-full}}{\delta_{v-total}} \quad [4.24]$$

4.2.1.4 Numerical model for shear

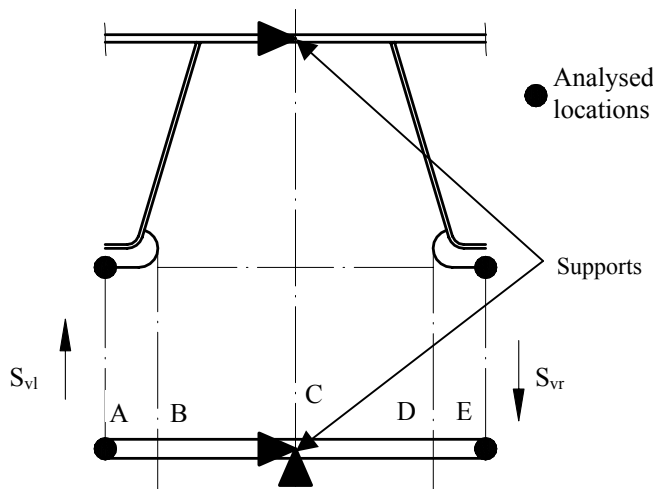


Fig. 4.16 Numerical model for in-plane shear

Fig. 4.16 shows the FE model for verification of the in-plane shear analysis. The web is modelled with shell elements; the bottom flange and the deck are modelled with line elements. The model is supported in the horizontal direction at the top and bottom of the centre line of the tooth and in the vertical direction at the bottom of the T-beam. The end cross sections of the web at the left hand side (A) and the right hand side (E) are forced to remain straight under loading to simulate the boundary conditions generated by the adjacent structure.

However, these sections are free to deflect and rotate. The nodes in the vertical cross sections A and E of the T-beams are constrained in the vertical direction and for the in-plane rotations to simulate the adjacent structure. The cross sections (A) and (E) in the centre lines of the troughs are loaded by unit loads. This means that the deflections directly give information about the shear stiffness of the whole system, as the bending and shear of the tooth is included.

4.2.2 Global model for the crossbeam in-plane analysis

4.2.2.1 Global bending analysis

The equivalent bending stiffness ratio c_b of the crossbeam, which can be used for the modeling of the global in-plane bending, is discussed in 4.2.1.1 and 4.2.1.2.

Fig. 4.17 shows a comparison of the equivalent bending stiffness ratio based on the analytical results from calculations with eqs. [4.6] to [4.11], indicated with “A”, which can also be obtained with eqs. [4.14], [4.15] and [4.11], and that based on numerical results obtained with the model described in 4.2.1.2, indicated with “FE”.

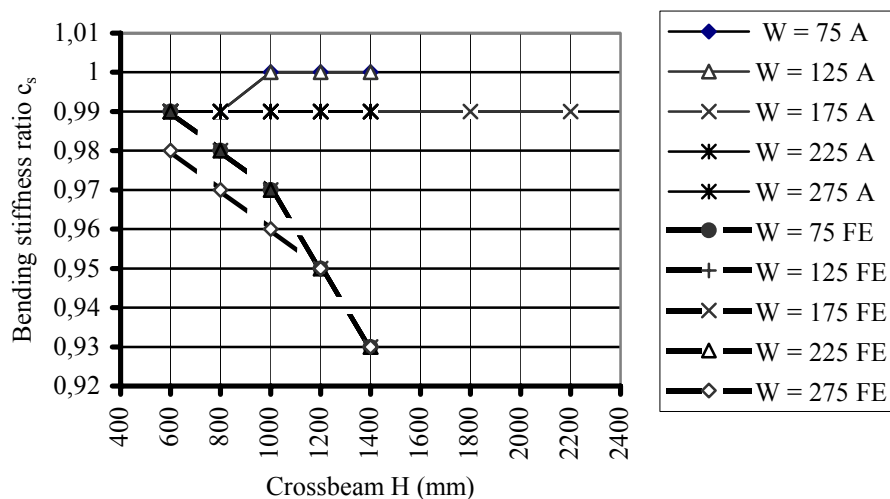


Fig.4.17 Equivalent bending stiffness ratio c_b

Based on the analytical model, values for c_b are found between 0.98 and 1.00 for $H = 600$ mm to $H = 1400$ mm and $W = 75$ mm to $W = 275$ mm. The FE model gives the same values for the lower beams with $H = 600$ mm, but marginally lower values for the deeper beams with $H = 1000 - 1400$ mm, i.e. 0.96 and 0.93 respectively.

From the above analyses, it can be concluded that the effect of the cut-out has a minor effect on the global in-plane bending stiffness, and in many cases the effect may be ignored.

4.2.2.2 Global shear analysis

Fig. 4.18 shows the analytical results from the eqs. [4.17] - [4.24] for the equivalent shear stiffness ratio c_s together with the FE results for crossbeams varying in depth $H = 600 - 2200$ mm. For each crossbeam the lever arm a_1 is indicated (in Fig. 4.18 as “al”)(see also Figs 4.11 and 4.12).

The c_s values calculated with the analytical model vary from 0.21 to 0.91. When the web depth increases from $H = 600$ mm to $H = 1400$ mm, i.e. a factor 2.33, c_s increases with an average factor of about 1.55. When the cut-out width decreases from 275 mm to 75 mm, i.e. with a factor 3.7, c_s increases with a factor 3.0 approximately when determined with the analytical method and with a factor 2.1 based on the FE method.

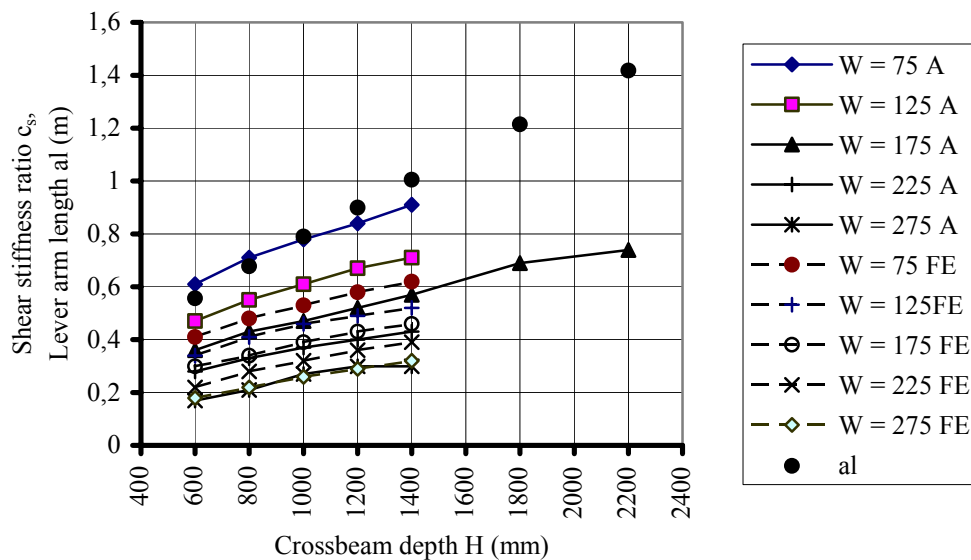


Fig.4.18 Equivalent shear stiffness ratio c_s and lever arms a_1

The results from the FE-analyses vary from 0.18 to 0.62. Increasing the web depth from $H = 600$ mm to $H = 1400$ mm, i.e. again by a factor 2.33, results in an increase of c_s with an average factor of about 1.65. Decreasing the cut-out width from 275 mm to 75 mm gives an average increase of c_s with a factor 2.1.

Fig. 4.19 shows the c_s values from the analytical model, divided by the values from the FE model.

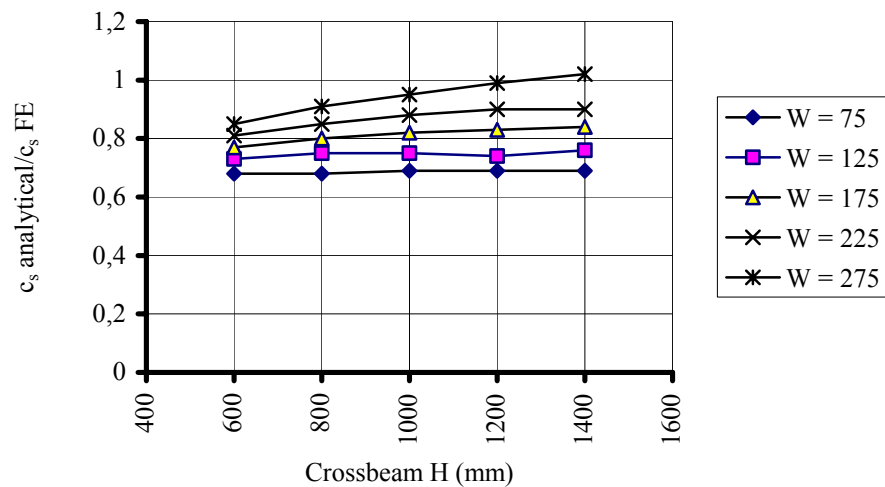


Fig. 4.19 Equivalent c_s from analytical procedure divided by c_s from FE analyses

The wider the cut-outs, the better the agreement between both results. The analytical results vary between 0.65 and 1.0 times the FE model results due to the assumptions for the dimensions of the rigid parts. The effect of the variation of the cut-out width has no relationship to the effect of the variation of the crossbeam web depth. However, the results for c_s in the crossbeams are obtained as a combination of both effects.

The difference between the analytical model and the FE model results can be explained as follows:

When the results from the FE-analyses (see 4.2.1.4) are considered in detail, it can be seen that the length of the tooth l_{IV} in the analytical model (see Fig. 4.11) does not correspond to the deformed shape in the numerical model. The curvature of the tooth is extended into the part, which is assumed to act as a rigid T-frame.

From the calculations the following conclusions can be drawn:

- The shear mechanism acts as anticipated, but the FE models are more flexible than the analytical models.
- A correction factor c_c , which adapts the length of the tooth in the calculations, is required in order to adjust the analytical values to the more precise values calculated with the FE-analyses.

For the determination of the correction factor c_c the total deflection in the analytical model over a length "c" (see Fig. 4.12), being the distance between the cross sections A and D of the FE model (see Fig. 4.16), is compared with the deflection of the FE model. The difference in the results is related to the length of the tooth l_{IV} , which is 350 mm in the analytical model. A correction factor c_c for this length is calculated in such a way that the deflection in the analytical model becomes the same as that of the FE model. The correction factors c_c have been checked by substitution

Table 4.2, Correction factors c_c for tooth length 350mm to be used in conjunction with analytical calculations

Crossbeam No.	Web depth H (mm)	Cut-out with cope hole width "W" (mm)				
		75	125	175	225	275
1	600	1.20	1.16	1.13	1.11	1.08
2	800	1.25	1.20	1.15	1.12	1.08
3	1000	1.30	1.23	1.18	1.13	1.09
4	1200	1.33	1.24	1.17	1.11	1.06
5	1400	1.33	1.24	1.16	1.10	1.04
7	1800	-	-	1.16	-	-
9	2200	-	-	1.16	-	-

Table 4.2 shows the correction factors c_c to be applied to tooth lengths of 350 mm for design purposes. The values for the beam types 7 and 9 are determined by extrapolation of the values for the beams 3, 4 and 5. For the more commonly used trapezoidal stiffeners with a cope hole width $W = 175$ mm the correction factor c_c is about 1.15.

4.2.3 Local cut-out behaviour

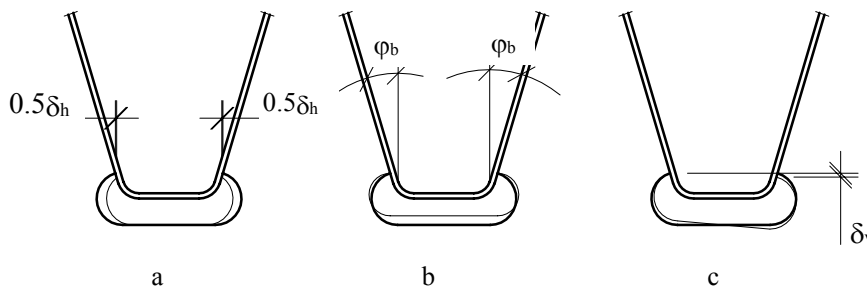


Fig. 4.20 Deformations of cope hole

In many structures, the load carrying parts affect other parts by imposed deformations. They may cause secondary normal forces, bending moments and shear forces often ignored in the design. This also applies to the

design of continuous closed stiffener connections in the orthotropic steel decks. Fig.4.20 shows the behaviour of a closed stiffener to crossbeam connection with a cope hole, under in-plane bending and shear deformations of the crossbeam.

The in-plane crossbeam bending causes cut-out and cope hole deformations. These result in relative horizontal translations $0.5\delta_h$ at each side, as shown in Fig. 4.20a, and the rotation ϕ_b , as shown in Fig.4.20b.

The in-plane crossbeam shear causes cut-out and cope hole deformations together with a relative vertical displacement δ_v as shown in Fig.4.20c. An external load may generate an additional displacement δ_{vP} .

4.2.3.1 Local closed stiffener mechanisms

Fig.4.21 shows the bottom of the closed stiffener modelled as a trapezoidal frame subjected to imposed displacements and rotations at the ends of the legs (S.4.2.bl and S.4.2.br). The contribution from P_v , the vertical force, in the vertical deformation is ignored, as the stresses are small.

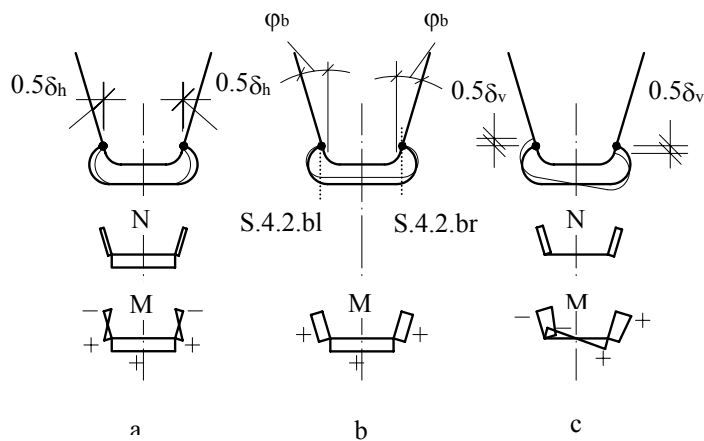


Fig. 4.21 Cope hole deformations, imposed forces and bending moments in closed stiffener bottom

Fig. 4.21a shows diagrams with normal forces N and bending moments M generated by the relative horizontal displacements due to crossbeam bending in the trough bottom part. A shortening of the distance between the locations S.4.2.bl and S.4.2.br causes a compression force N with compression stresses (-) in the stiffener, together with a bending moment resulting in tensile stresses (+) at the outside of the stiffener bottom and compression stresses (-) at the outside of the stiffener web near S.4.2.bl and S.4.2.br.

Fig. 4.21b shows a diagram for the bottom part of the trough with bending moments M generated by the rotations due to crossbeam bending. These cause tension stresses at the outside of the stiffener web and the stiffener bottom. The normal forces N are ignored.

Fig. 4.21c shows diagrams with normal forces N and bending moments M generated by the relative vertical displacements due to crossbeam shear. The normal force in both stiffener webs is equal but of opposite sign; the same applies to the bending moments in the closed stiffener bottom and webs. The difference in rotations due to shear in the crossbeam web at the locations S.4.2.bl and S.4.2.br was analysed separately, however, it was shown that the effect could be neglected.

The local frame model representing the trough bottom at the vicinity of the crossbeam behaves symmetrically under crossbeam bending and asymmetrically under crossbeam shear. The reaction forces generated by all these local deformations of the closed stiffeners are assumed to have a minor contribution to the crossbeam load transfer and therefore ignored. Carry-over effects between two adjacent crossbeams by torsion and distortion of the stiffeners are also ignored.

4.2.3.2 Local closed stiffener bottom models

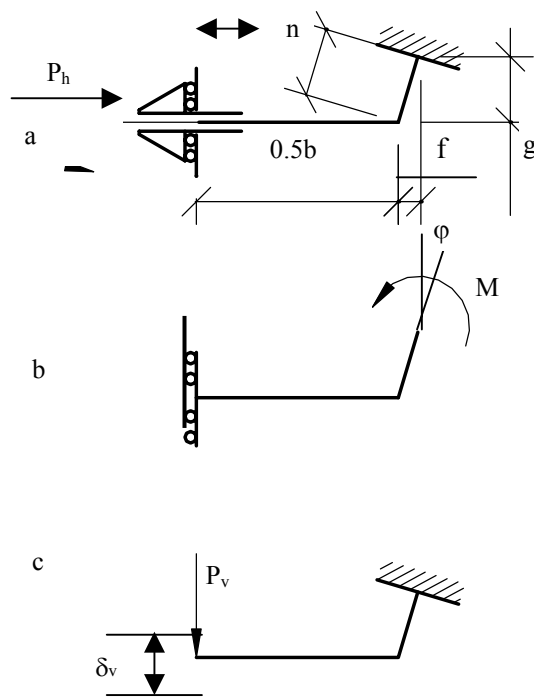


Fig. 4.22 Closed stiffener bottom models

The closed stiffener bottom and the free part of the web are modelled as a half trapezoidal frame e.g. clamped at the right hand side S.4.2.br of the cope hole. The width of the frame model chosen for the analyses is 1 mm. In real structures, the corners are curved, but for the calculations, these curvatures are not modelled because a separate sensitivity analysis showed that the deviations between models with two straight legs and those with curved legs are small. Fig. 4.22 shows the right hand models "a", "b" and "c". The model for the left hand side is not shown.

Model "a" is used for the simulation of the horizontal displacements caused by crossbeam bending. The left hand side end of the model is submitted to a horizontal displacement that causes a horizontal force P_h . This location is clamped for rotations, but free to move in horizontal and vertical directions.

Model "b" is used for the simulation of the rotations at S.4.2.br caused by the rotations due to crossbeam bending and to determine the moment M . The mid section is clamped for rotations and free to move in the vertical direction, but restrained in the horizontal direction.

Model "c" is used to simulate the vertical displacements of S.4.2.br due to crossbeam shear and to determine the vertical force P_v . The mid section is free to rotate and to move in vertical and horizontal directions.

When the results for unit loads, moments, rotations or displacements on the models "a", "b" and "c" are scaled to the real values and combined, the section forces and moments for the real crossbeam bending moments and shear forces can be obtained. From the section forces and moments the nominal stresses can be calculated and they can be modified to geometrical stresses by the use of geometrical stress concentration factors.

4.2.3.3 Local analyses for crossbeam bending

As discussed in 4.2.3.1, bending of the crossbeam results in horizontal displacements and rotations at the closed stiffener connections. Fig. 4.23 shows the relevant part of the structure.

Relative horizontal displacements

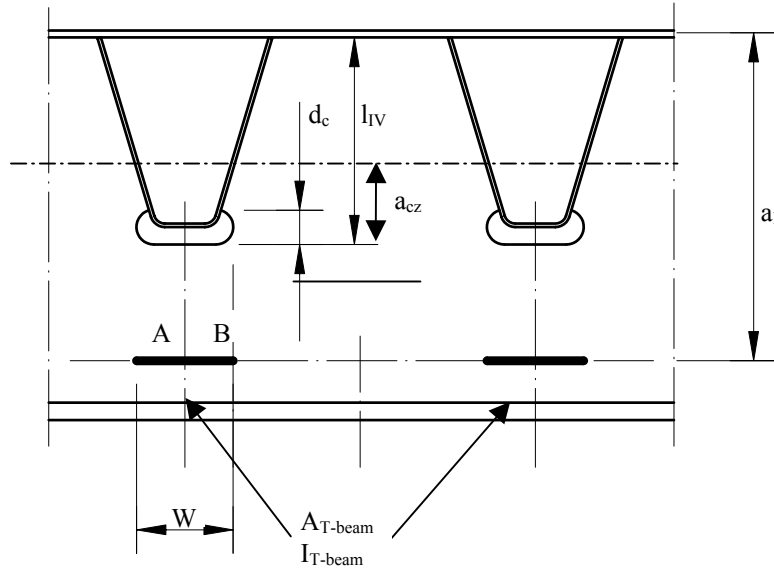


Fig. 4.23 Model for relative horizontal displacements caused by crossbeam bending

The displacements are calculated from the elongation (or contraction) of the T-beam over the length “W” due to the lever system and the effect of the secondary bending moment.

The first part of equation [4.24] deals with the elongation of the T-beam over half the cope hole and the second part deals with the effect of the secondary bending moment in the T-beam. The total elongation or shortening of

the distance between S.4.2.bl and S.4.2.br, see also Fig. 4.21, is found by multiplication with a factor

2.

$$\delta_h = 2 \left(\frac{M_l \cdot 0.5W}{a_1 \cdot E \cdot A_{T-beam}} - \frac{M_T \cdot 0.5 \cdot W \cdot (a_1 - l_{IV} + d_c)}{E \cdot I_{T-beam}} \right) \quad [4.24]$$

As an alternative to equation [4.24], equation [4.25] can be used with the $I_{cut-out}$ for the section over the cut-out. The notional bending stress at the level of S.4.2.bl and S.4.2.br is used to calculate the elongation or contraction of the distance between S.4.2.bl and S.4.2.br.

$$\delta_h = \frac{M \cdot a_{cz}}{I_{cutout}} \cdot \frac{W}{E} \quad [4.25]$$

In equation [4.25] a_{cz} is the distance from the neutral axis to the locations S.4.2.bl and S.4.2.br of the complete section over the cut-out.

The relationship between the relative horizontal displacements and the horizontal force (P_h) acting in the frame of Fig. 4.22a can be calculated with equation [4.26].

$$\delta_h = P_h \left(\frac{n \cdot g^2}{3 \cdot E \cdot I_{frame}} - \frac{n^2 \cdot g^2}{(0.5b + n) \cdot 4 \cdot E \cdot I_{frame}} \right) \quad [4.26]$$

Once P_h is known, the axial force (P) in the stiffener web can also be calculated with equation [4.27].

$$P = \frac{f}{n} * P_h \quad [4.27]$$

The bending moment (M) at the location S.4.2.br can be computed with equation [4.28]:

$$M = P_h \cdot g - \frac{P_h \cdot g \cdot n}{2(0.5b + n)} \quad [4.28]$$

Fig. 4.24 shows the calculated relative horizontal displacements between S.4.2.bl and S.4.2.br.

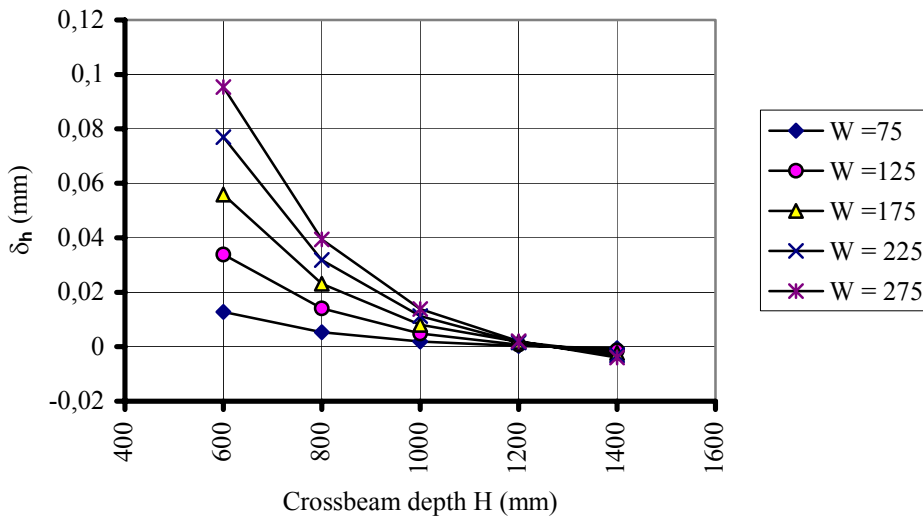


Fig.4.24 Relative horizontal displacements of S.4.2.bl and S.4.2.br

In those crossbeams, where the locations S.4.2.bl and S.4.2.br are situated above the neutral axis of the crossbeam, a contraction occurs and in those cases where these locations are below the neutral axis an elongation is found.

In case of contraction, the stresses at the outside of the trough web at the locations of S.4.2.bl and S.4.2.br will both be compressive. In the Beam Type 1, with $H = 600$ mm and $w = 75$ mm, the locations S.4.2.bl and S.4.2.br are below the neutral axis, so the stresses at the outer fibre of S.4.2.bl and S.4.2.br will be tensile.

With the eqs. [4.27] and [4.28], a resulting nominal stress of 30 N/mm^2 is found in the trough web for the crossbeam with $H = 600 \text{ mm}$ and $W = 75 \text{ mm}$. For a simple comparison, all calculated stresses in the trough web for other geometries are related to this value by dividing these stresses by 30 N/mm^2 (see Fig 4.25).

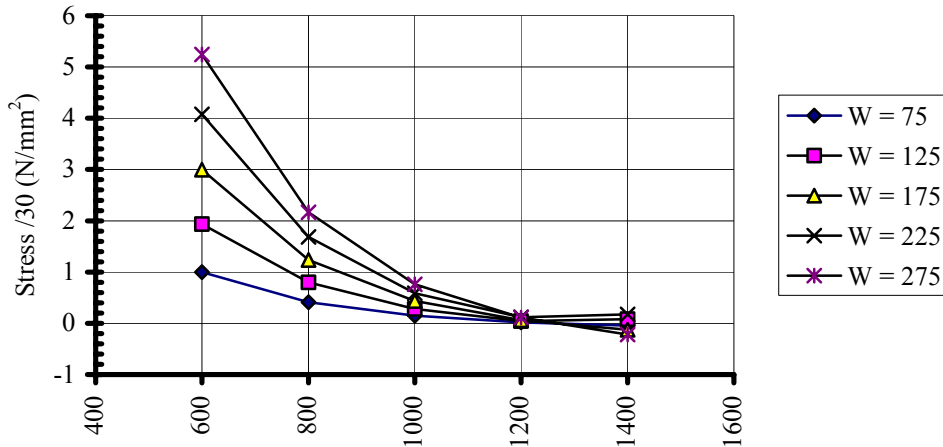


Fig.4.25 Nominal stresses due to relative horizontal displacements of S.4.2.bl and S.4.2.br

As mentioned in 4.1.3 the calculations were carried out for a crossbeam midspan bending moment with a magnitude of 700 kNm in the crossbeam with $H = 600 \text{ mm}$. This moment causes a working stress of 240 N/mm^2 in the bottom flange of the crossbeam.

As previously discussed, the maximum bending moments for other beam types can be determined in a similar way. Fig. 4.25 shows for all investigated crossbeams and cut-outs the nominal stresses in the trough web (divided by 30). As shown in Fig. 4.25, an increase of the cope hole width W gives a considerable increase in the stresses in the trough web. Increasing the web depth, results in a considerable reduction in the stresses.

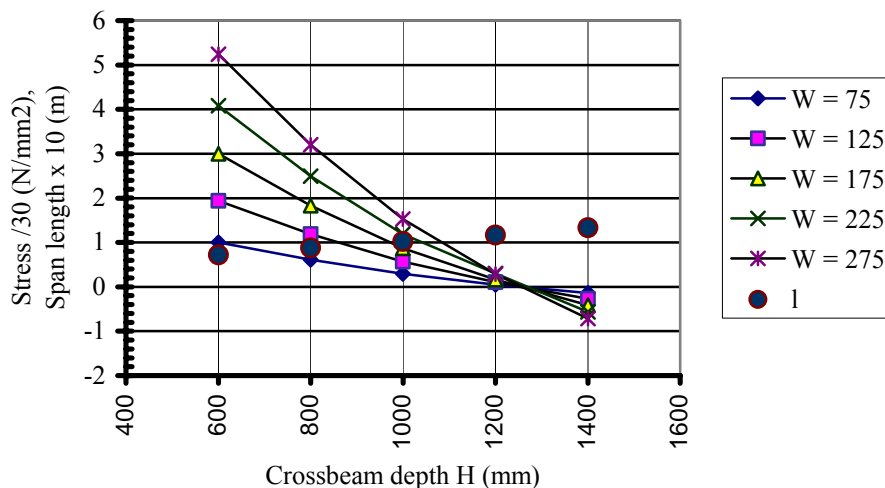


Fig.4.26 Nominal stresses due to relative horizontal displacements S.4.2.bl and S.4.2.br for an optimised bending capacity (span length l)

Fig 4.26 shows the relative nominal stresses in the trough web for various optimal span lengths determined with eqs. [4.3] to [4.5].

Compared to Fig. 4.25 the stresses for H = 600 mm are the same, but for the other depths the values increase due to the increased bending moments in the optimised crossbeams.

Influence of the "effective width" of the deck plate

In 4.1.2 it is shown that, depending on the standard used, for a simple span of 7200 mm the effective width $b_{\text{eff}} = 2400$ to 2600 mm.

The 1400 mm, as used in this study, applies only for interior spans. Therefore, additional analyses are carried out for the influence of an effective width of 1900 mm and 2400 mm.

Table 4.3 shows the notional strains between the locations S.4.2.cl and S.4.2.cr for an effective width $b_{\text{eff}} = 1400$ mm, $b_{\text{eff}} = 1900$ mm and $b_{\text{eff}} = 2400$ mm.

It can be concluded that for the smaller crossbeams the results are in the same range.

Table 4.3 Notional strains between S.4.2.cl and S.4.2.cr

Web depth H (mm)	$b_{\text{eff}}=1400$ (mm)	$b_{\text{eff}}=1900$ (mm)	$b_{\text{eff}}=2400$ (mm)
600	-4.08×10^{-4}	-4.49×10^{-4}	-4.74×10^{-4}
800	-1.19×10^{-4}	-1.60×10^{-4}	-1.83×10^{-4}
1000	-1.16×10^{-5}	-4.88×10^{-5}	-7.08×10^{-5}
1200	$+3.19 \times 10^{-5}$	-9.27×10^{-5}	-1.96×10^{-5}
1400	$+5.39 \times 10^{-5}$	$+2.33 \times 10^{-5}$	$+5.11 \times 10^{-6}$

However, for the deeper crossbeams an increasing effective width may have a considerable influence and may even change tension into compression.

As shown in Figs. 4.25 and 4.26 the magnitude of the stresses of the deeper crossbeams is considerably smaller than for the crossbeams with the smaller depths. Nevertheless, the effect has to be taken into account.

In-plane rotations of the closed stiffener connections

In Figs. 4.20 and 4.21, it is shown that in addition to the horizontal displacements, at the locations S.4.2.bl and S.4.2.br rotations also occur due to crossbeam bending. The rotation ϕ_b in cross section B can be used for the determination of the stresses due to rotation.

Analogous to the horizontal displacements, a simplified calculation can be carried out using equation [4.29].

$$\phi_l = -\phi_r = \frac{M \cdot w}{2E \cdot I_{\text{cut-out}}} \quad [4.29]$$

From the imposed rotation, the bending moment at the locations S.4.2.bl and S.4.2.br can be computed with equation [4.30].

$$\phi_b = \frac{M}{E \cdot I} \cdot \left[(0.5b + n) - \frac{(b + n)^2}{2 \cdot (b + \frac{2}{3} \cdot n)} \right] \quad [4.30]$$

Further, P_h can be calculated with equation [4.31].

$$P_h = M \cdot \frac{(b+n)}{g \cdot (b + \frac{2}{3}n)} \quad [4.31]$$

The axial force P in the leg can be obtained with equation [4.32].

$$P = \frac{f}{n} \cdot P_h \quad [4.32]$$

Fig. 4.27 shows the resulting rotations. The crossbeam with $H = 1400$ mm shows a rotation which is about 14.5% of the rotation for $H = 600$ mm.

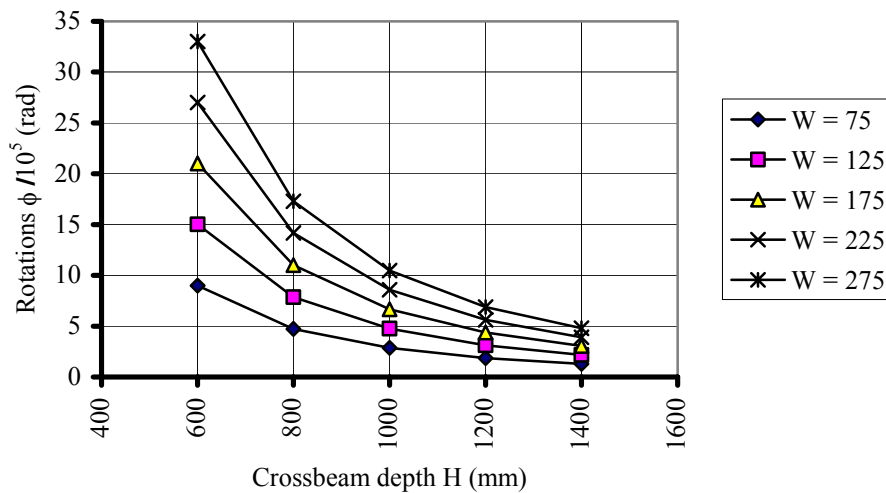


Fig.4.27 Rotations at S.4.2.bl and S.4.2.br from crossbeam bending

Fig.4.28 shows the nominal stresses due to rotations divided by 30. In comparison with the stresses in Fig. 4.25, it can be concluded that the stresses due to the imposed rotation are generally approximately a factor 5 smaller than the stresses due to the horizontal displacement.

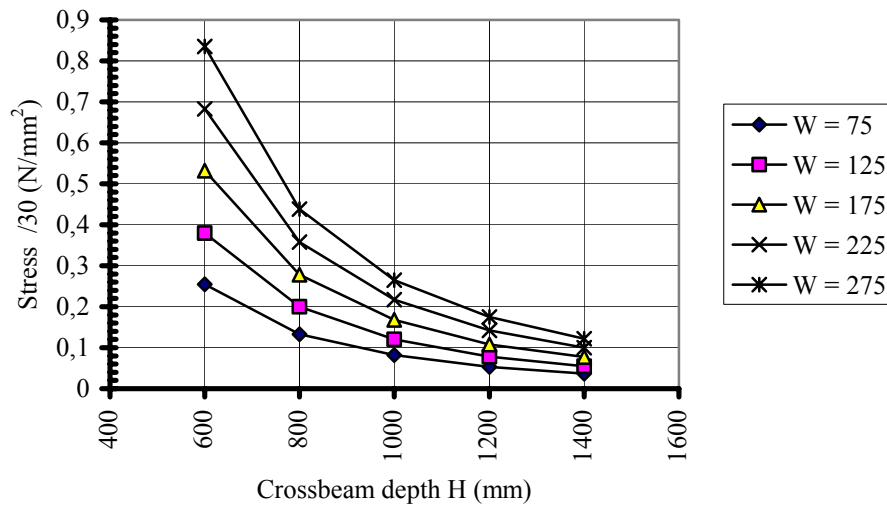


Fig.4.28 Nominal stresses caused by rotations of S.4.2.bl and S.4.2.br

The results for the crossbeams with the so-called “optimised bending capacity” are shown in Fig. 4.29. These show a similar tendency as those in Fig. 4.28.

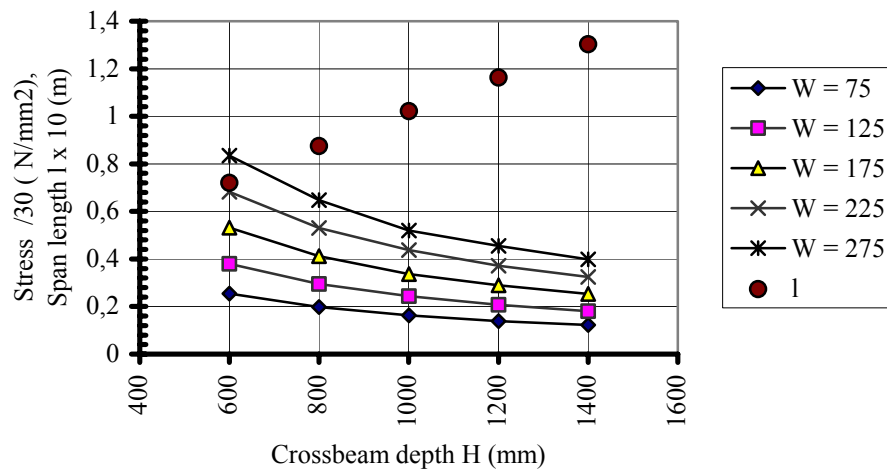


Fig.4.29 Nominal stresses caused by rotations of S.4.2.bl and S.4.2.br for crossbeams with an optimised bending capacity (span length l)

In simply supported crossbeams, the rotation due to a positive bending moment always causes a tensile stress at the locations S.4.2.bl and S.4.2.br

Influence of the "effective width" of the deck plate

Table 4.4 Notional rotations from crossbeam bending over cut-out

Web depth H (mm)	$b_{eff} = 1400$ (mm)	$b_{eff} = 1900$ (mm)	$b_{eff} = 2400$ (mm)
600	2.47×10^{-6}	2.30×10^{-6}	2.21×10^{-6}
800	1.28×10^{-6}	1.18×10^{-6}	1.12×10^{-6}
1000	7.73×10^{-7}	7.06×10^{-7}	6.67×10^{-7}
1200	5.063×10^{-7}	4.62×10^{-7}	4.34×10^{-7}
1400	3.589×10^{-7}	3.23×10^{-7}	3.00×10^{-7}

As mentioned before, the analyses presented are based on an effective width $b_{eff} = 1400$ mm.

Table 4.4 shows the specific rotations for $b_{eff} = 1400$ mm, $b_{eff} = 1900$ mm and $b_{eff} = 2400$ mm. The effective width of 2400 mm gives a specific rotation, which is 11 to 16% smaller than that for an effective width of 1400 mm. Table 4.5 gives an overview of the combined stress results from crossbeam bending.

Summary of the nominal stresses due to the relative horizontal displacements and relative rotations caused by crossbeam bending:

Table 4.5, Summary of nominal stresses in S.4.2.bl and S.4.2.br for the standard span length 7200mm due to a crossbeam bending moment of 700 kNm

		Nominal stresses (N/mm ²), for $b_{eff} = 1400$ (mm), due to:			Nominal stresses (N/mm ²), for $b_{eff} = 2400$ (mm), due to:		
Web depth H (mm)	Width of cut-out W (mm)	Horizontal translation	Rotation	Sum	Horizontal translation	Rotation	Sum
600	75	+1.00	+0.26	+1.26	+1.17	+0.23	+1.40
600	275	+5.24	+0.84	+6.08	+6.13	+0.11	+6.24
1400	75	-0.04	+0.12	+0.08	-0.00	+0.10	+0.01
1400	275	-0.72	+0.46	-0.26	-0.07	+0.38	+0.31

For the standard span crossbeam the following observations can be made with respect to the stresses in the stiffener due to crossbeam bending:

1. A wider cut-out leads to higher stresses (combined effect from horizontal translations and rotations).
2. Increasing the depth of the crossbeam reduces the relative displacement of locations S.4.2.bl and S.4.2.br due to the changing level of the neutral axis. This may also cause a change of sign of the stresses.
3. In addition to the effect mentioned under 2, the increased crossbeam depth causes a reduction of the displacements and rotations due to the higher stiffness of the beam.

Further, the following observations can be made:

- From equation [4.26], it can be concluded that the relationship between δ_h and P_h , is approximately proportional to n^3 . i.e. the leg length "n" (see Fig. 4.22) influences the stresses by approximately n^3 . Because of this marked effect, a reduction of the stresses can be expected by increasing the leg length "n".
- The stress sensitivity to the leg length "n" indicates that small deviations during assembly can lead to large variations in stresses in S.4.2.bl and S.4.2.br.

4.2.3.4 Local analyses for crossbeam shear

The shear forces S_V cause horizontal and vertical displacements of the locations S.4.2.bl and S.4.2.br.

The horizontal shear forces S_H in the tooth act in the same direction along the part of the crossbeam where the shear force doesn't change sign. The shear forces S_H in two adjacent teeth will have about the same magnitude, therefore, the horizontal displacements of the locations S.4.2.bl and S.4.2.br will also have the same magnitude and the relative horizontal displacements can be neglected.

Fig. 4.30 shows the model that is used for the calculation of the relative vertical displacements of the locations S.4.2.bl and S.4.2.br. derived from the shear model described in 4.2.1.3.

Vertical displacements caused by crossbeam shear:

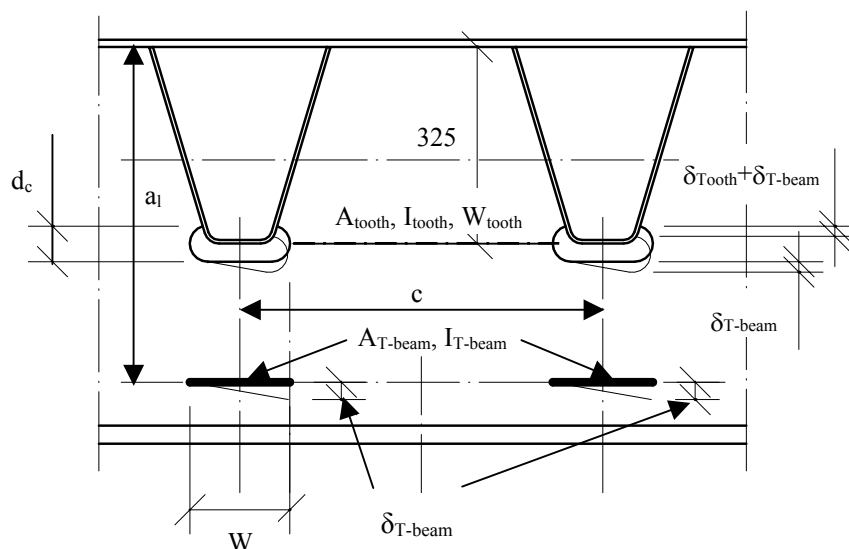


Fig. 4.30 Structure and model for relative vertical displacements of S.4.2.bl and S.4.2.br.

The relative vertical displacement of the locations S.4.2.bl and S.4.2.br with respect to the mid section of the cut-out are caused by the shear force S_V in the T-beam and by the shear force S_H in the tooth.

The displacements can be computed with equation [4.33]. The first term is the contribution from the shear deformation in the T-beam and the second term is the

deformation from the tooth bending. In this term, the corrected tooth height is used for the rotation over the height $(c_c \cdot I_{IV} - I_{IV} + d_c)$.

The contribution to the relative displacement is found, by combining the rotation with the distance 0.5c.

In equation [4.33] c = centre-to-centre distance of the closed stiffeners (see also Fig. 4.25), and the tooth length l_{IV} is shown in Fig. 4.11.

$$\delta_{vl} = \frac{S_v \cdot 0.5w}{G \cdot A_{F-beamweb}} + \frac{[S_h \cdot c_c \cdot l_{IV} + S_h \cdot (l_{IV} - d_c)] \cdot c \cdot (c_c \cdot l_{IV} - l_{IV} + d_c)}{2 \cdot 2 \cdot E \cdot I_{tooth}} \quad [4.33]$$

When a directly applied vertical load P_v acts on the tooth, it causes a normal force N and an eccentricity moment M_F in section F (for section F: see Fig. 4.11), this results in an additional δ_v as shown in equation [4.34]. In 4.2.4 it will be explained that in most cases $M_F \approx 0$.

$$\delta_{vP} = \frac{N \cdot d_c}{E \cdot A_{tooth}} + \frac{M_E \cdot d_c \cdot 0.5c}{E \cdot I_{tooth}} \quad [4.34]$$

The above determined displacements $\delta_{v,total}$ can be used again for the determination of the force P_v and stresses in the trough bottom frame by using equation [4.35].

$$\delta_{v-total} = \frac{P_v \cdot b^3}{24 \cdot E \cdot I_{frame}} + \frac{P_v \cdot b \cdot n}{4 \cdot E \cdot I_{frame}} \cdot \left(\frac{f}{3} + \frac{b}{2}\right) + \frac{P_v \cdot \left(\frac{b}{2} + f\right) \cdot n}{2 \cdot E \cdot I_{frame}} \cdot \left(\frac{2}{3} \cdot f + \frac{b}{2}\right) \quad [4.35]$$

The vertical displacement “ $\delta_{v-total}$ ” used in equation [4.35] is half of the total relative vertical displacement between S.4.2.bl and S.4.2.br.

For the locations S.4.2.bl and S.4.2.br the force P in Fig. 4.22c can be calculated with equation [4.36] and the bending moment M with equation [4.37].

$$P = P_v \cdot \frac{g}{n} \quad [4.36]$$

$$M = P_v \cdot \left(\frac{b}{2} + f\right) \quad [4.37]$$

The crossbeam H = 600 mm, W = 75 mm with a span length of 7200 mm is subjected to a maximum shear force $S_v = 390$ kN, due to a uniformly distributed load as discussed in 4.1.

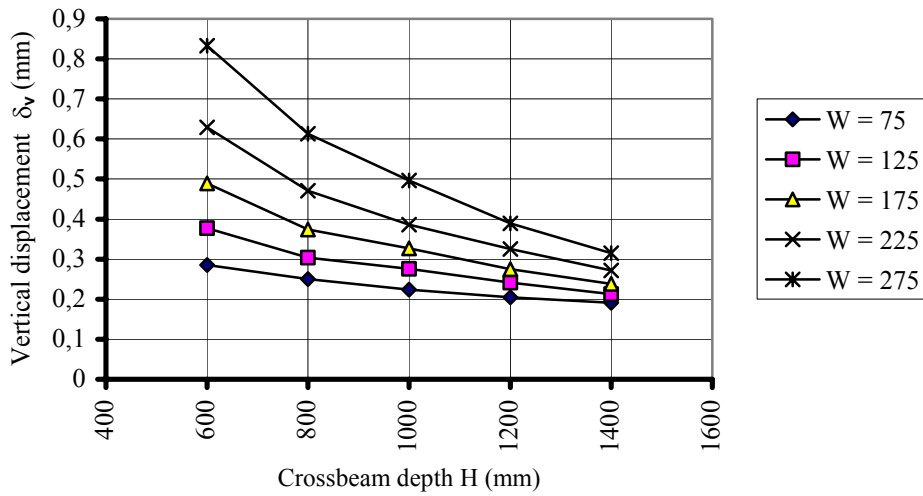


Fig.4.31 Relative vertical displacements of S.4.2.bl and S.4.2.br with respect to middle of cut-out

The relative vertical displacements due to the shear forces S_V and S_H at the locations S.4.2.bl and S.4.2.br with respect to the middle of the cut-out are shown in Fig.4.31.

This figure shows, that as the crossbeam depth increases displacements and the influence of the cope hole dimension reduce. As shown in Fig. 4.21c, due to the asymmetric frame behaviour the normal forces and bending moments cause stresses at S.4.2.bl and S.4.2.br, which are equal and have opposite sign.

Fig. 4.32 shows the stresses at the locations S.4.2.bl and S.4.2.br, divided by 30 N/mm^2 . Therefore, these relative stresses are directly comparable with the previously determined stresses due to the crossbeam bending.

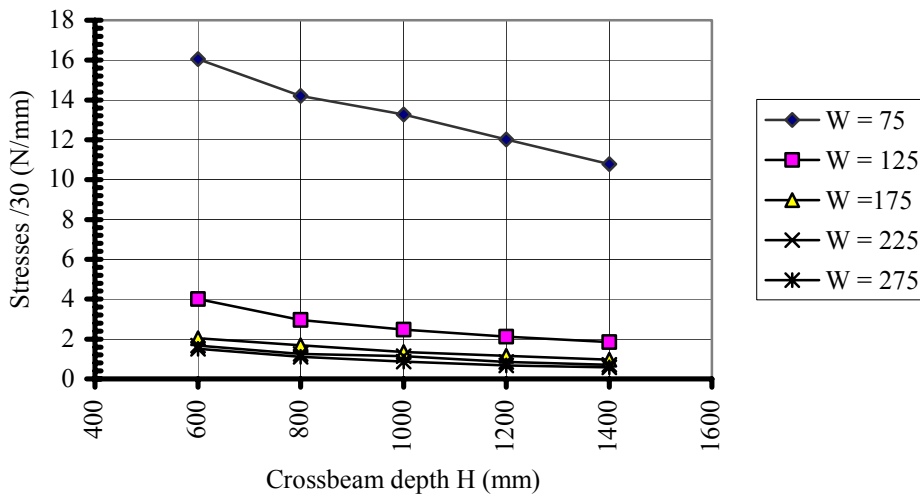


Fig.4.32 Nominal stresses from relative vertical displacement of S.4.2.bl and S.4.2.br

In Fig. 4.32, it can be seen that an increase in the cope hole width W gives a considerable decrease in the stresses in the trough web, which is very different from the situation for crossbeam bending, see Figs. 4.25 and Fig. 4.28. It must be recognized that $W = 75$ is only a theoretical cope hole dimension and that the trough bottom width would be very small, which leads to a very rigid frame model.

Summary of the relative nominal stresses due to the relative vertical displacements caused by crossbeam shear:

Table 4.6, Nominal stresses in S.4.2.bl and S.4.2.br due to the crossbeam shear for the standard span length 7200 mm

Web depth (mm)	Width of cut-out (mm)	Stresses (N/mm ²), for $b_{\text{eff}}=1400$ (mm), due to shear
600	75	-/+ 16.
600	275	-/+ 1.
1400	75	-/+ 12.5
1400	275	-/+ 0.6

Increasing the web depth results in a considerable reduction in the stresses, similar to that for crossbeam bending.

The rotations of S.4.2.bl and S.4.2.br are approximately the same. The effect of the rotations on the relative displacements is incorporated in equation [4.33].

Table 4.6 gives a brief overview

of the stresses caused by crossbeam shear. The stresses are indicated with a sign as the trough bottom shows an asymmetric behaviour due to crossbeam shear.

For the standard span crossbeams the following observations can be made with respect to the stresses in the stiffener due to crossbeam shear:

1. A wider cut-out leads to lower stresses in the locations S.4.2.bl and S.4.2.br. This is caused by the greater flexibility of the trough bottom for larger cut-out widths.
2. An increasing depth of the crossbeams reduces the relative displacement of locations S.4.2.bl and S.4.2.br due to the relationship between S_V and S_H and the higher shear stiffness of the T-beam, which results in lower stresses in the locations S.4.2.bl and S.4.2.br.

Similar to the conclusions for the effect of crossbeam bending, it can be concluded that, increasing the leg length “ n ” for a fixed cut-out width, results in a more flexible trough bottom and a decrease in the stresses, see equation [4.35].

4.2.4 Local in-plane behaviour of the crossbeam web with cut-outs

As shown in 4.2.1.1, the bending moment in the crossbeam generates both tension forces and secondary bending in the T-beam below the stiffener. Further, as discussed in 4.2.1.2, the shear force S_V in the crossbeam generates bending and shear in the T-beam and the shear force S_H results in bending and shear in the tooth.

4.2.4.1 Stresses in cut-out with cope hole

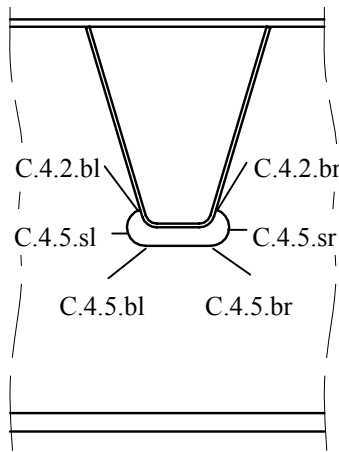


Fig. 4.33 Stress locations at cope hole

Fig. 4.33 shows the critical locations C.4.2.bl, C.4.5.sl, C.4.5.bl, C.4.2.br, C.4.5.sr and C.4.5.br in the crossbeam web.

Similarly to the stresses determined for the trough bottom the stresses at the locations C.4.2.bl and C.4.2.br are also generated by the global bending of the crossbeam, the secondary bending in the T-beam, the local bending due to crossbeam shear and eventually the normal forces in the tooth with their eccentricity moments.

When the stresses in the tooth are only based on the effects caused by the shear force S_V , eqs. [4.38] and [4.39] apply for the determination of the horizontal shear force S_H at the top and for the bending stress in the tooth at the level of the trough bottom:

$$S_h = \frac{S_{vr} \cdot 0.5c + S_{vl} \cdot 0.5c}{a_t} \quad [4.38]$$

$$\sigma = \frac{S_h \cdot (l_{IV} - 0.5d_c)}{W_{tooth}} \quad [4.39]$$

Fig. 4.34 shows the nominal stresses according to equation [4.39] due to tooth bending caused by S_h in locations C.4.5.s for $S_V = 3.9 \times 10^5$ N. Additionally, the stresses due to T-beam bending caused by S_V are indicated as dashed lines for C.4.5.b.

Further, for comparison, for $W = 175$ mm the stresses at the edge of the cut-out at the location C.4.5.s are also calculated below with the procedure, in accordance with the DIN-Fachbericht 103, but excluding the 15% reduction for the shear force.

The nominal stress, which is indicated in Fig. 4.34 with C.4.5.sG, is calculated with:

$$\sigma = \frac{S_h \cdot (l_{IV} - 0.5d_c)}{W_{tooth}} \quad [4.40]$$

where:

$$S_h = \tau \cdot t_w \cdot c \tag{4.41}$$

and the shear stress in the upper fibre of the crossbeam web is given by:

$$\tau = \frac{S_v \cdot t_{de} \cdot A_{fl} \cdot a_z}{t_w \cdot I_{cb}} \tag{4.42}$$

In which: t_{de} = equivalent thickness of the deck plate.

For the combination of stresses, Table 4.7 shows the nominal bending stresses from crossbeam bending at location C.4.5.b for the midspan bending moment $M_b = 700$ kNm.

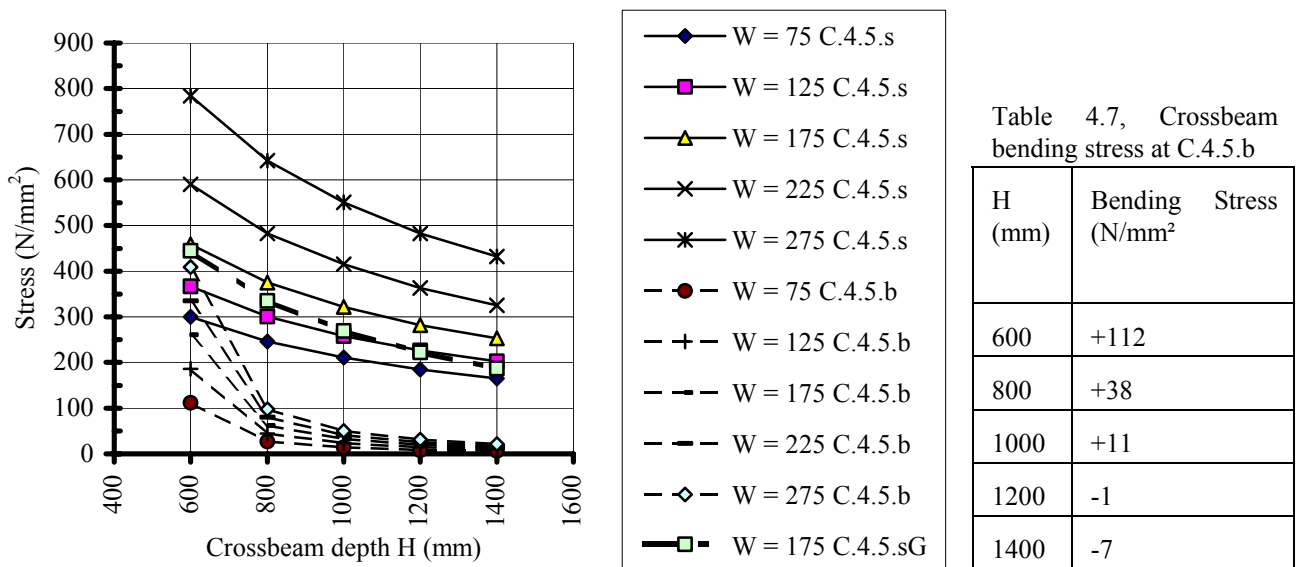


Fig .4.34 Nominal stresses in cope hole locations C.4.5.sl, C.4.5.bl, C.4.5.sr and C.4.5.br .

The wider the cope holes the larger the stresses. Increasing the crossbeam web depth shows a decrease of the stresses in C.4.5.s.

The comparison of the calculated stresses for $W = 175$ mm (C.4.5.s) shows that the stresses calculated with the method according to the DIN-Fachbericht 103 (C.4.5.sG), without the allowed reduction factor of 15%, gives a reasonable good agreement with those resulting from this study.

In order to obtain accurate stresses along the edge of the cope hole for fatigue assessments, the stresses, using geometrical stress concentration factors as discussed in chapter 5, have to be combined.

As an approximation the interaction of the tooth bending stresses and the T-beam bending stresses can be analysed with a Von Mises stress equation as shown in equation [4.43]. The stresses σ_V and σ_H should include the stress concentration effects. As will be discussed in chapters 5 and 7, the relevant stress concentration factors for σ_V are SCF = 2.1 and for σ_H SCF = 3.0.

$$\sigma_e = \sqrt{\sigma_V^2 + \sigma_H^2 - \sigma_V \cdot \sigma_H} \quad [4.43]$$

Here the stresses will be combined for the crossbeam with H = 1200 mm, for which, as shown in Table 4.7 the crossbeam bending stresses at the cope hole can be ignored. The resulting geometrical stresses including the SCF's are shown in Table 4.8.

Table 4.8 Concentrated (geometrical) stresses in Location C.4.5.s, C.4.5.b and resulting stresses between locations C.4.5.s and C.4.5.b

	w=75	W=125	w=175	w=225	w=275
C.4.5.s	389	475	592	762	1014
Between C.4.5.s and C.4.5.b	378	456	564	727	971
C.4.5.b	24	42	60	762	93

It can be seen that the stresses at the locations C.4.5.s are always higher than the stresses in C.4.5.b and in the location between them. However, for the crossbeams with a lower depth the stresses due to crossbeam bending at

location C.4.5.b can have a considerable contribution in the total geometrical stress, which could cause the “in between “ location to become critical.

4.2.4.2 Stresses in cut-out without cope hole

Fig. 4.35 shows the considered locations for a closed stiffener with a close fit. The nominal stresses in C.4.1.wl and C.4.1.wr can be calculated with equation [4.39]. Similarly as before, the stresses in C.4.1.bl and C.4.1.br can be calculated from the local and global bending moments in the crossbeam.

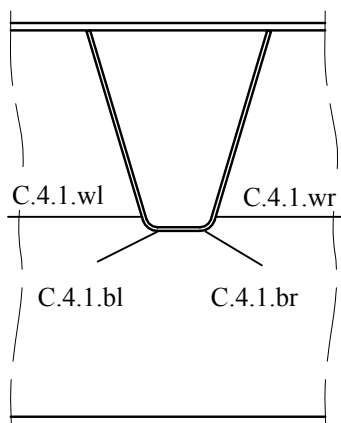


Fig. 4.35 Stress locations cross beam web without cope holes

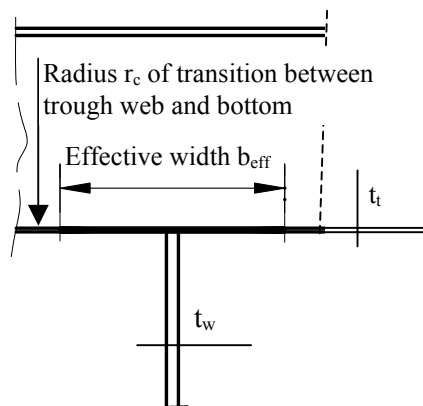


Fig. 4.36 Effective geometry for relation between trough and crossbeam stresses

Fig. 4.36 shows the geometry relevant for the determination of the local stresses in the crossbeam web caused by the stresses in the trough.

Fig. 4.37 shows the nominal stresses at the locations C.4.1.wl and C.4.1.wr in the tooth and at C.4.1.bl and C.4.1.br in the T-beam in tangential direction parallel to the weld toe. These stresses are the result from a distributed load of 108 N/mm^1 , resulting in a shear force $S_v = 390 \text{ kN}$ and a midspan bending moment of $M_b = 700 \text{ kNm}$.

For comparison, the crossbeams and cut-outs are identically indicated as for the crossbeams with cope holes, i.e. $w = 175 \text{ mm}$ means in reality here a trough bottom width of 105 mm , which equals the width of the effective cut-out.

Further, the nominal stresses due to a crossbeam bending moment $M_b = 700 \text{ kNm}$ are indicated by: "All W C.4.1.b". The stresses are not calculated for crossbeams with a cut-out $W = 75 \text{ mm}$, because these beams are not realistic.

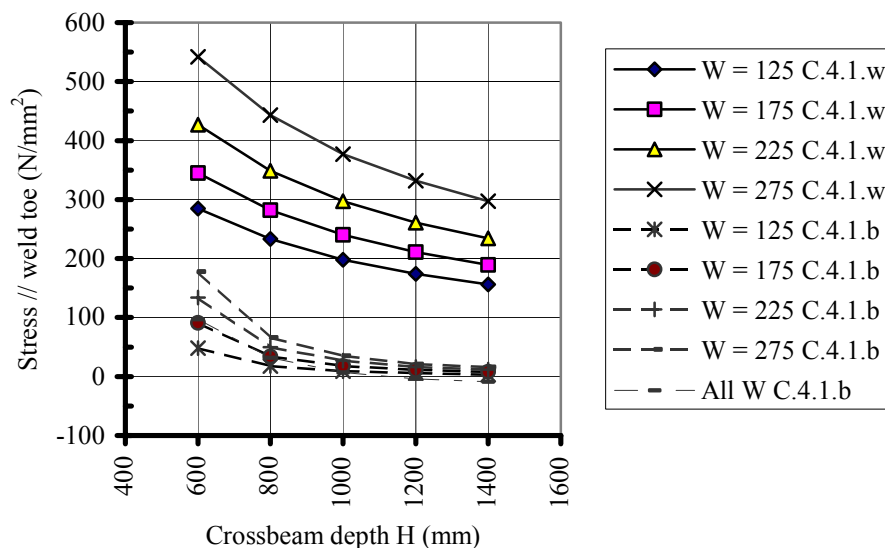


Fig.4.37 Nominal stresses in a crossbeam web parallel to the weld for continuous stiffeners with a close fit

As the direction of these calculated stress components is parallel to the weld toe of the trough to crossbeam connection, these stresses are less relevant for the fatigue strength of this connection.

The stresses perpendicular to the weld toe can be derived with the method presented below.

When the stresses parallel to the weld toe are assumed not only to act in the crossbeam web, but also in the effective width b_{eff} of the trough with a thickness t_t and a radius r_t , the radial stresses can be obtained as described by Roark and Young (1986). In analogy to a pressure vessel, the force between two locations can be calculated.

The geometrical stresses are obtained by dividing this concentrated force by the outer radius r_c of the trough bottom and the crossbeam web thickness t_w , and multiplying these stresses by the relevant stress concentration factor, see equation [4.44]. In equation [4.44] the stress concentration factor for the upper end of the curvature for C.4.1.wl and C.4.1.wr is taken as $SCF = 2.1$ and at the bottom end of the curvature for C.4.1.bl and c.4.1.br as $SCF = 3.0$.

$$\sigma_{wr} = \frac{SCF \cdot \sigma_s \cdot t_t \cdot 1.56 \sqrt{r_t \cdot t_t}}{r_c \cdot t_w} \quad [4.44]$$

The geometrical stresses in these locations perpendicular to the weld toe without the influence of crossbeam bending are indicated in Fig.4.38.

Table 4.9 shows the geometrical stresses at the locations C.4.1.bl and C.4.1.br from crossbeam bending due to a bending moment of 700 kNm. The mean radius r_t of the curved trough bottom is taken 28 mm which means that the outer radius r_c is 31 mm.

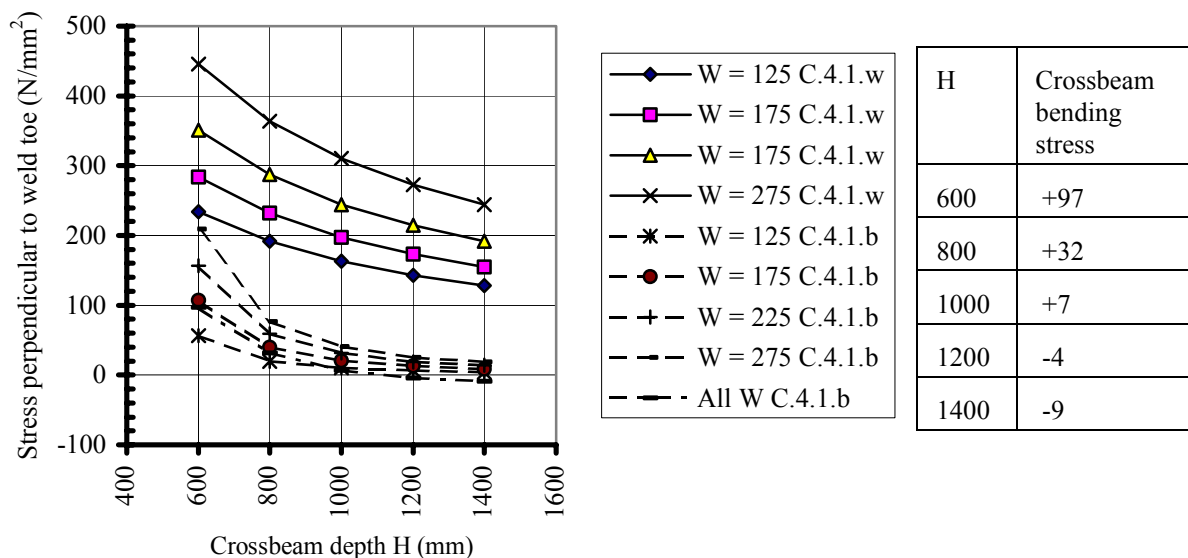


Fig. 4.38 Geometrical stresses in the crossbeam web perpendicular to the weld toe for a stiffener with a close fit

For the crossbeams with less depth, the stresses due to crossbeam bending at the bottom location C.4.5.b can have a considerable contribution in the total geometrical stress, which could cause that the bottom location becomes critical.

4.2.4.3 Influence of direct loads on the tooth

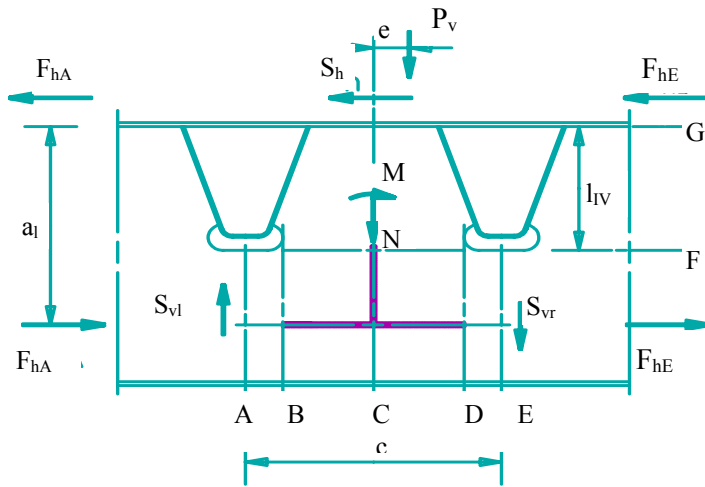


Fig. 4.39 Arrangement of internal forces and external loads on the crossbeam web

In addition to the previously mentioned loads from crossbeam shear and bending, a vertical force P_v can also act on the tooth.

This can be the result of a direct load on the tooth or be introduced by the stiffeners through the connecting welds. The force P_v can have an eccentricity e .

Summarizing, a normal force "N" (ΣP_v) and a bending moment "M" act on the tooth. The external forces and the section forces are shown in Fig. 4.39.

The external forces on the tooth, $S_{vl} \neq S_{vr}$ and the additional bending in the tooth from the load introduction would cause a horizontal displacement at the top of the tooth if it were not restrained by the deck plate.

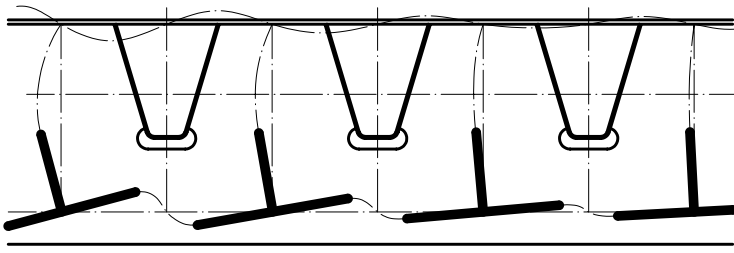


Fig. 4.40 Vierendeel system deformations

Fig. 4.40 shows that the deformation of one tooth depends on the deformations of the adjacent teeth as they are linked by the deck plate. Therefore, the top of the tooth can be considered as horizontally restrained.

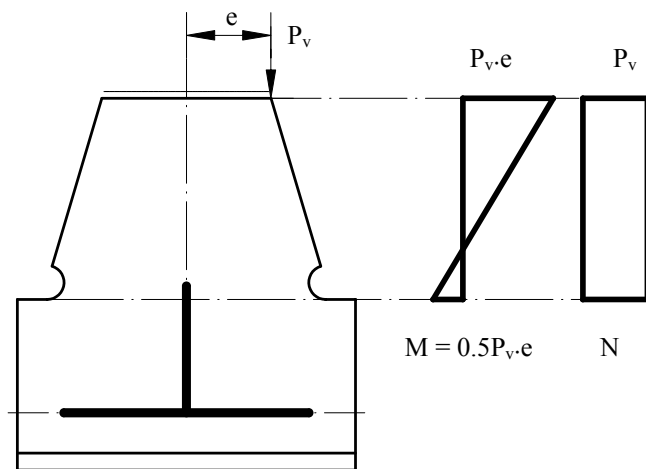


Fig. 4.41 Tooth acting as a column with a restrained top and clamped bottom

Because the tooth is assumed to be restrained at the top and clamped at the bottom at a distance $c_c \times l_{IV}$, the resulting moment diagram is as indicated in Fig. 4.41. This moment diagram shows that the location with zero bending is very close to the location of the bottom of the closed stiffener.

From this, it can be concluded that the eccentricity effect of direct loads can be ignored for the cut-out and cope hole locations. The stresses due to the normal forces are small compared to the effects from crossbeam shear and can be ignored.

4.3 Crossbeam out-of-plane analyses

4.3.1 Out-of-plane model

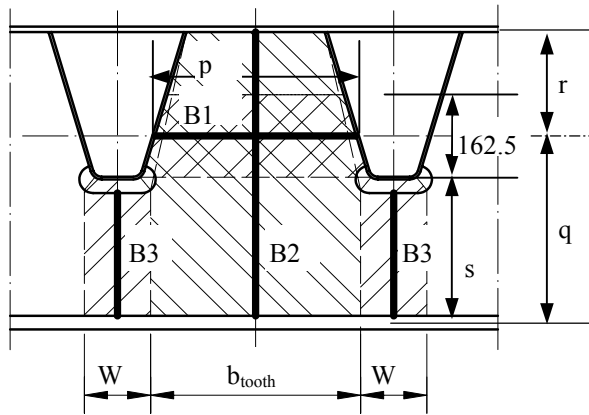


Fig. 4.42 Model for out-of-plane crossbeam behaviour

Vertical loads on the deck between the crossbeams cause out-of-plane rotations of the closed stiffener to crossbeam web connections. Due to these rotations, clamping moments are generated in the connections of the stiffeners to the crossbeams. They act in the web of the crossbeam between the stiffeners and in the crossbeam web below the stiffeners. In case of continuous stiffeners with a cope hole, no connection exists between the closed stiffener bottom and the crossbeam web. Therefore, this “connection” does not participate in the load transfer.

In Fig. 4.42, the tooth is divided into an upper area, which is considered not to participate in the static system and a lower part, which is modelled as a horizontal beam “B1” between the two troughs.

The crossbeam web below the level of the tooth is modelled as two vertical columns “B2” and “B3”. “B2” is connected to the horizontal beam “B1”, the deck plate and the bottom flange. The effective width of the column B2 is assumed not to be affected by the existence of the cope holes.

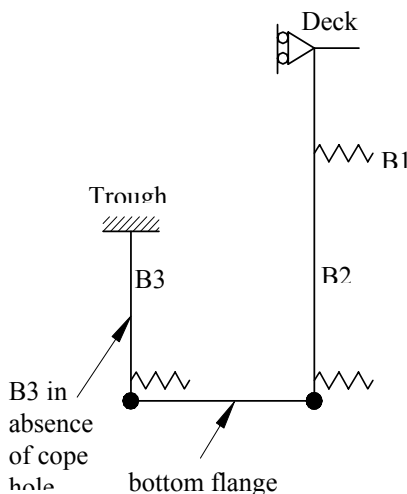


Fig. 4.43 System B1B2 and System B3 in crossbeam out-of-plane model

For crossbeams with close fit stiffeners, the web below the stiffener is modelled with a vertical beam “B3”, connected to the trough bottom and the crossbeam bottom flange. For B3 the width of the notional cut-out enlarged with a cope hole is assumed to be the effective width. Connections with cope holes do not have column B3. The complete system (B1, B2, B3) is shown in Fig. 4.43.

In the following analyses, the bottom flange of the crossbeam is assumed a rigid support in the horizontal direction.

A crossbeam out-of-plane rotation of two adjacent troughs causes bending in the beams B2 and B3.

Due to the stiffening influence from the bottom of the trough, the connection of B1 to the trough is considered clamped. The support of B2 at the deck plate level is considered a hinge; B2 is assumed connected to the bottom flange by a hinge.

The equivalent spring stiffness of the system B1B2 at the connection with the bottom flange can be determined from the stiffnesses of B1 and B2. When B3 exists, it is assumed to be clamped at the bottom of the trough and hinged to the crossbeam bottom flange.

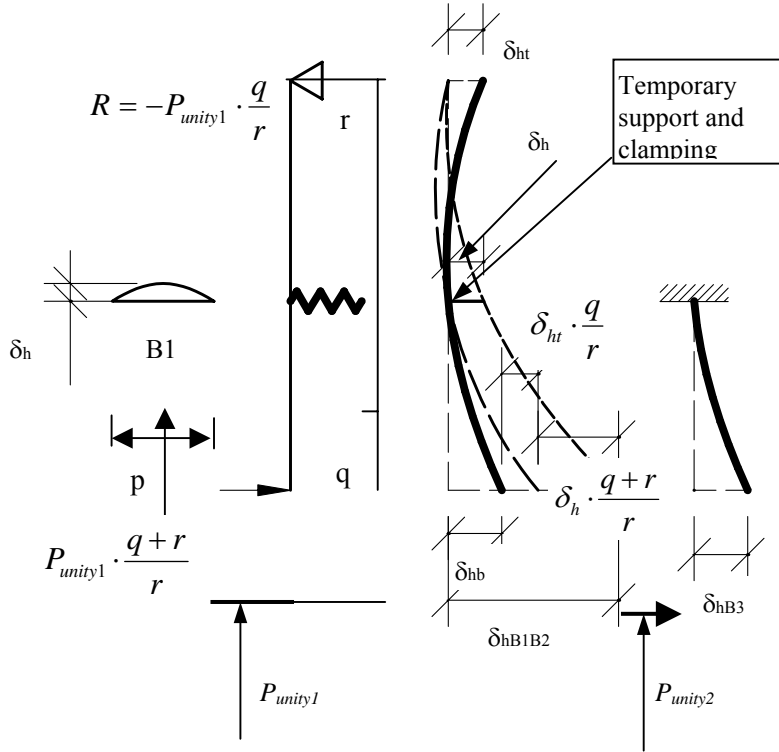


Fig. 4.44 Deflections of Elements in the Systems B1B2 and B3, due to unit loads

Fig. 4.44 shows the behaviour of the systems B1B2 and B3. Hereafter, a unit force P_{unity1} is applied to the System B1B2 at the connection with the bottom flange, which results in a point load on the connection with B1. Here, B1 acts like a spring support for B2.

If a temporary clamping is assumed at B1, the deflections δ_{hb} and δ_{ht} can be calculated.

By rotating Beam B2 about the support at B1 and taking the deformation δ_h of B1 into account, the deflection δ_{hB1B2} at the crossbeam bottom flange is found.

The deflection at the centre of B1, due to a load P_{unity1}

on the lower end of B2 can be calculated with equation [4.45].

$$\delta_h = \frac{r+q}{r} \cdot \frac{P_{unity1} \cdot r^3}{192 \cdot E \cdot I_{B2}} \quad [4.45]$$

The clamping moment M_{cw} at the ends of B1 follows from equation [4.46].

$$M_{cw} = \frac{r+q}{r} \cdot \frac{P_{unity1} \cdot P}{8} \quad [4.46]$$

If, for computation purposes, B2 is temporarily clamped at the connection of B1, the free deflections of B2 at top and bottom locations can be determined. The reaction force P_t at the top follows from equation [4.47].

$$P_t = P_{unity1} \cdot \frac{q}{r} \quad [4.47]$$

The deflection at the top δ_{ht} is calculated with equation [4.48]

$$\delta_{ht} = \frac{P_{unity1} \cdot q \cdot r^2}{3 \cdot E \cdot I_{B2}} \quad [4.48]$$

The deflection at the bottom δ_{hb} can be determined with equation [4.49].

$$\delta_{hb} = \frac{P_{unity1} \cdot q^3}{3 \cdot E \cdot I_{B2}} \quad [4.49]$$

The total deflection at the bottom location of B2 follows from equation [4.50].

$$\delta_{hB1B2} = \frac{q+r}{r} \cdot \delta_h + \frac{q}{r} \cdot \delta_{ht} + \delta_{hb} \quad [4.50]$$

The spring constant K_{B1B2} , which replaces the system B1B2 at the connection to the bottom flange, is found with equation [4.51].

$$K_{B1B2} = \frac{P_{unity1}}{\delta_{hB1B2}} \quad [4.51]$$

Fig. 4.44 also shows the deflection δ_{hB3} at the crossbeam flange level of the system B3 due to a unity load P_{unity2} . As before, the spring constant K_{B3} , replacing the system B3 can be derived, assuming the crossbeam web rigidly clamped in the trough. The horizontal deflection δ_{hB3} of the lower end of the column loaded by a force P_{unity2} is calculated with equation [4.52].

$$\delta_{hB3} = \frac{P_{unity2} \cdot s^3}{3 \cdot E \cdot I_{B3}} \quad [4.52]$$

The clamping moment M_{cb} at the support of the trough bottom is calculated with equation [4.53].

$$M_{cb} = P_{unity2} \cdot s \quad [4.53]$$

The spring constant K_{B3} can be determined from equation [4.54].

$$K_{B3} = \frac{P_{unity2}}{\delta_{hB3}} \quad [4.54]$$

In many bridges, the bottom flange of the crossbeam will act as an elastic support in horizontal direction instead of a fixed hinge support. However, the assumption of a fixed support is on the safe side as it results in the highest clamping moments at the trough to crossbeam connection. Often real bridges have a more complex behaviour.

4.3.2 Global model for the out-of-plane analysis

Since the bending stiffness of the deck plate with stiffeners is much higher than the rotational stiffness of the crossbeam and that of the stiffener to crossbeam connection the assumption that the clamping effect of the crossbeams can be neglected is justified.

4.3.3 Local load transfer analysis

Table 4.10 shows the generated relative force F_i on the crossbeam bottom flange for a unit rotation of the closed stiffener to crossbeam connection, using $H = 600$ mm and $W = 75$ mm as a unit reference. The distribution of these generated relative forces is given over the system B1B2 and the system B3 for a range of crossbeam web depths “H” and (notional) cope hole widths “W”.

For a crossbeam with cope holes, the values for B3 do not apply, but those for system B1B2 can still be used for comparison of the load transfer through the various crossbeams.

For the trough to crossbeam connections without cope holes, the rotational spring constant has a linear relationship with F_i in Table 4.10. The stiffness of the complete connection B1B2 with B3 can be derived from F_i with F_i for $H = 600$ and $W = 75$ as a reference. The values for B1B2 and B3 show the relative distribution.

In the case of trough to crossbeam connections with cope holes the rotational spring constant now has a linear relationship with the product of F_i and B1B2 only.

From Table 4.10 it can directly be concluded that the troughs with wider bottoms generate a slightly weaker behaviour of the B1B2 system and the larger the depth of the crossbeam web, the smaller the generated forces in both systems for both types of details. These observations are in full agreement with the expectations.

Table 4.10, Relative force transfer distribution F_i and distributions over B1B2, B3 at the connections C.4.1.wl, C.4.1.wr (trough web) and C.4.1.bl and C.4.1.br (trough bottom) due to a unit rotation of the stiffener. (For these locations see Fig. 4.45)

Web Depth H (mm)	Width of cut-out W (mm)				
	75	125	175	225	275
	F_i B1B2, B3	F_i B1B2, B3	F_i B1B2, B3	F_i B1B2, B3	F_i B1B2, B3
600	1.000 0.55, 0.45	1.312 0.43, 0.57	1.614 0.35, 0.65	1.905 0.29, 0.71	2.189 0.24, 0.76
800	0.385 0.70, 0.30	0.459 0.58, 0.42	0.529 0.49, 0.51	0.596 0.41, 0.59	0.662 0.35, 0.65
1000	0.208 0.75, 0.25	0.237 0.64, 0.36	0.264 0.55, 0.45	0.299 0.47, 0.53	0.316 0.41, 0.52
1200	0.131 0.78, 0.22	0.145 0.68, 0.32	0.158 0.59, 0.41	0.172 0.51, 0.49	0.185 0.44, 0.56
1400	0.089 0.80, 0.20	0.099 0.70, 0.30	0.106 0.61, 0.39	0.113 0.53, 0.47	0.121 0.47, 0.53
1800	-	-	0.057 0.64, 0.36	-	-
2200	-	-	0.036 0.66, 0.34	-	-

4.3.4 Local stresses

4.3.4.1 Stresses in the crossbeam connections without cope hole

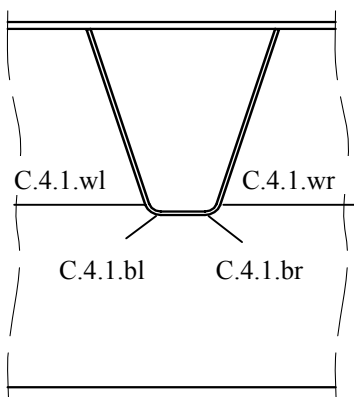


Fig. 4.45 Locations for stresses from out-of-plane rotations

Fig. 4.45 shows the relevant locations C.4.1.wl, C.4.1.wr, C.4.1.bl and C.4.1.br for the out-of-plane effects in the crossbeam web of the connection.

The stresses can be obtained by calculating the bending moments in C.4.1.wl, C.4.1.wr, C.4.1.bl and C.4.1.br from the internal forces in the systems B1B2 and B3. For the calculations of the stresses, the effective width of beam B1 is taken 162.5 mm, being half of the connected length of the stiffener web. For B3 the effective width is taken 105 mm, being the width of the standard trough bottom.

Fig. 4.46 shows, for a rotation of 0.01 rad the nominal bending stresses for the locations indicated in Fig. 4.45.

The stresses at the connection of the trough bottom C.4.1.bl and C.4.1.br are about 1.5 to 4.0 times higher than those at the connection to the trough web C.4.1.w.

It is further shown that the deeper the crossbeam web, the smaller the bending stresses at the connections. The figure also shows that, the wider the trough bottom the smaller the bending stresses at the location C.4.1.w.

This also confirms that trough to crossbeam connections with V-shaped stiffeners will result in higher stresses than trough to crossbeam connections with trapezoidal stiffeners.

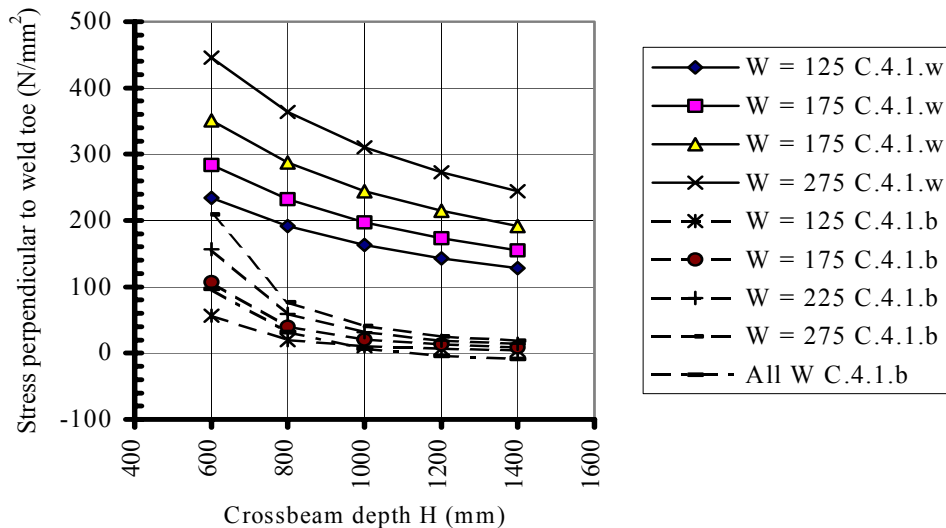


Fig. 4.46 Nominal stresses in the crossbeam web at the trough web and trough bottom connections due to an out-of-plane rotation of 0.01 rad

The fatigue tests in the ECSC research also showed that connections with V-shaped stiffeners have a much shorter fatigue life than connections with trapezoidal stiffeners.

4.3.4.2 Stresses in the crossbeam web at the cope hole

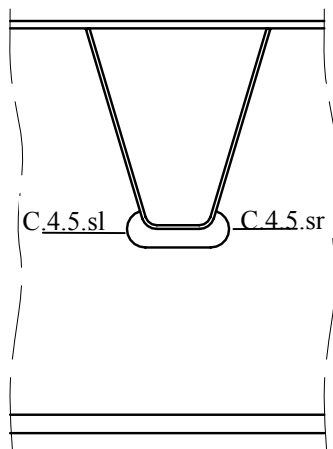


Fig. 4.47 shows the locations C.4.5.sl and C.4.5.sr at the cope hole edge which are relevant for the out-of-plane behaviour. Fig. 4.48 shows for the out-of-plane rotation of 0.01 rad the nominal stresses.

Similar to the locations described in 4.3.4.1 the stresses decrease when the crossbeam web depth increases. Widening the cope holes reduces the stresses. The stress levels are similar to those of the connections C.4.1.wl and C.4.1.wr.

Fig. 4.47 Stress locations at a cope hole

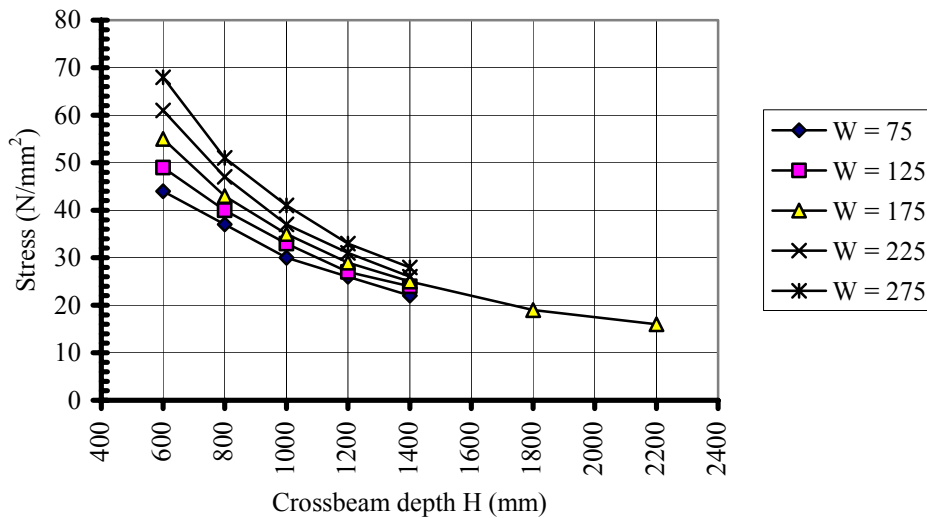


Fig.4.48 Nominal stresses at the crossbeam web cope hole locations C.4.2.sl and C.4.2.sr

4.4 Concluding remarks

4.4.1 Models

In-plane

- For crossbeam bending the conventional crossbeam can be modelled with “equivalent” bending stiffness; for shear with an “equivalent” web thickness, derived from a Vierendeel system.
- For the analysis of the local behaviour and the load transfer the conventional crossbeam can be modelled with a local model, derived from a Vierendeel system. With this model, the nominal stresses in all relevant locations can be obtained.

Out-of-plane

- The conventional crossbeam can be modelled as a beam grid. With this model, the nominal stresses in the relevant locations can be determined.

For the in-plane and out-of-plane crossbeam behaviour and the connection with the trough the local models are suitable for parameter studies.

4.4.2 Results of the analyses

In-plane

- For crossbeam bending the effect of the cut-out with cope holes can be neglected; the “equivalent” bending stiffness is equal to the stiffness of a crossbeam without cut-outs.
- For crossbeam shear the effect of the cut-outs can be taken into account by using a modified thickness for the crossbeam web.
- For the shear transfer in the crossbeam the deformation contribution due to bending of the T-beam below the cut-out can be ignored.
- The tooth length used in calculations for the bending deformation caused by crossbeam shear has to be corrected due to local deformations in the crossbeam web below the tooth.
- The stresses in the trough web caused by a crossbeam bending moment increase for larger cope hole widths
- The stresses in the trough web caused by a crossbeam bending moment depend on the position of the neutral axis of the crossbeam.
- The stresses in the trough web caused by crossbeam shear decrease for wider cope holes and deeper crossbeams.
- The effect of local loads on the troughs on the stresses in the trough to crossbeam connection at the cope hole can be ignored.
- The cope hole edge of wider cope holes shows higher stresses in the crossbeam than narrower cope holes.
- Deeper crossbeams show a decrease of the stresses at the cope hole edge in the crossbeam.
- For the investigated crossbeams, the largest stresses at the cope hole edge occur at the narrowest cross section of the tooth.
- The stresses perpendicular to the weld toe at the trough to crossbeam connection are lower in a connection with a close fit than in connections with a cope hole.

Out-of-plane

- An increase of the width of the trough bottom results in a larger stiffness of the connection for rotation.
- Wider trough bottoms also show an increase of the load transfer from the trough bottom to the crossbeam bottom flange and a decrease of the load transfer from the trough webs through the crossbeam web to the crossbeam bottom flange.
- Narrower troughs show larger stresses in the crossbeam web at the trough to crossbeam connection than wider troughs and deeper crossbeams show lower stresses than shallow crossbeams.

5 GEOMETRICAL STRESS CONCENTRATION FACTORS

5.1 Introduction

In the previous chapters, it has been shown that the closed trough to crossbeam connection is subjected to an in-plane crossbeam loading caused by the load transfer in the crossbeam and imposed out-of-plane rotations caused by the deflections of the troughs.

In 1.3.2.2 the closed trough to crossbeam connection details were classified as “a” and “b”. They are called "a" when the crossbeam web is continuous and the closed troughs are fitted between adjacent crossbeam webs and "b" when the closed trough is continuous and passes the crossbeam web.

In chapter 4 the closed trough connection behaviour was analysed and the nominal stresses were determined. This chapter presents models and a more detailed analysis of the local behaviour around the welded connection detail type "b". From these models the geometrical stress concentration factors (SCF's) due to the local behaviour of the trough to crossbeam connections are derived for the trough web, the crossbeam web and the cope hole.

For some locations, analytical models are only used to obtain insight into the mechanisms, and FE models are used to verify the analytical models and to obtain more accurate stress concentration factors. For some other locations, equations from Roark & Young (1986) are used for the determination of the stress concentration factors.

The fatigue analysis in this thesis will be based on extrapolated geometrical stresses and detail classifications, which means that both must be consistent with each other. In this chapter, the geometrical stress concentration factors near the weld toe are determined with a linear extrapolation, based on the stresses at distances of 0.4 and 1.0 times the plate thickness of the relevant part, as recommended by IIW commission XIII-XV (Hobbacher, 2003).

For most locations these geometrical stresses cannot directly be related to a nominal stress, thus the geometrical stress is related to a reference location, in this case the concentration factor also includes the relationship between the two locations and is indicated with: Concentration (relation) factor. In general, the following applies:

Connections with cope hole

In-plane:

All geometrical stresses at the trough to crossbeam connection are linked by relation factors to a reference stress in the trough web.

Out-of-plane:

All geometrical stresses at the trough to crossbeam connection are linked by relation factors to a reference stress in the crossbeam web.

Cope hole

In-plane and Out of plane: Geometrical stress concentration factors

Connections with close fit

In-plane and Out of plane: Geometrical stress concentration factors

5.2 Models

5.2.1 Connection with a cope hole - trough web

Fig. 5.1 shows the crossbeam and the trough with the welded connection with the analysed part of the structure (hatched areas) and the centre C of the connection.

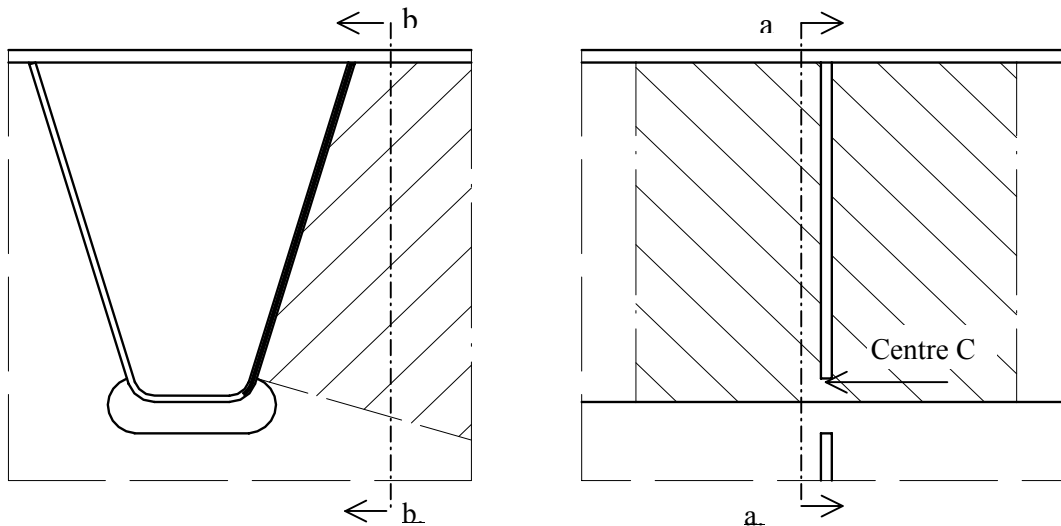
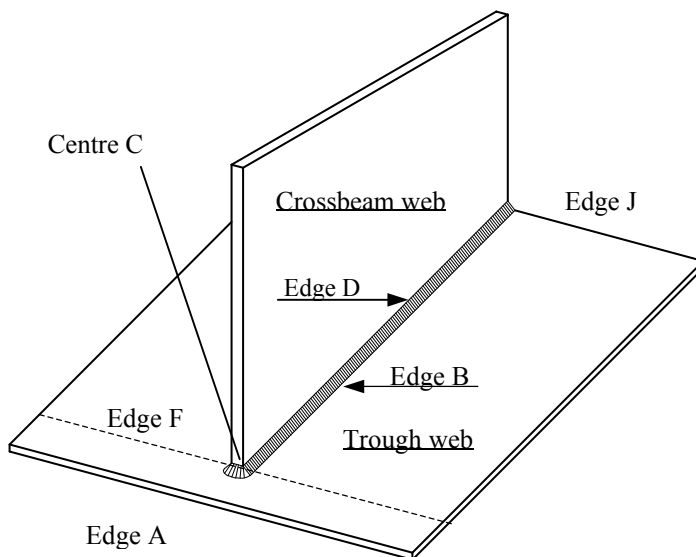


Fig. 5.1 Cross section of the trough (a) and cross section of the crossbeam (b) at the cope hole location

Fig. 5.2 shows an isometric view of the modelled part, the vertical plate represents the crossbeam web and the horizontal plate the trough web.



the crossbeam web with two fillet welds “a” (throat) = 5 mm, which is often used in practice.

Fig.5.2 Modelled part of the stiffener to crossbeam connection

The weld dimensions are taken into account in the analyses because of their relevance compared to the thicknesses of the crossbeam web and the trough.

In practice, the thicknesses of the troughs and crossbeams only vary in a small range.

Therefore, only one set of dimensions is selected for the analysis, namely:

- Crossbeam web plate thickness: $t = 10\text{mm}$.
- Trough thickness: $t = 6\text{ mm}$.
- The trough web is connected to the crossbeam web with two fillet welds “a” (throat) = 5 mm, which is often used in practice.
- The distance from the weld toe to the free edge is 25 mm.

The angle between two adjacent beams is 15° . The free edge is called Edge A and the weld toe at the trough web is called Edge B.

Each beam is considered to be clamped at Edge B, near the centre C. (See Fig. 5.3) The mutual interaction between the beams is ignored.

Edge A, the free end of the beams 1 – 6, is in reality the corner of the trough bottom. In order to obtain results that can be used in conjunction with the frame analyses of the trough bottom as described in chapter 4, the analyses for crossbeam in-plane loading are carried out for the conditions “Edge A hinged and clamped”. For crossbeam out-of-plane loading only the condition “Edge A clamped, but free to translate perpendicular to the plane of the trough web” is considered. The effect of the boundary conditions is further considered in 5.4. The fictitious Edges F of the trough web are assumed to be unsupported. The radial beam properties and boundary conditions are shown in Figs. 5.4 and 5.5 for the free and clamped condition of Edge A. The model is subjected to imposed unit displacements and rotations at Edge A.

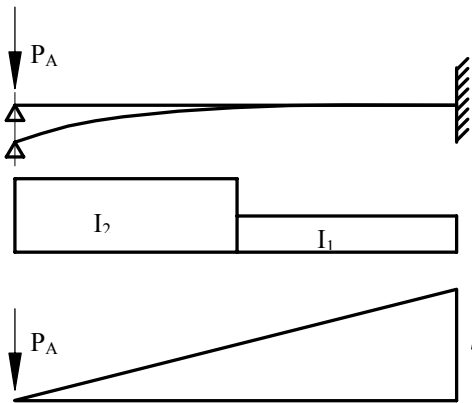


Fig. 5.4 Edge A free

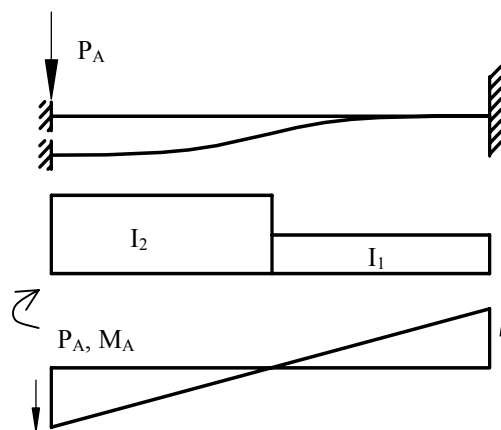


Fig. 5.5 Edge A clamped

Radial beam with end A free

The relationship between an applied force P_A and the rotation of the free end A of a beam with two equal parts with different moments of inertia can be calculated with equation [5.1].

$$\phi_A = \frac{P_A l^2}{8E} \cdot \left(\frac{3}{I_1} + \frac{1}{I_2} \right) \quad [5.1]$$

The relationship between an applied force P_A and the displacement of the free end A of a beam with two equal parts with different moments of inertia can be calculated with equation [5.2].

$$\delta_A = \frac{P_A l^3}{24E} \cdot \left(\frac{7}{I_1} + \frac{1}{I_2} \right) \quad [5.2]$$

The relationship between an applied bending moment M_A and the rotation of the free end A of a beam with two equal parts with different moments of inertia can be calculated with equation [5.3].

$$\phi_A = \frac{M_A l}{2E} \cdot \left(\frac{1}{I_1} + \frac{1}{I_2} \right) \quad [5.3]$$

The relationship between an applied bending moment M_A and the deflection of the free end A of a beam with two equal parts with different moments of inertia can be calculated with equation [5.4].

$$\delta_A = \frac{M_A l^2}{8E} \cdot \left(\frac{3}{I_1} + \frac{1}{I_2} \right) \quad [5.4]$$

In the above equations the rotation and deflection of the free end A were calculated for a load P_A and a bending moment M_A .

For a translation δ_A the load P_A^1 can be calculated with equation [5.5]:

$$P_A^1 = \frac{1}{\delta_A} \quad [5.5]$$

$$Q_A = \frac{P_A^1}{b^1} \quad [5.6]$$

The magnitude of the distributed load along edge A can be calculated by dividing the load P_A^1

by the projected width b^1 on Edge A:

The values of Q_A for the radial beams show the load distribution in the trough bottom.

Radial beam with end A clamped, but free to translate

$$\phi_A = \frac{P_A \cdot l}{8 \cdot E} \cdot \left(\frac{1}{I_1} + \frac{1}{I_2} \right) - \frac{M_A \cdot l}{2 \cdot E} \cdot \left(\frac{1}{I_1} + \frac{1}{I_2} \right) = 0 \quad [5.7]$$

The rotation of the clamped end A caused by a load P_A and the clamping moment at A must be zero, hence:

The translation of end A caused by a load P_A and the clamping moment is given by equation [5.8].

$$\delta_A = \frac{P_A \cdot l^3}{24 \cdot E} \cdot \left(\frac{7}{I_1} + \frac{1}{I_2} \right) - \frac{M_A \cdot l^2}{8 \cdot E} \cdot \left(\frac{3}{I_1} + \frac{1}{I_2} \right) \quad [5.8]$$

The moment M_A and the deflection δ_A can be calculated with equations [5.7] and [5.8] respectively

For unit translation the load P_A^1 and the bending moment M_A^1 can be calculated again with equation [5.5] in combination with equation [5.8].

The clamping moment for each beam at "Edge B" can be calculated with equation [5.9].

$$M_B = P_A^1 \cdot l - M_A^1 \quad [5.9]$$

The bending stresses σ_B at edge B are calculated with equation [5.10].

$$\sigma_B = \frac{M_B}{W_B} \quad [5.10]$$

In this model, the centre-to-centre distance of every beam at the weld toe location is 4 mm and for the further analysis in 5.3, the elastic section modulus is given by:

$$W_B = (4 \cdot 6^2)/6 = 24 \text{ mm}^3.$$

Radial beam with a torsion moment at end A:

When a torsion moment is applied to a beam consisting of two equal parts with two different polar moments of inertia, the rotation at the end A can be calculated with equation [5.11]:

$$\phi_{At} = \frac{M_t}{G} \cdot \left(\frac{l_1}{2I_{t1}} + \frac{l_2}{2I_{t2}} \right) \quad [5.11]$$

FINITE ELEMENT MODEL

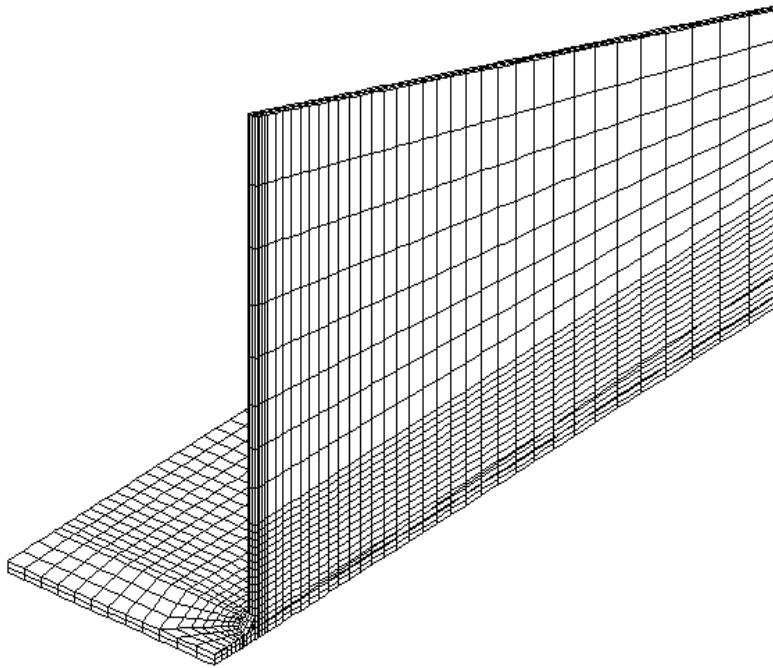


Fig. 5.6 Half FE model of the crossbeam web to trough connection

Half of the FE model of the detail, consisting of 20 node brick elements for the plates and 15 node triangular elements for the welds is shown in Fig. 5.6. It is used for the verification of the analytical model and to determine the geometrical stresses. In order to enable an easy comparison of the stresses from the analytical model with those of the FE model, the nodes of the elements at the weld toe have the same location as the end of the beams of the analytical model.

The imposed deformations (loads) and boundary conditions are also similar to those of the analytical model. Fig. 5.6 shows only a half model in order to display the fine mesh used.

The geometrical stresses at Edge B obtained with this model, are derived from the bending moments of the radial beams. As these bending moment diagrams are linear, the stresses agree with a linear extrapolation to the weld toe from the locations at $0.4t$ and $1.0t$.

5.2.1.1 In-plane behaviour

The in-plane behaviour of the crossbeam is simulated with a uniformly applied displacement of edge A of 1mm. This is simulated in the analytical model with 1 mm applied to each end of the radial beams.

Torsion in the radial beams of the analytical model is assumed to be of minor importance and therefore disregarded in the analyses.

5.2.1.2 Out-of-plane behaviour

The out-of-plane behaviour of the crossbeam is simulated with a rotation of edge A about beam 6, (see Fig. 5.3). This is simulated in the analytical model with different applied deformations to each end of the radial beams, the displacements simulate the applied unit rotation.

The out-of-plane forces, moments and stresses in the analytical model at the end of the radial beams at Edge B can be derived from the in-plane results by scaling.

$$\delta_A = \phi_{unity} \cdot l \cdot \cos \alpha \quad [5.12]$$

The applied end displacement δ_A (see Figs. 5.4 and 5.5) can be derived with equation [5.12]:

The applied unit rotation ϕ_{unity} of Edge A is 0.01 rad.

The end rotation ϕ_A of the radial beam depends on the direction of the radial beam and is found with equation [5.13]:

$$\phi_A = \phi_{unity} \cdot \sin \alpha \quad [5.13]$$

From eqs. [5.12] and [5.13] in combination with eqs. [5.7] to [5.9] the bending moment M_B for every radial beam can be calculated and thus the stresses at the weld toe.

Out-of-plane stiffness of the connection between the crossbeam web and the trough web

In the analyses described in chapter 4, it is assumed that the crossbeam web to closed trough connection acts as fully clamped. In reality, this is not true and the flexibility can be derived with the radial beam model described earlier in this chapter.

In order to investigate the effect of the flexibility on the load transfer through the connection, it is necessary to know the out-of-plane stiffness of the connection.

The clamping moment at location C (see Fig. 5.3) follows from the extrapolated bending and torsion moments in the radial beams at B. In this model, the distance between B and C is 12 mm (distance from weld toe to centre C). Consequently, the bending moment follows from the bending moment M_B and the contribution of the shear load at B, which is equal to P_A^1 .

The bending moment perpendicular to the crossbeam web is obtained by multiplying by $\cos \alpha$ as shown in equation [5.14]:

$$M_{cb} = (M_B + P_A^1 \cdot 12) \cdot \cos \alpha \quad [5.14]$$

The total moment resulting from the bending moments in the beams 1 - 6 and 1¹ - 5¹ is the sum of all moments M_{Cb} .

The torsion moment in each radial beam is found with equation [5.15]

$$M_t = \frac{\phi_{At} \cdot G}{\left(\frac{l_1}{2I_{t1}} + \frac{l_2}{2I_{t2}} \right)} \quad [5.15]$$

The component relevant for out-of-plane behaviour of the connection can be found with equation [5.16]:

$$M_{Ct} = M_{Bt} \cdot \sin \alpha \quad [5.16]$$

In addition to the contribution of the stiffness of the radial beams, the bending stiffness of the trough web perpendicular to the crossbeam web has to be considered. The contribution of this part can be derived from equation [5.17]:

$$M_{Sb} = \frac{6 \cdot E \cdot I_{troughweb} \varphi}{l} \quad [5.17]$$

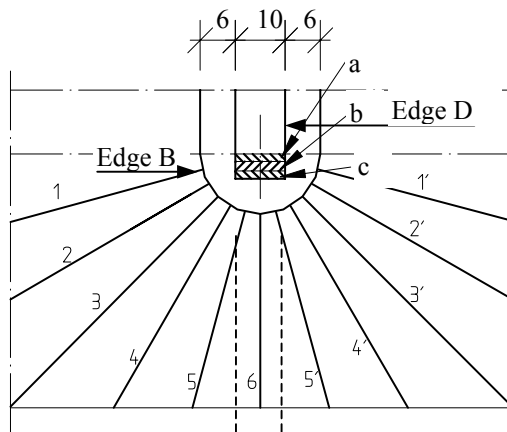
The total out-of-plane bending moment on the crossbeam web for an out-of-plane unit rotation of 0.01 rad at Edge A with respect to location C is given by equation [5.18].

$$M_C = M_{Cb} + M_{Ct} + M_{Sb} \quad [5.18]$$

The rotational spring stiffness of the detail can be determined from the moment M_C and the unit rotation of 0.01 rad.

5.2.2 Connection with a cope hole - crossbeam web

5.2.2.1 In-plane behaviour



The stresses in the crossbeam web at the locations C.4.2 and C.4.3 (in Fig. 5.7 at “c”) can be determined with the load transfer in the radial beams of the trough web model. For the in-plane behaviour, only the support reactions of the radial beams at the Edge B are relevant. The “supporting” area at the Edge D of the crossbeam web in this model is subdivided into three areas for the load introduction of the radial beams. The width of these areas is based on the crossing of the axes of the radial beams with the boundary of the crossbeam web.

Fig. 5.7 In-plane load introduction in crossbeam web

The support reactions are directly related to the imposed deformation of the trough web. These support reactions of the radial beams 1 and 1' are introduced in a part of the web “a” with a cross sectional area of 21.14 mm^2 . The support reactions of beams 2 and 2' are introduced in area “b” with a cross sectional area of 18.3 mm^2 and the support reactions of beams 3, 3', 4, 4', 5, 5' and 6 are introduced in “c” with a cross sectional area of 10.56 mm^2 . The stresses in the area “c” of the crossbeam web are represented by σ_F .

The relationship between the stresses σ_F and the bending stresses of beam 6 at Edge B, for this case with a constant width and constant properties (dotted lines), can be considered to be a “stress concentration factor”.

5.2.2.2 Out-of-plane behaviour

In Fig. 4.42, a global model with Beams B1 and B2 is shown for the out-of-plane load transfer between the trough and the crossbeam.

The Beam B1 has a width of 162.5mm, half the length of the welded connection between the crossbeam web and the trough web.

In this section, the load transfer is described with a simple analytical line model and also with a FE solid model.

Figs. 5.8a and 5.8b show the analytical model for the determination of the geometrical stress concentration factors at the welded connection (Edge D) between the crossbeam web and the trough web. The model in 5.2.1 represents the trough to crossbeam connection between location C and the trough bottom and this model represents the trough to crossbeam connection between location C and the deck plate.

The FE model is shown in Fig. 5.4.

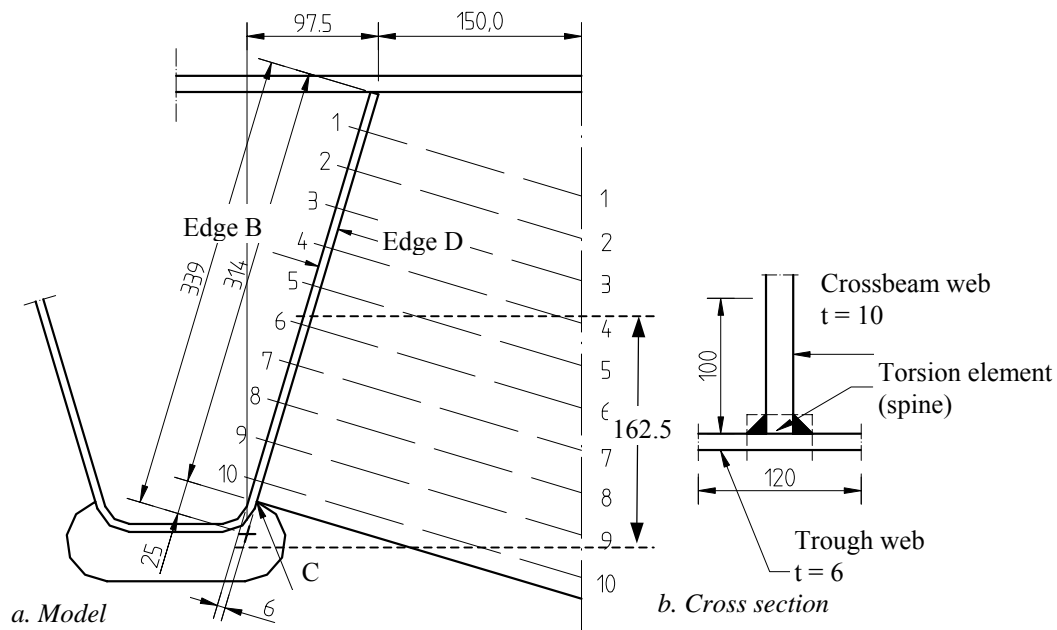


Fig. 5.8 Trough web to crossbeam web connection (dimensions in mm)

The analytical line element model of this connection consists of a spine along the welded connection of 10 elements connected to the middle of the crossbeam web with 10 elements. The spine elements are subjected to torsion and the crossbeam web elements are subjected to bending. The torsion stiffness of the spine depends on the box shape established by the welds, the crossbeam web and the trough web as shown in Fig. 5.8b. The torsion stiffness I_T can be calculated using Roark and Young (1986), Table 20, Item 23. The crossbeam web thickness is 10 mm, the trough web thickness is 6 mm and the two fillet welds have a throat thickness “a” of 5 mm. At each side, a total width of ten times the thickness of each element is assumed to contribute to the torsion stiffness. This will be for the trough web 60 mm and for the crossbeam web 100 mm. The beams are clamped in the middle between two troughs.

For a particular rotation at C, the torsion moment M_C in beam 10 follows from the bending moments in the beams 1 to 10 and the torsion moment at the upper end of the spine.

The stresses calculated in chapter 4 for the beam B1, with a width of 162.5 mm (indicated with dotted lines) are (nominal) reference values in relation to the stress distribution found with the beam model shown in Fig. 5.8a.

The FE model with solid elements and the same dimensions as the analytical model is also used to determine M_C and the stresses at the weld toe Edge D of the crossbeam web.

5.2.3 Crossbeam - cope hole location

For the crossbeam web locations C.4.5.s and C.4.5.b the stress concentration factors for in-plane and out-of-plane loading can also be determined using Roark and Young (1986). The results are compared with the FE calculations for the ECSC 3rd Phase specimens.

5.2.4 Model for the connection with a close fit

5.2.4.1 In-plane behaviour

For the crossbeam web locations C.4.1.w and C.4.1.b (see Fig. 4.45), the stress concentration factors can be determined using Roark and Young (1986).

5.2.4.2 Out-of-plane behaviour

In Roark and Young (1986), no references are available for the determination of stress concentration factors for the loading conditions of this detail.

Therefore, to estimate the stress concentration factors, the results of FE calculations with shell element models carried out in the ECSC 3rd Phase program and in the ECSC 4th Phase program, are used in conjunction with the measured stresses.

5.3 Analyses

5.3.1 Connection with a cope hole - trough web

5.3.1.1 In-plane behaviour

The nominal stresses determined in 4.2.3.3 and 4.2.3.4 for the trough web of a connection with an oval cope hole (Location S.4.2, see Fig.3.4) and for a connection with a “Haibach” cope hole (Location S.4.3, see Fig. 3.5), are obtained from calculations with local strip elements. These elements with a constant width of 4 mm and a length equal to the modified radial beam 6, shown with dotted lines in Fig. 5.7, are subjected to an imposed displacement at Edge A of 1 mm.

Table 5.1 Reference values for the determination of force/stress concentrations

	Edge A free	Edge A clamped
P_A (N)	2.90×10^3	9.30×10^4
Q_A (N/mm ¹)	7.27×10^2	2.00×10^3
M_B (Nmm)	7.26×10^4	1.89×10^5
σ_B (N/mm ²)	3020	6050

Table 5.1 shows the results for the conditions:

Free, respectively clamped at Edge A and clamped in Edge B.

As the imposed deformations are much smaller in practice, the generated forces are much smaller too.

The results at Edge B of Table 5.1 can be used as reference values for the determination of geometrical stress concentration (relation) factors, as radial beam model of Fig. 5.3 is subjected to the same imposed displacement of 1 mm. The forces, moments and stresses from the analytical model with the radial beams (Fig. 5.3) and the above mentioned strip model are shown in Table 5.2.

Table 5.2. Load transfer by radial beam models and strip models with constant width

Type of result, (Beam Nr.)	Edge A free			Edge A Clamped		
	Radial beam model	Strip model	Ratio	Radial beam model	Strip model	Ratio
Q_A (6) N/mm	3.14×10^2	7.26×10^2	0.433	1.92×10^2	2.90×10^3	0.664
M_B (6) Nmm	7.84×10^4	7.25×10^4	1.080	1.89×10^5	1.45×10^5	1.299
σ_B (6) N/mm ²	3270	3020	1.080	7881	6050	1.303
σ_B (5) N/mm ²	3010	-	0.995	7281	-	1.203

Figs. 5.9 and 5.10 show the bending stresses at the weld toe, Edge B for an imposed displacement of Edge A of 1 mm.

The stresses from the analytical models are indicated by “A”, the stresses from the FE results linearly extrapolated from 0.4t and 1.0t to the weld toe by “T” and the reference stresses “Ref” from the constant width strip model.

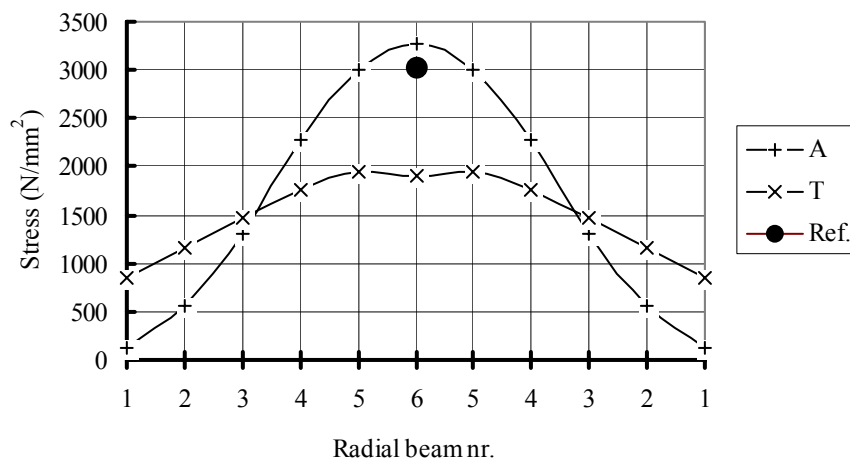


Fig.5.9 Stresses at weld toe (Condition Edge A: free)

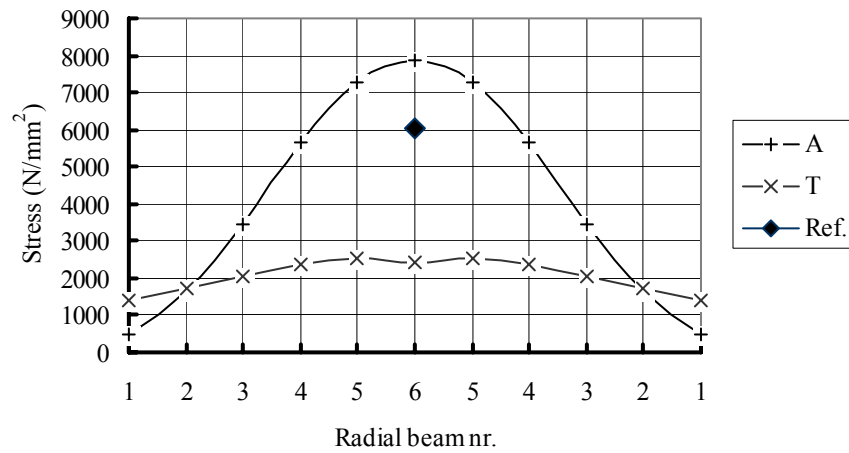


Fig.5.10 Stresses at weld toe (Condition Edge A: clamped)

For both types of boundary conditions at edge A, the FE results for beams 4, 5 and 6 are lower than the analytical results, which indicates that the plate structure redistributes the applied force and shows that the radial beam model of 5.2.1 is extremely conservative.

The division of the beams into two parts with stiffnesses equal to the stiffnesses at the respective ends is too approximate and influences the analytical results, however, treating the radial beams as separate elements has the greatest effect.

The geometrical stress concentration factors for beams 1 - 6 at Edge B are shown in Fig. 5.11, where all factors relate to the reference stress for the clamped location of the strip with constant width at Edge B.

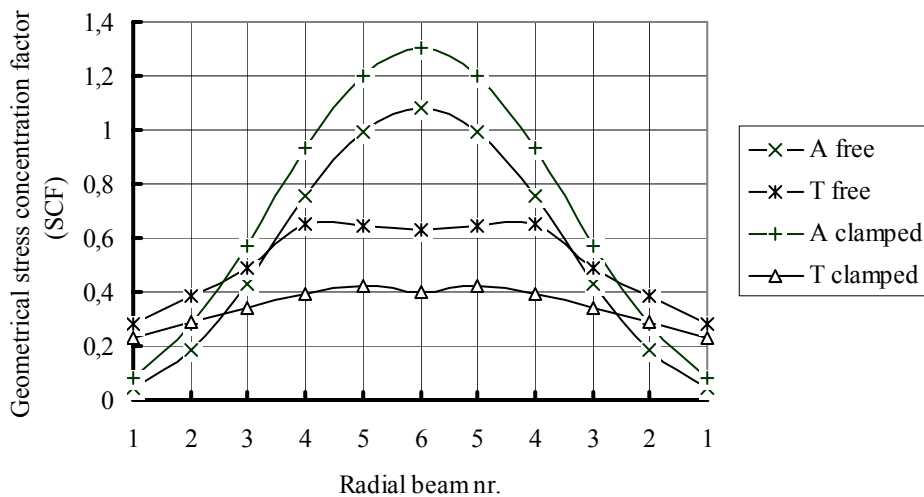


Fig. 5.11 Geometrical stress concentration (relation) factors for the through web in relation to the through web reference for crossbeam in-plane loading

5.3.1.2 Out-of-plane behaviour

The stiffness of the connection and the bending moment in the crossbeam web between the troughs can be derived from the moment at C (see Fig. 5.3) for a relative rotation of 0.01 rad at Edge A.

Table 5.3 shows the analytically determined contributing moments and the moment at C resulting from the FE analysis.

Table 5.3 Moments at C (in kNm) due to a rotation of 0.01 rad of Edge A with respect to C

Contribution from	Analytical method	FE
Bending in radial beams (equation [5.14])	0.168	-
Torsion in radial beams (eqs. [5.15], [5.16])	0.046	-
Bending in the trough webs (equation [5.17])	0.227	-
Sum (equation [5.18])	0.441 kNm	0.446 kNm

From the moment at C (analytical method) the spring constant for the rotation of the connection is:

$$K_{RCa} = 44.1 \text{ kNm/rad}$$

The FE analysis gives:

$$K_{RCn} = 44.6 \text{ kNm/rad}$$

Thus, the spring constant found with the analytical method agrees very well with that of the FE analysis.

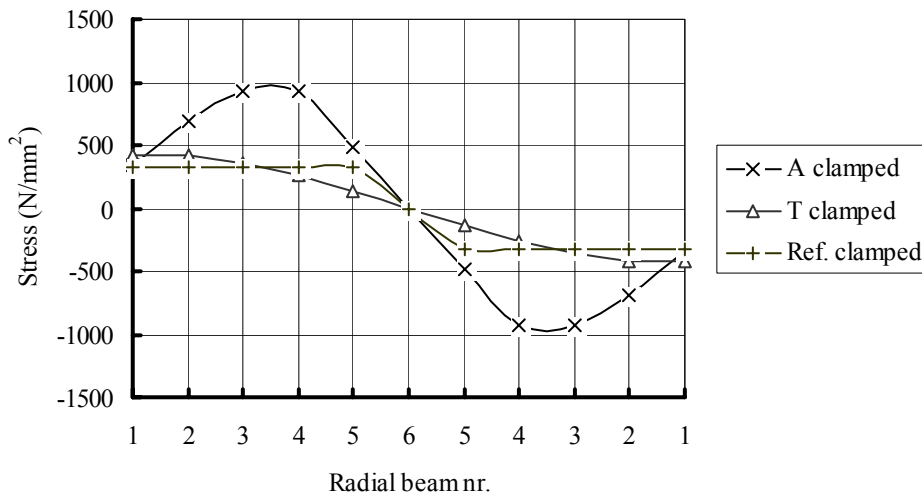


Fig. 5.12 Stresses at weld toe of crossbeam web for crossbeam out-of-plane

The nominal calculated bending stress in the strip B1 of Fig. 4.42 due to the moment M_C (for $b = 162.5$) is taken as the reference stress for the determination of the stress concentration factors. The stresses in the notional beams of the model shown in Fig. 5.3 and the adjacent trough webs can be calculated with a similar procedure as used for the in-plane bending stresses. They are shown in Fig.5.12, together with the reference (nominal) stress in beam B1 from the FE model at the weld toe, indicated by “Ref. clamped”.

The maximum stresses from the analytical procedure “A clamped” are much higher than the extrapolated stresses to the weld toe “T clamped” determined with the FE model. The maximum analytical stresses occur at the beams 3 and 4 and at beam 2 in the FE results.

The stresses obtained with the FE model show that the load transfer takes place over a larger distance along the crossbeam web than is assumed with the analytical radial beam model. In addition, in the analytical model the carry-over effects between the radial beams are ignored, therefore, the results from the FE models will be used in further analyses.

The stress concentration (relation) factors related to the reference stress in beam B1 are shown in Fig.5.13.

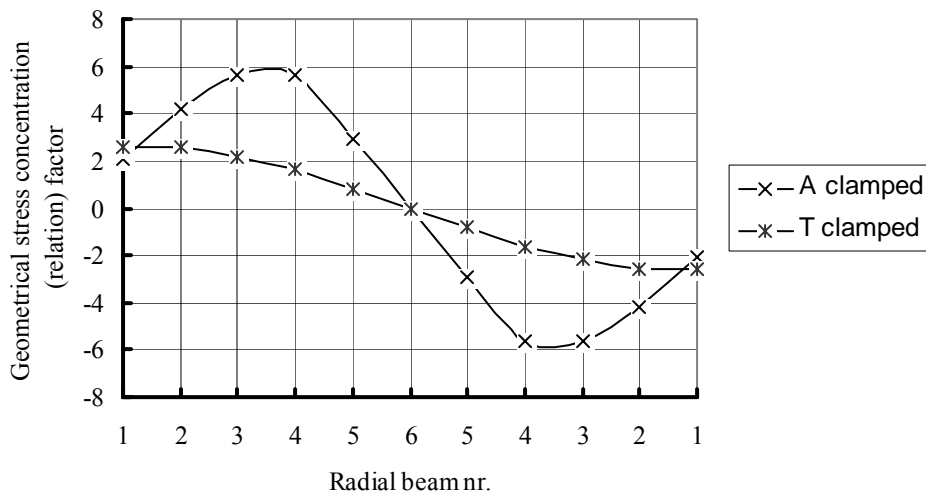


Fig. 5.13 Stress concentration (relation) factors at weld toe of trough web for crossbeam out-of-plane

5.3.2 Connection with a cope hole - crossbeam web

5.3.2.1 In-plane behaviour

For the crossbeam web with an oval cope hole (Location C.4.2, see Fig. 3.4) and a “Haibach” cope hole (Location C.4.3, see Fig.3.5), the load transfer is determined with the model shown in Fig. 5.7. In the analytical model, the load transfer is determined for small elements over a distance of 5 mm (areas “a”, “b” and “c”).

For the condition where Edge A is free a maximum stress is found of 1341 N/mm² and for the condition where Edge A is clamped a maximum stress is found of 8542 N/mm² due to a displacement of Edge A of 1 mm.

These stresses are much higher than the stresses extrapolated to the weld toe (Edge D), found with the FE model (T) and shown in Fig. 5.14.

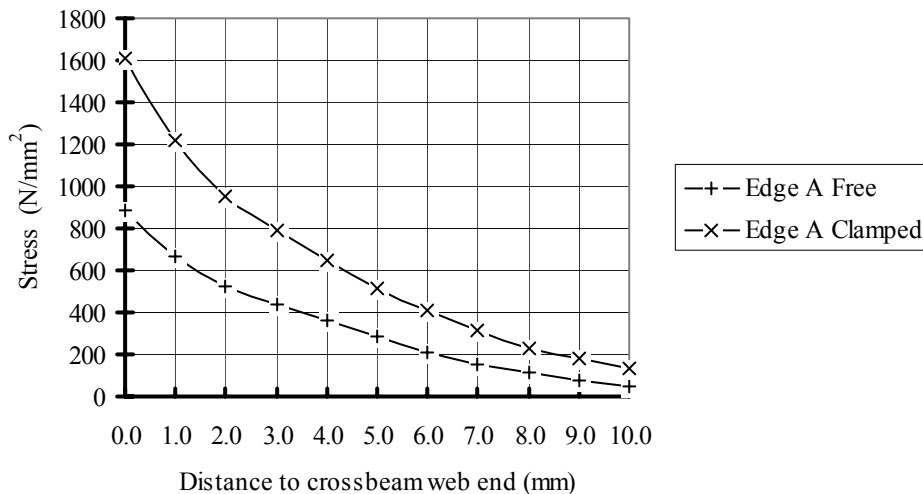


Fig.5.14 Stresses (FE) extrapolated to the weld toe (Edge D) for crossbeam web in-plane at weld toe

The stresses at the end of the crossbeam web are extrapolated. In the analytical model the load transfer was based on the assumption that the radial beams would directly introduce their loads into the crossbeam web.

From the results of the FE model, it is concluded that the trough web distributes the stresses much more effectively than is assumed in the model with separate radial beams. The extrapolated stresses from the FE model can be related to the bending stress in the trough web for the strip model at beam 6 (see Table 5.2) and based on these stresses the resulting stress concentration (relation) factors are:

- Edge A free: SCF = 0.29
- Edge A clamped: SCF = 0.27

For the further analyses a stress concentration (relation) factor SCF = 0.3 is adopted.

5.3.2.2 Out-of-plane behaviour

Fig. 5.15 shows the geometrical stress concentration factors determined with the analytical method (indicated with A) and the stress concentration (relation) factors determined with the FE model (T) all related to the reference nominal bending stresses in B1 (Ref. value B1)(Figs 4.42).

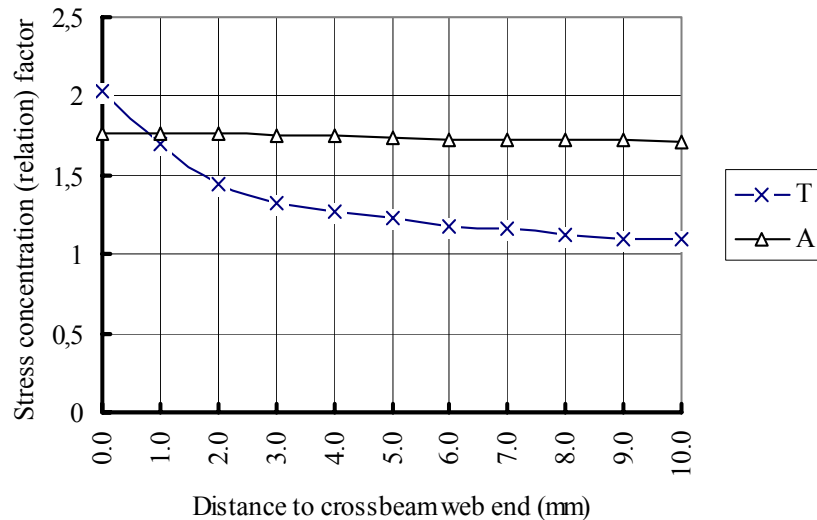


Fig. 5.15 Stress concentration (relation) factors

With the analytical beam model of Fig. 5.8a and b, the stress concentration (relation) factors are determined from the bending moments in the beams 1 – 10. For the FE model the stress concentration (relation) factors are directly derived from the bending stresses in the crossbeam web.

The following geometrical stress concentration (relation) factors are derived with respect to the reference stress in B1:

Analytical model: SCF = 1.77
 FE model (extrapolated): SCF = 2.03

The analytical beam model can be considered to be less accurate, as the beam models are discontinuous and torsion constraints etc. are ignored; therefore the stress concentration (relation) factor from the FE model will be used for further analyses.

5.3.3 Crossbeam - cope hole location

5.3.3.1 In-plane behaviour

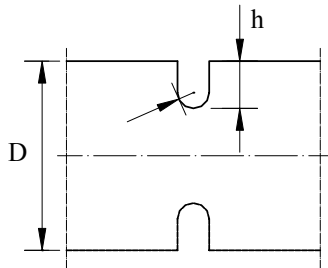


Fig. 5.16 Geometry parameters for scf

For the determination of the geometrical stress concentration factors at the cope hole locations (Locations C.4.5.s and C.4.5.b, see Figs. 3.4, 3.5 and 4.33) use is made of Roark and Young (1986), Table 37, ref. 1b, see Fig. 5.16.

In practice, the depth of the cut-out with cope hole shows some variation, but it is always near 350 – 360 mm. Here, for location C.4.5.b the value h is taken as 360 mm, which is the depth of the cut-out with cope hole of the crossbeam tested for the ECSC 4th Phase program. D is taken as twice the distance from the neutral axis of the T-beam of the test crossbeam below the cope hole to the deck which is 1330 mm. The cope hole radius r is 35 mm, so the value $h/r = 360/35 = 10.39$. For the crossbeams described in chapter 4, h/r is $350/25 = 14.00$. D is different for each crossbeam, e.g. for the crossbeam with $H = 1400$ mm $D = 2010$ mm. The geometrical SCF is calculated with:

$$SCF = K_1 + K_2 \cdot \left(\frac{2h}{D}\right) + K_3 \cdot \left(\frac{2h}{D}\right)^2 + K_4 \cdot \left(\frac{2h}{D}\right)^3 \quad [5.19]$$

For location C.4.5.b: SCF = 2.7 (for the ECSC 4th Phase crossbeam)
 SCF = 3.0 (for the crossbeam of chapter 4 with
 H = 1400 mm)

For location C.4.5.s the same model is used, but now h is half the length of the cut-out being $175/2 = 87.5$. The radius r of the ECSC crossbeam is again 35 and h/r becomes 2.5. D is taken as the centre-to-centre distance of the troughs and equals 600 mm. The geometrical SCF is again calculated with equation [5.19]. For all crossbeams described in chapter 4, r is 25 mm and the dimensions are similar to the ECSC crossbeam.

For location C.4.5.s: SCF = 2.4 (for the ECSC 4th Phase crossbeam)
 SCF = 2.7 (for all crossbeam depths of chapter 4)

The measured SCF value at location C.4.5.s found in the ECSC research is 2.5. As discussed in 2.5.1, depending on the shape and the curvature of the cope hole, for location C.4.5.s, SCF values are found ranging from 1.6 – 3.3.

5.3.3.2 Out-of-plane behaviour

The stress concentration factors for the cope hole locations C.4.5.s and C.4.5.b are again calculated using Roark and Young (1986) Table 37, but now with ref.1c, which has different values for the factors K. The geometry is similar to that in 5.3.3.1 and the geometrical stress concentration factors are calculated with equation [5.19].

For location C.4.5.b: SCF = 2.2 (for the ECSC 4th Phase crossbeam)
 SCF = 2.6 (for the crossbeam of chapter 4 with
 H = 1400 mm)

For location C.4.5.s: SCF = 1.7 (for the ECSC 4th Phase crossbeam)
 SCF = 1.8 (for all crossbeam depths of chapter 4)

5.3.4 Connection with a close fit - crossbeam web

5.3.4.1 In-plane behaviour

The stress concentration factors for the cope hole locations (Locations C.4.1.w and C.4.1.b, see Figs. 3.3 and 4.35) are also calculated using Roark and Young (1986) Table 37, ref.1b.

For location C.4.1.b the value h is taken as 325 mm, which is the depth of the cut-out of the crossbeam. D is taken as twice the distance from the neutral axis of the T-beam of the test crossbeam to the deck and is 1302 mm. The radius r of the close fit is 31 mm, so the value h/r = 360/31 = 10.48. The geometrical SCF is calculated with:

$$SCF = K_1 + K_2 \cdot \left(\frac{2h}{D}\right) + K_3 \cdot \left(\frac{2h}{D}\right)^2 + K_4 \cdot \left(\frac{2h}{D}\right)^3 \quad [5.20]$$

For location C.4.1.b: SCF = 3.1

For location C.4.1w the same ref. 1b is used, but now h is half the length of the cut-out, being 105/2 = 52.5. The radius r is again 31 and h/r becomes 1.69. D is taken as the centre-to-centre distance of the troughs and equals 600 mm. The geometrical SCF is again calculated with equation [5.19]:

For location C.4.1.w: SCF = 1.7

It should be noted that the Roark model results could not be verified with measurements of the ECSC 4th Phase program, however, it is expected that the calculated SCFs will be higher than the actual ones due to the effective part of the trough being ignored.

5.3.4.2 Out-of-plane behaviour

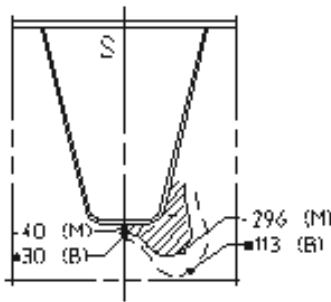


Fig. 5.17 Stress distribution at close fit connection

For the connection with a close fit the stress concentration factors are based on the measured and calculated value in location C.4.1.w in the ECSC 3rd Phase program and in the ECSC 4th Phase program.

Fig. 5.17 shows an example of the distribution of the stresses perpendicular to the weld around the connection for a vertical load on the deck in combination with an out-of-plane rotation. The load causes the membrane stresses (M) due to in-plane load transfer and the bending stresses (B) due to out-of plane rotations, obtained with a FE shell element model for the ECSC 3rd Phase program.

The concentration effect at C.4.1.b for out-of plane bending is approximately 1.6.

From similar FE calculations for the ECSC 4th Phase program a stress concentration factor of 1.3 was derived. As an arbitrary solution is chosen:

$$\text{For location C.4.1.b: } SCF = 1.6$$

Fig. 5.17 shows that the bending stress due to out-of-plane behaviour is almost constant over the curved part of the trough bottom, but the load and boundary conditions of this test specimen do not represent the “built in” situation in real structures.

$$\text{For location C.4.1.w: } SCF = 1.0, \text{ in relation to the nominal stress in beam B2 of the crossbeam web}$$

5.4 Boundary condition effects

5.4.1 In-plane support conditions

The stress concentration factors for the in-plane crossbeam behaviour have been calculated in 5.3.2.1 and 5.3.2.1 for the boundary conditions of Edge A “free” and “clamped”. As a simplification however, the maximum values of these analyses were chosen for the use in further calculations.

5.4.2 Out-of-plane support conditions

The rotation stiffness K_{RC} at C as determined in 5.3.1.2 influences the moment transfer in the connection between the trough web and the crossbeam web.

The results of the analyses in 4.3.3 and 4.3.4 for the connection of beam B1, shown in Fig. 4.42, are related to a rigid connection; however, in reality the connection is flexible.

By comparing the moment in a flexible connection with that for a rigid connection the clamping ratio C_R can be determined and it is possible to estimate whether the results in chapter 4 are directly applicable for further analysis, or have to be reduced.

W	C_R
75	0.80
125	0.79
175	0.78
225	0.75
275	0.58

Table 5.4 shows the clamping ratio C_r ; these are based on the bending moments determined with the rotational spring stiffness at C based on the FE analyses (see 5.3.1.2) divided by the clamping moment for a rigid connection.

The conclusion is, that the “fully clamped” condition is a conservative assumption for a fatigue damage calculation, because for realistic cut-out widths a moment reduction of 20% could be used.

5.5 Summary of concentration factors

Figs. 5.19 and 5.20 show the locations of the reference stresses and the locations of the stress concentration (relation) factors at the weld toe (C 4.2b) of a connection with a cope hole. Figs. 5.19 and 5.20 also show the locations of the geometrical stresses at the ends of the radial beams 1, 2, etc. near the weld toe at edge B (Location S 4.2, see Figs. 3.4 and location S 4.3, see Fig.3.5) for the trough in decks with cope hole connections and the locations of the crossbeam web (Location C.4.2b, see also Figs. 3.4 and 4.33, Location C.4.3, see also Figs.3.5 and 4.35).

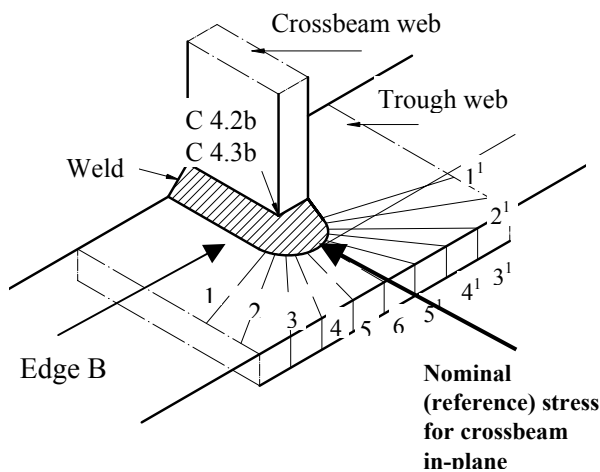


Fig. 5.19 Stress concentration factor locations for crossbeam in-plane loading for a cope hole

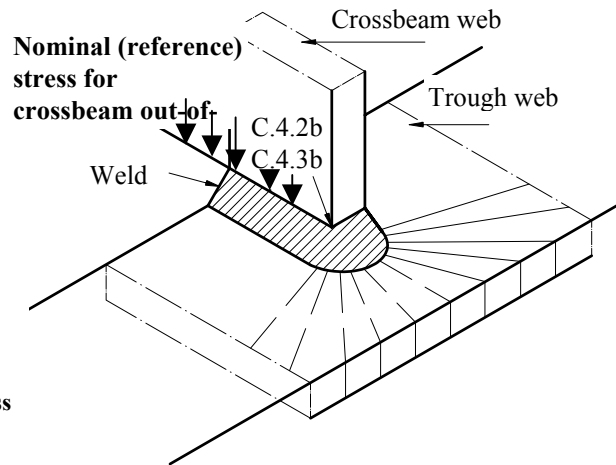


Fig. 5.20 Stress concentration factor locations for crossbeam out-of-plane loading for a cope hole

Figs. 5.21 and 5.22, show the remaining locations at the crossbeam web.

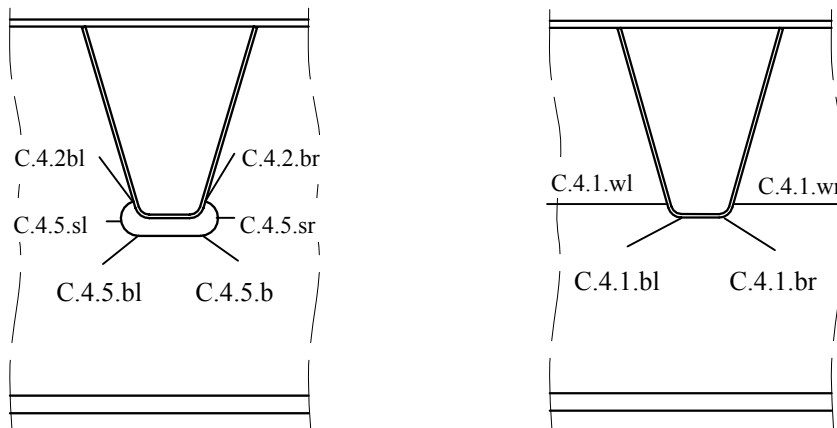


Fig. 5.21 Locations for connection with cope hole Fig. 5.22 Locations for connection without cope hole

An overview of all stress concentration (relation) factors is presented in Table 5.5, which is a brief summary of all stress relations determined in this chapter.

Table 5.5 Overview of stress concentration (relation) factors

Locations		Crossbeam In-plane Loading		Crossbeam Out-of-plane Loading	
Edge B	Radial Beam	$\sigma_{nom.}$ at trough web is nominal (reference) stress		$\sigma_{nom.}$ at crossbeam web (B1) is nominal (reference) stress	
S.4.2					
S.4.3	1	0.3 (1)		2.6 (1)	
	2	0.4 (1)		2.6 (1)	
	3	0.5 (1)		2.2 (1)	
	4	0.7 (1)		1.6 (1)	
	5	0.6 (1)		0.8 (1)	
	6	0.6(1)		0	
Crossbeam web Locations C.4.2b, C.4.3b		0.3 (1)		2.0 (1)	
		Nominal stress in cross section of tooth is reference stress		Nominal stress in cross section of tooth is reference stress	
Cope hole		r = 35		r = 25	
Location C.4.5.s		2.4	2.7	2.2	1.7
Location C.4.5.b			3.0	2.6	1.8
Crossbeam web close fit Location C.4.1.w Location C.4.1.b		1.7 (1) 3.1 (1)		1.2* (1) or 1.1** 1.6 (1) *(with stress below trough as nominal (reference) stress) ** (with stress at considered location as reference stress)	

r = radius of cope hole,

(1) = includes relation between two different locations

Note:

The stresses for the in-plane behaviour of the crossbeam are related to the nominal stress at the weld toe in the trough web at the cut-out (Reference stress in-plane). The stresses for the out-of-plane behaviour of the crossbeam are related to the stresses at the weld toe of the crossbeam web at the cut-out edge (Reference stress out-of-plane).

Where available, the highest concentration (relation) factors resulting from the FE analyses for Edge A free and clamped have been selected for further analyses in the following chapters.

5.6 Concluding remarks

The stress distributions determined in this chapter are based on analytical and FE models and give a good indication where high stresses can be found. Further, the geometrical stress concentration (relation) factors determined are easy to use in conjunction with the nominal stresses at the reference locations and the fatigue detail classifications. The analytical models are suitable for obtaining insight into the behaviour of the connections but are not sufficiently accurate for use in real applications.

6 TRANSFER FUNCTIONS

6.1 Introduction

The mechanical system acting in the crossbeams and the nominal stresses resulting from in-plane unit loads and out-of-plane unit rotations have been described in chapter 4. The Hot Spot stresses can be calculated with the geometrical stress concentration factors as determined in chapter 5.

This chapter deals with the transfer of traffic load effects from the deck to the crossbeams and shows how the histories of the crossbeam section forces, the histories of the imposed deformations (rotations) and the histories of the deck bending moments can be calculated.

The vehicle configurations and the individual axle loads affect the time histories of the reactions, the rotations and the deck bending moments of the trough to crossbeam connection. The time histories are derived for the typical vehicles in ENV 1991-1-3, Fatigue load model 2 (Frequent loads, FLM2) with the influence lines that are determined for single axle loads. From these load, rotation and deck bending moment histories, the maximum intervals can be calculated, using the vehicle type distributions in ENV 1991-3, Table 4.7 (Set of equivalent lorries) and they can be used for the determination of the equivalent number of cycles for each lorry and for all lorries on a particular crossbeam.

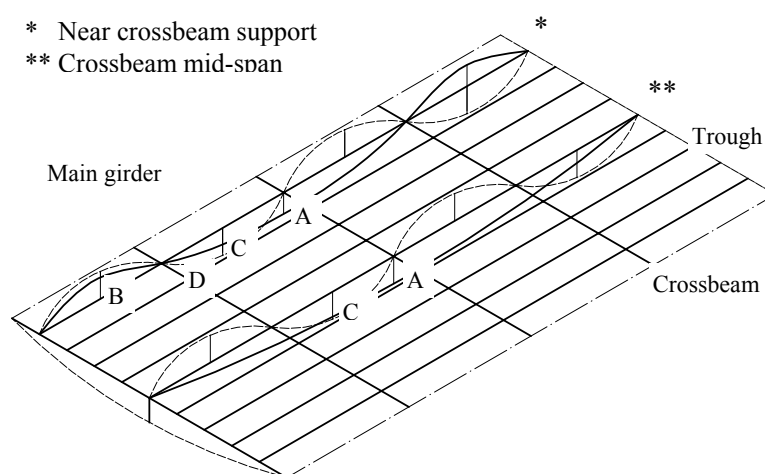


Fig.6.1 Bridge deck troughs with typical influence lines for the middle crossbeam

Fig. 6.1 shows typical influence lines for crossbeam loads (continuous lines) and reactions (dotted lines) of the middle crossbeam and trough to crossbeam connection rotations in relation to moving loads travelling in the direction of the troughs. The influence lines near the main girder are for beams on rigid supports and those at the crossbeam mid-span location are for beams on flexible supports.

The influence lines with extreme values A and B are for crossbeam loads and those with C and D are for trough to crossbeam connection rotations.

In this chapter, the effects of rigid and flexible supports are considered in more detail for the influence lines and the traffic induced load histories, rotation histories and the deck bending moment histories. The following models are used:

1. Analytical model of a deck, substituted by a continuous beam on 5 spring supports
2. FE 2D beam model on 5 spring supports
3. 3D FE model with shell elements, comprising a deck plate with trapezoidal troughs supported by 5 crossbeams.

The 2D and 3D FE models are used to verify the influence lines resulting from the analytical model and the 2D FE model is used for additional parameter studies.

6.2 Structural dimensions and properties investigated

The crossbeam dimensions analysed in chapters 4 and 5 are used as a basis for the analyses presented in this chapter. Two typical cross sections of the conventional crossbeam are shown in Fig. 6.2.

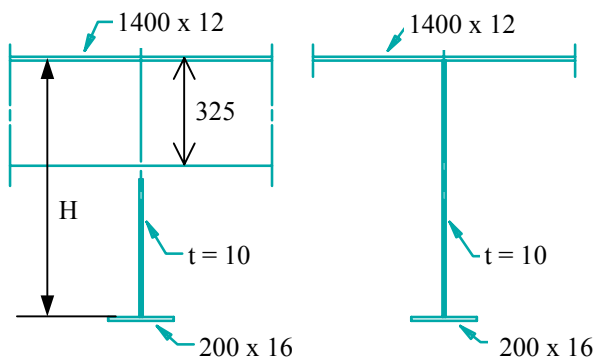


Fig. 6.2 Typical cross sections of conventional crossbeams

Table 6.1 gives an overview of the crossbeams analysed and, using the abbreviations listed below, the analyses carried out and the results to be derived from the analyses

The analysed conventional crossbeam web depths are the same as those considered in chapter 4 with the addition of type 7 ($H = 1800$ mm and $W = 175$ mm) and type 9 ($H = 2200$ mm and $W = 175$ mm).

In this case, only beams with a span of 7200 mm are analysed.

Abbreviations used in Table 6.1:

	Method	Abbreviation
Analyses	Analytical	A
	FE beam grid model	FE-G
	FE shell model	FE-S
	Selected value for a spring stiffness	Z
Type		
Results	Crossbeam spring stiffness based on equivalent crossbeam properties	K_C^1
	Deck spring stiffness including the effect of the equivalent crossbeam stiffness of two crossbeams at both sides of the considered crossbeam	K_D^1
	Influence line for the vertical reaction	I_{Ps}
	Influence line for the trough to crossbeam rotation	I_{Rs}
	Influence line for the bending moment in the deck (lane)	I_{Mds}
	Vertical reaction history for a trough span of 3500, 4000 and 4500 mm	H_{Pr}, H_{Ps}, H_{Pt}
	Trough to crossbeam rotation history for a trough span of 3500, 4000 and 4500 mm	H_{Rr}, H_{Rs}, H_{Rt}
	Bending moment history in the deck (lane) for a trough span of 4000 mm	H_{Mds}

The values of “Z” for K_C^1 are arbitrarily chosen in order to investigate the effect of higher crossbeam stiffnesses; they can be linked to deeper crossbeams not investigated in the study.

Table 6.1 Overview of crossbeam types and calculation results and abbreviations

Crossbeam type	Web depth (mm)	Cope hole width W (mm)				
		H	W=75	W=125	W=175	W=225
1	600	-	-	$K_C^1, K_D^1: A$ $I_{Ps}, I_{Rs}, I_{Mds}: A$ $H_{Ps}: A, FE-G; H_{Pr}, H_{Pt}: A, FE-G$ $H_{Rs}: A, FE-G; H_{Rr}, H_{Rt}: A, FE-G;$ $H_{Md}: A$	$K_C^1, K_D^1: A$	$K_C^1, K_D^1: A$
2	800					
3	1000					
4	1200					
5	1400					
7	1800	-	-	-	-	-
9	2200	-	-	-	-	-
10	-	-	-	$K_C^1: Z, K_D^1: A$ $I_{Ps}, I_{Rs}, I_{Mds}: A$ $H_{Ps}: A, FE-G; H_{Pr}, H_{Pt}: A, FE-G$ $H_{Rs}: A, FE-G; H_{Rr}, H_{Rt}: A, FE-G;$ $H_{Md}: A$	-	-
11	-	-	-		-	-
12	-	-	-		-	-
13	-	-	-		-	-

6.3 Modelling of the deck with the crossbeams

For the analytical model and the 2D FE model, the deck is modelled as a single continuous beam with equivalent mechanical properties EI_D , representing the stiffened deck plate on spring supports K^1_C , emulating the crossbeams (see Fig 6.3).

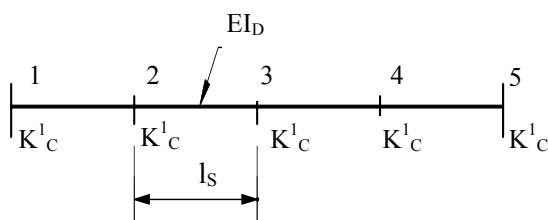


Fig. 6.3 Beam on vertical spring supports

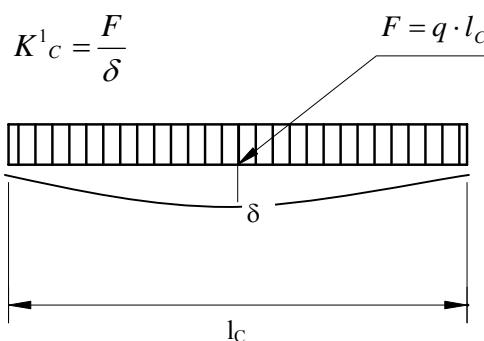


Fig. 6.4 Equivalent spring stiffness K^1_C of crossbeam

The crossbeam spring stiffness K^1_C is defined here as the total uniformly distributed load on the crossbeam, divided by the deflection at mid-span, see Fig. 6.4. The analyses of partially loaded crossbeams are described in 6.4.2.

In these calculations, the rotational stiffness of the crossbeams (out-of-plane) is ignored, since the bending stiffness of the deck is much higher than the rotational stiffness of the crossbeam and the local out-of-plane bending stiffness of the crossbeam web.

6.3.1 Equivalent vertical spring properties for the fully loaded crossbeam

In the analytical models and the 2D FE model, the crossbeams are represented by vertical spring supports.

In the AISC Design Manual (1963), the bending moments were considered to be the only cause of the deflection. A symmetric sinusoidal loading was assumed to cause a sinusoidal in-plane deflection line due to bending of the crossbeam. The deck and crossbeam behaviour was linked by Fourier functions.

Comparison of a deflection line caused by bending due to a symmetrical sinusoidal load with a parabolic deflection line caused by a uniformly distributed load showed that the results were about the same and that a parabolic deflection line is a good approximation.

Therefore, in the analysis presented here, uniformly distributed line loads are used to calculate the crossbeam in-plane deflections due to bending moments and shear forces. The loads are identical to those in chapter 4.

The sum of the loads is:

$$F = q \cdot l_C \quad [6.1]$$

The deflection at mid-span from bending is:

$$\delta_M = \frac{5 \cdot F \cdot l_C^3}{384 \cdot E \cdot I_C^1} \quad [6.2]$$

The equivalent bending stiffness in equation [6.2] is $EI_C^1 = c_b \cdot EI_C$ as described in 4.2.1.1.

The deflection at mid-span due to shear is:

$$\delta_{Sh} = \frac{F \cdot l_C}{4 \cdot G \cdot A_C^1} \quad [6.3]$$

The equivalent shear stiffness in equation [6.3] is $GA_C^1 = c_s \cdot GA_C$ as described in 4.2.1.3.

The total deflection δ_{total} is the sum of the deflections from bending δ_M and shear δ_{Sh} , including the effect from the equivalent section properties due to the cut-outs.

$$\delta_{total} = \delta_M + \delta_{Sh} \quad [6.4]$$

The spring constant K_C^1 of a spring, which substitutes the crossbeam with equivalent properties for bending and shear is as given in equation [6.5]:

$$K_C^1 = \frac{F}{\delta_{total}} = \frac{1}{\frac{5 \cdot l_C^3}{384 \cdot E \cdot I_C^1} + \frac{l_C}{4 \cdot G \cdot A_C^1}} \quad [6.5]$$

6.3.2 Equivalent vertical spring properties for the deck

As stated above, in the analytical model and the 2D FE model, the deck (deck plate with troughs) is represented by a continuous single beam, supported by vertical springs.

For the determination of the properties of this beam, a parabolic deflection line is assumed for the crossbeam due to a uniformly distributed load.

The deck bending stiffness EI_D can be derived from the bending stiffness of an individual trough with the deck plate EI_S , because the shear deformation of the deck plays a negligible role. The deflection line of the deck in transverse direction at the crossbeam location will have the same shape as the deflection line of the crossbeam.

Due to the parabolic deflection line of the crossbeam and thus of the deck in transverse direction, the effective bending stiffness of the whole deck plate with troughs $E \cdot I_D$ (for trough distances of 600 mm) can be calculated with equation [6.6].

$$E \cdot I_D = \frac{2}{3} \cdot \frac{l_c}{600} \cdot E \cdot I_s \quad [6.6]$$

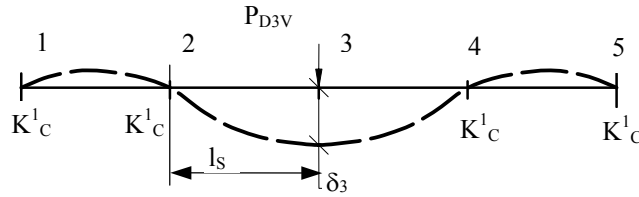


Fig. 6.5 Equivalent vertical spring model of deck

The resulting deck model is a stiffened deck structure substituted by a line element with equivalent properties $E I_D$.

Fig. 6.5 shows the model for the determination of the spring constant K^1_{D3} of the stiffness of the deck plate with troughs, including the effect of the spring stiffness of the adjacent crossbeams, 1, 2, 4 and 5 at the location of the missing crossbeam 3.

The analyses for the deck are carried out with "half" models, using symmetrical and asymmetrical boundary conditions. The deflection at crossbeam 3 due to a unit load P_{D3V} ($= 0.5P$) on a "half" model can be calculated for the boundary condition $\varphi_3 = 0$

The deflection of the deck at crossbeam 3 can be calculated with equation [6.7].

$$\delta_3 = P_{D3V} \cdot \left\{ \frac{5}{2 \cdot K^1_c} + \frac{l_s^3}{3 \cdot E \cdot I_D} \right\} - \frac{\left\{ \frac{3}{K^1_c \cdot l_s} + \frac{5 \cdot l_s^2}{6 \cdot E \cdot I_D} \right\}^2}{4 \left\{ \frac{1}{K^1_c \cdot l_s^2} + \frac{2l_s}{3 \cdot E \cdot I_D} \right\}} \quad [6.7]$$

The vertical spring constant K^1_{D3} for the deck at crossbeam 3, including the effect of the crossbeams 1, 2, 4 and 5 with equivalent properties is determined with equation [6.8]:

$$K^1_{D3} = \frac{P_{D3V}}{\delta_3} \quad [6.8]$$

6.3.3 Equivalent rotational spring properties for the deck

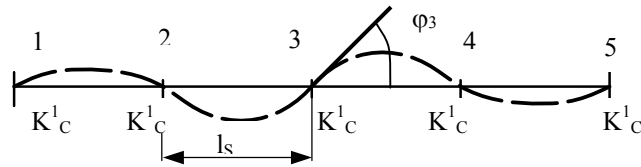


Fig. 6.6 Rotational spring model of the deck

Similarly, a model for the rotations can be derived. At the location of crossbeam 3 (see Fig. 6.6), a unit moment is applied to a continuous four span beam on spring supports. Here, a half beam from crossbeam 1 to crossbeam 3 is considered with the boundary condition $\delta_3 = 0$.

The out-of-plane rotation stiffness of the crossbeam itself is considered negligible in relation to the bending stiffness of the deck. This does not apply in general, e.g. if vertical stiffeners of the crossbeam web are connected to one or more troughs of the deck plate, the crossbeam may have a rotational stiffness that cannot be neglected. In real structures, this spring stiffness depends on both the torsion and warping stiffness of the crossbeam, and on local clamping effects.

The external moment-rotation relationship is given in equation [6.9]:

$$\phi_3 = M \cdot \left\{ 2 \cdot \left\{ \frac{1}{K^1_C \cdot l_s^2} + \frac{2 \cdot l_s}{3 \cdot E \cdot I_D} \right\} - \left\{ \frac{3}{K^1_C \cdot l_s} + \frac{5 \cdot l_s^2}{6 E \cdot I_D} \right\} \frac{\left\{ \frac{3}{K^1_C \cdot l_s} + \frac{5 \cdot l_s^2}{6 \cdot E \cdot I_D} \right\}}{\left\{ \frac{5}{K^1_C} + \frac{2 \cdot l_s^3}{3 \cdot E \cdot I_D} \right\}} \right\} \quad [6.9]$$

6.4 Crossbeam and deck spring constants

6.4.1 Fully loaded crossbeam

Fig.6.7 shows the spring constants K^1_C for the conventional crossbeam types 1 – 9, calculated with eqs. [6.1] to [6.5].

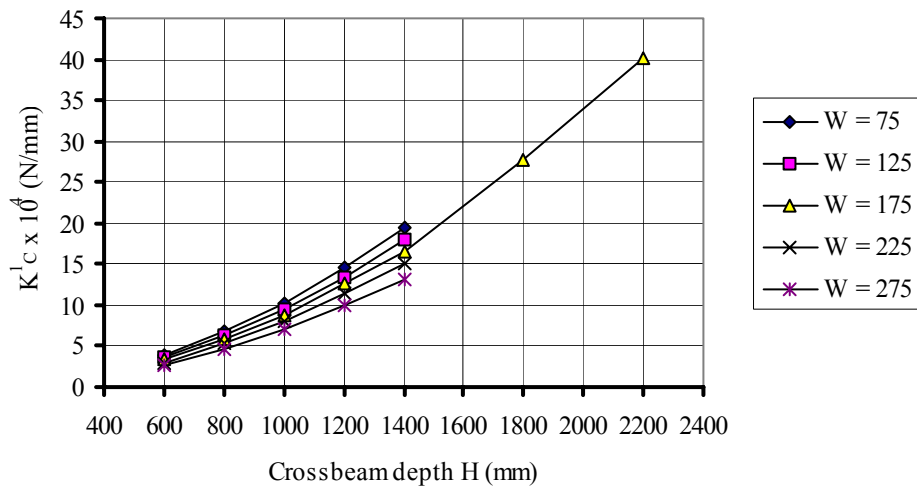


Fig.6.7 Spring constants K^1_C of crossbeams

The crossbeam spring constants K^1_C for the conventional types 1 to 5 with different cut-out widths W show a similar tendency for increasing crossbeam depths. The crossbeams with the cut-outs $W = 75$ mm have about a 15% higher stiffness than those with a cut-out width $W = 175$ mm, which is the standard width used in the Netherlands.

The crossbeams with the cut-outs $W = 275$ mm have a stiffness that is about 20% less than those with a cut-out width $W = 175$ mm. As these effects are almost the same for each crossbeam type, only results for $W = 175$ mm are calculated for the crossbeam types 7 ($H = 1800$ mm) and 9 ($H = 2200$ mm).

The crossbeams show increasing spring stiffness for deeper webs. Fig. 6.8 shows the values for K^1_D for decks with conventional crossbeams calculated with equations. [6.7] and [6.8].

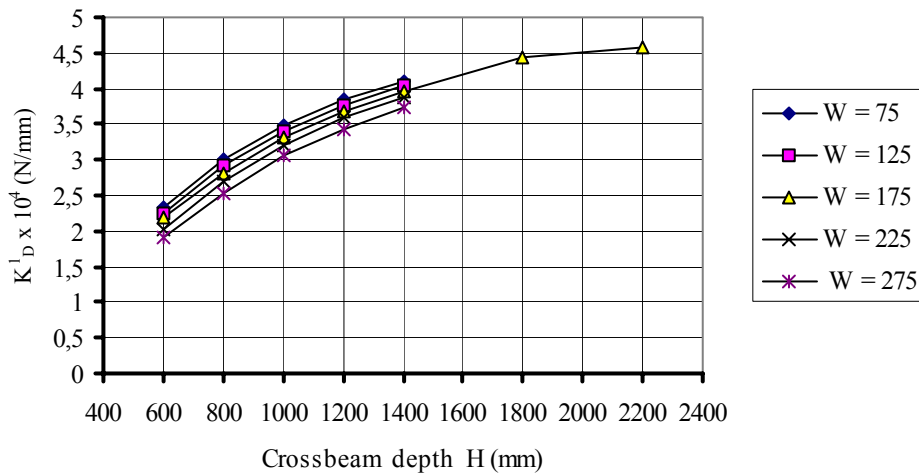


Fig. 6.8 Spring constants K_D^1 of the deck at crossbeam 3

The K_D^1 values for the deck with conventional crossbeams show an almost constant effect of the cut out width. With increasing web depth and thus rigidity of the crossbeam the value of K_D^1 converges to a maximum. For rigid crossbeams, the spring stiffness of the deck is based only on the deck bending stiffness.

With the spring constants K_C^1 for the crossbeam and K_D^1 for the deck structure, it is possible to calculate which portion of a vertical load applied on the deck above a crossbeam is transferred to the crossbeam situated directly under the load and which portion is transferred by the deck to the adjacent crossbeams. Fig. 6.9 shows the portion of the external load introduced into the crossbeam (distribution factor).

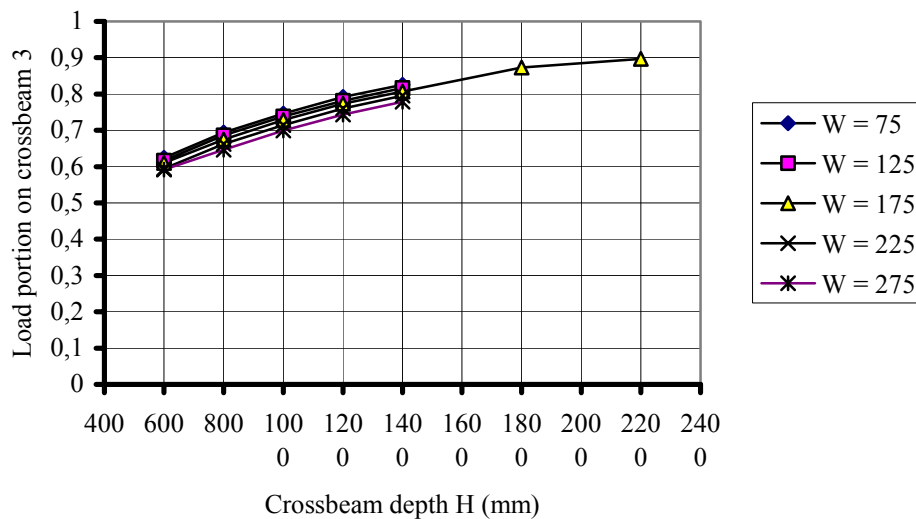


Fig. 6.9 Portion of external load on deck at crossbeam 3, transferred into crossbeam 3

As expected, deeper crossbeams with a higher stiffness result in a more direct load transfer into the crossbeam. It can be seen that the width of the cut-outs (with cope holes) only has a marginal effect on the load distribution and for this reason, in further analyses, only crossbeams with cut-outs $W = 175 \text{ mm}$ are considered.

6.4.2 Partially loaded crossbeams

The crossbeams discussed in 6.3.1 and 6.4.1, are loaded in-plane by a uniformly distributed load over the full span length and the equivalent spring stiffness applies for the midspan location (see also Fig. 6.10). The assumption of a parabolic deflection line for the crossbeam means that the beam model representing the deck includes 4800 mm ($2/3$ of 7200 mm), or 8 troughs.

The majority of real bridges however, show traffic loads F_L that are applied to the crossbeam over the width of the vehicle, with their centres approximately at the centre of the traffic lane. From measurements and calculations it follows, that in this case, a vehicle can be considered supported by approximately 5 troughs (3000 mm) when there is a thick wearing course and by 3 when there is a thin wearing course (1200 mm). Fig. 6.11 shows a concentrated load at a distance "x" from the left support.

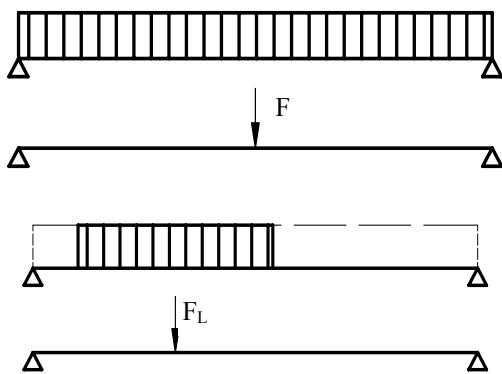


Fig. 6.10 Lane load positions

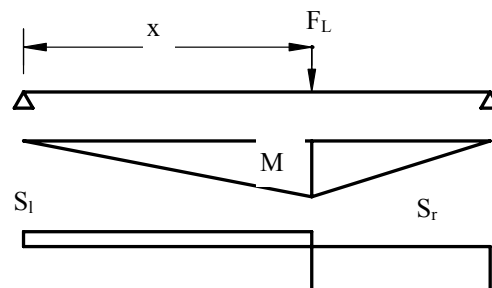


Fig.6.11 Lane load resultant, bending and shear diagrams

For a load applied at a location $0 < x < 0.5 \cdot l$, in which l is the crossbeam span. The crossbeam spring stiffness K_c^1 can be calculated with equation [6.10]:

$$K_c^1 = \frac{1}{\frac{x^2 \cdot (l_c - x)^3}{3 \cdot E \cdot I_c^1 \cdot l_c^2} + \frac{x \cdot (l_c - x)}{G \cdot A_c^1 \cdot l_c}} \quad [6.10]$$

Fig. 6.12 shows the quotient K_D^1/K_C^1 for 8 fully loaded crossbeams with $W = 75$ to 275 with a span of 7200 mm, together with the K_D^1/K_C^1 values for notional lanes with a width of 2400 mm (approximately the vehicle width). The centre of the lane indicated with $x = 1200$ is at a distance of 1200 mm from the support and the centre of the lane indicated with $x = 3600$ at a distance of 3600 mm from the support.

For partially loaded crossbeams, only a part of the deck in longitudinal direction (traffic lane) is effective, which has to be taken into account by scaling the deck spring stiffness. The included spring stiffness of the adjacent crossbeams is then also scaled but the effect is negligible.

The quotients K_D^1/K_C^1 for these partially loaded crossbeams are very close to those of the much higher fully loaded crossbeams due to the smaller width of the effective deck (lane) in longitudinal direction, which reduces the spring stiffness K_D^1 . The lane at $x = 1200$ mm is supported by a more rigid spring K_C^1 due to the position of the load in relation to crossbeam bending.

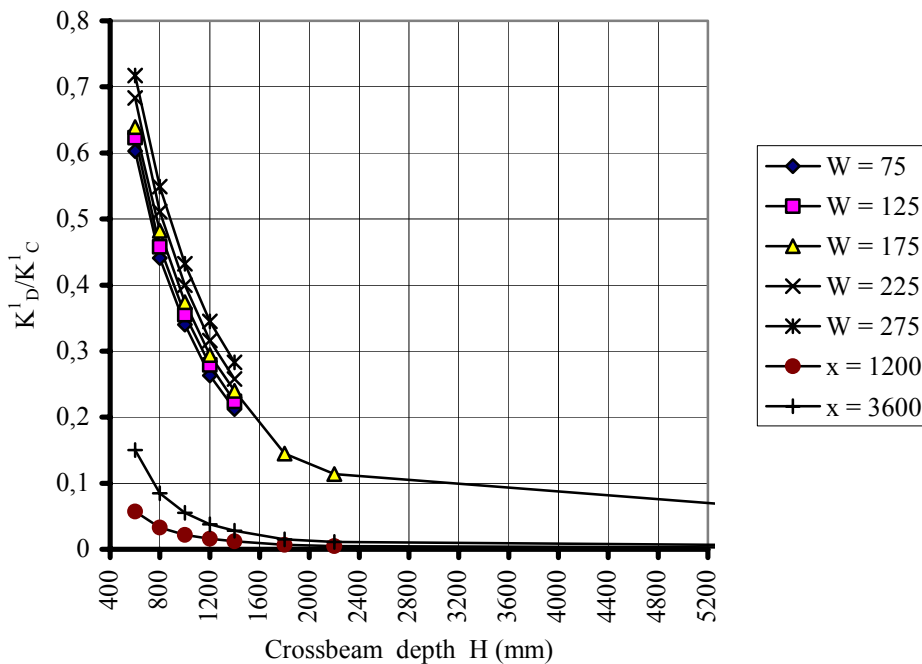


Fig.6.12 Quotients of K_D^1/K_C^1 for various crossbeams

6.5 Influence Lines

The influence lines are the basis for the determination of the load introduced into the crossbeam, the imposed rotation and the deck bending moment intervals at the trough to crossbeam connections.

Initially, to determine the crossbeam load and rotation histories, a model consisting of a beam on a continuous elastic foundation with the crossbeam spring stiffness “smeared out” over the trough span length was tried. The results were compared with those of an FE beam grid model but it was concluded that, although the crossbeam load interval matched fairly well for single point loads, this model was not suitable for axle load configurations and the rotation intervals of the beam on an elastic foundation did not comply at all with the FE beam grid model results.

Therefore, the influence lines for the crossbeam loads and trough to crossbeam connection rotations in this study are determined with an analytical model and checked with a 2D FE model, including elastic supports for the crossbeams.

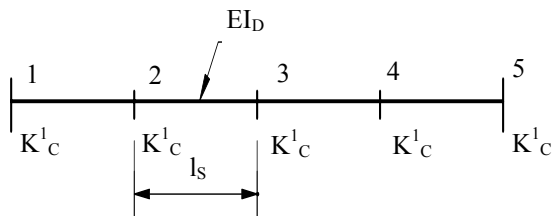


Fig. 6.12 Beam on spring supports for the determination of influence lines with the analytical and 2D FE models

The influence lines for the bending moments in the deck are determined with a simple 2D FE model only.

Fig. 6.12 shows the model of a beam (deck) on five spring supports (crossbeams).

For the determination of the influence lines with the maximum and minimum values and their locations with the analytical model, the virtual work analogy was used, which means that a deformation or rotation is applied at crossbeam 3.

The “deflection line” of the deck, due to a unit load P_{3DV} applied on the deck at crossbeam 3 gives the influence line for the reaction of crossbeam 3.

The “deflection line” of the deck, due to a unit rotation φ_3 applied to the deck at crossbeam 3, gives the influence line for the bending moment in the trough to crossbeam connection of crossbeam 3.

The “deflection line” of the deck, due to unit moments M_{D3} applied to the cross section of the deck at crossbeam 3 gives the influence line for the bending moment in the deck at crossbeam 3.

6.5.1 Influence lines for crossbeam loads

The spring constants of the deck K_{D3}^1 and the crossbeam K_{C3}^1 determine the load distribution between the deck and the crossbeam at the location of crossbeam 3.

a. Load between crossbeams 2 and 3, i.e. $0 < x \leq 4000$

The general form of the equation for the influence line for the crossbeam 3 load is given by equation [6.12].

Here $x = 0$ at crossbeam 3 and y is the load on crossbeam 3 due to a unit load at a distance x from crossbeam 3.

$$y = \delta_3 - \frac{M_{D3} \cdot x^2}{2 \cdot E \cdot I_D} + \frac{P_{C3V} \cdot x^3}{12 \cdot E \cdot I_D} \quad [6.12]$$

with the following relationship between M_{D3} and P_{C3V} :

$$M_{D3} = \frac{P_{C3V}}{4} \cdot \frac{\left\{ \frac{3}{K_C^1 \cdot l_s^2} + \frac{5 \cdot l_s^2}{6 \cdot E \cdot I_D} \right\}}{\left\{ \frac{1}{K_C^1 \cdot l_s^2} + \frac{2 \cdot l_s}{3 \cdot E \cdot I_D} \right\}} \quad [6.13]$$

In equation [6.12] δ_3 is the deflection of the deck at crossbeam 3 and $(1-\delta_3)$ is the deflection of the crossbeam, both due to a unit load at crossbeam 3.

b. Load between crossbeams 1 and 2, i.e. $4000 < x \leq 8000$

The deflection line is calculated with equation [6.14]:

$$y = \delta_3 - \frac{M_{D3} \cdot x^2}{2 \cdot E \cdot I_D} + \frac{P_{C3V} \cdot x^3}{12 \cdot E \cdot I_D} + \frac{1}{6} \cdot \left\{ \frac{M_{D3}}{l} - P_{C3V} \right\} (x - l_s)^3 \cdot \frac{1}{E \cdot I_D} \quad [6.14]$$

The crossbeam load interval at location 3 for a single load can be derived from the maximum and minimum values of the influence line. The locations of the maximum and the minimum reaction can be found with the derivatives to x of the influence function.

c. Location of an extreme value for a load between crossbeams 2 and 3, i.e. $0 < x \leq 4000$

Support 3 will always be the absolute maximum.

d. Location of an extreme value for a load between crossbeams 1 and 2, i.e. $4000 < x \leq 8000$

When $y^1 = 0$, the function has an extreme at a location x :

$$y^1 = -M_{D3} \cdot x + \frac{1}{4} \cdot P_{C3V} \cdot x^2 + \frac{1}{2} \cdot \left\{ \frac{M_{D3}}{l} - P_{C3V} \right\} (x^2 - 2 \cdot x \cdot l_s + l_s^2) \quad [6.15]$$

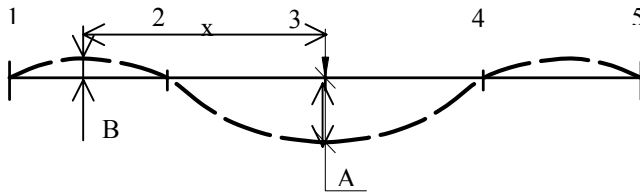
If no value for "x" is found, the load amplitude is varying between 0 and the maximum at crossbeam 3.

For a load at "x", the load P_{C3Vx} on crossbeam 3 is found with equation [6.16].

$$P_{C3Vx} = P_{D3V} \cdot \frac{\delta_x}{\delta_3} \quad [6.16]$$

6.5.1.1 Crossbeam load intervals due to unit loads

Fig. 6.13 shows a typical influence line for the crossbeam load P_{C3V} on crossbeam 3 with the maximum "A" and minimum "B". The values for A and B and the intervals ΔP_{C3V} to be taken into account for a fatigue damage calculation (rainflow procedure) fatigue literature are given in Table 6.2.



Based on an S-N line with a single slope $m = 3$, the "relative" fatigue damage can be calculated, with equation [6.17]:

Fig.6.13 Model of influence lines for support reactions P_{C3V}

$$D_{rel} = 0.5 \cdot (B)^3 + 2 \cdot 0.5 \cdot (A + B)^3 + 0.5 \cdot (B)^3 \quad [6.17]$$

This method is further described in detail in 6.6.1.1 and in chapter 8.

Table 6.2 shows that the relative fatigue damage from a single axle load on the crossbeam is strongly affected by the stiffness of the crossbeam relative to the stiffness of the deck, e.g. in case of a very stiff crossbeam (type 7), the relative fatigue damage is four times that of beam type 1.

Table 6.2, Relative load amplitudes and relative fatigue damage for single axle loads

CONVENTIONAL CROSSBEAMS (l = 7200 mm, W = 175 mm)						
Beam Type	Web Depth H (mm)	Maximum "A"	Minimum "B"	Distance x from crossbeam 3 (mm)	ΔR_{C3V}	D_{rel}
1	600	0.610	-	-	0.610	0.227
2	800	0.675	-	-	0.675	0.308
3	1000	0.728	-	-	0.728	0.386
4	1200	0.773	-0.042	7244	0.042, 0.815	0.541
5	1400	0.807	-0.054	6644	0.054, 0.861	0.638
7	1800	0.873	-0.089	6164	0.089, 0.962	0.891
9	2200	0.897	-0.100	6044	0.100, 0.997	0.992
$K_C^{l=\infty}$	-	1.000	-0.169	5702	0.169, 1.169	1.603

6.5.1.2 Influence lines for the crossbeam in-plane loading for load arrangements

The results in Table 6.2 are based on single loads and are not applicable to other load configurations. The fatigue assessment of real bridges with many vehicles with axle distances shorter than a branch of an influence line cannot be based on the maximum and minimum values only, but requires a summation of the influences of various axle loads for different vehicle positions. Therefore, the influence lines for vertical loads on crossbeam 3 are calculated for load positions on the deck between crossbeams 1 and 3. The influence lines for load positions on the deck between crossbeams 1 and 3 and between crossbeams 3 and 5 are symmetrical with respect to crossbeam 3.

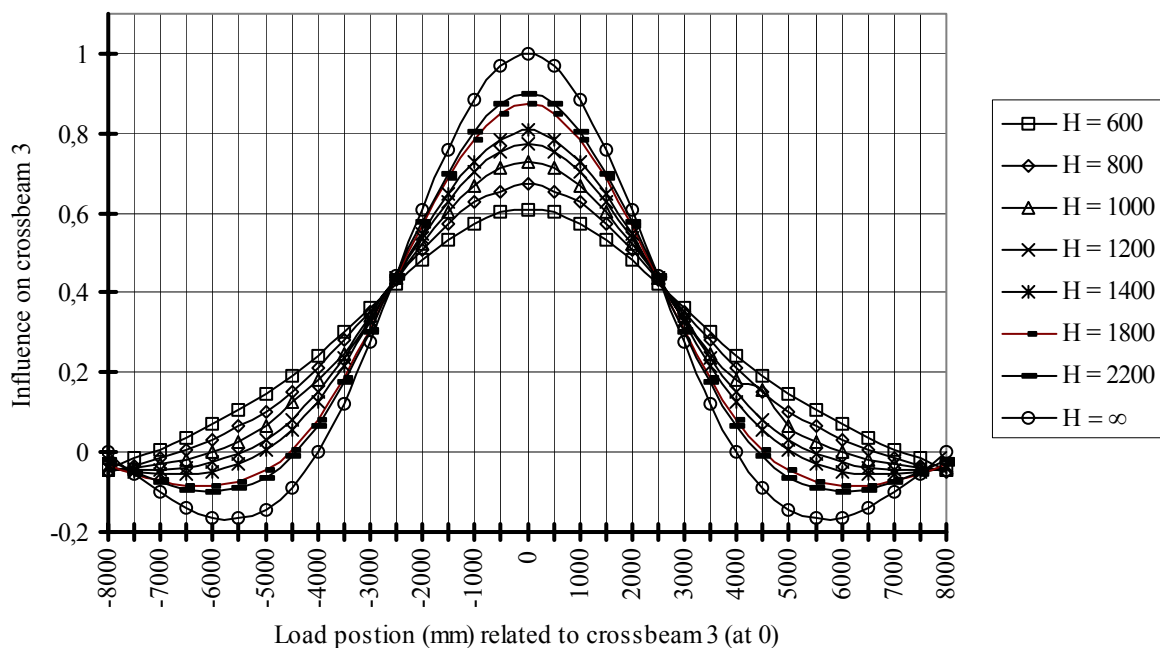


Fig. 6.14 Influence lines for the load on crossbeam 3 for spans 1-2, and 2-3

Fig. 6.14 shows the influence lines for the crossbeam load P_{C3V} for the crossbeam types 1 – 9. The crossbeam types are as indicated in Table 6.2.

Due to the flexibility of the crossbeams, the ordinates at the supports (even at a distance of 8000 mm) is generally not zero. If these influence lines are used for a deck with more spans, the influence of adjacent spans at a larger distance than 8000 mm from crossbeam 3 can be ignored, as the error is small.

For decks with relatively flexible crossbeams, almost all ordinates have the same sign and consequently all axle loads, even of long vehicles contribute to the maximum crossbeam load. On a deck with rigid supports, a small negative amplitude, then a large positive amplitude and finally a small negative amplitude occur. The load intervals caused by long vehicles will be a resultant of positive and negative influence values but the load intervals caused by short vehicles will be a resultant of influence values with the same sign and can therefore be larger.

A good agreement is shown when the influence lines determined with the analytical procedure are compared with the results of the FE model of a beam on spring supports. This is further shown in 6.6.1.2.

6.5.2 Influence lines for trough to crossbeam connection rotations

The rotations can be found in a similar way to the reactions, by applying a relative unit rotation to the deck at crossbeam 3.

a. Load between crossbeams 2 and 3, i.e. $0 < x \leq 4000$

The general form of the influence line for the rotations of support 3 (equal to the crossbeam rotation) is given by the deflection line equation [6.18]. It is assumed that the torsional rigidity of the crossbeam is very low, so the clamping moments can be neglected. Here, y is the rotation at crossbeam 3 due to a unit load on a distance x from crossbeam 3.

$$y = \phi_3 \cdot x - \frac{M_{D3}}{2 \cdot E \cdot I_D} \cdot x^2 + \frac{R_{C3V}}{6 \cdot E \cdot I_D} \cdot x^3 \quad [6.18]$$

The relationship between the bending moment M_{D3} in the deck and the support reaction R_{C3V} at support 3 is given by equation [6.19].

$$M_{D3} = R_{C3V} \cdot \frac{\left\{ \frac{5}{K^1_c} + \frac{2 \cdot l_s^3}{3 \cdot E \cdot I_D} \right\}}{\left\{ \frac{3}{l_s \cdot K^1_c} + \frac{5 \cdot l_s^2}{6 \cdot E \cdot I_D} \right\}} \quad [6.19]$$

b. Load between crossbeams 1 and 2, i.e. $4000 < x \leq 8000$

The deflection line is given by equation [6.20]:

$$y = \phi_3 \cdot x - \frac{M_{D3}}{2 \cdot E \cdot I_D} \cdot x^2 + \frac{R_{C3V}}{6 \cdot E \cdot I_D} \cdot x^3 + \frac{\frac{M_{D3}}{l} - 2 \cdot R_{C3V}}{6 \cdot E \cdot I_D} (x - l_S)^3 \quad [6.20]$$

The equations [6.18] and [6.19] give the values for ϕ_3 for a load at a distance “x” from support 3.

The crossbeam rotation interval at location 3, for a single load can be derived from the maximum and minimum values of the influence line. The locations for the maximum and the minimum rotation can be found with the first derivative to x of the influence function.

c. Location of an extreme for a load between crossbeams 2 and 3, i.e. $0 < x \leq 4000$

$$y' = 1 - \frac{M_{D3} \cdot x}{E \cdot I_D} + M_{D3} \cdot \frac{\left\{ \frac{3}{l_S \cdot K^1_C} + \frac{5 \cdot l_S^2}{6 \cdot E \cdot I_D} \right\}^2}{\left\{ \frac{1}{l_S^2 \cdot K^1_C} + \frac{2 \cdot l_S}{3 \cdot E \cdot I_D} \right\}} \cdot \frac{x^2}{2 \cdot E \cdot I_D} \quad [6.21]$$

When $y' = 0$, the function y has an extreme at a location x_1 .

d. Location of an extreme for a load between crossbeams 1 and 2, i.e. $4000 < x \leq 8000$

$$y' = 1 - \frac{M_{D3} \cdot x}{E \cdot I_D} + M_{D3} \cdot \frac{\left\{ \frac{3}{l_S \cdot K^1_C} + \frac{5 \cdot l_S^2}{6 \cdot E \cdot I_D} \right\}}{\left\{ \frac{1}{l_S^2 \cdot K^1_C} + \frac{2 \cdot l_S}{3 \cdot E \cdot I_D} \right\}} \cdot \frac{x^2}{2 \cdot E \cdot I_D} + \frac{1}{2} \cdot \left\{ \frac{M_{D3}}{l_S} - 2 \cdot R_{C3V} \right\} \frac{(x - l_S)^3}{E \cdot I_D} \quad [6.22]$$

When $y' = 0$, the function y has an extreme at a location x_2 .

The equations [6.18] and [6.20] give the influence values for the moment at 3 due to a load at a distance "x" from support 3 in relation to the moments at 3 caused by an applied unit rotation ($\phi_3 = 1.0$). The rotation at crossbeam 3 related to a unit load at a distance “x” from support 3 is found with equation [6.23].

$$\phi_3 = \frac{y}{2 \cdot M_{D3}} \quad [6.23]$$

Alternatively, to the above-described method, the influence line can be determined with a simple FE model consisting of a beam on spring supports.

6.5.2.1 Crossbeam rotation intervals due to unit loads

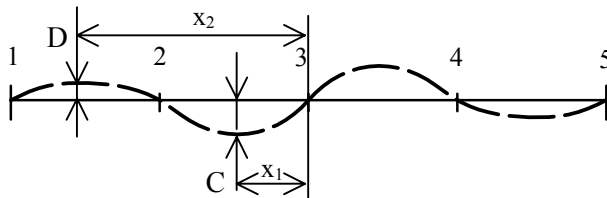


Fig.6.15 Influence line for rotations ϕ_3

Fig. 6.15 shows a typical influence line for the trough to crossbeam rotation ϕ_3 at support 3 with the maximum value "C" and the minimum value "D". The values for C and D and the intervals $\Delta\phi_3$ to be taken into account for a fatigue damage calculation of a trough to

crossbeam connection (rainflow procedure) are given in Table 6.3. In this table, the maximum and minimum amplitudes are given in relation to the maximum rotation amplitude for a beam on rigid supports.

For an S-N line with a single slope $m = 3$, a "relative" fatigue damage caused by a single axle load can be calculated, with equation [6.24]:

$$D_{rel} = 0.5 \cdot (D)^3 + 2 \cdot 0.5 \cdot (C + D)^3 + 0.5 \cdot (2C)^3 + 0.5 \cdot (D)^3 \quad [6.24]$$

Table 6.3 shows that the relative fatigue damage due to crossbeam rotations caused by a single axle load is strongly affected by the stiffness of the crossbeam in relation to the stiffness of the deck. For example, in case of a very stiff crossbeam type 7, the relative fatigue damage is only about 15% of that of beam type 1.

Table 6.3 Relative rotation amplitudes and relative fatigue damage for single axle loads

CONVENTIONAL CROSSBEAMS (l = 7200, W = 175)						
Beam Type	Web Depth H (mm)	Maximum "C"	Distance "x ₁ " (mm) from crossbeam 3	Minimum "D"	Distance "x ₂ " (mm) from crossbeam 3	D _{rel}
1	600	2.370	2361	-	-	66.56
2	800	1.911	2232	-	-	34.89
3	1000	1.593	2006	-	-	20.21
4	1200	1.468	1917	-	-	15.82
5	1400	1.357	1686	-	-	12.49
7	1800	1.196	1699	-0.148	6593	9.274
9	2200	1.159	1671	-0.128	6241	8.362
K = ω	-	1.000	1532	-0.316	5660	6.311

6.5.2.2 Influence lines for the crossbeam out-of-plane rotation for load arrangements

The results in Table 6.3 are based on single loads and not applicable to other load configurations. The fatigue assessment of real bridges with many vehicles with axle distances shorter than a branch of an influence line can not be based on the maximum and minimum values only, but requires the summation of the influences of various axle loads for different vehicle positions.

The influence lines for the rotations of the trough to crossbeam connection at crossbeam 3 are calculated for load positions on the deck between crossbeams 1 and 3. The influence lines for load positions on the deck between crossbeams 1 and 3 and between crossbeams 3 and 5 are asymmetrical with respect to crossbeam 3.

Fig. 6.16 shows the influence lines for the crossbeam rotation φ_3 for the crossbeam types 1 – 9 as indicated in Table 6.3 in relation to a unit load of 100 kN.

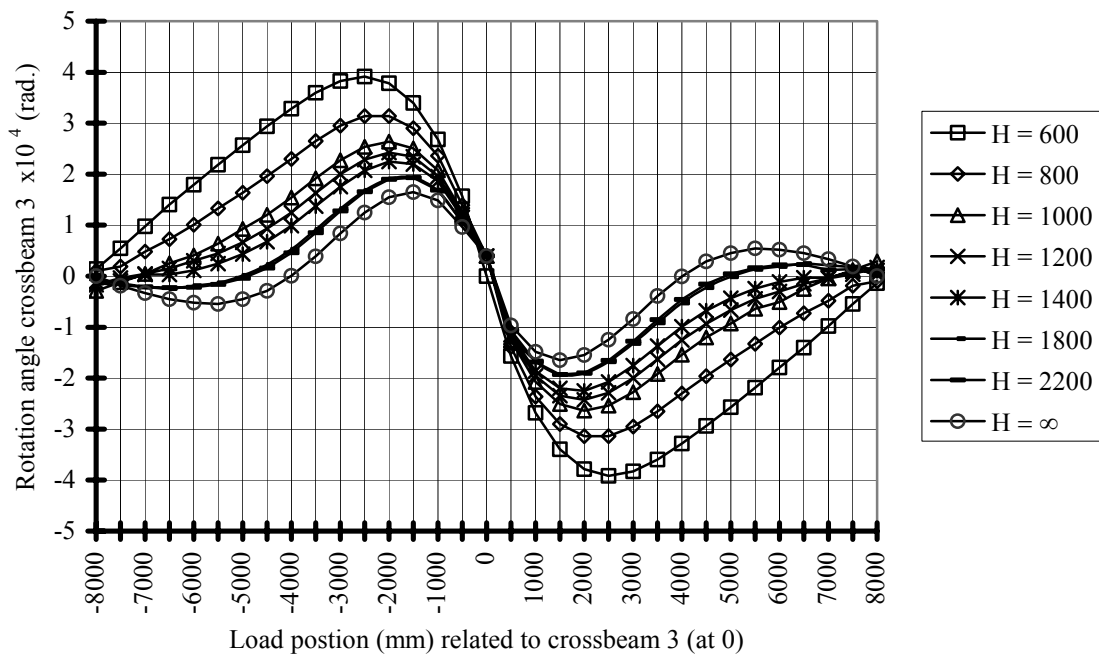


Fig.6.16 Influence lines for rotations (spans 1-2 and 3-4)

Due to the flexibility of the crossbeams, the ordinates at the supports (even at a distance of 8000 mm) is generally not zero. The influence of adjacent spans at a larger distance than 8000 mm from crossbeam 3 is ignored, as the error is small.

The largest amplitudes are found for the most flexible crossbeams. Crossbeams that are more rigid show more, but smaller, intervals.

A good agreement is shown when the influence lines determined with the analytical procedure are compared with the results of the FE model of a beam on spring supports. This is further shown in 6.6.2.2.

6.5.3 Influence lines for deck bending moments at crossbeam 3

Since the analytically determined influence lines for the crossbeam loads and the crossbeam rotations show a good agreement with those determined with an FE model, the influence lines for the bending moment in the deck M_{D3} at crossbeam 3 are only determined with an FE model consisting of a beam on spring supports.

Fig. 6.17 shows the influence lines for the deck bending moment M_{3D} in relation to a moving load of 100 kN for the crossbeam types 1 – 9 as indicated in Tables 6.2 and 6.3. The influence lines for load positions on the deck between crossbeams 1 and 3 and load positions between crossbeams 3 and 5 are symmetrical with respect to crossbeam 3.

As discussed earlier, the ordinate at support 1 will generally not be zero due to the flexibility of the crossbeams, but the values are small. The largest intervals are found for the most flexible crossbeams and the smallest intervals are found at the most rigid crossbeams.

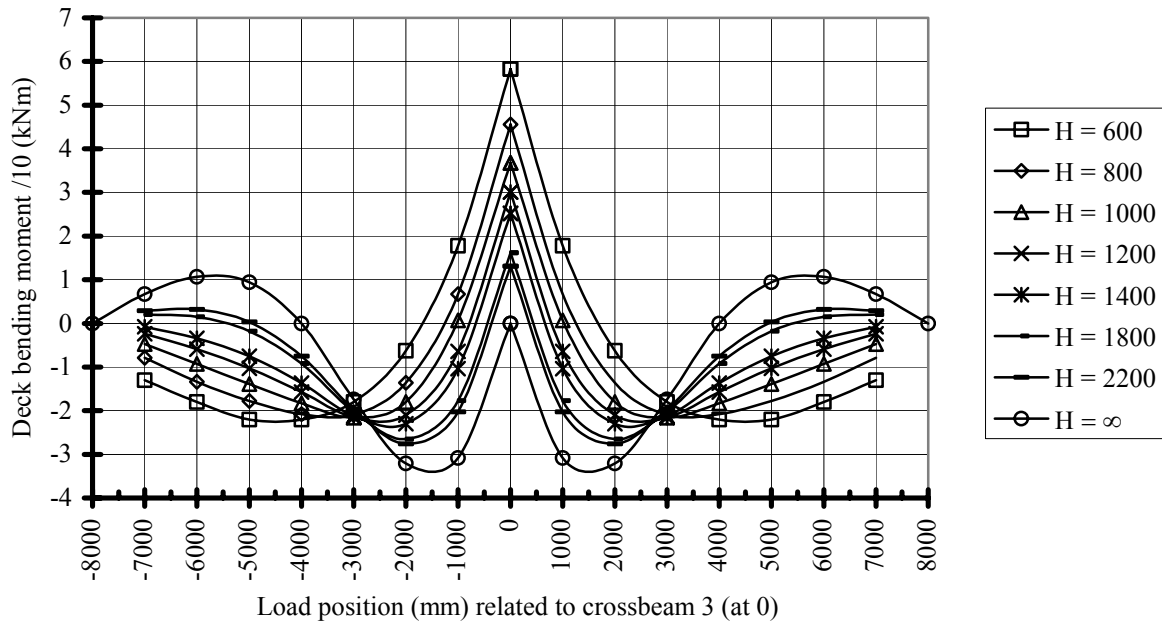


Fig.6.17 Influence lines for the deck bending moment at crossbeam 3

6.6 Crossbeam load, rotation and deck bending moment histories due to unit loads and vehicle loads

The Fatigue Load Model 2 (FLM2) given in ENV 1991-3 (and EN 1991-2) was discussed in 3.4 and should be used to verify whether the fatigue life is unlimited, which is the case when the maximum stress intervals are below the constant amplitude limit $\Delta\sigma_D$. The maximum stress intervals are derived from the load, rotation and bending moment histories. Therefore, it was decided to also calculate the equivalent numbers of cycles n_{eq} for each lorry of FLM2 and for all lorries, assuming that the lorry distribution of FLM2 is equal to that of FLM4. How the maximum vehicle loads, rotations and deck bending moments can be transferred into vehicle loads, rotations and deck bending moments for FLM4 is described in chapter 8.

Table 6.4 (which is the same as Table 3.1) shows the axle loads, together with the total lorry load ΣP , the axle distances and the lorry percentages taken from FLM4. (The values between brackets relate to EN 1991-2:2003)

The various wheel print geometries hardly affect the crossbeam loadings, rotations and the deck bending moments in these analyses; therefore, the effect of the various wheel print geometries is neglected. Further, it is assumed that the vehicle resultants coincide with the lane centres.

Table 6.4 Lorry silhouettes, frequent loads, equivalent loads

Lorry		Axle type	Frequent loads FLM2 (kN)		Equivalent loads FLM4 (kN)			Axle spacing (m)
			Axle load	Lorry load	Axle load	Lorry load	Lorry percentage Long distance	
1	2 axles ↓↓	A	90	280	70	200	20 (20)	4.50
		B	190		130			
2	3 axles ↓↓↓	A	80	360	70	310	5 (5)	4.20 1.30
		B	140		120			
		B	140		120			
3	Semi-trailer 2 axles, 3 axles ↓↓↓↓↓	A	90	630	70	490	40 (50)	3.20 5.20 1.30 1.30
		B	180		150			
		C	120		90			
		C	120		90			
4	Semi-trailer 2 axles, 2 axles ↓↓↓↓	A	90	560	70	390	25 (15)	3.40 6.00 1.80
		B	190		140			
		B	140		90			
		B	140		90			
5	Trailer combination 2 axles, 3 axles ↓↓↓↓↓	A	70	590	70	450	10 (10)	4.80 3.60 4.40 1.30
		B	180		130			
		C	120		90			
		C	110		80			
		C	110		80			

6.6.1 Crossbeam in-plane load histories

6.6.1.1 Analytical procedure

With the previously derived influence lines, the crossbeam in-plane load amplitudes “A” (see Fig. 6.18) are calculated for each crossbeam type, by positioning a unit load of 100 kN and the frequent vehicles in accordance with ENV 1991-3 in successive positions on the deck

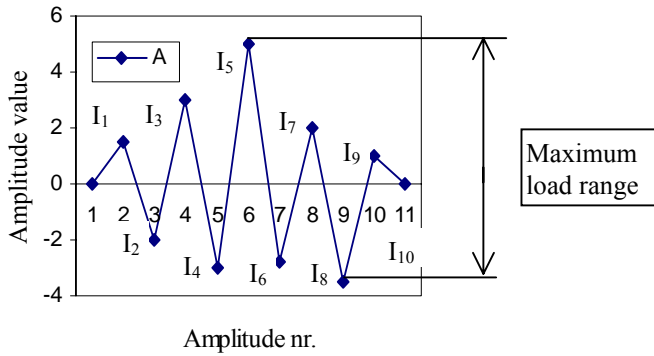


Fig. 6.18 Load amplitudes (A), load intervals (I) and the maximum load range

between crossbeam 1 and 5. The load intervals “I” (see Fig. 6.18) are derived from the crossbeam load amplitudes and the maximum load range is determined from the maximum amplitudes, as indicated in Fig. 6.18. The successive load intervals caused by a vehicle are called the load history.

For each crossbeam type and each frequent vehicle the equivalent numbers of cycles related to the maximum load interval are calculated with a “simplified” rainflow procedure for a S-N slope

$m = 3$ (indicated with “a”) and for $m = 5$ (indicated with “b”), both without a cut-off limit for fatigue. This simplified summation rule assumes that every load interval “I” has 0.5 cycles. This method is also discussed more in detail in chapter 8.

For a vehicle type “i” the equivalent number of cycles $n_{eq,i}$ for a specific crossbeam type is calculated for a S-N line with $m = 3$:

$$n_{eq,i} = a \cdot n_i \quad [6.25]$$

with:

$$a = 0.5 \cdot \sum \left[\left(\frac{I_1}{I_{i\max}} \right)^3 + \left(\frac{I_2}{I_{i\max}} \right)^3 + \left(\frac{I_3}{I_{i\max}} \right)^3 + \dots + \left(\frac{I_n}{I_{i\max}} \right)^3 \right] \quad [6.26]$$

and further for a S-N line with $m = 5$:

$$n_{eq,i} = b \cdot n_i \quad [6.27]$$

with:

$$b = 0.5 \cdot \sum \left[\left(\frac{I_1}{I_{i\max}} \right)^5 + \left(\frac{I_2}{I_{i\max}} \right)^5 + \left(\frac{I_3}{I_{i\max}} \right)^5 + \dots + \left(\frac{I_n}{I_{i\max}} \right)^5 \right] \quad [6.28]$$

In a similar way, for a particular crossbeam type, the equivalent number of cycles for all vehicles with respect to the maximum load interval caused by FLM2 is calculated.

The equivalent number of cycles for the long distance traffic on a particular crossbeam type is indicated with “c” for $m = 3$ and with “d” for $m = 5$. For this calculation, it is assumed that the lorry type distribution for the “frequent lorries” of FLM2 is similar to the distribution of the “equivalent lorries” of FLM4. For the analyses, the distribution “Long Distance” is chosen (see Table 6.4).

The equivalent number of cycles for the load intervals of a particular lorry type “i” for a slope $m = 3$ or $m = 5$ of the S-N curve are further indicated with a_i and b_i , respectively. “p” is the fraction (percentage) of the lorry type in relation to all vehicle types.

The equivalent number of cycles n_{eq} for all lorry types on a particular crossbeam for a S-N line for $m = 3$ is now determined with:

$$n_{eq} = c \cdot n \quad [6.29]$$

with:

$$c = p_1 \cdot a_1 \cdot \left(\frac{I_{1,max}}{I_{max,max}} \right)^3 + p_2 \cdot a_2 \cdot \left(\frac{I_{2,max}}{I_{max,max}} \right)^3 + p_3 \cdot a_3 \cdot \left(\frac{I_{3,max}}{I_{max,max}} \right)^3 + p_4 \cdot a_4 \cdot \left(\frac{I_{4,max}}{I_{max,max}} \right)^3 + p_5 \cdot a_5 \cdot \left(\frac{I_{5,max}}{I_{max,max}} \right)^3$$

and for $m = 5$:

$$n_{eq} = d \cdot n \quad [6.30]$$

with:

$$d = p_1 \cdot b_1 \cdot \left(\frac{I_{1,max}}{I_{max,max}} \right)^5 + p_2 \cdot b_2 \cdot \left(\frac{I_{2,max}}{I_{max,max}} \right)^5 + p_3 \cdot b_3 \cdot \left(\frac{I_{3,max}}{I_{max,max}} \right)^5 + p_4 \cdot b_4 \cdot \left(\frac{I_{4,max}}{I_{max,max}} \right)^5 + p_5 \cdot b_5 \cdot \left(\frac{I_{5,max}}{I_{max,max}} \right)^5$$

Here $I_{i,max}$ is the maximum interval per lorry, and $I_{max,max}$ is the maximum of the five lorries for a particular crossbeam.

Table 6.5 gives the crossbeam in-plane load histories P_{C3V} for a unit load of 100 kN on the deck and for the frequent lorries in accordance with ENV 1991-3. Further, it gives the equivalent number of cycles for the load intervals of each lorry type “i” for a particular crossbeam type. For each crossbeam and each lorry the maximum load intervals $I_{i,max}$ in Table 6.5 are underlined and the maximum load interval $I_{max,max}$ for a particular crossbeam type is indicated as **bold and underlined**.

The total load interval for each lorry type is indicated in Table 6.5 as ΔP_T . The total load interval only differs in some cases from the maximum interval over the complete history.

All load histories are determined for 7 crossbeam depths of conventional crossbeams with a span length l of 7200 mm and a cut-out width $W = 175$ mm.

Table 6.5 Crossbeam in-plane load intervals ΔP_{C3V} and equivalent nr. of cycles

LOAD INTERVALS ON CROSSBEAMS (kN) due to FLM2 with the distribution of FLM4							
Beam Type	Single Axle100 kN (Unit Load)	Lorry Type, Total Load, Axle Loads					n_{eq} for ΔP_{max} .
		1	2	3	4	5	
		$\Sigma P=280$ kN	$\Sigma P=360$ kN	$\Sigma P=630$ kN	$\Sigma P=560$ kN	$\Sigma P=610$ kN	
		90,190	80,140,140	90,180,120,120,120	90,190,140,140	90,180,120,110,110	
1 H = 600	61 $\Delta P_T=61$	134/134 a. 1.0 b. 1.0 $\Delta P_T=134$	181/181 a. 1.0 b. 1.0 $\Delta P_T=181$	184/26/54/ 212 a. 0.837 b. 0.747 $\Delta P_T=212$	164/164 a. 1.0 b. 1.0 $\Delta P_T=164$	170/170 a. 1.0 b. 1.0 $\Delta P_T=170$	c. 0.584 d. 0.444
2 H = 800	68 $\Delta P_T=68$	1/144/143 a. 0.990 b. 0.983 $\Delta P_T=144$	1/196/195 a. 0.991 b. 0.985 $\Delta P_T=196$	1/177/15/83/ 224 a. 0.749 b. 0.643 $\Delta P_T=225$	1/175/174 a. 0.991 b. 0.985 $\Delta P_T=175$	1/174/175/2 a. 0.991 b. 0.985 $\Delta P_T=175$	c. 0.551 d. 0.405
3 H = 1000	73 $\Delta P_T=73$	3/153/150 a. 1.0 b. 1.0 $\Delta P_T=153$	3/211/217/9 a. 0.971 b. 0.932 $\Delta P_T=217$	3/164/6/77/ 234 a. 0.959 b. 0.934 $\Delta P_T=237$	3/185/182 a. 0.696 b. 0.592 $\Delta P_T=185$	3/180/185/8 a. 0.976 b. 0.961 $\Delta P_T=185$	c. 0.539 d. 0.395
4 H = 1200	4/81/4 $\Delta P_T=81$	4/159/155 a. 0.963 b. 0.941 $\Delta P_T=159$	4/214/221/11 a. 0.954 b. 0.925 $\Delta P_T=221$	4/241/ 249 /4 a. 1.0 b. 1.0 $\Delta P_T=249$	4/195/191 a. 0.969 b. 0.950 $\Delta P_T=195$	4/185/25/13/177/9 a. 0.997 b. 0.912 $\Delta P_T=189$	c. 0.639 d. 0.536
5 H = 1400	5/86/5 $\Delta P_T=86$	5/171/166 a. 0.959 b. 0.934 $\Delta P_T=177$	4/220/229/13 a. 0.944 b. 0.910 $\Delta P_T=229$	5/254/ 259 /10 a. 0.972 b. 0.954 $\Delta P_T=259$	5/202/204/7 a. 0.985 b. 0.975 $\Delta P_T=204$	5/186/28/16/177/8 a. 0.933 b. 0.891 $\Delta P_T=189$	c. 0.638 d. 0.526
7 H = 1800	9/98/9/ $\Delta P_T=98$	8/174/166 a. 0.937 b. 0.899 $\Delta P_T=182$	7/234/228/21 a. 0.921 b. 0.875 $\Delta P_T=248$	8/256/ 270 /22 a. 0.926 b. 0.883 $\Delta P_T=270$	8/215/225/18 a. 0.937 b. 0.899 $\Delta P_T=225$	8/194/47/38/194/17 a. 1.011 b. 1.001 $\Delta P_T=203$	c. 0.636 d. 0.516
9 H = 2200	10/100/10 $\Delta P_T=100$	8/178/187/170 a. 0.932 b. 0.891 $\Delta P_T=187$	8/242/256/22 a. 0.922 b. 0.877 $\Delta P_T=256$	9/280/ 294 /23 a. 0.932 b. 0.891 $\Delta P_T=294$	7/220/233/20 a. 0.921 b. 0.875 $\Delta P_T=233$	9/198/58/40/200/19 a. 0.997 b. 0.976 $\Delta P_T=208$	c. 0.597 d. 0.480
$H = \infty$	16/116/16 $\Delta P_T=116$	15/198/183 a. 0.892 b. 0.831 $\Delta P_T=215$	13/266/294/41 a. 0.872 b. 0.804 $\Delta P_T=294$	14/304/ 332 /42 a. 0.885 b. 0.822 $\Delta P_T=332$	14/245/266/35 a. 0.892 b. 0.831 $\Delta P_T=266$	14/209/56/53/224 a. 0.922 b. 0.854 $\Delta P_T=227$	c. 0.577 d. 0.451

Further also for crossbeams with an infinite stiffness $H = \infty$. In general, a lorry generates only one large and two smaller load amplitudes on the crossbeam support (see also Fig. 6.19). The graphs show that the lorry type and the crossbeam stiffness influence the number of cycles of the load history ΔP_{C3V} .

As shown in Table 6.5 for all lorry types and all crossbeam types, the crossbeam load interval is only a percentage of the total lorry load. This percentage of the maximum load interval introduced into crossbeam Type 1 with $H = 600$ mm, varies between 28% and 48% and introduced into a crossbeam with $K^1_C = \infty$ (rigid supports) between 37% and 82%. This is for single axles 61% and 116% respectively.

Fig. 6.19 shows the reaction amplitudes (kN) for single axle loads of 100 kN and for the frequent lorries of FLM2 of ENV 1991-1-3 in relation to the crossbeam stiffness. Every axle and lorry is assumed to travel from left to right. As already discussed, the lorry type and the crossbeam stiffness influence the load history significantly.

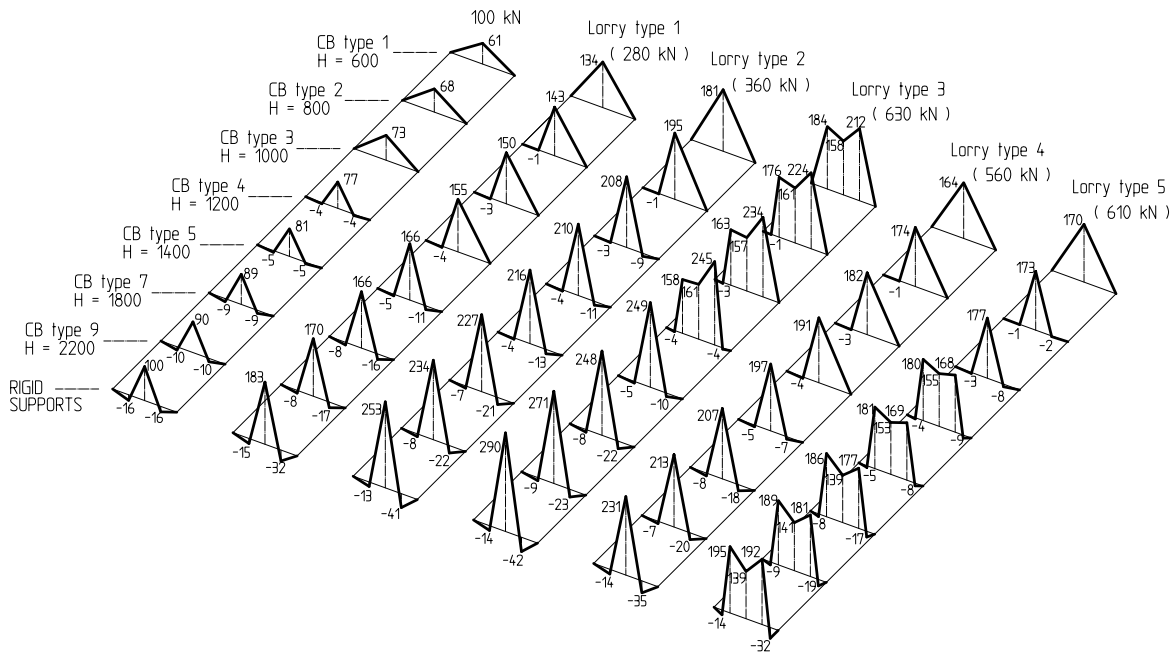


Fig. 6.19 Vehicle loads and Reaction amplitudes

The equivalent numbers of cycles for the maximum load intervals $\Delta P_{C3Vmax.}$, for various crossbeam depths derived from Table 6.5, are graphically presented in Fig. 6.20. In general it can be concluded that for $m = 3$ the equivalent number n_{eq} is between 0.50 and 0.65 and for $m = 5$, n_{eq} is between 0.40 and 0.54 times the total number of lorries.

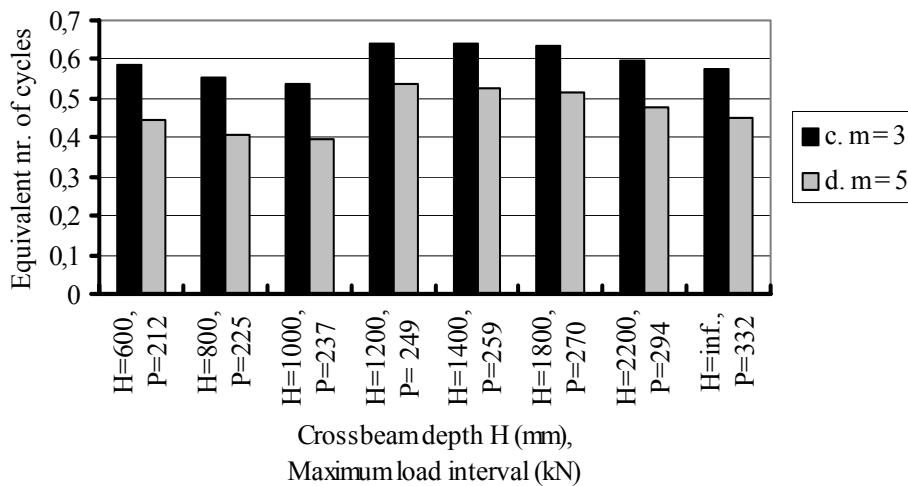


Fig.6.20 Maximum reaction intervals “ ΔP_{C3V} ” (indicated with “P”) with equivalent nr. of cycles “c” and “d”

This is a safe assumption as the equivalent numbers of cycles are linked to the maximum load intervals. In this way, the damage calculation is simplified to a constant amplitude damage calculation with an equivalent number of cycles, representing all traffic effects on a particular crossbeam. When the equivalent numbers of cycles n_{eq} of all crossbeams for $m=3$ and for $m=5$ are related to the maximum load interval found for $H = \infty$, the values become as shown in Fig. 6.21.

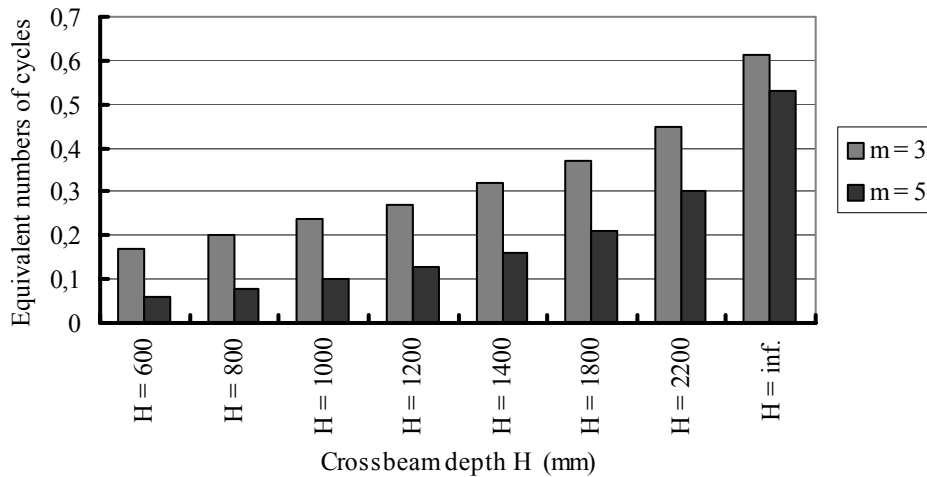


Fig. 6.21 Equivalent numbers of cycles for all crossbeams related to $\Delta P_{C3V} = 332$ kN of $H = \infty$

Combining the equivalent number of cycles n_{eq} and the crossbeam load intervals shows the relative fatigue damage D_{rel} of the crossbeam and the effect of flexible, related to rigid crossbeams, see Table 6.6.

Table 6.6 Relative damages D_{rel}

Crossbeam	ΔP_{C3V}	c for m = 3	D_{rel}	d for m = 5	D_{rel}
H = 600 mm	212	0.58	0.26	0.44	0.10
H = 1200 mm	249	0.64	0.36	0.54	0.28
H = 2200 mm	294	0.60	0.72	0.48	0.58
H = ∞	332	0.58	1	0.45	1

In Table 6.6 the $H = \infty$ with $\Delta P_{C3V} = 332$ kN and $n_{eq} = 0.58$ for $m=3$ and $n_{eq} = 0.45$ for $m=5$ is assumed to give a reference damage 1.

The effect of the load intervals and equivalent numbers of cycles for a selection of other crossbeam types are presented by their value of D_{rel} . For $H = 600$ mm, D_{rel} can be derived from that of $H = \infty$ with a scaling of the load intervals and the equivalent numbers of cycles: $(212/332)^3 \cdot (0.58/0.58) = 0.26$ for $m = 3$ and $(212/332)^3 \cdot (0.44/0.45) = 0.10$ for $m = 5$ respectively. The values D_{rel} for the other crossbeam types are determined in a similar way.

From Fig. 6.20 and Table 6.6 it can be concluded that for the locations governed by the in-plane behaviour of the crossbeam, the fatigue life of the crossbeam is underestimated when only influence lines are used for beams on rigid supports. Compared to the rigid crossbeam, the relative fatigue damage of a very flexible crossbeam is here only 26% for $m = 3$ and 10% for $m = 5$.

Based on Figs. 6.20 and 6.21, a very safe assumption for the in-plane load effect ΔP_{C3V} for all crossbeam types is: $\Delta P_{C3V} = 332$ kN (rigid supports), in combination with $n_{eq} = 0.60$ for $m = 3$ and $n_{eq} = 0.45$ for $m = 5$.

6.6.1.2 FE simulations for load intervals

The foregoing results from the analytical procedure are verified by and extended with computer simulations for additional influences such as trough span length and additional crossbeam stiffness (represented by spring constants). The model is the same as shown in par. 6.5.1.1.

In Table A2.1, the load intervals ΔP_{C3V} from the FE simulation is given. In addition to the crossbeam spring constants K_C^1 , the ratio between the deck stiffness and the crossbeam stiffness K_D/K_C^1 is indicated, as this can be used as a reference value for further analyses. The crossbeam distances are indicated with r, s and t:

r. =	Crossbeam centres	3500 mm
s. =	Crossbeam centres	4000 mm
t. =	Crossbeam centres	4500 mm

The computer simulations cover a larger range of crossbeam spring stiffnesses than the calculations with the analytical model. The values in Table A2.1 demonstrate that for a crossbeam with a stiffness ten times that of the crossbeam with a depth $H = 2200$ mm, already values are obtained that are close to those for a crossbeam on rigid supports. This means that the analytical procedure covers a range of crossbeam stiffnesses that is large enough to represent all stiffnesses.

Table A2.1 also shows the effect of the crossbeam distances 3500 mm, 4000 mm and 4500 mm. The ΔP_{C3V} values found with the computer simulations comply very well with those from the analytical model (values between brackets). This observation applies for the unit loads and for the amplitudes caused by the complete vehicles. It demonstrates that, even with estimated positions of the lorries, reasonable results are obtained with the analytical model.

As an example, the results of the analyses for lorry type 3 are shown in Fig. 6.22.

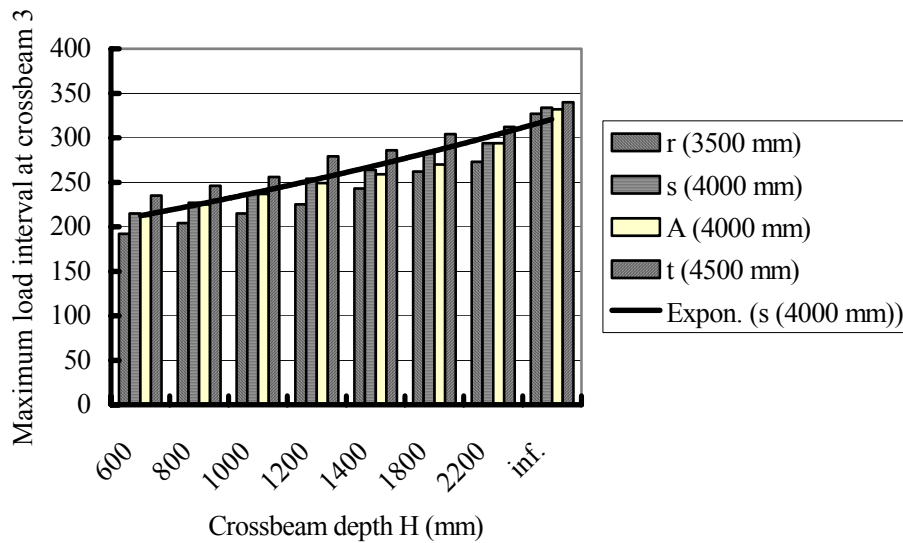


Fig. 6.22 Load intervals ΔP_{3CV} for Lorry 3 from FE calculations and analytical model (A)

As shown in Table A2.1 and Fig. 6.22, for the flexible crossbeams, the load amplitude for a crossbeam distance of 3500 mm is approximately 90% and that for a crossbeam distance of 4500 mm is 110% of that for a distance of 4000 mm.

When the crossbeams are deeper, the results tend to converge to those for a crossbeam distance of 4000 mm. This phenomenon is observed for the load amplitudes of single axles as well as for lorries. Although not reported here, the numbers of cycles are almost the same and the numbers of cycles found with the analytical procedure are equal to those found with the FE method.

6.6.2 Trough to crossbeam connection; out-of-plane rotation histories

6.6.2.1 Rotation results from the analytical method

Similar to the in-plane load amplitudes, the trough to crossbeam connection rotation amplitudes are calculated for each crossbeam type with the previously derived influence lines, by positioning a unit load of 100 kN with respect to the frequent vehicles in accordance with ENV 1991-3 in successive positions on the deck between crossbeam 1 and 5.

The rotation intervals are derived from the trough to crossbeam connection rotation amplitudes. The successive rotation intervals caused by a vehicle are called the rotation history. For each crossbeam type and each frequent vehicle the equivalent numbers of cycles related to the maximum rotation interval are calculated with a “simplified” rainflow procedure, for a S-N slope $m = 3$ (indicated with “e”) and for $m = 5$ (indicated with “f”). The simplified summation rule assumes that every load interval “I” has 0.5 cycle.

For a vehicle type “i” the equivalent number of cycles $n_{eq,i}$ for a specific crossbeam type is calculated for an S-N line with $m = 3$:

$$n_{eq,i} = e \cdot n_i \quad [6.31]$$

with:

$$e = 0.5 \cdot \Sigma \left[\left(\frac{I_1}{I_{imax}} \right)^3 + \left(\frac{I_2}{I_{imax}} \right)^3 + \left(\frac{I_3}{I_{imax}} \right)^3 + \dots + \left(\frac{I_n}{I_{imax}} \right)^3 \right] \quad [6.32]$$

and for an S-N line with $m = 5$:

$$n_{eq,i} = f \cdot n_i \quad [6.33]$$

with:

$$f = 0.5 \cdot \Sigma \left[\left(\frac{I_1}{I_{imax}} \right)^5 + \left(\frac{I_2}{I_{imax}} \right)^5 + \left(\frac{I_3}{I_{imax}} \right)^5 + \dots + \left(\frac{I_n}{I_{imax}} \right)^5 \right] \quad [6.34]$$

In a similar way, as before, although not in line with the intended use of FLM2, the equivalent number of cycles for all vehicles with respect to the maximum rotation interval is calculated for a particular crossbeam type.

The equivalent number of cycles for the long distance traffic on a particular crossbeam type is indicated with “g” for $m = 3$ and with “h” for $m = 5$. For this calculation, it is assumed that the lorry type distribution for the “frequent lorries” of FLM2 is similar to the distribution of the “equivalent lorries” of FLM4. For the analyses, the distribution “Long Distance” is chosen.

The equivalent number of cycles for the rotation intervals caused by a particular vehicle type “i” for a slope $m = 3$ or $m = 5$ of the S-N curve are further indicated with e_i and f_i , respectively. “p” is the fraction (percentage) of the vehicle type in relation to all vehicle types.

The equivalent number of cycles n_{eq} for all vehicle types on a particular crossbeam for an S-N line for $m = 3$ is now determined with:

$$n_{eq} = g \cdot n \quad [6.35]$$

with:

$$g = p_1 \cdot e_1 \cdot \left(\frac{I_{1,max}}{I_{max,max}} \right)^3 + p_2 \cdot e_2 \cdot \left(\frac{I_{2,max}}{I_{max,max}} \right)^3 + p_3 \cdot e_3 \cdot \left(\frac{I_{3,max}}{I_{max,max}} \right)^3 + p_4 \cdot e_4 \cdot \left(\frac{I_{4,max}}{I_{max,max}} \right)^3 + p_5 \cdot e_5 \cdot \left(\frac{I_{5,max}}{I_{max,max}} \right)^3$$

and for $m = 5$:

$$n_{eq} = h \cdot n \quad [6.36]$$

with:

$$h = p_1 \cdot f_1 \cdot \left(\frac{I_{1,\max}}{I_{\max,\max}} \right)^5 + p_2 \cdot f_2 \cdot \left(\frac{I_{2,\max}}{I_{\max,\max}} \right)^5 + p_3 \cdot f_3 \cdot \left(\frac{I_{3,\max}}{I_{\max,\max}} \right)^5 + p_4 \cdot f_4 \cdot \left(\frac{I_{4,\max}}{I_{\max,\max}} \right)^5 + p_5 \cdot f_5 \cdot \left(\frac{I_{5,\max}}{I_{\max,\max}} \right)^5$$

Here $I_{i,\max}$ is the maximum interval per lorry, and $I_{\max,\max}$ is the maximum of the five lorries for a particular crossbeam.

Table 6.8 gives the crossbeam out-of-plane rotation histories $\Delta\phi_3$ for a unit load of 100 kN on the deck and for the frequent vehicles in accordance with ENV 1991-3 and it gives the equivalent number of cycles for the rotation intervals of each vehicle type “i” for a particular crossbeam type.

In addition it gives the equivalent number of cycles for all lorries for a particular crossbeam type with respect to the maximum load interval indicated with “g” for $m = 3$ and with “h” for $m = 5$.

The maximum rotation intervals for each crossbeam and each vehicle given in Table 6.8 are underlined and the maximum load interval for a particular crossbeam type is indicated as **bold and underlined**. All rotation histories are determined for 7 crossbeam depths of conventional crossbeams with a span length l of 7200 mm and a cut-out width $W = 175$ mm and for crossbeams with an infinite stiffness $H = \infty$. For the individual lorries, the equivalent number of rotations for the crossbeam with $H = 600$ is between 0.64 and 1.13 for the maximum rotation interval for $m = 3$ and varies between 0.51 and 0.80 for $m = 5$. For a deck on rigid supports the equivalent number of cycles varies between 0.73 and 1.50 for $m = 3$ and between 0.60 and 1.26 for $m = 5$. The number of rotation intervals due to one lorry presented in Table 6.8 is about twice the number found for the in-plane load interval that can be derived from in Table 6.5. The equivalent numbers of cycles for the maximum rotation intervals $\Delta\phi_{3\max}$ for various crossbeam depths given in Table 6.8, are graphically presented in Fig. 6.23.

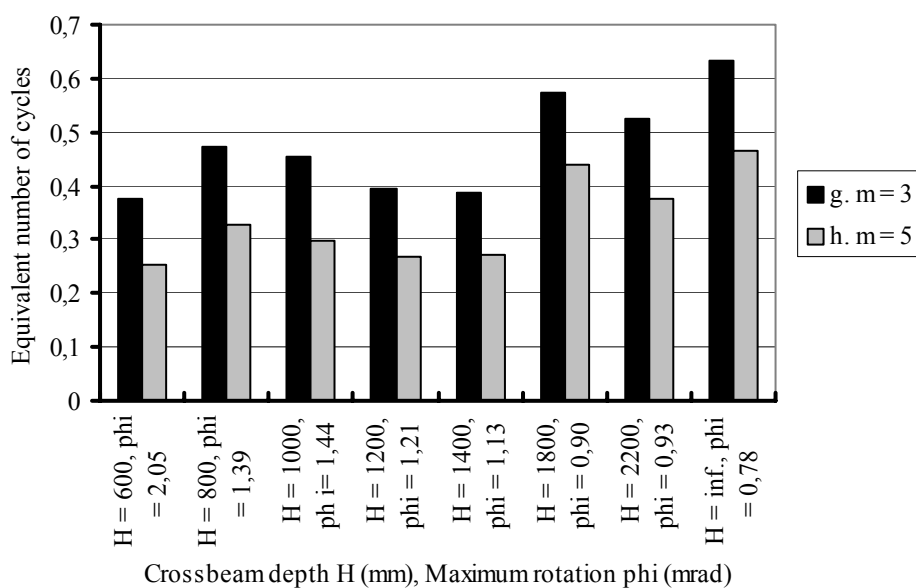


Fig.6.23 Maximum rotation intervals (indicated with phi) and equivalent nr. of cycles ”g” and ”h”

Table 6.8 Rotation intervals $\Delta\phi_3$ and equivalent nr. of rotations

ROTATION INTERVALS TROUGH TO CROSSBEAM CONNECTION (10^{-1} mrad) due to FLM2 with the distribution of FLM4							
Beam Type	Single Axle 100 kN (Unit Load)	Lorry Type, Total Load, Axle Loads					n_{eq} for $\Delta\phi_{3max}$
		1	2	3	4	5	
		$\Sigma P=280$ kN	$\Sigma P=360$ kN	$\Sigma P=630$ kN	$\Sigma P=560$ kN	$\Sigma P=610$ kN	
		90,190	80,140,140	90,180,120,120,120	90,190,140,140	90,180,120,110,110	
1 H = 600	3.9/7.8/3.9	3.5/10.9 e. 0.67 f. 0.51	7.3/18.1/10.8 e. 0.64 f. 0.54	8.7/20.5/11.8 e. 0.64 f. 0.54	6.9/7.9/3.0/ 11.7/9.7 e. 1.13 f. 0.80	5.7/13.8/8.1 e. 0.64 f. 0.54	g. 0.375 h. 0.253
2 H = 800	3.1/6.8/3.1	2.8/8.8/6.0 e. 0.68 f. 0.58	5.3/13.7/8.4 e. 0.64 f. 0.55	4.3/13.9/9.6 e. 0.68 f. 0.58	5.4/7.8/5.6/ 11.0/7.8 e. 0.98 f. 0.71	3.8/0.7/1.7/3.3/ 0.9/0.2/7.1/6.5 e. 1.02 f. 0.86	g. 0.472 h. 0.328
3 H = 1000	2.6/5.2/2.6	2.4/7.4/5.0 e. 0.67 f. 0.57	4.6/11.1/6.5 e. 0.64 f. 0.60	5.6/13.3/7.7 e. 0.63 f. 0.54	7.0/14.4/7.4 e. 0.63 f. 0.54	2.6/0.7/0.9/4.7/ 2.7/5.7/5.0 e. 1.22 f. 1.16	g. 0.454 h. 0.297
4 H = 1200	2.4/4.8/2.2	2.2/6.8/4.6 e. 0.67 f. 0.57	4.0/10.2/6.2 e. 0.64 f. 0.54	5.3/12.1/6.8 e. 0.63 f. 0.54	3.2/9.1/5.9 e. 0.85 f. 0.56	2.2/0.8/1.6/4.8/ 2.4/5.1/4.5 e. 1.37 f. 1.16	g. 0.395 h. 0.268
5 H = 1400	2.2/4.4/2.2	2.0/6.3/4.3 e. 0.68 f. 0.58	1.8/0.2/1.9/ 9.2/5.7 e. 0.63 f. 0.50	5.2/11.3/6.1 e. 0.63 f. 0.53	2.7/0.7/2.0/9.0/5 .0 e. 0.65 f. 0.53	2.0/3.0/1.6/3.9/ 2.4/5.0/3.9 e. 1.19 f. 0.85	g. 0.386 h. 0.271
7 H = 1800	0.2/1.9/3.8/ 1.9/0.2	1.9/3.1/1.6/ 3.7/3.9/0.4 e. 1.27 f. 1.06	0.2/4.3/9.0/ 5.2/0.4 e. 0.65 f. 0.55	0.2/2.2/0.7/3.3/9 0/4.1 e. 0.60 f. 0.52	0.2/2.2/5.7/7.9/8 7/4.9/0.4 e. 1.11 f. 0.90	1.3/2.1/3.3/3.9/ 3.9/6.0/3.5 e. 0.98 f. 0.68	g. 0.574 h. 0.438
9 H = 2200	0.2/1.9/3.8/ 1.9/0.2	1.9/3.2/1.7/ 3.8/4.0/0.5 e. 1.28 f. 1.07	0.2/4.3/8.9/ /4.8/0.6 e. 0.64 f. 0.54	0.2/2.1/0.6/2.9/8 2/4.6/0.6 e. 0.62 f. 0.54	0.2/2.2/7.4/9.3/8 .0/4.6/0.5 e. 1.14 f. 0.91	1.5/2.7/3.8/3.8/5.9 /3.4 e. 0.92 f. 0.65	g. 0.526 h. 0.375
$H = \infty$	0.5/1.5/3.0/ 1.5/0.5	0.2/1.6/3.5/ 2.5/3.1/3.6/0.9 e. 1.50 f. 1.26	0.4/3.2/6.0/ 4.6/1.3 e. 0.73 f. 0.60	0.5/4.7/7.7/4.9 e. 0.77 f. 0.64	0.5/1.9/5.1/7.8/6 7/3.8/1.2 e. 1.02 f. 0.81	1.3/2.2/1.6/2.8/4.7 /5.1/3.5/1.0 e. 1.21 f. 0.94	g. 0.632 h. 0.467

In general, it can be concluded that for $m = 3$, the equivalent number n_{eq} is between 0.37 and 0.63 and for $m = 5$, n_{eq} is between 0.25 and 0.47 for the total number of vehicles. With these values, the calculation procedure can be simplified.

When the equivalent numbers of cycles for all crossbeams are related to the maximum rotation interval found for $H = 600$ mm, the values become as presented in Fig. 6.24.

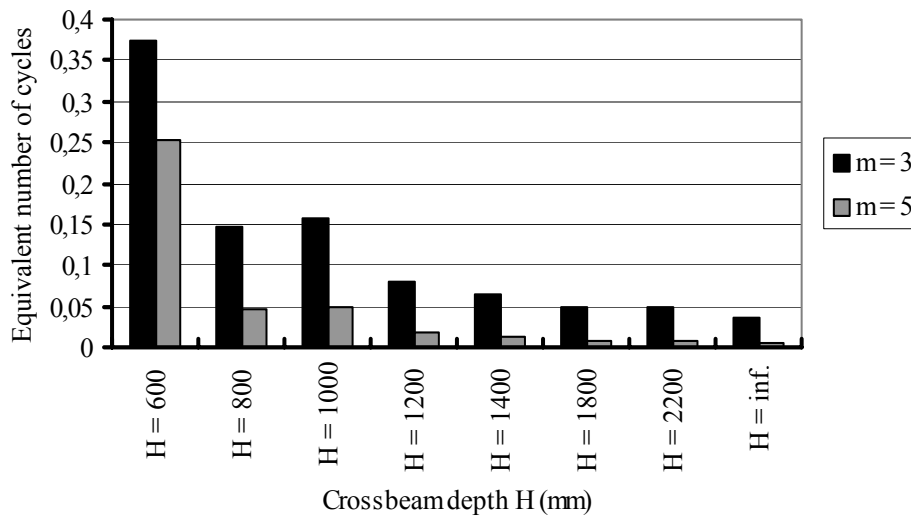


Fig. 6.24 Equivalent numbers of cycles in relation to $\Delta\varphi_3$ of 2.0 mrad of $H = 600$ mm

Combining the equivalent number of cycles and the rotation intervals, shows the relative fatigue damage D_{rel} of the crossbeam and the effect of flexible versus rigid crossbeams, see Table 6.9.

In Table 6.9 the $\Delta\varphi_3$ of $1.22 \cdot 10^{-3}$ rad for $H = \infty$ with $n_{eq} = 0.61$ for $m = 3$ and $n_{eq} = 0.53$ for $m = 5$ is assumed to given a reference damage 1.

Table 6.9 Relative damages

Crossbeam	$\Delta\varphi$ (mrad)	n_{eq} for $m=3$	D_{rel}	n_{eq} for $m=5$	D_{rel}
H=600	2.05	0.38	11.0	0.25	66.7
H=1200	1.21	0.40	2.4	0.27	5.2
H=2200	0.93	0.53	1.4	0.38	2.0
H=inf.	0.78	0.63	1	0.47	1

The rotation intervals and equivalent numbers of cycles for a selection of other crossbeam types are presented by their value of D_{rel} . For $H = 600$ mm. D_{rel} can be derived from that of $H = \infty$ with a scaling of the load intervals and the equivalent numbers of cycles: $(2.05/0.78)^3 \cdot (0.38/0.61) = 11.0$ for $m = 3$ and $(2.05/0.78)^5 \cdot (0.25/0.47) = 66.7$ for $m = 5$. The values D_{rel} for the other crossbeam types are determined in a similar way.

From Table 6.9 it can be concluded that for the locations governed by the out-of-plane behaviour of the crossbeam, the fatigue life is overestimated when influence lines are used for beams on rigid supports. The relative damage for the very flexible crossbeam is 11 times (for $m = 3$) and 67 times (for $m = 5$) the damage for rigid crossbeams. For crossbeams with an intermediate stiffness, the fatigue damage is about 2.4 (for $m = 3$) and is about 5 (for $m = 5$) times this damage for rigid crossbeams.

Based on Figs. 6.23 and 6.24, a very safe assumption for all crossbeam types is: $n_{eq} = 0.37$ for $m = 3$ and $n_{eq} = 0.26$ for $m = 5$, in combination with $\Delta\varphi_3 = 2.0$ mrad.

6.6.2.2 FE simulations for rotation histories

In a similar procedure to that used for the crossbeam load histories, the rotation histories determined with the analytical method are verified by and extended with computer simulations for additional influences such as trough span length and additional crossbeam stiffnesses (represented by spring constants). The model is the same as shown in par. 6.5.2.1.

Tables A2.2a, A2.2b and A2.2c show the rotation intervals $\Delta\phi_3$. The calculations with the analytical model are determined for crossbeam distances of 4.0 m only. With the FE model, the crossbeam distances of 3.5 m and 4.5 m are also analysed. All indications in the tables are similar to those used in the previous tables. The centre-on-centre crossbeam distances are again indicated with r, s and t:

r. =	Crossbeams	centres 3500 mm
s. =	Crossbeams	centres 4000 mm
t. =	Crossbeams	centres 4500 mm

For most crossbeams, the maximum $\Delta\phi_3$ values found with the computer simulations comply rather well with those from the analytical model (values between brackets). This observation applies for the unit loads and for the intervals caused by the lorries.

It demonstrates that even with estimated positions of the lorries, reasonable results are obtained with the analytical model.

The computer simulations cover a larger range of crossbeam spring stiffnesses, but the values in Tables A2.2a, A2.2b and A2.2c demonstrate that for a crossbeam stiffness ten times higher than that of the crossbeam with a depth $H = 2200$ mm, already rotations are obtained that are very close to those for a beam on infinite rigid supports. This means that the analytical procedure covers a range of crossbeam stiffnesses that is large enough for all stiffnesses.

Tables A2.2a, A2.2b and A2.2c also show the effect of the crossbeam distances 3500 mm, 4000 mm and 4500 mm, respectively. For the flexible crossbeams, the rotation interval for a span of 3500 mm is approximately 90% and for a span of 4500 mm about 110% of that for a span of 4000 mm. For the deeper crossbeams, these values are about the same, but for a crossbeam on rigid supports values of about 70% and 130% are found. The number of cycles found with the analytical procedure, are roughly equal to those found with the FE method. The numbers of cycles increase with an increasing stiffness of the crossbeams.

As an example, the results of the analysis for lorry type 3 are shown in Fig. 6.25.

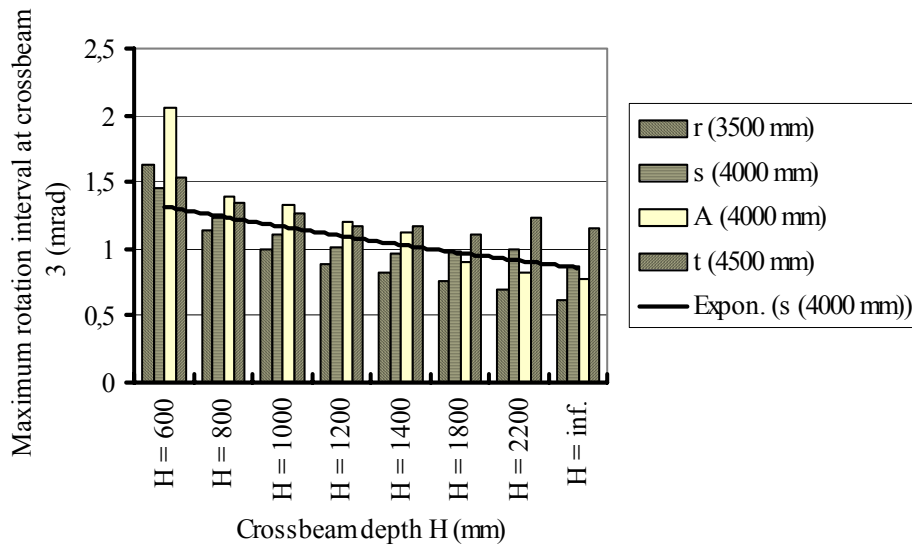


Fig. 6.25 Rotation intervals $\Delta\varphi_3$ for Lorry 3 from FE calculations and analytical model (A)

6.6.3 Deck bending moment histories

6.6.3.1 Calculations with FE models

The previous analyses showed a good agreement between the analytical method, where the reaction and rotation histories were determined with the estimated positions of the vehicles and the histories determined with the FE model. Therefore, the deck bending moment histories are determined with the influence lines determined in 6.5.3, by positioning the vehicles in subsequent locations. As before, for the crossbeam in-plane load amplitudes and the trough to crossbeam connection, the rotation amplitudes and deck bending moment amplitudes are calculated for each crossbeam type. In this calculation, the previously derived influence lines are used. A unit load of 100 kN with respect to the frequent vehicles in accordance with ENV 1991-1-3 are positioned in successive locations on the deck between crossbeam 1 and 5.

The deck bending moment intervals are derived from the trough to crossbeam connection rotation amplitudes. The successive rotation intervals caused by a vehicle are called the rotation history. For each crossbeam type and each frequent lorry type the equivalent numbers of cycles related to the maximum rotation interval are calculated with a “simplified” rainflow procedure, for a S-N slope $m = 3$ (indicated with “j”) and for $m = 5$ (indicated with “k”). A simplified summation rule assumes that every load interval “I” has 0.5 cycle.

For a vehicle type “i” the equivalent number of cycles $n_{eq,i}$ for a specific crossbeam type is calculated for an S-N line with $m = 3$:

$$n_{eq,i} = j \cdot n_i \quad [6.37]$$

with:

$$j = 0.5 \cdot \Sigma \left[\left(\frac{I_1}{I_{i\max}} \right)^3 + \left(\frac{I_2}{I_{i\max}} \right)^3 + \left(\frac{I_3}{I_{i\max}} \right)^3 + \dots + \left(\frac{I_n}{I_{i\max}} \right)^3 \right] \quad [6.38]$$

and further for a S-N line with $m = 5$:

$$n_{eq,i} = k \cdot n_i \quad [6.39]$$

with:

$$k = 0.5 \cdot \Sigma \left[\left(\frac{I_1}{I_{i\max}} \right)^5 + \left(\frac{I_2}{I_{i\max}} \right)^5 + \left(\frac{I_3}{I_{i\max}} \right)^5 + \dots + \left(\frac{I_n}{I_{i\max}} \right)^5 \right] \quad [6.40]$$

In a similar way, although not in line with the intended use of FLM2, again the equivalent number of cycles for all vehicles with respect to the maximum rotation interval is calculated for a particular crossbeam type and a particular vehicle. The equivalent number of cycles for the long distance traffic on a particular crossbeam type is indicated with “l” for $m = 3$ and with “m” for $m = 5$. It is assumed that the vehicle type distribution for the “frequent lorries” of FLM2 is similar to the distribution of the “equivalent lorries” of FLM4. For the analyses, the distribution “Long Distance” is chosen.

The equivalent number of cycles for the bending moment intervals caused by a particular vehicle type “i” for a slope $m = 3$ or $m = 5$ of the S-N curve are further indicated with j_i and k_i , respectively. “p” is the fraction (percentage) of the vehicle type in relation to all vehicle types.

The equivalent number of cycles n_{eq} for all vehicle types on a particular crossbeam for an S-N line with $m = 3$ is now determined with:

$$n_{eq} = l \cdot n \quad [6.29]$$

with:

$$l = p_1 \cdot j_1 \cdot \left(\frac{I_{1,\max}}{I_{\max,\max}} \right)^3 + p_2 \cdot j_2 \cdot \left(\frac{I_{2,\max}}{I_{\max,\max}} \right)^3 + p_3 \cdot j_3 \cdot \left(\frac{I_{3,\max}}{I_{\max,\max}} \right)^3 + p_4 \cdot j_4 \cdot \left(\frac{I_{4,\max}}{I_{\max,\max}} \right)^3 + p_5 \cdot j_5 \cdot \left(\frac{I_{5,\max}}{I_{\max,\max}} \right)^3$$

and for $m = 5$:

$$n_{eq} = m \cdot n \quad [6.30]$$

with:

$$m = p_1 \cdot k_1 \cdot \left(\frac{I_{1,\max}}{I_{\max,\max}} \right)^5 + p_2 \cdot k_2 \cdot \left(\frac{I_{2,\max}}{I_{\max,\max}} \right)^5 + p_3 \cdot k_3 \cdot \left(\frac{I_{3,\max}}{I_{\max,\max}} \right)^5 + p_4 \cdot k_4 \cdot \left(\frac{I_{4,\max}}{I_{\max,\max}} \right)^5 + p_5 \cdot k_5 \cdot \left(\frac{I_{5,\max}}{I_{\max,\max}} \right)^5$$

Here $I_{i,\max}$ is the maximum interval per lorry, and $I_{\max,\max}$ is the maximum of the five lorries for a particular crossbeam.

Table 6.10 gives the deck bending moment intervals for a unit load of 100 kN on the deck and for the frequent vehicles in accordance with ENV 1991-3 and it gives the equivalent number of cycles for the load intervals of each vehicle type “i” for a particular crossbeam type. The equivalent numbers of cycles for a specific crossbeam type due to a vehicle type for a S-N slope $m = 3$ are indicated with “j” and for $m = 5$ indicated with “k”. In addition it gives the equivalent number of cycles for all vehicles for a particular crossbeam type with respect to the maximum load interval indicated with “l” for $m = 3$ and with “m” for $m = 5$.

The maximum bending moment intervals for each vehicle in Table 6.10 are underlined and the maximum bending moment interval for a particular crossbeam type is indicated as **bold and underlined**.

All bending moment intervals are determined for 7 crossbeam depths of conventional crossbeams with a span length l of 7200 mm and a cut-out width $W = 175$ mm and for crossbeams with an infinite stiffness $H = \infty$. For individual lorries the equivalent number of deck bending moments varies for the crossbeam $H = 600$ mm and for $m = 3$ between 0.70 and 1.20 and between 0.58 to 1.14 for $m = 5$. For a deck on rigid supports the equivalent number of cycles for individual lorries varies between 0.80 and 1.75 for $m = 3$ and between 0.65 and 1.46 for $m = 5$.

Fig. 6.26 shows the equivalent numbers of cycles (l and m) for the maximum deck bending moment intervals M_{D3} for various crossbeam depths as given in Table 6.11.

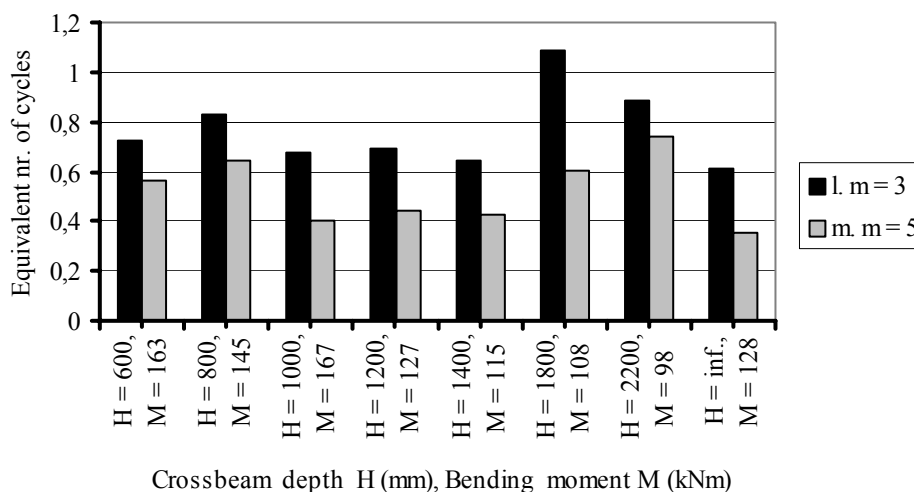


Fig. 6.26 Maximum deck bending moment intervals M_{D3} (indicated with M) and equivalent nr. of cycles

Table 6.10 Bending moment intervals ΔM_{D3} (kNm x10)

DECK BENDING MOMENT INTERVALS (kNm) due to FLM2 with the distribution of FLM4							
BEAM TYPE	SINGL E AXLE 100kN	LORRY TYPE					N _{eq} for ΔM_{3D}
		1 $\Sigma P=280$ kN	2 $\Sigma P=360$ kN	3 $\Sigma P=630$ kN	4 $\Sigma P=560$ kN	5 $\Sigma P=610$ kN	
		90, 190	80, 140, 140	90, 180, 120, 120, 120	90, 190, 140, 140	90, 180, 120, 110, 110	
H = 600	8.030	2.0/11.1/13.3/ 4.2 j. 0.953 k. 0.857	1.8/7.8/12.0/ 5.9 j. 0.702 k. 0.576	4.0/7.7/16.1/ 13.0/ 7.2/14.0 j. 1.200 k. 1.023	2.0/8.0/16.3/ 14.3/11.9/7.9 j. 1.154 k. 1.149	2.0/8.0/7.3/6.4/ 9.2/4.6 j. 1.194 k. 0.884	l. 0.728 m. 0.564
H = 800	9.650	6.2/13.0/11.0/ 4.2 j. 0.850 k. 0.725	1.8/6.7/10.4/ 5.5 j. 0.709 k. 0.576	4.0/6.9/14.2/ 14.5/ 9.7/6.2 j. 1.185 k. 0.991	2.0/6.4/14.2/ 12.4/7.5/4.9 j. 0.926 k. 0.779	2.0/2.7/5.6/9.0/ 4.3/3.0 j. 0.979 k. 0.700	l. 0.831 m. 0.645
H = 1000	5.840	2.0/2.0/5.8/ 11.3/ 9.6 /4.2 j. 1.143 k. 0.752	6.2/8.7/7.9/5.4 j. 1.178 k. 0.950	4.7/7.0/13.3/ 16.7/ 12.6/6.8 j. 1.051 k. 0.798	1.9/5.7/13.6/ 12.6/8.0/5.2 j. 1.062 k. 0.593	2.0/6.7/9.1/9.2/ 3.7/4.9/8.8/5.9/ 4.6 j. 1.916 k. 1.575	l. 0.680 m. 0.404
H = 1200	5.160	2.0/2.0/6.0/ 10.4/8.6/ 4.2 j. 0.960 k. 0.778	2.3/1.7/6.6/7.8/6 .3/ 5.7 j. 1.278 k. 1.002	3.4/5.4/12.7/ 10.3/ 5.9/6.5 j. 0.929 k. 0.708	3.2/2.3/7.8/ 10.1/6.7/5.2 j. 0.953 k. 0.709	2.1/2.6/7.1/9.6/ 10.5/8.1/4.2/3.5 j. 1.327 k. 1.032	l. 0.690 m. 0.443
H = 1400	4.820	2.1/2.3/6.6/ 10.2/8.3/ 4.5 j. 0.951 k. 0.737	2.2/1.5/7.1/7.1/6 .0 j. 1.319 k. 1.219	2.1/3.7/7.6/6.0 j. 0.811 k. 0.787	3.0/1.7/4.4/8.2/1 0.9/11.5/8.4/5.3 j. 1.308 k. 1.104	2.3/2.7/7.1/5.3/ 6.2/8.1/4.8/4.5 j. 1.381 k. 1.014	l. 0.644 m. 0.424
H = 1800	4.270	2.4/2.7/7.7/9.9/ 7.8/ 5.1 j. 1.056 k. 0.798	1.5/1.0/7.9/6.9/0 .3/ 1.8 j. 0.843 k. 0.754	6.5/8.1/10.8/ 5.5/7.1 j. 1.200 k. 0.820	2.3/0.5/5.1/8.6/8 .4/5.8/4.9/ 6.0/0.3 j. 1.501 k. 1.171	1.8/2.7/7.8/8.5/ 7.0/4.5/5.5/0.4 j. 1.769 k. 1.596	l. 1.091 m. 0.607
H = 2200	4.040	2.5/3.1/6.2/5.6 j. 0.965 k. 0.821	1.0/1.7/9.4/6.6/4 .0/ 6.1 j. 0.854 k. 0.653	6.8/5.6/9.8/4.9/ 3.3/7.0 j. 1.017 k. 1.048	2.1/0.3/5.7/8.7/7 .8/4.7/0.3/ 2.7/0.7 j. 1.135 k. 0.850	2.1/2.6/7.9/7.3/ 7.4/7.5/7.9/9.0/ 7.4/6.2/0.7 j. 2.534 k. 1.927	l. 0.887 m. 0.742
H = ∞	4.290	1.0/9.1/10.2/ 2.1 j. 0.860 k. 0.783	0.9/10.6/12.4/ 2.7 j. 0.814 k. 0.730	8.1/4.3/3.5/1.0/ 1.9/10.3/2.2 j. 0.802 k. 0.654	1.0/10.25.9/ 2.4/3.1/5.0/ 10.2/2.5 j. 1.749 k. 1.457	1.0/2.2/7.9/12.8/ 7.3/8.0/6.8/4.0/ 3.2/5.6 j. 0.978 k. 0.655	l. 0.616 m. 0.357

In general it can be concluded that for $m = 3$ the equivalent number n_{eq} is between 0.6 and 1.1 and for $m = 5$, n_{eq} is between 0.4 and 0.8 times the total number of lorries.

Comparing the maximum deck bending moment intervals and the equivalent numbers of cycles of $H = 600$ mm, $H = 800$ mm and $H = 1000$ mm with the influence lines, it is observed that the zero intercept of the influence lines is shifted about 500 mm for each successively deeper type of crossbeam, which influences, together with the lorry configurations, the positive and negative contributions in the resulting bending moment. In addition, the maximum and minimum amplitudes change considerably. A similar observation can be made for the crossbeams $H = 1800$ mm, $H = 2200$ mm and $H = \infty$.

Fig. 6.27 shows the adapted equivalent numbers of cycles for all crossbeams if all would be subjected to the maximum deck bending moment M_{D3} of the crossbeam with $H = 1000$ mm.

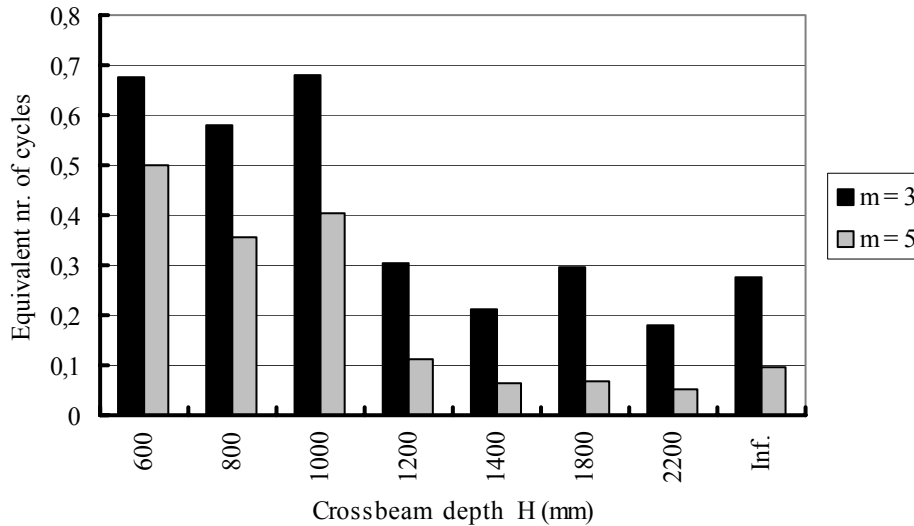


Fig. 6.27 Equivalent numbers of cycles in relation to M_{D3} of 167 kNm of $H = 1000$ mm

Combining the equivalent number of cycles n_{eq} and the crossbeam intervals shows the relative damage D_{rel} of the deck and the effect of flexible, versus rigid crossbeams, see Table 6.11. In Table 6.11 the M_{3D} of 128 kNm for $H = \infty$ with $n_{eq} = 0.62$ for $m = 3$ and $n_{eq} = 0.36$ for $m = 5$, is assumed to give a reference damage 1.

Table 6.11 Relative damages

Crossbeam	ΔM_D (kNm)	n_{eq} for $m=3$	D_{rel}	n_{eq} for $m=5$	D_{rel}
H=600	163	0.73	2.4	0.56	5.2
H=1200	127	0.69	1.1	0.44	1.2
H=2200	98	0.89	0.6	0.74	0.5
H=inf.	128	0.62	1	0.36	1

The deck bending moment intervals and equivalent numbers of cycles for a selection of other crossbeam types are presented by their value of D_{rel} . For $H = 600$ mm. D_{rel} can be derived from that of $H = \infty$ with a scaling of the load intervals and the equivalent numbers of cycles: $(163/128)^3 \cdot (0.73/0.62) = 2.4$ for $m = 3$ and $(163/128)^3 \cdot (0.56/0.36) = 5.2$ for $m = 5$. The values D_{rel} for the other crossbeam types are determined in a similar way.

From Table 6.11 it can be concluded that for the locations governed by the bending moments in the deck for a flexible crossbeam with $H = 600$ mm, using influence lines for a beam on rigid supports, the fatigue damage is underestimated. The relative damage for this very flexible crossbeam is about 2 times (for $m = 3$) and 5 times (for $m = 5$) the damage for rigid crossbeams.

For crossbeams with an intermediate stiffness, the fatigue damage varies from about 0.6 to 1.2 (for $m = 3$) and 0.5 to 1.2 (for $m = 5$) times the damage for rigid crossbeams.

Based on Figs. 6.26 and 6.27, a very safe assumption for all crossbeam types is: $n_{eq} = 0.7$ for $m = 3$ and $n_{eq} = 0.5$ for $m = 5$, in combination with $M_{D3} = 167$ kNm.

6.7 Partially loaded crossbeams

For the loading of the crossbeam and the deck to crossbeam connection in a partially loaded deck, use is made of the relationship between the spring constants of the deck K_D^1 and that of the fully loaded crossbeam K_C^1 .

6.7.1 Crossbeam load intervals

From the quotient K_D^1/K_C^1 (see Fig. 6.12) the relevant influence line can be selected for crossbeam 3. The maximum load intervals ΔP_{C3V} and the equivalent numbers of cycles for the crossbeam can be directly determined with Table 6.5 and Fig. 6.20.

6.7.2 Crossbeam rotation intervals

From the quotient K_D^1/K_C^1 (see Fig. 6.12) the relevant influence line can be selected for crossbeam 3. The rotation intervals $\Delta\phi_3$ and the equivalent numbers of cycles can be derived from Table 6.8 and Fig. 6.23. However, the actual rotations are obtained by scaling with the factor c_d , which corrects the rotations for the smaller deck bending stiffness.

$$c_d = \frac{b_l}{4800} \quad [6.43]$$

in which b_l is the lane width and 4800 is 2/3 of the span length of the standard crossbeam.

6.7.3 Deck bending moments

From the quotient K_D^1/K_C^1 (see Fig. 6.12) the relevant influence line can be selected for crossbeam 3. The maximum deck bending moment interval ΔM_{D3} and the equivalent numbers of cycles can be derived from Table 6.10 and Fig. 6.26.

6.8 Concluding remarks

Crossbeam reactions

For the crossbeam load histories for fully loaded crossbeams, the calculation with influence lines for beams on rigid supports overestimates the crossbeam load effects for shallow crossbeams.

Trough to crossbeam connection rotations

For the rotation histories, the calculation with influence lines for fully loaded crossbeams on rigid supports underestimates the deck to crossbeam connection rotation effect for shallow crossbeams.

Bending moments in the deck

For the deck bending moment histories, the calculation with influence lines for beams on rigid supports may underestimate the deck bending moment effect for shallow crossbeams

Agreement between analytical method and computer simulations

In general, a good agreement was found between the two methods.

Wider application of the results

With the quotient K_D^1/K_C^1 , the reaction, rotation and deck bending results can be used for all types of crossbeams, crossbeam depths and crossbeam spans.

For partially loaded crossbeams, the support conditions for the deck tend to be close to those of the more rigid fully loaded crossbeams.

7 VALIDATION OF ANALYTICAL CALCULATION METHODS WITH FE CALCULATIONS AND MEASUREMENTS

7.1 Introduction and objective

In chapters 4, 5, and 6 the calculation results from the analytical models were compared with the results from FE models. Most of these FE analyses were carried out with the DIANA program.

This chapter describes a further validation of the analytical models. The results from analytical models and various FE analyses with the DIANA and the ANSYS programs are compared with those of strain gauge measurements. The analyses consider the behaviour of the conventional crossbeams, with geometrical stress concentration factors.

In 7.2, the analyses of the ECSC 3rd Phase specimens tested at Delft University of Technology are described and the differences between the fatigue resistances found in these tests and similar tests in the UK are explained.

The analyses and measurements of the ECSC 4th Phase specimens used for the full-scale crossbeam tests are presented in 7.3

7.2 Single trough specimens

7.2.1 Test specimen

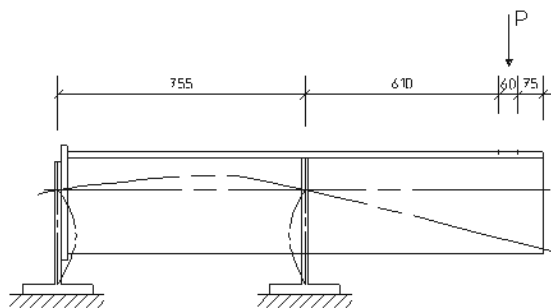


Fig. 7.1 shows one of the ECSC 3rd Phase test specimens, used for the single trough tests, together with a deflection line. The deck plate is stiffened with one trapezoidal stiffener FKH 2/325/6 and has a length of 1500 mm. The specimen has two fixed line supports, at the left and near the centre. The load is applied at the right hand end.

Fig.7.1 Test specimen ECSC Research Phase 3

7.2.2 Measurements and Models

7.2.2.1 Measurements

Strain gauges were applied to the test specimens at all relevant locations in the vicinity of the trough to crossbeam connection. (See Kolstein et al. (1995a))

7.2.2.2 Models

The behaviour was calculated with an analytical model consisting of a cantilever beam supported by two columns. In addition, the complete test specimens were modelled with the DIANA program with 4-node shell elements. The weld geometry was not modelled. The models were loaded by a line load in the transverse direction on the deck plate with a resultant equal to the applied test load. The support conditions replicated those of the test specimens.

7.2.2.3 Comparison of analyses with strain gauge measurements

The comparison of the analyses with the strain gauge measurements has been described in Leendertz et al. (1995a).

As an illustration of the stress patterns of the three details tested, Fig. 7.2 shows an overview of the calculated stresses with the FE program along and parallel to the connection of the trough to the crossbeam or along and parallel to the edge of the cope hole in the crossbeam web. The in-plane membrane effect (M) is shown, together with the out-of-plane bending effect (B).

In these specimens, the membrane stresses (M) generated by the in-plane behaviour are mainly caused by the load introduction and do not include the Vierendeel behaviour of the crossbeam.

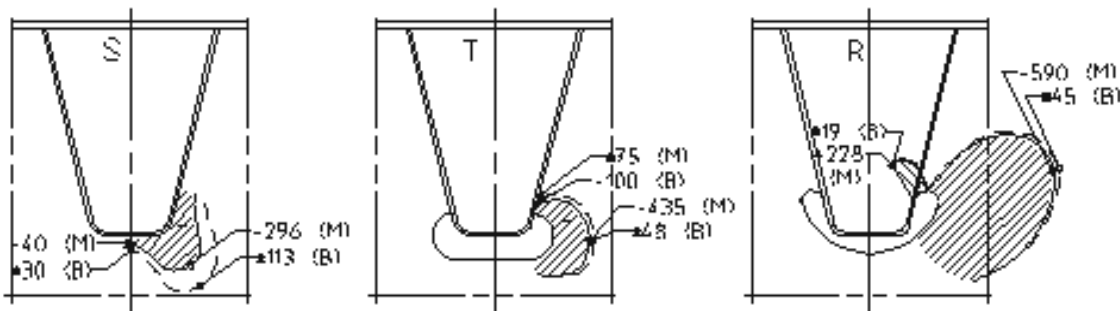


Fig. 7.2 Calculated membrane stresses (M) and bending stresses (B) for test specimens S, T and R

The stress patterns in Fig. 7.2 show that the out-of-plane bending stresses (B) for both details with cope holes have the same magnitude (48 & 45). The highest stresses due to bending are found in the specimen without a cope hole (113). The membrane stresses (M) in the specimen with the “Haibach” cope hole (right)(590) are much higher than those in the specimen with the oval cope hole (middle)(435), but the lowest membrane stresses are found in the specimen without a cope hole (left)(296).

These stresses, which were obtained with FE shell models, are not fully representative near the trough to crossbeam connection, because of the absence of the weld geometry in the connection details.

However, the stress patterns of the three details can still be used for a qualitative comparison. This applies for those cases, where the measured strains are in the same direction as the principal stress and the analytically determined stress and the measured stresses are not influenced by plate thicknesses and weld geometries.

7.3 Full scale crossbeam test specimen

7.3.1 Introduction

The measurements and FE analyses of the full-scale crossbeam specimen in the 4th Phase ECSC Research were carried out for a further validation of the analytical method with the crossbeam in-plane and out-of-plane models as described in chapter 4 and the geometrical stress concentration factors as described in chapter 5.

In order to achieve a realistic in-plane and out-of-plane behaviour, the crossbeam and its details had dimensions as used in practice. The support and boundary conditions of the specimen also represented realistic "built in" conditions and the in-plane loading and out-of-plane rotation conditions were representative for those in real bridges.

7.3.2 Dimensions and materials

Table 7.1 Dimensions and properties of full-scale test specimen

Item	Dimensions (mm)	Properties
Span	4800	-
Web	l=4800, h=772, t=10	-
Deck plate	b=2000, t=12	S355
Bottom flange	Strip 200x16	S355
Vertical end plate	Strip 200x16	S355
Deck edge stiffeners	Strip 200x16	S355
Support	Strip 300x10	S355
Cut-outs	4x for FKH 2/325/6 with oval cope hole W = 175 mm, R = 35 mm 4x for FKH 2/325/6 with close fit	-
Trough stiffeners	8x FKH 2/325/6 l=2000	FE 510 KQ
Welds	All welds, excluding weld to end plate: fillet welds a=4mm End plate vertical welds: 1/2 V=5mm	-

Fig. 7.3 shows the drawing of the crossbeam, including the structural details used for the manufacture of the test specimen and Table 7.1 gives the relevant dimensions and properties.

The FKH 2/325/6 closed stiffeners were used in most bridges recently built in The Netherlands. The total width of the oval cope hole is 175 mm; the radii are 35 mm. The trough centre-to-centre distance of 600 mm is commonly used. The crossbeam depth of 800 mm is sometimes used for smaller bridges.

The end supports of the specimen consist of vertical supporting plates (strips) generating an in-plane rotational spring stiffness, which is less than 0.1% that of the crossbeam end. Thus, in-plane, the support acts like a hinge. The strips are wide enough to provide a clamping for the crossbeam out-of-plane rotations at the supports.

Validation of analytical calculation methods with FE calculations and measurements

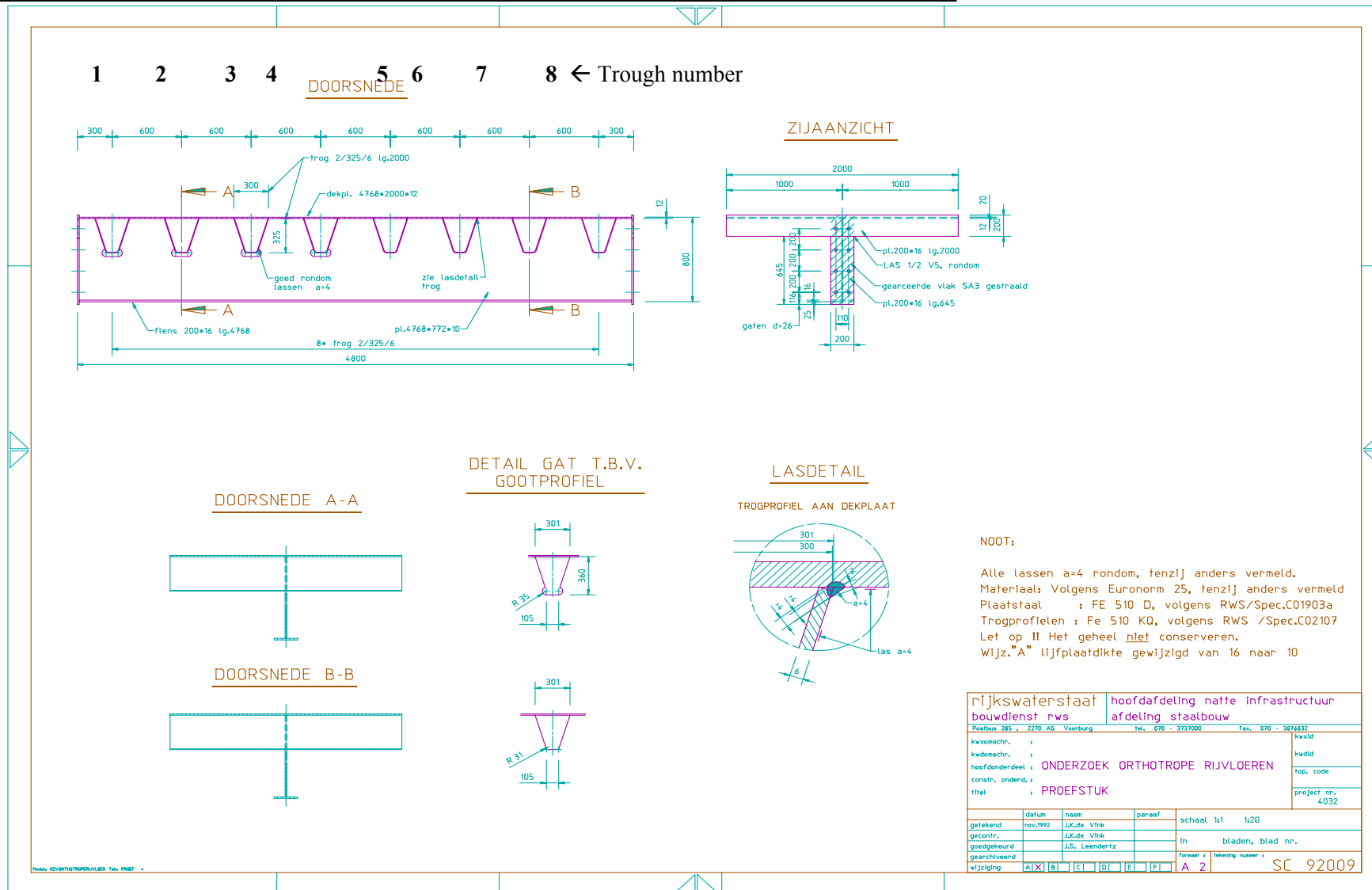


Fig. 7.3 Drawing of the full-scale test specimen (text in Dutch)

7.3.3 Calculation models

7.3.3.1 FE shell elements model

Initially, an FE shell element model was used, which consisted of 8-node shell elements. This meant that the stresses were only reliable at locations that were not highly affected by the local structural geometry. (e.g. plate and weld thickness). Thus, the local stresses near the trough to crossbeam connections were not reliable. This also applies to locations where elements generated “hard” supports and singularities.

The results were contour plots of principal stresses and the stress results presented in the Tables 7.5 - 7.8, 7.13 - 7.16 of this chapter are indicated with “FESh”

7.3.3.2 FE solid elements model

In order to obtain a better insight into the stresses for those locations influenced by the plate and weld thickness, an additional FE model with small 8-node solid elements was used.

Figs 7.4a and 7.4b show two characteristic element meshes at the trough to crossbeam connections.

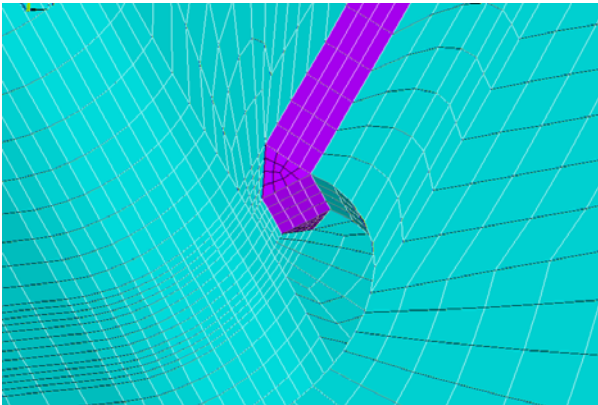


Fig. 7.4a FE model with solid elements, connection with cope hole (troughs 1 – 4)

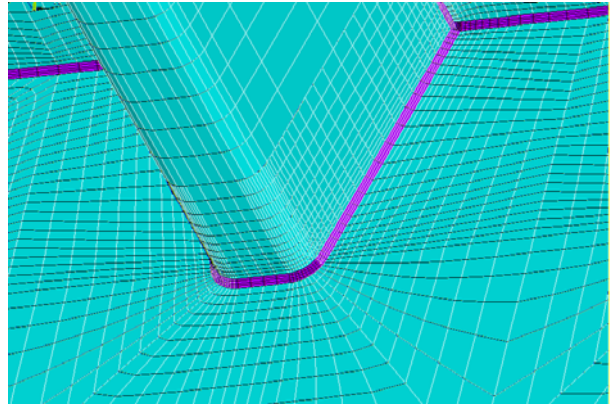


Fig. 7.4b FE model with solid elements, connection with close fit (trough 5 – 8)

The results of this model are indicated with “FESo”.

7.3.3.3 Analytical model

The crossbeam modelling presented in chapter 4 was used to calculate the section forces, bending moments and nominal stresses due to in-plane and out-of-plane crossbeam loading. The geometrical stress concentration factors determined in chapter 5 were used to obtain the geometrical stresses.

The in-plane analysis using the analytical model, considered the relative horizontal and vertical displacements and the rotations at the ends of the trough to crossbeam connections. Although the theoretical tooth length in the analyses of chapter 4 was 350 mm and was actually 360 mm in the test specimen, this deviation is considered to be small and with a negligible influence on the correction factor c_c for the tooth length, given in Table 4.2, which is also used here.

For the specimen considered, the equivalent web thickness for shear due to the cut-outs and cope holes is 67% of the original thickness, i.e. 6.7 mm.

The effective widths of the top flange of the crossbeam were considered in accordance with EN 1993-1-5, i.e. $b_{\text{eff.1.2}} = 803$ mm for the cross section at trough 2 and $b_{\text{eff.1.3}} = 877$ mm for the cross section at trough 3, based on a triangular shaped bending moment diagram. For uniformly distributed loads the $b_{\text{eff.2.2}} = 1436$ mm for the cross section at trough 2 and $b_{\text{eff.2.3}} = 1565$ mm for the cross section at trough 3.

The analytical results are indicated with “A”. In some cases, a stress in the principal direction is indicated with “A_1” and the stress perpendicular to the main direction with “A_2” or with A_perp. When two stresses are given in a Table, the first, indicated with (Q) applies for a crossbeam with an effective width for a uniformly distributed loading (Q) and the second, indicated with (P) for an effective width for a point loading.

7.3.3.4 Loads

The test specimen was loaded with four vertical loads, resulting in a total load interval of 300 kN ($R=1.0$) and an imposed out-of-plane rotation interval on the crossbeam of 0.008 rad (+/-0.004 rad) as shown in Figs. 7.5 to 7.7.

Table 7.2 gives an overview of all applied loads on the test specimen, and those used in the FE and the analytical models.

Table 7.2 Loads and rotations on test specimen

Loading configuration numbering			Applied loads, rotations	Distance of loads	Locations
Test load nr.	FE nr.	Analytical model nr.			
1A	5	1A	2x150kN	1200mm	in web plane
1C	2	-	4x75kN	1200mm	end of trough
2A	6	2A	2x150kN	1800mm	in web plane
2C	4	-	4x75kN	1800mm	end of trough
3	1	3	+/- 0.004rad	-	About crossbeam axis
4* (1A+3)	1+5	1A+3	-	1200mm (vert. loads)	in web plane + rot.
Static tests: Load configuration 1A, 1C, 2A, 2C					
Fatigue test: Load configuration 4 is a combination in time of tests 1A and 3 (see Fig.7.6)					

Tests 1 to 3 were used to measure the stresses under various static loading conditions and Test 4 was used to determine the fatigue behaviour. In Tests 1 and 2, the load distances chosen were 1200 mm and 1800 mm to compare the effect of loads on or between the troughs.

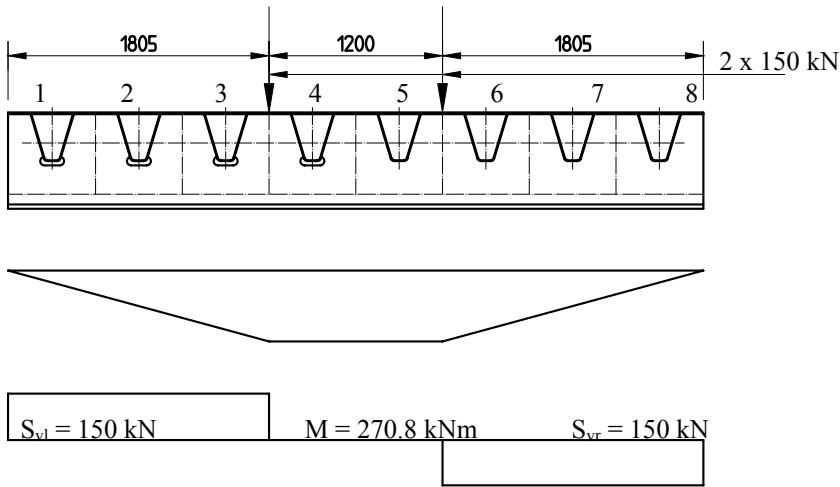


Fig. 7.5 Test load arrangement of Case 1A

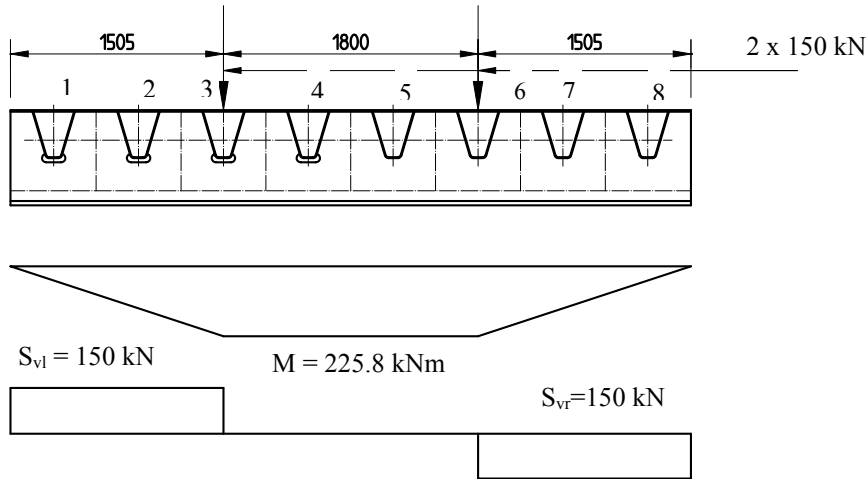


Fig. 7.6 Test load arrangement of Case 2A

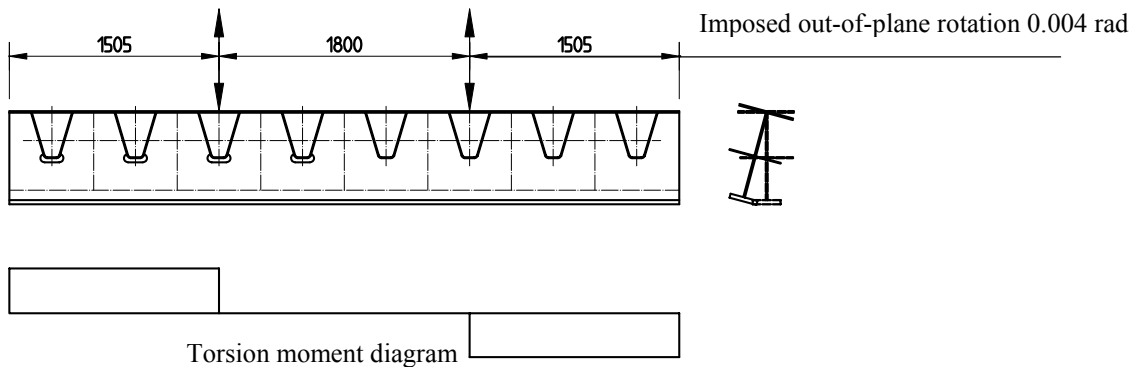


Fig. 7.7 Test load arrangement of Case 3

In addition, in these tests, the effect of the position of the loads was investigated, i.e. with two loads of 150 kN directly in the plane of the crossbeam (1A and 2A) or with four loads of 75 kN at the ends of the troughs (1C and 2C).

In Test 3, the specimen was only subjected to an out-of-plane rotation. Test 4 was a fatigue test, in which the test specimen was subjected to a combination of in-plane loads in the crossbeam web plane, together with out-of-plane rotations.

Figs. 7.5 - 7.7 show the test load arrangements for the tests 1A, 2A and 3, respectively.

In-plane section forces and bending moments in the crossbeam

Table 7.3 Section forces and bending moments in test crossbeam

Test	Load distance	Shear forces (kN), Bending moments (kNm)			
		Trough nr.	2,7	3,6	4,5
1A	1200	Shear	150	150	0
		Moment	136	226	271
2A	1800	Shear	150	75	0

Table 7.3 gives the crossbeam shear forces and in-plane bending moments for the tests 1A and 2A in the relevant cross sections, as the section forces and moments are the basis for all nominal stresses determined with the models in chapter 4.

7.3.4 Stresses at a cope hole for Test load 1A (in-plane)

The geometry of the tooth at the left hand side of trough 1 differs from the general geometry, as it includes the vertical support. At troughs 4 and 5 local loads are introduced in the deck plate and stiffeners. Therefore, the stress results are only presented for the cut-outs for troughs 2 and 3. All considered locations are indicated in Fig. 7.8 and explained in Table 7.4.

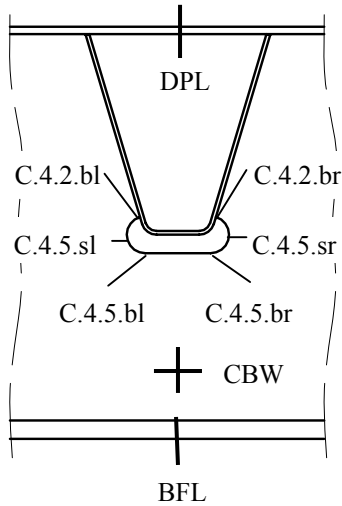


Table 7.4 Analysed and measured locations

Location	
DPL	Deck plate at the centre line of the trough
C.4.2l	Connection tooth to trough, left side, 145 mm from the centre of cope hole along the free edge
C.4.5sl	Free edge of tooth, left side, 106 mm from the centre of cope hole along the free edge
C.4.5bl	Transition area of tooth to T-beam, left side, 81 mm from the centre of cope hole along the free edge
C.4.2r	Connection tooth to trough, right side, 145 mm from the centre of cope hole along the free edge
C.4.5sr	Free edge of tooth, right side, 106 mm from the centre of cope hole along the free edge
C.4.5br	Transition area of tooth to T-beam, right side, 81 mm from the centre of cope hole along the free edge
CBW	Strain gauge location on web of T-beam, at approx 105 mm above bottom flange
BFL	Bottom flange underside

Fig. 7.8 Relevant locations for fatigue

For the Tests 1A and 2A, the stresses for the deck plate, the crossbeam web and the bottom flange are shown in the Tables 7.5 to 7.8.

Table 7.5 Stresses at Trough 2 of Test 1A

Location	FESh	FESo	M	A (Q)	A (P)
DPL	-	-12	-13	-11	-20
CBW	-	+28	+27	+32	+27
BFL	+38	+39	-	+34	+35

Table 7.6 Stresses at Trough 3 of Test 1A

Location	FESh	FESo	M	A (Q)	A (P)
DPL	-	-22	-17	-18	-30
CBW	-	+47	+49	+47	+47
BFL	+63	+66	-	+56	+58

Table 7.7 Stresses at Trough 2 of Test 2A

Location	FESh		M	A (Q)	A (P)
DPL	-		-	-11	-20
	-		+27	+32	+27
BFL	+38		-	+34	+35

Table 7.8 Stresses at Trough 3 of Test 2A

Location	FESh		M	A (Q)	A (P)
DPL	-		-	-18	-30
CBW	-		+47	+47	+47
BFL	+63		-	+56	+58

The stresses determined with the FE shell model are indicated with “FESh”; those, with the FE solid model with “FESo”. The measured stresses are indicated with “M” and the stresses along the weld toe calculated with the analytical model are indicated with “A”. The stresses determined with the FE analyses, the measurements and the analytical model show a good compliance, except those calculated for the deck plate with an effective width in relation to point loads. It should be kept in mind that these stresses at the locations DPL, CBW and BFL are only affected by the global crossbeam behaviour.

The compliance of the stresses at the locations C.4.2.l, C.4.5.sl, C.4.5.bl, C.4.2.r, C.4.5.sr and C.4.5.br is shown in “path plots” for load case Test1A.

Figs. 7.9 and 7.10 show the path plots for the principal stresses S1 and S3 calculated by the solid element model (FESo) together with the measured stresses in the direction of the edge (M), the principal stresses from the shell element model (FESh) and the stresses in the direction of the edge determined with the analytical method (A).

S1 is the maximum (in relation to tension) and S3 the minimal principal stress. Here, on the left side, the principal stress S1 is in the cope hole edge direction for the part in tension at 60 – 100 mm from the trough (cope hole) centre and at the right side the principal stress S3 for the part in compression at 60 – 100 mm from the trough centre, based on analyses of vector plot analyses. In general, a rather good agreement is found between all stresses of the four methods, except for the analytically determined stresses for the deck plate with an effective deck plate width for point loads.

However, from a comparison of the results it follows that the two selected locations where the analytical stresses are calculated for the free edge of the cope hole do not include the locations with the maximum values. These locations depend on the interaction of the crossbeam bending and the Vierendeel effect in the tooth and reversed T-beam below the trough. In deeper crossbeams however, the influence of the crossbeam bending and the reversed T-beam is smaller, which also means that the analytically determined stresses do represent the relevant stresses for a fatigue assessment

Due attention should be paid to steep gradients (about $10 \text{ N/mm}^2/\text{mm}^1$) for the locations near to the welds.

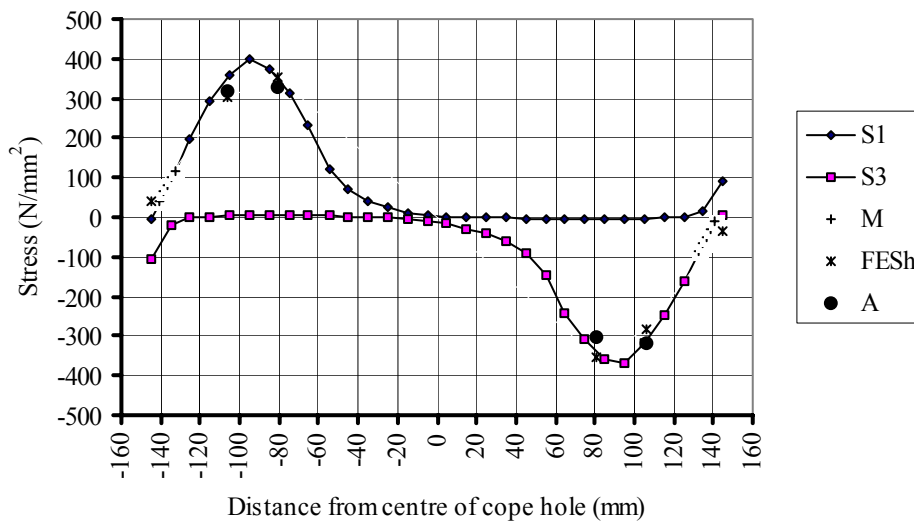


Fig. 7.9 Stresses along free edge of cope hole at Trough 2

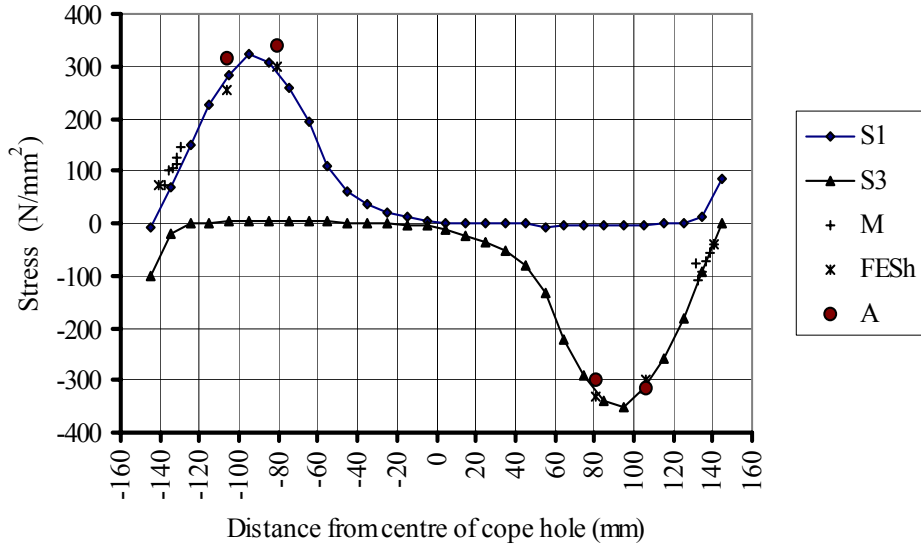


Fig. 7.10 Stresses along free edge of cope hole at Trough 3

7.3.5 Stresses in the trough web for a connection with a cope hole for Test load 1A (in-plane)

For Test 1A, the stresses determined with the analytical model (A) are compared with the measured stresses (M) and those obtained with the FE-model with solid elements (FESo).

As the stresses calculated with the analytical model depend on the imposed deformations of the trough bottom due to bending and shear in the crossbeam as described in chapter 4, it is essential that the effect of the used simplifications for the analytical models is investigated in detail.

The influence of the effective width of the deck plate (the top flange) on the relative displacements and rotations of the trough to crossbeam connections is shown in Table 7.9. This influence is related to the shear forces and the bending moments in the crossbeam.

It is clear that the effective width has a large influence on the horizontal displacements $\delta_{h,rel}$ of the trough to crossbeam connections, however, this is strongly affected by the position of the neutral axis of the crossbeam.

Table 7.9 Relative displacements of trough to crossbeam connections

Loading condition		Trough 2	Trough 3
	Crossbeam shear force (kN)	150	150
	Crossbeam bending moment (kNm)	140	230
Distributed loads	b_{eff} (mm)	1436	1565
	$\delta_{h,rel}$ (mm)	+0.0038	+0.0068
	$\Delta(\varphi_{rel})$ (rad)	+0.000033	+0.000054
	δ_v (mm)	+0.213	+0.213
Point loads	b_{eff} (mm)	803	877
	$\delta_{h,rel}$ (mm)	+0.0011	+0.0027
	$\Delta(\varphi_{rel})$ (rad)	+0.000040	+0.00065
	δ_v (mm)	+0.213	+0.213

In the analytical model, the section forces in the trough bottom and web are calculated with a simple trapezoidal model composed of two sub models (left and right) as shown in Fig. 7.11.

In the foregoing analyses in chapter 4, the effect of the curved transition between the trough bottom and web is disregarded for these sub models. In order to achieve a more accurate comparison between results from the analytical models, the FE models and the measurements, the effect of the curvature is here analysed more in detail.

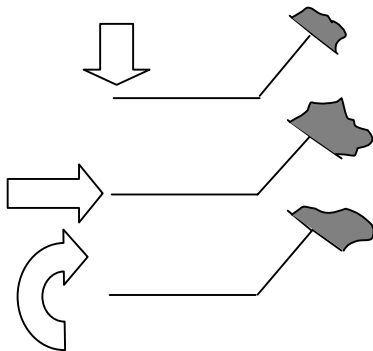


Fig.7.11 Line models for half trough bottom

The sub models are loaded by imposed displacements and rotations. In one model the curved part of the trough bottom is modelled with a polygon of four straight lines. Another model has a straight bottom with a straight trough web as shown in Fig. 7.11 and is similar to the model used in chapter 4.

Both types of trough bottom models are submitted to identical horizontal and vertical unit displacements of the mid section of the trough bottom and an imposed unit rotation of the trough to crossbeam web connection.

Table 7.10 Comparison of relative section forces and bending moments in models with a straight and a “curved” trough bottom

Imposed displacement	Polygon bottom	Straight bottom
Horizontal	N=100% M=100%	N=110% M=101%
Vertical	N=100% M=100%	N=117% M=120%
Rotation	N=100% M=100%	N=104% M=97%

Table 7.10, gives the relative section forces (N) and relative bending moments (M). It shows that, for the imposed displacements the model with two straight elements reacts more rigidly. For rotation, the model with the straight elements reacts somewhat more rigidly for the normal forces and somewhat flexibly for the bending moment. The differences are relatively small, which means that only small deviations occur in the stresses when the straight-line model is used. The polygon model, however, is more suitable for an accurate stress comparison between the strain gauges at the full-scale specimen and is used in the analyses below.

Table 7.11 shows the stresses resulting from the analytical model (A) at a distance of 5 mm from the weld toe. This location at the trough was selected for comparison of the measured stresses with the calculated stresses, because it is less affected by stress concentrations due to the weld geometry than the straight part of the trough web near the welded connection with the crossbeam web.

The stresses are calculated from the section forces and bending moments in Table 7.3 with the relative displacements and rotations of Table 7.9. The curvature between the trough web and the trough bottom causes a stress reduction at the outer surface. This stress reduction factor (0.93) was calculated with the formulae given by Roark & Young (1986) and included in the resulting stresses.

Table 7.11 Stress determination with analytical method for Test load case 1A

	Effective widths for:							
	Distributed loads				Point loads			
	Trough 2		Trough 3		Trough 2		Trough 3	
	Left	Right	Left	Right	Left	Right	Left	Right
$\sigma_{\delta v}$	-145	+145	-145	+145	-145	+145	-145	+145
$\sigma_{\delta h}$	+11	+11	+19	+19	+3	+3	+8	+8
$\sigma_{\delta \phi}$	+2	+2	+4	+4	+3	+3	+4	+4
σ_{Tnom}	-132	+158	-122	+168	-125	+137	-120	+142
Stress results	-123	+147	-114	+156	-116	+127	-112	+132

The stresses calculated with the analytical model show, that the crossbeam shear deformation makes the largest contribution to the resulting stresses. As lorry axles are considered to be local loads, here, the effective widths in the deck plate related to point loads are used for further stress calculations to be used for comparisons.

Figs. 7.12 and 7.13 show the path plots for the principal stresses S1 and S3 calculated by the solid element model (FESo) in combination with the measured stresses (M) and the stresses determined with the analytical method (A). Here, on the right side, the principal stress component S1 is in the strain gauge direction for the part in tension at 55 – 72 mm from the trough bottom centre and on the left the stress component S3 for the part in compression at 55 – 72 mm from the trough centre, based on vector plot analyses.

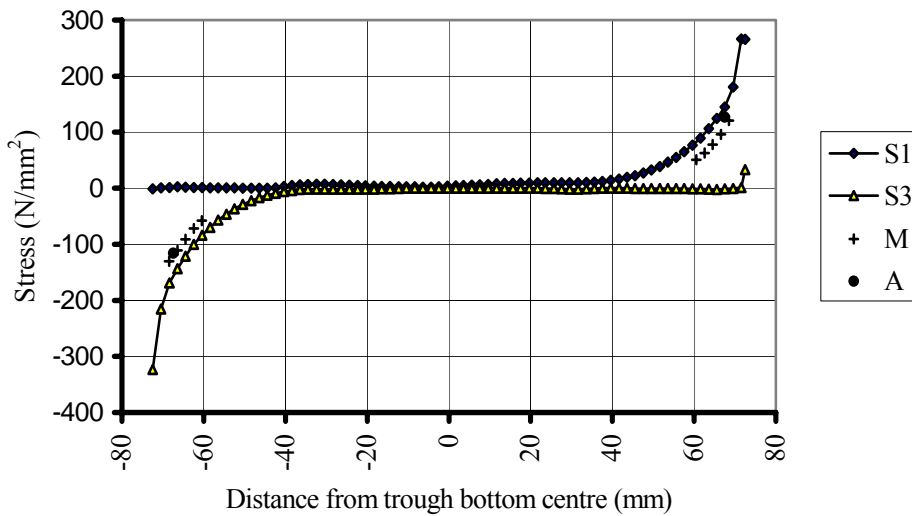


Fig. 7.12 Principal stresses, results from measurements and stresses from analytical method for bottom of Trough 2

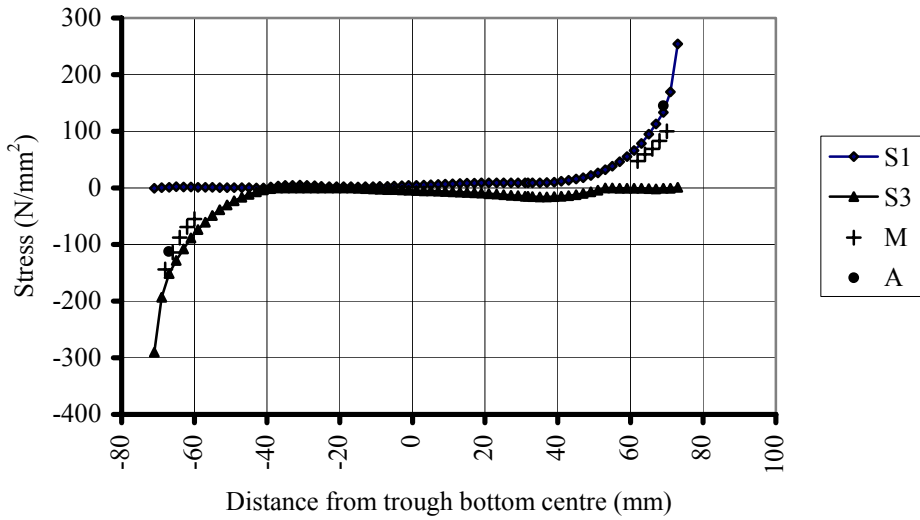


Fig. 7.13 Principal stresses, results from measurements and stresses from analytical method for bottom of Trough 3

Comparison of the stresses shows that the stresses determined with all three methods are fairly close. However, the detailed analyses of the measurements shows that the stress gradient in this area is so steep that over a 2 mm distance the stresses change in the order of 15 N/mm².

Enlarging the depth of the cope hole by raising the lower end of the trough to crossbeam connection will reduce this effect.

7.3.6 Stresses at a cope hole for Test load 3 (out-of-plane)

Fig. 7.14 shows the path plot for the principal stresses S3 at trough 3, calculated by the solid element model (FESo) in combination with the measured stresses (M) in the direction of the edge, the principal stress results from the shell element model (FESh) and the stresses in the direction of the edge determined with the analytical method (A).

The strain gauges were positioned at 16.3 mm from the free edge of the cut-out at C.4.5.sl and C.4.5.sr, which are located at 107.5 mm distance from the centre of the cope hole, measured along the free edge. Here, the principal stress component S3 is shown along the free edge of the cope hole, in the cope hole edge direction for the parts at 50 – 145 mm from the trough bottom centre.

The FESo stress pattern shows the influence of the support, situated left of trough 1, by being not symmetrical. The analytically determined stresses do not consider the support influence, therefore these results are symmetrical.

From Figure 7.14 it can be concluded that the analytical model gives in general too low stresses, but the most relevant locations C.4.5.sl and C.4.5.sr, which results are generally used for the calculations, do comply rather well.

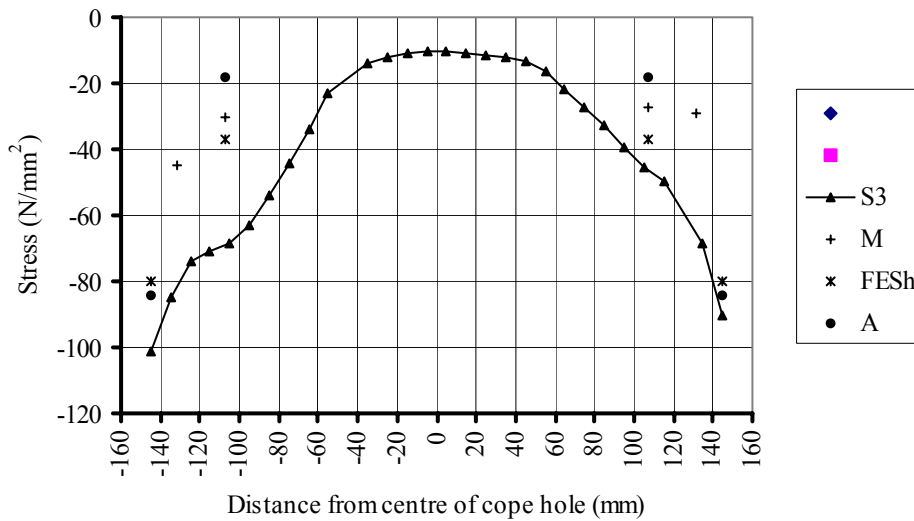


Fig. 7.14 Stresses along free edge of cope hole at Trough 2

7.3.7 Stresses in a close fit connection for Test load 1A (in-plane)

The geometry of the tooth at the right side of trough 8 differs from the general geometry as it includes the vertical support; at troughs 4 and 5 local loads are introduced in the deck plate and stiffeners.

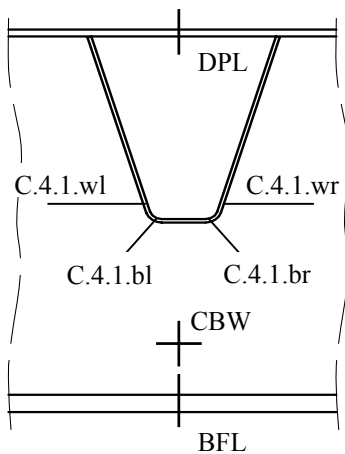


Fig.7.15 Relevant locations for fatigue

Table 7.12 Analysed and measured locations

Location	
DPL	Deck plate at the centre line of the trough
C.4.1.wl	Connection tooth to trough, left side, crossbeam web at 77 mm from the centre of the trough bottom along the weld toe.
C.4.1.bl	Transition area of tooth to T-beam, left side, crossbeam web at 57 mm from the centre of the trough bottom along the weld toe.
C.4.1.wr	Connection tooth to trough, right side, crossbeam web at 77 mm from the centre of the trough bottom along the weld toe.
C.4.1.br	Transition area of tooth to T-beam, right side, crossbeam web at 57 mm from the centre of the trough bottom along the weld toe.
CBW	Strain gauge location on web of T-beam, crossbeam web at approx. 100 mm above bottom flange
BFL	Bottom flange underside

Therefore, the stress results are not presented for the cut-outs for troughs 5 and 8. For the Test loads 1A and 2A the stresses for the deck plate, the crossbeam web and the bottom flange are shown in the Tables 7.13 to 7.16. Similarly to the connection with a cope hole, the stresses determined with the FE shell model are indicated with “FESh”; those, with the FE solid model with “FESo”.

The measured stresses are indicated with “M” and the stresses along the weld toe, calculated with the analytical model are indicated with “A”. When two stresses are given, the first applies to a crossbeam with an effective width for a uniformly distributed loading (Q) and the second for an effective width for a point loading (P).

Table 7.13 Stresses at Trough 6 of Test 1A

Location	FESh	FESo	M	A (Q)	A (P)
DPL	-	-22	-18	-18	-31
CBW	-	+48	+46	+47	+47
BFL	+62	+62	-	+56	+58

Table 7.14 Stresses at Trough 7 of Test 1A

Location	FESh	FESo	M	A (Q)	A (P)
DPL	-	-12	-12	-11	-20
CBW	-	+29	+28	+27	+28
BFL	+35	+38	-	+34	+35

Table 7.16 Stresses at Trough 7 of Test 2A

Location	FESh	M	A (Q)	A (P)
DPL	-	-	-11	-20
CBW	-	+49	+47	+47
BFL	+60	-	+56	+58

Table 7.15 Stresses at Trough 6 of Test 2A

Location	FESh	M	A (Q)	A (P)
DPL	-	-13	-11	-20
CBW	-	+31	+27	+28
BFL	+37	-	+34	+35

Except for the analytical stresses in the deck plate DPL for the condition (P), the stresses determined with the FE analyses, with measurements and with the analytical model show a good compliance. The deviation is due to the assumed effective width of the deck plate at the cross section at troughs 6 and 7. It should be borne in mind that these stresses at the locations DPL, CBW and BFL are only affected by the global crossbeam behaviour.

Fig. 7.16 shows the “path plots” for the principal stresses (S1, S2, S3) along the weld toe, calculated with the solid element model (FESo) in combination with the measured stresses in the direction of the edge (M). Here, on the right side at 40 – 90 mm from the trough bottom centre (0), the principal stress component S1 is in the tension, parallel to the weld toe direction. On the left side at 40 – 90 mm from the centre (0), S3 is in compression in the direction of the weld toe. S2 is on both sides at 40 – 90 mm from the trough bottom centre (0), perpendicular to the weld toe. The statements on the directions are based on vector plots analyses.

Fig. 7.16 also shows the principal stresses from the shell element model (FESh, distinguishing stresses in weld toe direction // and the stresses perpendicular to the weld toe FESh_perp), stresses determined with the analytical method for the direction of the weld (A_1) and the stresses perpendicular to the weld (A_2).

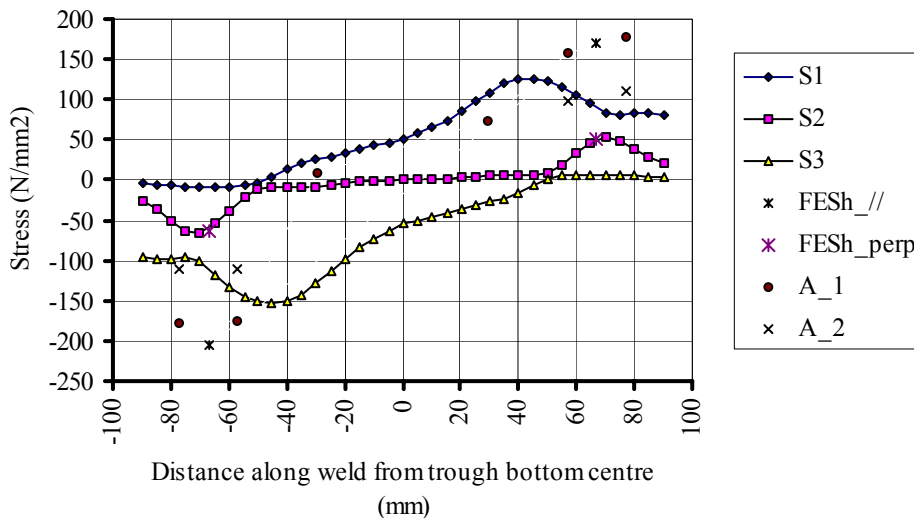


Fig. 7.16 Stresses along the weld toe at Trough

The principal stresses determined with the solid element model between -40 and $+40$ mm from the trough bottom centre (0), should not be used for comparison with stresses from other analyses, due to the unknown direction of the principal stresses.

Fig. 7.16 shows that, for the relevant locations C.4.1.wl and C.4.1.wr at 77 mm distance from the trough bottom centre the analytical method and the FESh model overestimate the stresses parallel to the weld toe direction if compared to the FESo model. The perpendicular stresses from the analytical method overestimate the stresses, compared to the FESo and FESh models.

For the connections of troughs 5 to 8 with a close fit, the stress perpendicular to the weld toe is most relevant for fatigue. As the principal stress S2 at the indicated places is almost perpendicular to the weld toe, this is the most relevant stress resulting from the FESo calculations relevant for fatigue. It has to be compared with FESh_perp and A_2.

The stresses were measured on the crossbeam web, near to the locations C.4.1.bl and C.4.1.br, both at a distance of 57 mm from the trough bottom centre (measured along the weld toe). The position of the sets of strain gauges was on two lines perpendicular to the weld toe as indicated in Fig. 7.17.

The measured stresses at C.4.1.bl along this line to the weld toe are shown in Figure 7.18 and those at C.4.1.br in Figure 7.19.

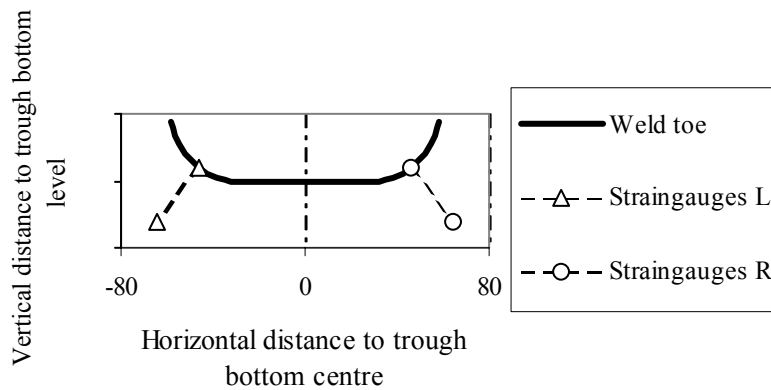


Fig. 7.17 Weld toe and strain gauge positions on crossbeam web

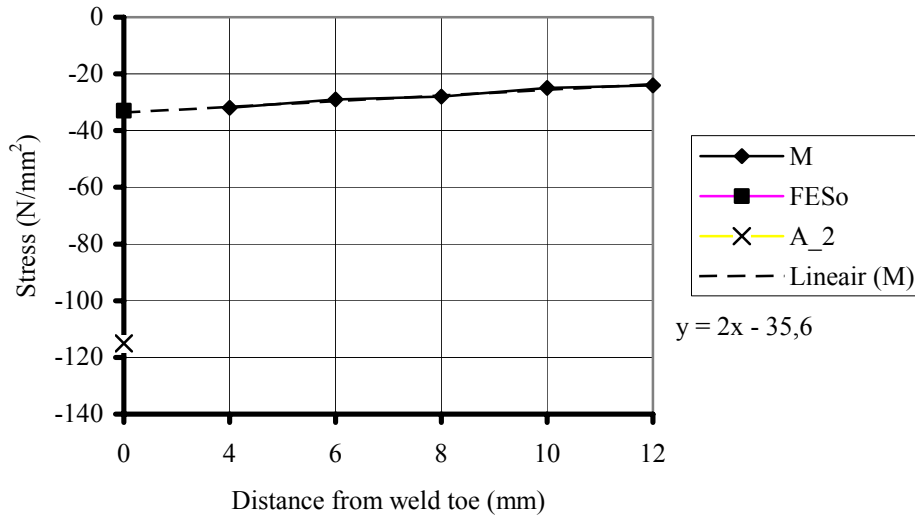


Fig. 7.18 Stress gradient at C.4.1.bl crossbeam web trough 6 (left)

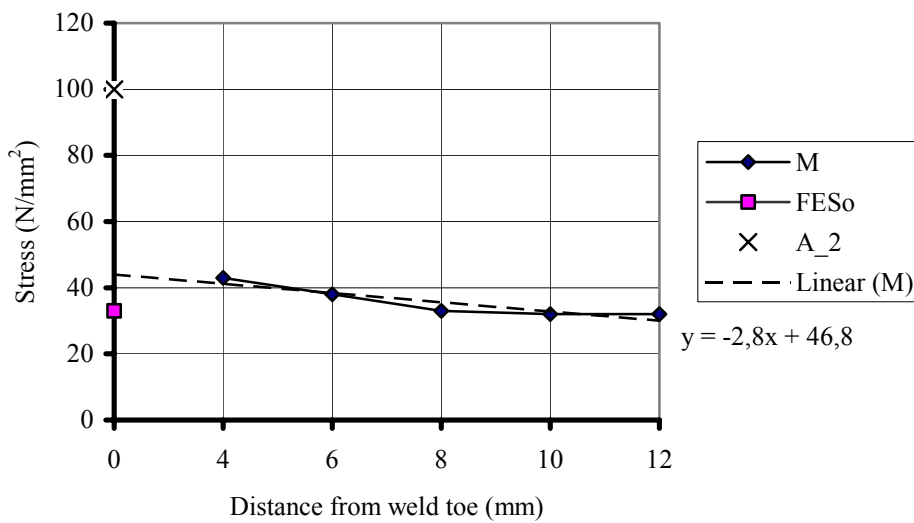


Fig. 7.19 Stress gradient at C.4.1.br crossbeam web trough 6 (right)

The linear extrapolation of the stresses from the first 5 strain gauges would result in a stress of -36 N/mm^2 at the left hand side and $+47 \text{ N/mm}^2$ at the right hand side. The right hand side measurements are less clear for an adequate extrapolation due to the curved shape of the graph, which connects the stress measurements.

The stresses found with the FE solids model (FESo) are lower at these locations, but the analytically determined stresses are (also in absolute value) much higher than those determined with the FE models and the measurements.

Fig. 7.20 shows the stresses for the crossbeam web at Trough 7. The abbreviations apply as for Fig. 7.16.

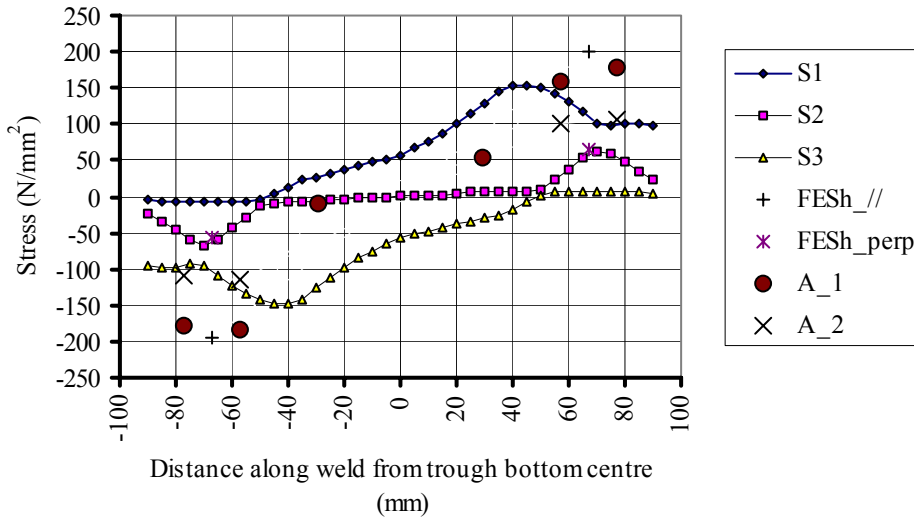


Fig. 7.20 Stresses along the weld toe at Trough 7

The stresses shown in Fig. 7.20 are similar to those of Fig. 7.16. The measured stresses for C.4.1.bl are shown in Figure 7.21 and those at C.4.1.br in Figure 7.22 in analogy to Fig.7.17.

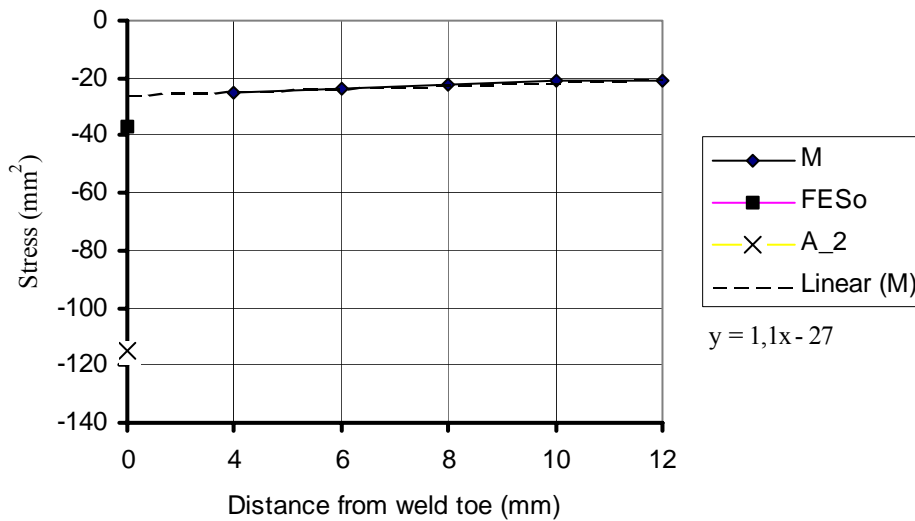


Fig. 7.21 Stress gradient at C.4.1.bl crossbeam

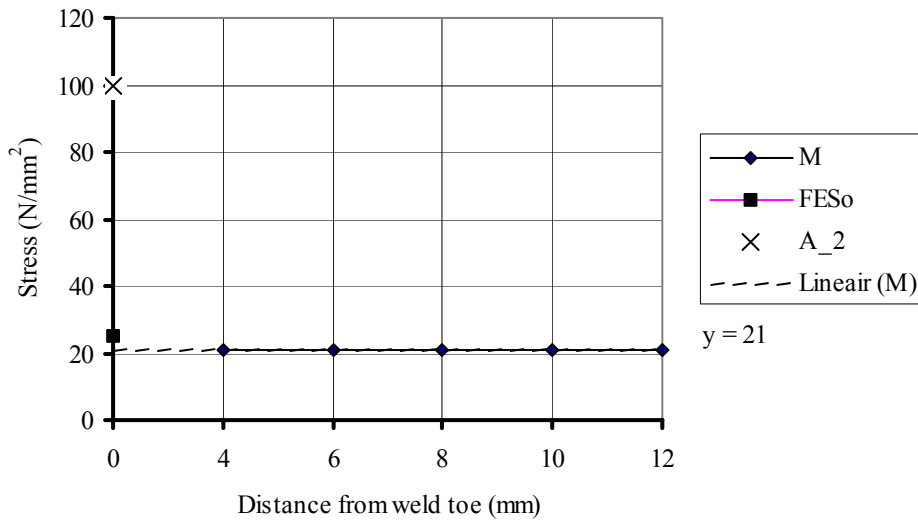


Fig. 7.22 Stress gradient at C.4.1.br crossbeam web trough 7 (right)

The linear extrapolation of the stresses from the first 5 strain gauges would result in a stress of -27 N/mm^2 at the left hand side and $+21 \text{ N/mm}^2$ at the right hand side. The stresses found with the FE solids model (FESo) are somewhat higher at these locations.

It can be concluded that, generally, the stresses calculated with the solid element model are sometimes somewhat higher (in absolute value) or lower than the extrapolated stresses from measurements. In addition, the analytically determined stresses with the method given in chapter 4 always strongly overestimate the stresses as determined with FE models. Therefore, using the stresses from chapter 4 for an analysis is very conservative.

7.3.8 Stresses in a close fit connection for Test load 3 (out-of-plane)

Fig. 7.23 shows the path plot for the principal stresses S3 at the weld toe, calculated by the solid element model (FESo). Here, the principal stress component S3 is perpendicular to the weld toe for the part at 40 – 90 mm from the trough centre, based on vector plot analyses.

Fig. 7.23 also shows the principal stresses from the shell element model (FESh // parallel to the weld toe and FESh_perp perpendicular to the weld toe) and the stresses determined with the analytical method for the direction perpendicular to the weld toe (A_perp).

The FE solid model and shell model stresses show the influence of the support, but the analytically determined stresses do not consider the support influence. The FE shell model apparently overestimates the stresses, probably due to the absence of the welds in the model, but in general, the stress pattern shows a similar behaviour to the FE solid model, including the effect of the support.

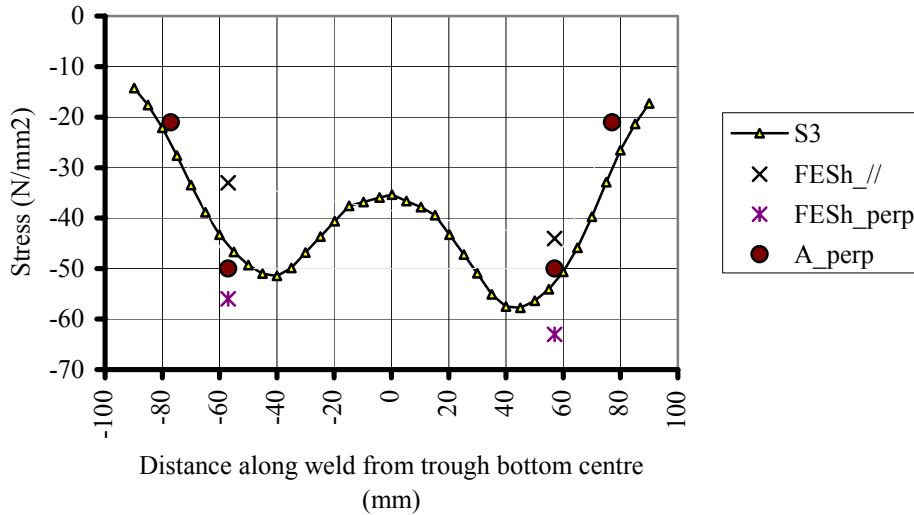


Fig. 7.23 Stresses at crossbeam side weld toe of trough 6 (out-of-plane)

In fact, the measured stresses near C.4.1.bl and C.4.1.br are less suitable for extrapolation, due to the shape of the graph that connects the measured values. However, a simple linear extrapolation is carried out to the weld toe, as was done above for the in-plane behaviour. The stresses from the extrapolation of the measurement, the analytical method and the FE solid element models are shown in Figs 7.24 and 7.25 in analogy to Fig. 7.17.

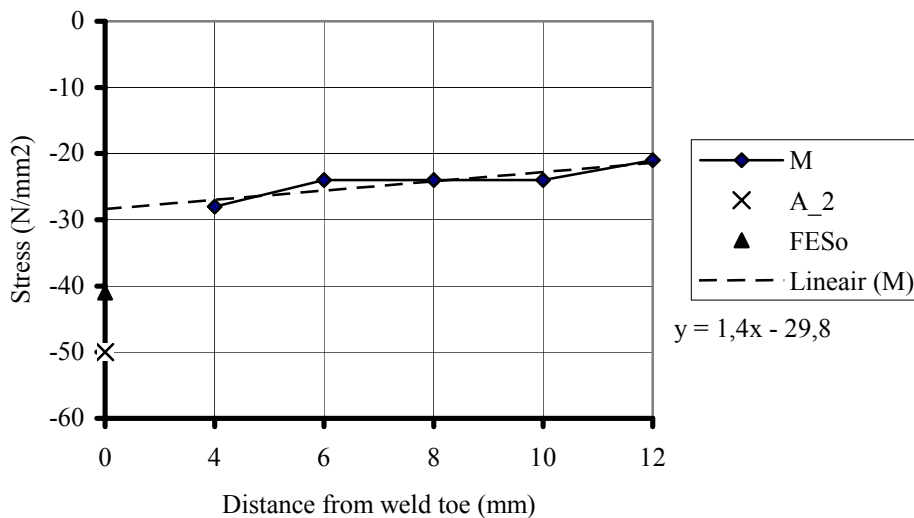


Fig. 7.24 Stress gradient at C.4.1bl crossbeam web trough 6 (left)

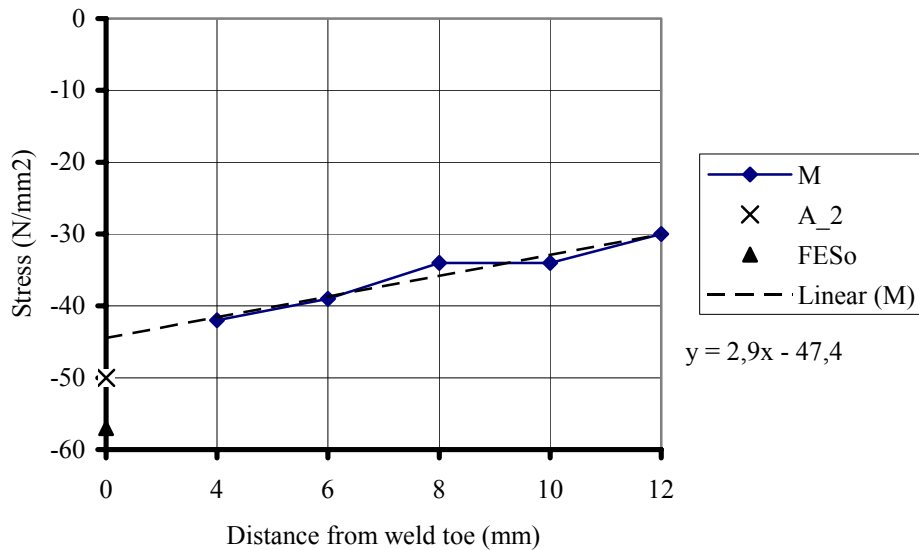


Fig. 7.25 Stress gradient at C.4.1bl crossbeam web trough 6 (right)

A linear extrapolation of the stresses from the first 5 strain gauges would result in a stress of -30 N/mm^2 at the left hand side and -47 N/mm^2 at the right hand side. The stresses found with the FE solids model (FESo) are much higher (in absolute value) at these locations. The stresses determined with the analytical method are much higher at the left side somewhat higher (in absolute value) at the right side.

Generally, for the most critical locations, it can be concluded that the analytically determined stresses are on the very safe side, if compared to FE models and measurements.

7.3.9 Conclusions for the full-scale test specimen

Part with cope holes

In-plane

For the global behaviour the analytical results compare very well with the FE results and the measurements. At the cope hole edge the analytical results are sometimes higher, sometimes lower than the FE results which compare well with the measurements. See Figs. 7.9, 7.10, 7.12 and 7.13.

Out-of-plane

The analytical results are lower or equal to the FE results. The latter compare well with the measurements. See Fig. 7.14.

Part without cope holes

In-plane

For the global behaviour the analytical results compare very well with the FE results and the measurements. At the weld toe the analytical results are higher than the FE results which compare well with the measurements. See Figs. 7.16, 7.18, 7.19, 7.20, 7.21 and 7.22.

Out-of-plane

For the most critical locations, the analytically determined stresses are on the very safe side, compared to FE models and measurements. See Figs. 7.23, 7.24 and 7.25.

General

- For many locations, the analytical model gives results, which are reasonably in agreement with the measurements, and the results of the FE-models. Near the welds, however, their accuracy depends on proper stress concentration factors.
- The stresses in the trough bottom are mainly caused by crossbeam shear and less by crossbeam bending.
- The stresses in the trough have a steep gradient near the connection to the crossbeam web. This means that fabrication inaccuracies can have a large influence on actual stresses.

Remarks:

As the influence of apparently small details such as manufacturing tolerances can cause stresses that deviate substantially from the theoretical stresses, it is advisable to aim to keep the stresses low. In practice this means: “With a sufficient margin below the constant amplitude fatigue limit in relation to ENV 1991-3, Fatigue Load Model 2”

7.4 Concluding remarks

- FE-models with shell elements are only reliable for the determination of the geometrical peak stresses for locations not affected by the weld geometry and can give, in conjunction with fatigue tests, a contribution to the fatigue classification of the details. For other locations FE element models with solid elements should be used, as these can be very accurate.
- The analytical models give a good representation of the behaviour of the structure.
- Where geometrical peak stresses have to be determined, due attention should be paid to the use of appropriate stress concentration factors.
- In trough to crossbeam connections with a cope hole, the stresses in the trough web below the trough to crossbeam web connection are very sensitive for the location considered and for small changes in the geometry.
- The stress gradients at some locations are high, and this can mean that the actual stresses in the structure may deviate significantly from the calculated stresses
- The theoretical design stress intervals at locations with high stress gradients should be kept low.
- For an exact determination of the fatigue detail classes, FE solid models can be used in combination with test specimens. Appropriate FE models with solid elements can give such accurate results, that extrapolation from strain gauge measurements to the weld toe can be abandoned for determination of the stresses, as long as the FE model is based on the exact dimensions including manufacturing deviations. In this case, only a few strain gauge measurements for calibration will be needed. Consequently, fatigue detail categories based on this procedure are well in line with the designers need, but may deviate from the current values.

8 Assessment procedures

8.1 Introduction and objective

Chapter 3 describes the steps in the assessment procedure and chapter 4 describes the method for the calculation of the nominal stresses in the closed stiffener to crossbeam connection for in-plane loads and out-of-plane rotations. In chapter 5, the geometrical stress concentration factors are calculated.

The maximum intervals and the associated equivalent numbers of cycles for the lane loads, the out-of-plane rotations of the stiffener to crossbeam connection and the deck bending moments are calculated in chapter 6. The history for the geometrical hot spot stress intervals due to the crossbeam in-plane load effects can be calculated from the lane load intervals.

The geometrical hot spot stress intervals for the crossbeam out-of-plane effects can be determined in a similar way from the rotation intervals of the stiffener to crossbeam connection. This also applies to the geometrical hot spot stress intervals in the stiffeners due to the deck bending moments.

An overview of the complete fatigue assessment procedure is given in 8.2.

In 8.3, the fatigue damage calculation procedure including the criteria for infinite fatigue life and limited fatigue life and the relationship between the fatigue load models (FLM2 and FLM4) of ENV 1991-3 (EN 1991-2) and how they can be used, is shown.

How the effects from the various traffic lanes interact and how the in-plane and out-of-plane effects should be combined is shown in 8.4.

Finally, in order to enable the fatigue life calculations, a selection of the detail classifications for fatigue is given in 8.5

Some concluding remarks are given in 8.6.

8.2 Assessment procedure overview

An overview of the assessment procedure is shown in Table 8.1 and is described in detail.

Table 8.1 Assessment procedure

Step no.	Aspect	Method	Requirement
1. General	Design life	-	<ul style="list-style-type: none"> Standards Contract
2. Loads	<ul style="list-style-type: none"> Lorry loads Axle loads Wheel prints Axle and wheel distances 	-	<ul style="list-style-type: none"> Standards (EN 1991-2 with or without NA) Contract
3. Determination of stresses	<ul style="list-style-type: none"> Crossbeam load transfer Global and local behaviour Nominal stresses Geometrical stresses 	<ul style="list-style-type: none"> Analytical method (see ch 4) with geometrical stress concentration factors (see ch 5) Beam grid FE-model with geometrical stress concentration factors FE shell element model FE solid element model 	-
4. Fatigue damage assessment	<ul style="list-style-type: none"> Transfer functions Stress histories Fatigue detail classes (ch8, EN 1993-2, EN 1993-1-9) Interaction effects for loads and mechanical behaviour Damage assessment 	<ul style="list-style-type: none"> Fatigue load models (see ch 6, ch 8) Analytical model (see ch 6) Simulation Interaction lane Interaction effect stress components in-plane and out-of-plane effects Damage 	<ul style="list-style-type: none"> Standards Contract
5. Inspection and repair	<ul style="list-style-type: none"> Inspection Repair 	<ul style="list-style-type: none"> Non-destructive inspection method Welding 	<ul style="list-style-type: none"> Contract

As the general requirements and the loads are given in the contract and/or standards, the detailed steps described here for a fatigue assessment of the trough to crossbeam connection, are only Step 3 and Step 4:

Step 3 Determination of nominal stresses for unit loads and unit rotations

In step 3, the geometrical stresses are calculated for a defined uniformly distributed load, (or in-plane lane loads) over the width of the respective traffic lanes on the crossbeam and for a defined rotation of the trough to crossbeam connections.

In-plane

Calculate the nominal stresses and relative displacements for the in-plane lane loads (crossbeam bending and shear) with the procedures described in 4.2.3.3, 4.2.3.4, 4.2.4.1 and 4.2.4.2. The stresses at the crossbeam web location C.4.1.w (See Figs. 4.35 or 5.22) for connections with a close fit are determined with a stress concentration factor due to the curvature of the tooth base.

If the dimensions of the crossbeam (height H and web thickness t) and the cut-outs (cope hole width W , trough thickness and the trough depth) are within the range of the analysed crossbeams in chapter 4, the nominal stresses in the trough web for trough to crossbeam connections with cope holes can be derived from Figs. 4.25, 4.28, 4.32 and for connections with a close fit from Figs. 4.34 and 4.37.

The stress concentration factors of chapter 5 can be used to obtain geometrical stresses.

Out-of-plane

Calculate the nominal stresses due to a unit rotation with the procedure described in 4.3.

If the dimensions of the crossbeam and the cut-outs are within the range of those of the analysed crossbeams in chapter 4, the nominal stresses in the crossbeam web can be derived from Fig. 4.46 for trough to crossbeam connections with and without cope holes (locations C.4.1.w, C.4.1.b, C.4.2.w) and from Fig. 4.48 for the cope hole locations (C.4.5.s). The stresses for other crossbeam web thicknesses can be derived from these stresses, considering that the stresses depend linearly on the crossbeam web thickness.

The stress concentration (or relation) factors of chapter 5 can be used to obtain geometrical stresses.

Step 4 Fatigue damage assessment

In step 4, the load, rotation, and deck bending moment intervals are determined. With these intervals, the stress intervals and equivalent numbers of cycles in relation to loads on various lanes are calculated for FLM2. If these stress intervals are above the constant amplitude limit, the intervals should be scaled down to the level corresponding with FLM4 and damage calculations have to be carried out.

Step 4a

Determine the equivalent crossbeam properties c_b and c_s in relation to the in-plane behaviour as described in 4.2.1.1 for crossbeam bending and in 4.2.1.3 for crossbeam shear, including the effect of the correction factor c_c on the tooth length given in table 4.2. If the dimensions of the crossbeam (height H and thickness t) and the cut-outs (width W , thickness and trough depth) are in the range of those of the analysed crossbeams in chapter 4, the values for c_b to obtain the equivalent moment of inertia and c_s to obtain the equivalent crossbeam web thickness for shear can be taken from Figs.4.17 and 4.18 respectively.

Step 4b

Determine the in-plane spring stiffnesses of the crossbeam locations at the centre lines of the traffic lanes with the methods given in 6.3 and 6.4.2 and select the applicable influence lines for crossbeam in-plane loads, out-of-plane rotations, and the deck (or lane) bending moments.

Step 4c

Calculate the maximum load, rotation and deck bending moment intervals for the fatigue load model FLM2 at the connection, together with the equivalent numbers of cycles for the in-plane load intervals with the influence lines given in 6.5.1.2. For the trough to crossbeam rotations, the influence lines given in 6.5.2.2 and for the deck bending moments, those given in 6.5.3 can be used.

The load, rotation, and deck bending moment intervals given in Tables 6.5, 6.8 and 6.11 respectively, are only applicable for the analysed crossbeam spring stiffnesses and crossbeam centre-to-centre distances of approximately 4.0 m.

The influence of shorter (3.5 m) and longer spans (4.5 m) is indicated in 6.6.1.2 for crossbeam loads and in 6.6.2.2 for trough to crossbeam connection rotations.

Step 4d

Scale the concentrated stresses calculated with the procedures given in step 3 for the unit loads and rotation due to the load, rotation, and deck bending moment intervals, in order to obtain the concentrated stress intervals.

Step 4e

Increase the stress intervals in the crossbeam web, caused by the crossbeam in-plane loads, with half the stress intervals caused by the trough to crossbeam rotations under a particular traffic lane as described hereafter in 8.4.2. and 8.4.3. The stresses due to the loads on the adjacent traffic lane are added as far as the in-plane loads are concerned, as described in 8.4.1. and 8.4.3.

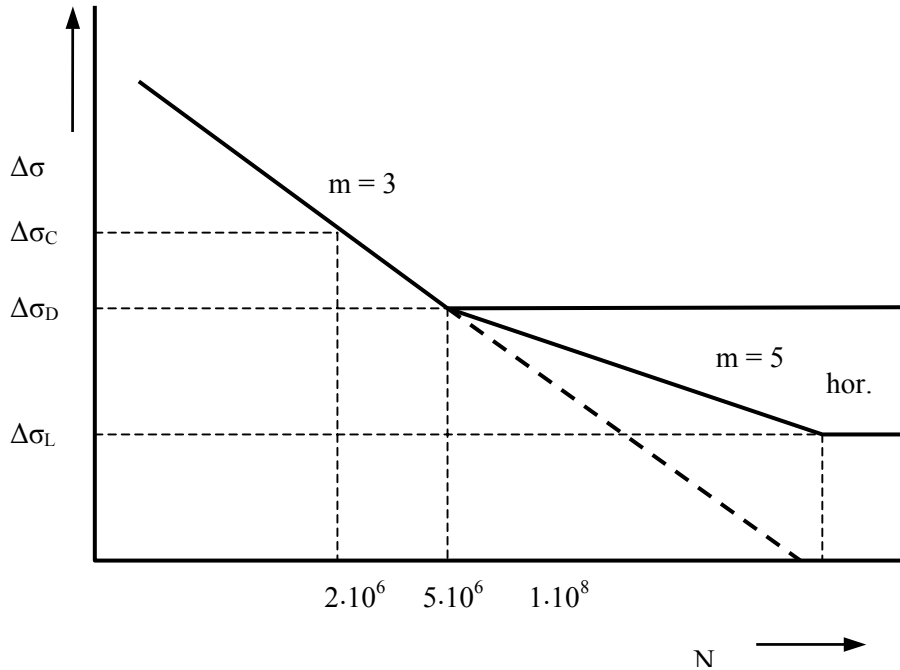
Step 4f

If the maximum stress intervals due to FLM2 are below the “Constant amplitude stress $\Delta\sigma_D$ ” of the fatigue resistance, associated to the fatigue detail classes as recommended in 8.5, the fatigue life is considered infinite.

If the maximum stress intervals due to FLM2 are above the constant amplitude limit, a damage calculation should be carried. For the damage calculation the maximum stress intervals for FLM4 should be used with the equivalent numbers of cycles as described in 8.4. The maximum stress intervals of FLM4 can be obtained by scaling of the stress intervals of FLM2.

8.3 Fatigue damage calculation procedure

The fatigue strength of a detail is characterised by a linear log-log relationship between the stress intervals $\Delta\sigma$, also called “stress ranges” and the number of cycles N as shown in Fig. 8.1 (also called S-N line).



The S-N lines used in EN 1993-1-9 for axial and bending stresses due to random loading have three linear parts, one with a slope $m = 3$, a second with $m = 5$ and third a horizontal part.

The design category is indicated with $\Delta\sigma_C$ for $N_C = 2 \cdot 10^6$ cycles. The transition between the lines for $m = 3$ and $m = 5$ is equal to the constant amplitude fatigue limit, with the stress range $\Delta\sigma_D (= 0.737 \cdot \Delta\sigma_C)$ at $N_D = 5 \cdot 10^6$ cycles.

Fig. 8.1 Stress cycles for Palmgren-Miner damage calculation

If all stress intervals are below $\Delta\sigma_D$, no fatigue is to be expected. If some of the stress intervals are above $\Delta\sigma_D$, a damage assessment must be carried out. The transition between the line with $m = 5$ and the horizontal part is called the cut-off limit $\Delta\sigma_L (= 0.405 \Delta\sigma_C)$ at $N_L = 1 \cdot 10^8$. The stress intervals below this level are considered not to contribute to fatigue damage.

The quotient of an applied number of cycles n_i and a number of cycles to failure N_i gives the damage D_i :

$$D_i = \frac{n_i}{N_i} \tag{8.1}$$

According to Palmgren-Miner, for various stress intervals and the associated numbers of cycles, the total fatigue damage is the sum of the individual damage contributions with eq. [8.2]:

$$D = \Sigma(D_1 + D_2 + D_3 + \dots + D_n) \tag{8.2}$$

Generally, a stress history is analysed with a “rainflow” analysis, see Matsuishi et al. (1968), in order to obtain a stress spectrum. This spectrum consists of different stress intervals, each with its associated number of cycles. This spectrum of stress intervals can be transferred into a stress interval $\Delta\sigma_C$ with an equivalent number of cycles $n_{eq,C}$, giving the same damage.

As one complete stress cycle consists of two stress interval, as a simplification in this study, the stress intervals shown in Fig. 8.2, (I_1, I_2, I_3, I_4 etc.) produced by the passage of one lorry, are considered as half cycles.

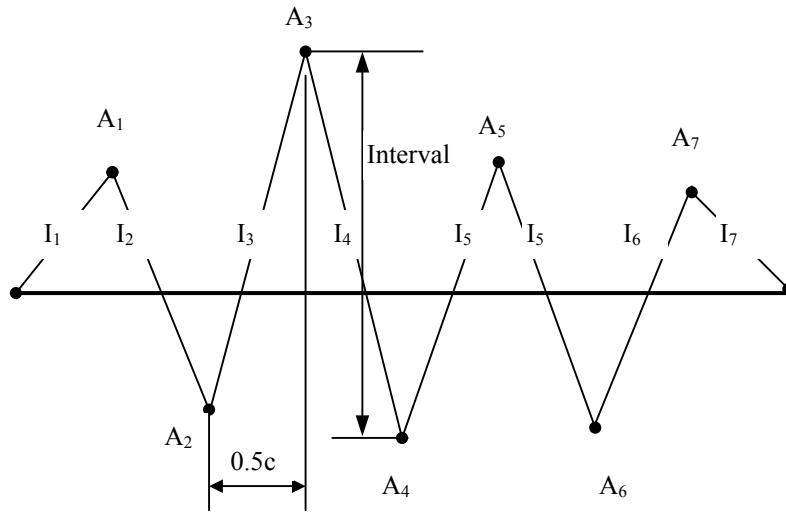


Fig. 8.2 Stress amplitudes and intervals

For all intervals, caused by the passage of the lorry “i”, the equivalent number of cycles $n_{eq,i}$ in relation to the maximum stress interval $\Delta\sigma_{max,i}$ produced by this lorry can be calculated with eq. [8.3].

$$n_{eq,i} = 0.5 \left(\frac{\Delta\sigma_1}{\Delta\sigma_{max,i}} \right)^3 + 0.5 \left(\frac{\Delta\sigma_2}{\Delta\sigma_{max,i}} \right)^3 + \dots + \left(\frac{\Delta\sigma_D}{\Delta\sigma_{max,i}} \right)^3 \cdot \left\{ 0.5 \left(\frac{\Delta\sigma_{21}}{\Delta\sigma_{max,i}} \right)^5 + 0.5 \left(\frac{\Delta\sigma_{22}}{\Delta\sigma_{max,i}} \right)^5 + \dots \right\} \quad [8.3]$$

In eq. [8.3] it is assumed, that all stress intervals up to $\Delta\sigma_{21}$ are larger than $\Delta\sigma_D$ and are related to the S-N line with $m = 3$. The other intervals (e.g. $\Delta\sigma_{21}$) are below $\Delta\sigma_D$ and are related to the S-N line with the slope $m = 5$. In eq. [8.3], the stress intervals below $\Delta\sigma_D$, are initially related to $\Delta\sigma_D$ and then the equivalent number of cycles is corrected for the relation to $\Delta\sigma_{max}$. The stress intervals below $\Delta\sigma_L$ are not considered, as they do not contribute to the damage. This deviates from the procedure in chapter 7, where either all stress intervals are assumed to be on the $m = 3$ or the $m = 5$ part of the S – N line.

If the total number of lorries type “i” is n_i , the total number of cycles related to $\Delta\sigma_C$ ($N_C = 2 \times 10^6$ cycles) for five lorries becomes:

$$\begin{aligned} n_{eq,C} = & n_{eq,1} \cdot n_1 \cdot \left(\frac{\Delta\sigma_{max,1}}{\Delta\sigma_C} \right)^m + n_{eq,2} \cdot n_2 \cdot \left(\frac{\Delta\sigma_{max,2}}{\Delta\sigma_C} \right)^m + n_{eq,3} \cdot n_3 \cdot \left(\frac{\Delta\sigma_{max,3}}{\Delta\sigma_C} \right)^m + \\ & + n_{eq,4} \cdot n_4 \cdot \left(\frac{\Delta\sigma_{max,4}}{\Delta\sigma_C} \right)^m + n_{eq,5} \cdot n_5 \cdot \left(\frac{\Delta\sigma_{max,5}}{\Delta\sigma_C} \right)^m \end{aligned} \quad [8.4]$$

If $\Delta\sigma_{max}$ is above $\Delta\sigma_D$, $m = 3$, for the $\Delta\sigma_{max}$ below $m = 5$ $\Delta\sigma_D$, and a correction factor $\left(\frac{\Delta\sigma_D}{\Delta\sigma_{max,i}} \right)^3$ shall be used. The number of lorries $n_{eq,C}$ can directly be related to the fatigue life, number of cycles N_C .

The foregoing method for the calculation of the fatigue damage is not identical to a rain flow method. Therefore, for Lorry type 3 of ENV 1991-3 the results of the above mentioned “interval method” were compared to those of a rain flow analysis and the difference was small.

According to ENV 1991-3 (EN 1991-2), no further damage calculation needs to be carried out when the maximum stress interval for the frequent load model FLM2 of ENV 1991-3 is below $\Delta\sigma_D$. When the maximum stress interval belonging to FLM2 is above $\Delta\sigma_D$, Fatigue Load Model 4 (Equivalent lorries) should be used for a damage calculation. The stress intervals of FLM4 can be derived from those of FLM2 with a scale factor and n_{eq} of FLM2 can be used.

In chapter 6, the maximum stress intervals have been determined for the maximum crossbeam load, rotation and deck bending moments for each lorry of the frequent loads (FLM2).

Although not in line with the intended use of FLM2, the equivalent numbers of cycles n_{eq} have been calculated for FLM2 with the vehicle distribution “Long Distance”, as given for the equivalent loads (FLM4).

The interval method was used to perform a simplified damage calculation. It was assumed, that all cycles could be related to stress intervals in conjunction with $m = 3$ or $m = 5$ of the S-N line.

Table 8.2 Relationship between FLM2 and FLM4 vehicle loads

Lorry	Percentage	Vehicle load (kN)		Load ratio FLM4/FLM2
		FLM2	FLM4	
1	20	280	200	0.71
2	5	360	310	0.86
3	50	630	490	0.78
4	15	560	390	0.70
5	10	610	450	0.74

Table 8.2 shows the vehicle load ratio between FLM4 and FLM2, with the “Long Distance” lorry distribution of EN 1991-2.

A very conservative assumption for the reduction factor would be 0.86, but based on the lorries with the higher occurrence, 0.8 is a logical and safe assumption.

Table 8.3 Relationship between FLM2 and FLM4 axle loads

Lorry	Percentage	Axle load (kN)		Load ratio FLM4/FLM2
		FLM2	FLM4	
1	20	90	70	0.78
		190	130	0.68
2	5	80	70	0.88
		140	120	0.86
		140	120	0.86
3	50	90	70	0.78
		180	150	0.83
		120	90	0.75
		120	90	0.75
4	15	90	70	0.78
		190	140	0.74
		140	90	0.64
5	10	90	70	0.78
		180	130	0.72
		120	90	0.75
		110	80	0.73
		110	80	0.73

The axle load ratio between FLM4 and FLM2 is shown in Table 8.3.

For lorry type 2, the maximum ratio is 0.88, for lorry type 3: 0.83 and for lorry type 4: 0.78, equal to that of lorry type 1. If the maximum occurrence of the lorry types is taken into account, it can be concluded that the ratio 0.8 of the axle loads of lorry type 3 is a safe factor.

Concluding, the scale factor of 0.8 is a safe assumption for deriving FLM4 lorry and axle loads from FLM2.

8.4 Combination of load effects

8.4.1 Multi-lane effects

Usually, crossbeams in bridges will carry several traffic lanes with different traffic volumes. Consequently, for the fatigue assessment of a specific detail of the crossbeam, the various traffic lane effects must be combined.

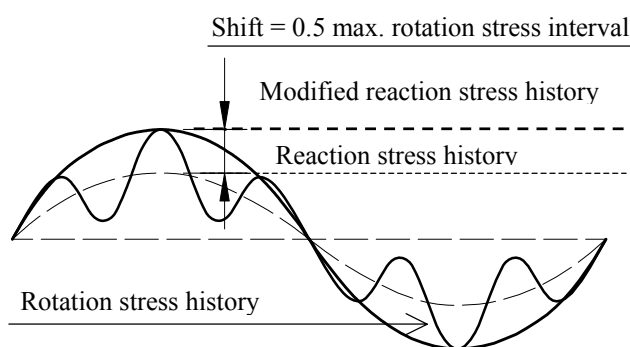
According to ENV 1991-3 and EN 1991-2, 10% of the number of lorries in the slow lane should be considered in the fast lane. However, measurements on bridges in the Netherlands indicate that for some bridges the number of lorries in the fast lane varies between 25% and 40% of that in the slow lane. Due to traffic regulations, the number of lorries on the third lane will be negligible. On bridges with parallel roads, specific analyses of the traffic flow on each lane must be made. This also applies to bridges with specific lanes for heavy traffic such as lorries, buses etc.

In these analyses, 25 % of the lorries on the slow lane are assumed to coincide with lorries on the fast lane. For simplicity, no distinction is made between the combination of a heavy lorry on one lane and a light one on the other lane.

8.4.2 Combination of crossbeam in-plane loads and out-of-plane rotations of the trough to crossbeam connection

For those locations, subjected to stress intervals due to in-plane loads and out-of-plane rotations, the stresses generated by crossbeam in-plane bending and shear and out-of-plane rotations are in the same direction, but have different magnitudes and may have different numbers of cycles.

As shown in Table 6.5 and Fig. 6.19, depending on the type of lorry and the stiffness of the crossbeam, the passage of one lorry causes a number of load intervals between one and four and Table 6.8 shows that the number of rotation intervals varies between three and nine cycles.



Because the stress intervals generated by rotation of the trough to crossbeam connection cause more cycles than that of the crossbeam in-plane loads, the rotation contribution should be considered as an addition to the in-plane load effect.

This is a safe assumption, as the same lorry causes both the stress intervals. The total damage is the sum of the damage due to this modified reaction stress history and the out-of-plane stress history.

Fig. 8.3 Combination of stress intervals

8.4.3 Combined numbers of cycles

The resultant number of cycles for the fatigue life depends on:

1. Lorries on the slow lane per day, Lane 1 $\{f_1 \cdot n_d\}$
2. Lorries on the fast lane per day, Lane 2 $\{f_2 \cdot n_d\}$
3. Stress intervals due to lorries on the slow lane only $\{(f_1-f_2) \cdot n_d\}$
4. Stress intervals due to simultaneous lorries on the slow and the fast lane $\{f_2 \cdot n_d\}$
5. Equivalent number of cycles n_{eq} in relation to the maximum stress interval due to in-plane, out-of-plane and deck bending moment for a particular traffic type. The maximum stress interval depends on a specified relationship between the bending stiffness of the deck per lane and the spring stiffness provided by the crossbeam (K_D^1/K_C^1)
6. Total number of lorries in one direction per working day “ n_d ”
7. Number of working days “ d ” per year
8. Number of design years “ y ”

The resultant number of cycles can be modified into an equivalent number of cycles $n_{eq,C}$ in relation to the fatigue class $\Delta\sigma_C$. This relation covers the relationship between the maximum stress intervals from the analyses derived from the in-plane load intervals, out-of-plane rotation intervals and the deck bending moment intervals.

Table 8.4 shows an example damage calculation procedure. The considered location is subjected to:

- Stress intervals caused by in-plane loads from the lorries on Lane 1 only, increased by 0.5 times the stress intervals due to out-of-plane rotations from the Lorries on Lane 1
- Stress intervals caused by the out-of-plane rotations from the lorries on Lane 1 only
- Stress intervals caused by the simultaneous lorries on Lane 1 and Lane 2, increased by 0.5 times the stress intervals due to out-of-plane rotations from those on Lane 1

The calculation starts with the stress intervals related to FLM2. If all stress intervals are equal to, or below $\Delta\sigma_D$, the location has an unlimited fatigue life. If not, a damage calculation with FLM4 must be carried out. The stress intervals for FLM4 can be obtained by multiplying those of FLM2 by 0.8 (see tables 8.2 and 8.3). Each stress interval equal to or below $\Delta\sigma_L$, makes no contribution to the fatigue damage.

The numbers of cycles for a stress interval under consideration are calculated with the n_{eq} , which can be different for each stress interval, the fraction f_1 (for lorries on Lane 1 only) or f_2 (for lorries on Lane 1 and Lane 2), the total number of lorries per day n_d and the number of design years “ y ”. The result “ n ” is modified with the factor C_f , which relates the maximum stress intervals for a particular load combination to the stress intervals $\Delta\sigma_C$. These equivalent numbers of cycles in relation to the detail class n_C are summed.

If $2 \cdot 10^6$ is divided by Σn_C and multiplied with the reference number of years y , the expected design life in years “ y ” is obtained.

For other locations in the crossbeam, other combinations of damage contributions are possible; e.g. the calculation may be based on the stress intervals caused by the in-plane and the out-of-plane behaviour due to lorries on lane 2 only, or only on in-plane loads due to lorries on lane 1 and lane 2.

Table 8.4 Example of Design life calculation procedure

Wearing course “thick” or “thin”							
Load on	Mode	FLM2		FLM4		n	n _C
		$\Delta\sigma_{\max 2}$	$\Delta\sigma_{\max 2} < \Delta\sigma_D$	$\Delta\sigma_{\max 4}$	$\Delta\sigma_{\max 4} < \Delta\sigma_L$		
Lane 1	In-plane	$\Delta\sigma_{L1ip}$	Y/N (1)	$\Delta\sigma_{L1p}$	Y/N (2)	$(f_1-f_2) \cdot n_{eq} \cdot n_d \cdot d \cdot y = n_{L1ip}$ (3)	$C_f \cdot n_{L1ip} = n_{CL1ip}$ (4)
	Out-of-plane	$\Delta\sigma_{L1op}$	Y/N (1)	$\Delta\sigma_{L1op}$	Y/N (2)	$f_1 \cdot n_{eq} \cdot n_d \cdot d \cdot y = n_{L1op}$ (3)	$C_f \cdot n_{L1op} = n_{CL1op}$ (4)
Lane 1 and Lane 2	In-plane	$\Delta\sigma_{L1+L2ip}$	Y/N (1)	$\Delta\sigma_{L1+L2ip}$	Y/N (2)	$f_2 \cdot n_{eq} \cdot n_d \cdot d \cdot y = n_{L1+L2ip}$ (3)	$C_f \cdot n_{L1+L2} = n_{CL1+L2}$ (4)
Σn_C							Σn_C
Fatigue life (y)							“y”

Explanation to Table 8.4

- $\Delta\sigma_{L1ip}$ Modified stress interval caused by crossbeam in-plane load transfer, due to loads on Lane 1 (The stress interval includes $0.5\Delta\sigma_{L1op}$)
- $\Delta\sigma_{L1op}$ Stress interval caused by trough to crossbeam out-of-plane rotation, due to loads on Lane 1
- $\Delta\sigma_{L1+L2ip}$ Modified stress interval caused by crossbeam in-plane load transfer, due to loads on Lane 1 (The stress interval includes $0.5\Delta\sigma_{L1op}$)
- n Equivalent number of cycles for maximum stress interval of FLM4 during design life
- n_C Equivalent number of cycles of FLM4 in relation to $\Delta\sigma_C$ during design life
- n_d Lorries per day
- d Working days per year
- y Reference number of years
- $\Delta\sigma_{\max 2}$ Maximum stress interval for FLM2
- $\Delta\sigma_{\max 2} > \Delta\sigma_D$ Fatigue life assessment with FLM4
- (1) $\Delta\sigma_{\max 2} \leq \Delta\sigma_D$ Unlimited fatigue life, if fulfilled
- $\Delta\sigma_{\max 4}$ Maximum stress interval for FLM4
- $\Delta\sigma_{\max 4} > \Delta\sigma_L$ Fatigue life assessment with FLM4
- (2) $\Delta\sigma_{\max 4} \leq \Delta\sigma_L$ No damage, if fulfilled
- (3) n_{eq} Equivalent number of cycles in relation to one lorry, which can be different for each stress interval
- (4) C_f Factor that relates the maximum stress interval $\Delta\sigma$ to the $\Delta\sigma_C$ (is different for each stress interval)
- “y” Fatigue life in years

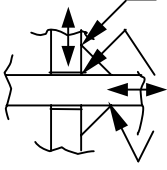
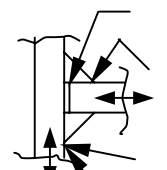
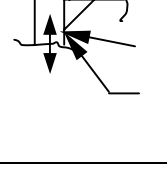
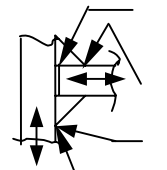
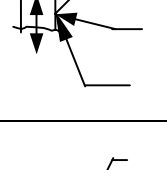

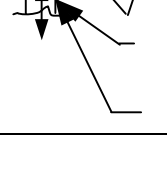
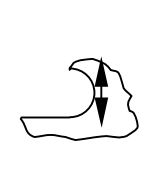
8.5 Recommended detail classifications and partial factors

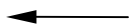
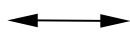
In order to enable fatigue assessments for design, the fatigue detail classes for the closed stiffener to crossbeam connection are given as recommended design values, together with a recommended partial safety factor γ_{Mf} for the fatigue resistance of the details. The evaluation of existing structures can be carried out with an average value of the detail classification, which is not given here. The recommended fatigue detail classifications are, where possible, based on a comparison of the IIW Recommendation for Fatigue design of Welded Joints and Components by Hobbacher et al. (2005) and the fatigue design classifications given in EN 1993-1-9.

In general, these design classifications are based on a 75% confidence level of 95% probability of survival, analysed with the assessment procedure given in EN 1990 Annex D.

Except for the continuous open stiffener to crossbeam connection, the data shown in Table 8.5 have been used to select the appropriate categories for calculation purposes presented in the Tables 8.6 to 8.9.

Table 8.5 Assembly of detail classifications

Loc.	Detail	EN 1993-1-9		IIW		Remark	Stress
		Class	Table	Class	Ref.		
Trough fitted between crossbeams							
S.3		80 nom. Toe	8.5	-	-	-	NWT NWR
		36 nom. Root	8.5	-	-	-	
		36 nom. Root	8.8	36 nom. Root	Tab. {3.2}-1 item 416	-	
C.3		80 nom. Toe	8.4	80 nom. Toe	Tab. {3.2}-1 item 511	-	NWT
Continuous trough in close fit							
C.4.1		36 nom. Root	8.5	36 nom. Root	Tab. {3.2}-1 item 414	-	NWR
		80 nom. Toe	8.5	63 nom. Toe	Tab. {3.2}-1 item 413	-	
S.4.1		80 nom. -	8.8	-	-	-	NWT
		80 nom. -	8.4	71 nom. -	Tab. {3.2}-1 item 511	-	
Continuous trough with cope hole							
C.4.2		36 nom. Root	8.5	36 nom. Root	Tab. {3.2}-1 item 414	-	NWT
		80 nom. Toe	8.5	63 nom. Toe	Tab. {3.2}-1 item 413	-	
S.4.2		80 nom. -	8.8	-	-	-	NWT
		80 nom. Toe	8.4	80 nom. Toe	Tab. {3.2}-1 item 511	-	
C.4.2		80 nom. Toe	8.5	-	-	-	NWT
		-	-	100 geom. Toe	Tab. {3.3}-1 item 4	-	
S.4.2		56 nom. Toe	8.4	71 nom. Toe	Tab. {3.2}-1 item 512	1)	NWT
		-	-	100 geom. Toe	Tab. {3.3}-1 item 4	-	
C.4.5		140 nom. Edge 125 nom. Edge	8.1	140 nom. Edge 125 nom. Edge	Tab. {3.2}-1 item 121	2)	GHS N
		71 (112) nom. Edge	8.8	-	-	3)	

 = Location
 = Stress interval

Explanation:
 NWT = Nominal stress at weld toe location
 NWR = Nominal stress at weld root location in accordance with EN 1993-1-9
 GHS = Geometric stress at edge of parent material
 N = Nominal stress at edge of parent material

Remarks:

- 1) Out of range for EN 1993-1-9 and IIW
- 2) Incl.geometric concentration, Class depends on finish
- 3) Depends on method of calculation

8.5.1 Closed stiffener fitted between crossbeams, detail "a"

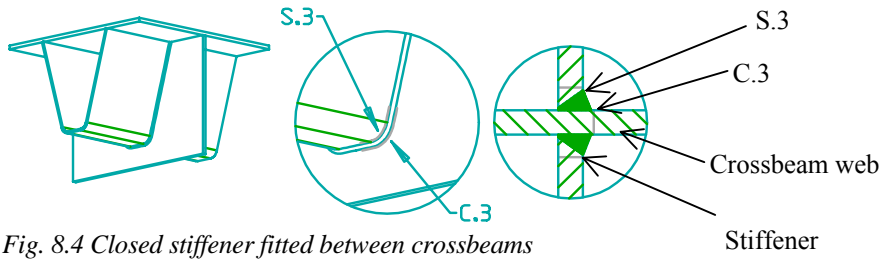


Fig. 8.4 Closed stiffener fitted between crossbeams

Fig. 8.4 shows the detail and the relevant locations and Table 8.6 gives the fatigue detail classification recommendations.

Table 8.6

Location Fig. 8.5	Design fatigue class	Stress type	Failure mode Root = R Toe = T	γ_{Mf}	Weld shape
S.3	36	Nominal stress in weld in accordance with EN 1993-1-9	R	1.0	Fillet en butt welds
C.3	80	Nominal stress in crossbeam web	T	1.0	Fillet welds

Root failure is most likely to occur in location S.3, as local bending is of minor importance. At C.3, toe failure is most likely to occur due to a combination of crossbeam in-plane behaviour with out of-plane rotations. The classifications in EN 1993-1-9 are identical to those in the IIW document. The partial factor γ_{Mf} has been chosen as 1.0, because the failure of the connection does not immediately threaten the overall structural integrity of the orthotropic deck.

8.5.2 Continuous closed stiffener through crossbeam with close fit, detail "b1"

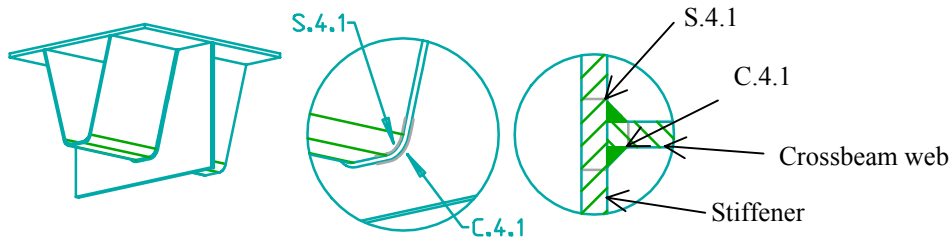


Fig. 8.5 Continuous closed stiffener through crossbeam with close fit

Fig. 8.5 shows the detail and the relevant locations and Table 8.7 shows the fatigue detail classification recommendations.

Table 8.7

Location Fig. 8.6	Design fatigue class	Stress type	Failure mode Root = R Toe = T	Note	γ_{Mf}
S.4.1	80	Nominal stress in stiffener at weld toe	-	-	1.0
C.4.1	80	Nominal stress in crossbeam web at weld toe, including trough bottom curvature effects	T	-	1.15

At C.4.1, toe failure is most likely to occur due to a combination of crossbeam in-plane behaviour with out of-plane rotations. In spite of the lower values in the IIW document, the classifications from EN 1993-1-9 have been used, as the conditions are similar to those of the locations S.3 and C.3.

The partial factor γ_{Mf} has been chosen as 1.0, for S.4.1 and 1.15 for C.4.1 because crack growth in the stiffener does not threaten the overall structural integrity of the orthotropic deck. Crack growth in the tooth and the reversed T-beam below the trough could immediately threaten the overall structural integrity of the orthotropic deck.

8.5.3 Continuous closed stiffener through a cut out in the Crossbeam with an oval cope hole or with a "Haibach" cope hole, detail "b2" and "b3"

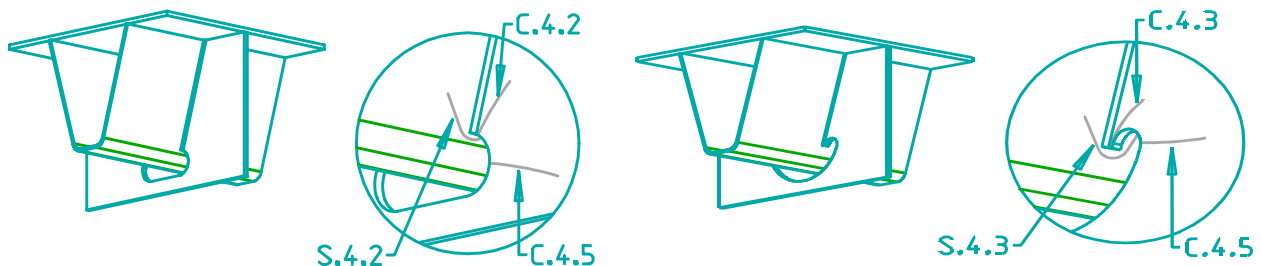


Fig. 8.6 Closed stiffener through crossbeam with oval cope hole

Fig. 8.7 Closed stiffener through crossbeam with "Haibach" cope hole

Figs. 8.6 and 8.7 show the detail and the relevant locations and Table 8.8 gives the fatigue detail classification recommendations.

Table 8.8

Location Figs 8.7 and 8.8	Design fatigue class	Stress type	Failure mode Root = R Toe = T	Note:	γ_{Mf}
S.4.2 and S.4.3	80	Nominal stress in stiffener at weld toe	T	For web	1.0
	100	Geometrical stress in stiffener at weld toe	T	Around bottom of connection	1.0
C.4.2 and C.4.3	100	Nominal stress in stiffener at weld toe	T	-	1.0
C.4.5	140	Geometric stress in crossbeam	T	-	1.15

Based on the comparison of the detail classifications given in Table 8.5, fatigue class 80 is recommended for an assessment with nominal stresses for the vertical weld to the trough web (S.4.2 and S.4.3), in line with EN 1993-1-9.

For the locations around the lower end of the fillet weld of the trough to the crossbeam web however, the geometrical Hot Spot stresses from the IIW document should be used. At these locations, the geometrical stress concentration factors in chapter 5 are used, based on FE models with solid elements. The extrapolated stresses have been determined in a similar way.

For the locations S.4.2, S.4.3, C.4.2 and C.4.3, the partial factor γ_{Mf} has been chosen as 1.0, because the failure of the connection does not immediately threaten the overall structural integrity of the orthotropic deck. For C.4.2 and C.4.3, γ_{Mf} should be chosen as 1.15 in combination with larger inspection intervals.

For the cope hole location C.4.5, it is recommended that the fatigue classification 140 is used, in conjunction with a partial factor γ_{Mf} of 1.15, because, although the tooth has a good inspectability, the crack can propagate quickly, due to the load transfer in the tooth.

8.6 Concluding remarks

The procedure in 8.2 leads to nominal and geometrical stress intervals, which can be used for a fatigue assessment using the calculation procedures given in 8.3 and 8.4.

The fatigue loads model FLM2 can be related to FLM4 with a factor 0.8, which enables a direct transfer of the stresses used for the assessment for unlimited fatigue life into stresses for an assessment for a limited fatigue life.

The fatigue design classifications given as examples in 8.5 are based on the state of the art and their accuracy could be refined with further work.

9 CALCULATION EXAMPLE FOR A TROUGH TO CROSSBEAM CONNECTION IN THREE TYPES OF CROSSBEAMS

9.1 Introduction

In this chapter, the methods and results from the chapters 4, 5, 6 and 8 are used for fatigue assessments. Three types of trough to crossbeam connections in typical crossbeams are analysed; Crossbeam “AA” with continuous troughs and cope holes, Crossbeam “BB” with continuous troughs through close fitting cut-outs and Crossbeam “CC” with trough stiffeners fitted between the crossbeams.

The design assumptions are set out in 9.2 and the structural dimensions are given in 9.3. The material is described in 9.4 and the basis for the traffic loads is given in 9.5.

The static properties are described in 9.6; the determination of the equivalent crossbeam properties is described in 9.7 and the equivalent deck properties in 9.8.

The selection of the appropriate influence lines and subsequently the load, rotation and deck bending moment histories are described in 9.9 and the relevant load, rotation and deck bending moment intervals that are derived from it, are described in 9.10.

Paragraph 9.11 gives an overview of the relevant shear force intervals, the rotation intervals and the deck bending moment intervals that are the basis for further calculations of the locations around trough number 8, which is selected for further analysis. The detail analyses for Crossbeam “AA”; stress intervals, stress interval combinations and a fatigue assessment are given in 9.12. For Crossbeam “BB” these analyses are described in 9.13 and for Crossbeam “CC” in 9.14 respectively. Finally, 9.15 gives the concluding remarks.

9.2 General

The analysed orthotropic steel deck is intended for a twin deck plate girder bridge situated on a three-lane motorway, so each deck carries three traffic lanes and an emergency lane.

Fig. 9.1 shows a cross section of one deck of the motorway, including the safety barriers, the parapets and the positions of the traffic lanes. The total width of the deck between the parapets is 18.0 m. The analyses are carried out for the connection of trough number 8 to the crossbeam, which is considered to be subjected to crossbeam in-plane, crossbeam out-of-plane and deck bending, as a most adverse combination of effects.

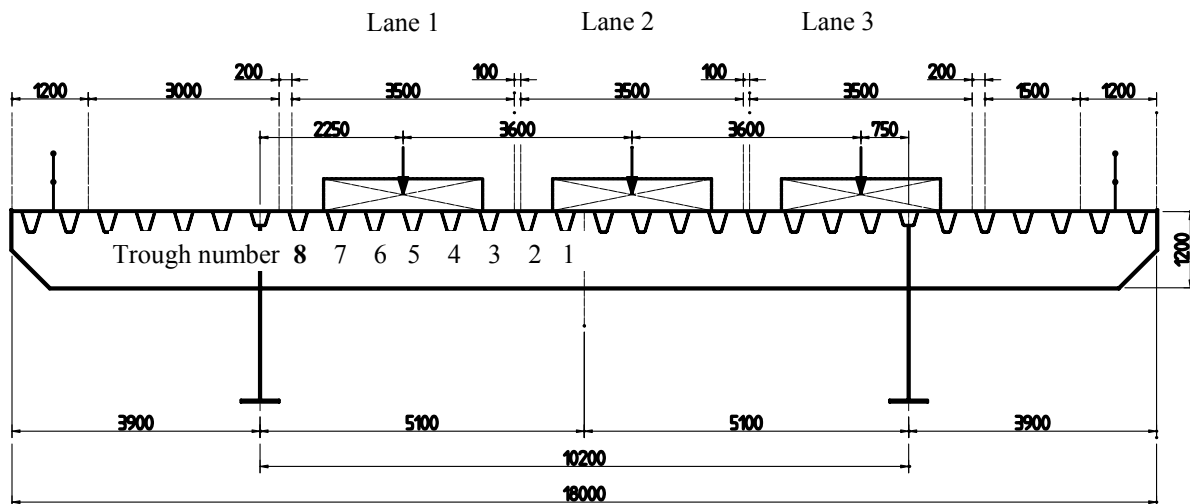


Fig. 9.1 Cross section of bridge deck with crossbeam in elevation

The assumed traffic flow complies with the static and fatigue traffic load models given in ENV 1991-3 (EN 1991-2), except for the total number of lorries in the traffic categories, which is taken as 8.000 per working day in one direction distributed as follows: On the slow lane, "Lane 1", 0.8 times 8000, i.e. 6400 and on the adjacent fast lane, "Lane 2", 0.2 times 8000, i.e. 1600. The second fast lane, "Lane 3", is not considered as being loaded by lorries affecting the fatigue strength, as the number on this lane is negligible due to traffic regulations. The same applies to the emergency lane and the space between "Lane 3" and the safety barrier. A year is assumed to have 250 working days.

The analyses for trough no. 8 are carried out for the maximum shear force interval in the crossbeam caused by the lorries. The influence length of the deck for one lorry is assumed to be covered by the model consisting of five crossbeams as used in chapter 6.

9.3 Dimensions

The chosen deck plate thickness is 16 mm, stiffened in the longitudinal direction by troughs with the dimensions of the former Krupp: FKH 2/325/6 product. The crossbeam web has a depth of 1200 mm and a thickness of 10 mm. The centre-to-centre distance of the stiffeners is 600 mm. The distance between the main girders is 10.200 mm. The crossbeams have two cantilever parts with lengths of 3900 mm. The centre-to-centre distance of the crossbeams is 4000 mm.

Three types of crossbeams are considered:

Crossbeam type "AA"

The stiffeners are continuous and pass through cut-outs with oval cope holes with a total horizontal length of 175 mm and radii of 35 mm.

Crossbeam type "BB"

The stiffeners are continuous and pass through close fitting cut-outs.

Crossbeam type "CC"

The stiffeners are fitted between the crossbeams.

In general, two types of wearing courses are used on steel decks:

- “Thick wearing courses” consisting of mastic asphalt with a thickness from 50 – 60 mm on fixed bridges
- “Thin wearing courses” consisting of an epoxy layer with a thickness of approximately 10 mm on moveable bridges

A thicker wearing course results in substantial composite action between the wearing course and the deck plate. This causes the axle loads to be distributed over more stiffeners under moving loads than occurs with a thin wearing course, where, due to the small layer thickness, the effect of the wearing course (composite action) can be neglected. In the calculations presented here, a thick wearing course has a thickness of approximately 50 mm and a thin wearing course has a thickness of approximately 10 mm. The thickness of the wearing course is included in a typical deck plate stiffness to determine the effective number of troughs carrying the traffic lane. Simple calculations, not reported here, led to the following conclusion:

Thick wearing course

The effective deck lane width for axle loads includes five stiffeners.

Thin wearing course

The effective deck lane width for axle loads includes three stiffeners.

9.4 Material

The selected material is the commonly used steel for bridges: S355 in accordance with EN 10025.

9.5 Loads

The static loads are derived from ENV 1991-3 (EN 1991-2), clause 4.3.1. The fatigue loads are derived from ENV 1991-3, clause 4.6.3 Fatigue Load Model 2 "Set of frequent lorries" FLM2 and Fatigue Load Model 4 "Set of equivalent lorries" FLM4. (Additional requirements such as the Netherlands National Annex are ignored.)

9.6 Section properties

9.6.1 Deck plate

The deck plate has a thickness of 16 mm.

9.6.2 Trough stiffener with deck plate

Fig. 9.2 shows the cross section of the trough stiffener with deck plate assembly, the section properties for a single trough with deck plate are shown in Table 9.1.

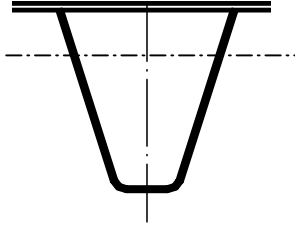


Table 9.1 Section properties of trough with deck plate

Effective width	b_{eff}	600 mm
Area	A	$1.43 \cdot 10^4 \text{ mm}^2$
Moment of Inertia	I_S	$1.66 \cdot 10^8 \text{ mm}^4$
Upper part section modulus	W_{Su}	$2.34 \cdot 10^6 \text{ mm}^3$
Lower part section modulus	W_{Sl}	$6.16 \cdot 10^6 \text{ mm}^3$

Fig. 9.2 Trough stiffener with deck plate

9.6.3 Lane deck stiffness

a. Thick wearing course

The axle loads are assumed to be distributed transversely over five troughs with deck plate. The effective moment of inertia $I_{D,L5}$ for one lane becomes:

$$I_{D,L5} = 5 \cdot I_S = 5 \cdot 1.66 \cdot 10^8 = 8.30 \cdot 10^8 \text{ mm}^4$$

The lane bending stiffness: $E \cdot I_{D,L5} = 174.3 \cdot 10^{12} \text{ Nmm}^2$

b. Thin wearing course

As axle loads are assumed to be distributed transversely over a smaller number of stiffeners, three troughs with deck plate are considered to carry the traffic loads. The effective moment of inertia $I_{D,L3}$ for one lane becomes:

$$I_{D,L3} = 3 \cdot I_S = 3 \cdot 1.66 \cdot 10^8 = 4.98 \cdot 10^8 \text{ mm}^4$$

The lane bending stiffness: $E \cdot I_{D,L3} = 104.6 \cdot 10^{12} \text{ Nmm}^2$

9.6.4 Full deck stiffness

The moment of inertia I_D for the deck, including all (16) trough stiffeners between the main girders, acting as supports for the traffic lanes, becomes, as described in 6.3.2 with equation [6.6]:

$$I_D = 2/3 \times 16 \times I_S = 17.7 \cdot 10^8 \text{ mm}^4$$

The full deck bending stiffness: $E \cdot I_D = 371.8 \cdot 10^{12} \text{ Nmm}^2$

9.6.5 Crossbeam properties

The resistances of the crossbeams Type "AA", "BB", and "CC" have been verified with a global static calculation, not reported here.

Fig. 9.3 shows the cross section of the crossbeam at locations with and without cut-out.

The dimensions of the parts of the crossbeam that are used to derive the properties for the crossbeams with cope holes at cross section "A" (see also Figs. 4.2 and 4.3), are given in Table 9.2, together with the section properties for the cross section "C".

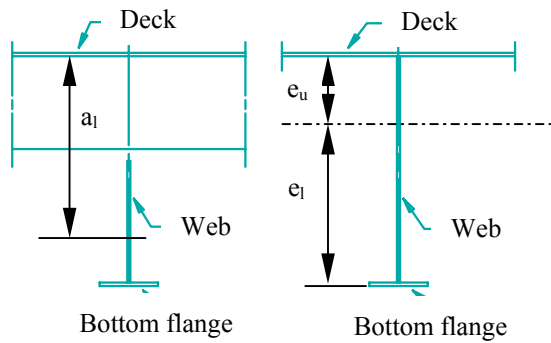


Fig. 9.3 Typical cross sections “A” and “C”

Table 9.2 Section properties of crossbeam with full section

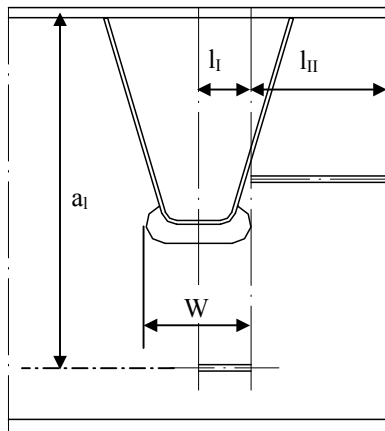
Part		
Deck plate		2470 x 16 mm
Crossbeam web (full section)		1200 x 10 mm
Bottom flange		300 x 20 mm
Property		
Moment of Inertia	I_C	$111.0 \cdot 10^8 \text{ mm}^4$
Distance from neutral axis to centre of deck plate	e_u	262mm
Upper part section modulus	W_u	$422.5 \cdot 10^6 \text{ mm}^3$
Distance from neutral axis to centre of bottom flange	e_i	957mm
Lower part section modulus	W_l	$114.0 \cdot 10^6 \text{ mm}^3$
Lever arm	a_1	963 mm

9.7 Equivalent crossbeam properties

9.7.1 In-plane bending

The equivalent bending stiffness c_b for a crossbeam with cut-outs (and cope holes) is determined in accordance with the methods, presented in 4.2.1:

$\phi_{A\text{-cutout}}$ for a crossbeam with cut-outs:	$\phi_{A\text{-cutout}} = \frac{M_{unity}}{E} \cdot \left(\frac{l_I}{I_{cutout}} + \frac{l_{II}}{I_{full}} \right)$	[4.14]
$\phi_{A\text{-full}}$ for a crossbeam without cut-outs:	$\phi_{A\text{-full}} = \frac{M_{unity}}{E} \cdot \frac{l_I + l_{II}}{I_{full}}$	[4.15]
c_b :	$c_b = \frac{\phi_{A\text{-full}}}{\phi_{A\text{-cutout}}}$	[4.11]



In equations [4.14] and [4.15] the lengths l_I , l_{II} and a_1 are as shown in Fig. 9.4:

- l_I = 0.5 W = half cut-out (including cope hole) width
- l_{II} = half centre-to-centre distance of troughs minus half cut-out width
- a_1 = lever arm (distance between centre of the deck plate and the centroid of reversed T-beam below the trough)

Fig. 9.4 Model of crossbeam with cut-out and cope hole

The following abbreviations are used:

M_{unity}	=	unity bending moment in the crossbeam
$I_{\text{cut-out}}$	=	moment of inertia of the crossbeam at the cut-out
I_{full}	=	moment of inertia of the crossbeam without cut-outs
$\phi_{\text{A-cut-out}}$	=	rotation at cross section A with respect to cross section C due to the unit moment over the parts $l_I + l_{II}$ with and without cut-out
$\phi_{\text{A-full}}$	=	rotation at cross section A with respect to cross section C due to the unit moment over the parts $l_I + l_{II}$ if there were no cut-out

Calculation results reported in 4.2.2.1, showed that for the crossbeams “AA” and “BB” the influence of cut-outs on the crossbeam bending stiffness is insignificant due to the position of the centroid. Therefore, the value of c_b for the crossbeams “AA” and “BB” can be taken as 1.0.

9.7.2 In-plane shear

For the calculation of the effective shear stiffness by means of an effective crossbeam web thickness, the method presented in 4.2.1.3 is used, including the correction for the tooth length given in Table 4.2:

S_h :	$S_h = \frac{S_{vl} \cdot 0.5c + S_{vr} \cdot 0.5c}{a_l}$	[4.17]
δ_h due to bending and shear:	$\delta_h = \frac{S_h \cdot c_c \cdot l_{IV}^3}{3 \cdot E \cdot I_{\text{tooth}}} + \frac{S_h \cdot c_c \cdot l_{IV}}{G \cdot A_{\text{tooth}}}$	[4.18]
δ_{vl} due to bending and shear:	$\delta_{vl} = \frac{S_{vl} \cdot l_I^3}{3 \cdot E \cdot I_{T\text{-beam}}} + \frac{S_{vl} \cdot l_I}{G \cdot A_{T\text{-beam}}}$	[4.19]
δ_{vr} due to bending and shear:	$\delta_{vr} = \frac{S_{vr} \cdot l_{III}^3}{3 \cdot E \cdot I_{T\text{-beam}}} + \frac{S_{vr} \cdot l_{III}}{G \cdot A_{T\text{-beam}}}$	[4.20]
The additional vertical displacements of the T-beam ends due to the tooth deformations:	$0.5\delta_{v\text{-add}} = \frac{\delta_h}{a_l} \cdot 0.5c$	[4.21]
The total vertical deformation:	$\delta_{v\text{-total}} = \delta_{vl} + \delta_{vr} + \delta_{v\text{-add}}$	[4.22]
The total vertical deformation for a crossbeam web without cut-outs:	$\delta_{v\text{-full}} = \frac{S_v \cdot c}{G \cdot A_{\text{web}}}$	[4.23]
The equivalent shear stiffness ratio c_s :	$c_s = \frac{\delta_{v\text{-full}}}{\delta_{v\text{-total}}}$	[4.24]

In equations [4.17] to [4.20] the lengths are as indicated in Fig. 9.5:

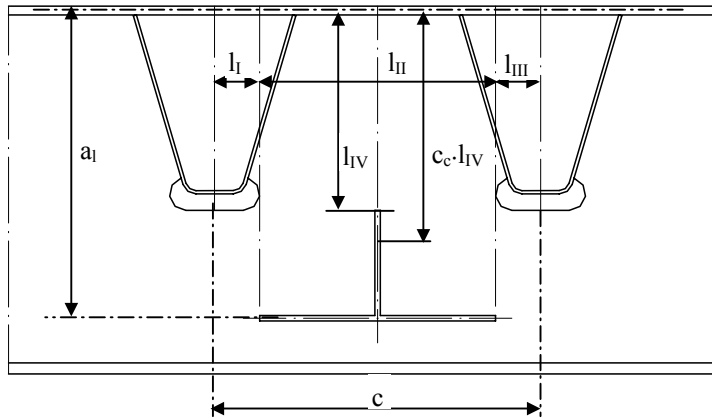


Fig. 9.5 Model of crossbeam web with cut-out and cope hole

With:

- c = centre-to-centre distance of troughs
- l_I = $0.5 W$ = half cut-out (including cope hole) width
- l_{II} = centre-to-centre distance of troughs minus cut-out width
- l_{III} = $0.5 W$ = half cut-out (including cope hole) width
- l_{IV} = tooth length
- a_1 = length of lever arm between T-beam centroid below the trough and the deck plate centre
- c_c = correction factor for tooth length (see Table 9.3)

The following abbreviations are

used:

- S_{vl} = vertical shear force (left side)
- S_{vr} = vertical shear force (right side)
- S_h = horizontal shear force
- I_{tooth} = moment of inertia of the tooth
- I_{T-beam} = moment of inertia of the T-beam
- A_{tooth} = area of tooth
- A_{T-beam} = area of T-beam
- δ_h = horizontal deformation of tooth, see Fig. 4.12
- δ_{vl} = vertical deformation of T-beam (left side), see Fig. 4.12
- δ_{vr} = vertical deformation of T-beam (right side), see Fig. 4.12
- δ_{v-add} = additional vertical deformation due to tooth deformation, see Fig. 4.12
- $\delta_{v-total}$ = total vertical deformation, see Fig. 4.12
- δ_{v-full} = vertical deformation of crossbeam part without cut-outs

Table 9.3 (equivalent to Table 4.2), Correction factors c_c for tooth length 350 mm to be used in conjunction with analytical calculations

Beam No.	Web depth (mm)	Cut-out with cope hole width "W" (mm)				
		75	125	175	225	275
1	600	1.20	1.16	1.13	1.11	1.08
2	800	1.25	1.20	1.15	1.12	1.08
3	1000	1.30	1.23	1.18	1.13	1.09
4	1200	1.33	1.24	1.17	1.11	1.06
5	1400	1.33	1.24	1.16	1.10	1.04
7	1800	-	-	1.16	-	-
9	2200	-	-	1.16	-	-

As an alternative to this calculation, the values from Fig. 4.18 can be used. For both crossbeams "AA and BB" with $H = 1200$ mm, the value of $c_s = 0.430$, as the difference between the widths of the cope holes ($W = 175$ and 105 mm) proves to have a negligible influence. Crossbeam "CC" has no cut-outs, so c_s is irrelevant.

9.7.3 Equivalent crossbeam properties

The equivalent properties for the crossbeams “AA” and “BB” to be used for the determination of the crossbeam spring stiffness K_C^1 and the deck spring stiffness K_D^1 for Lane 1 and Lane 2 become:

$$A_C^1 = c_s \cdot A_C \quad [9.1]$$

$$A_C^1 = 51.6 \cdot 10^2 \text{ mm}^2$$

$$I_C^1 = c_b \cdot I_C \quad [9.2]$$

$$I_C^1 = 111.0 \cdot 10^8 \text{ mm}^4$$

9.7.4 Equivalent crossbeam spring stiffness in-plane

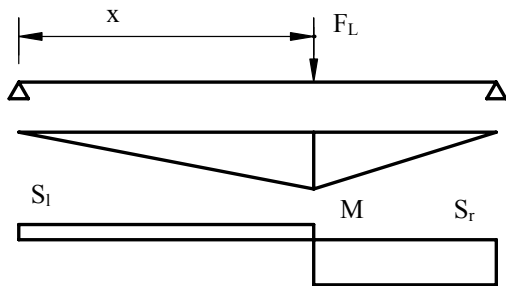


Fig.9.6 Lane load,, bending and shear diagrams

The effective spring stiffnesses K_C^1 of the partially loaded crossbeam, together with the effective spring stiffnesses of the deck K_D^1 , are essential for the selection of the appropriate influence lines and the reaction and rotation histories to be used for further calculations.

The spring stiffness is calculated with equation [6.10] for partially loaded crossbeams, acting as supports of Lane 1 and Lane 2 respectively:

$$K_C^1 = \frac{1}{\frac{x^2 \cdot (l_C - x)^3}{3 \cdot E \cdot I_C^1 \cdot l_C^2} + \frac{x \cdot (l_C - x)}{G \cdot A_C^1 \cdot l_C}} \quad [6.10]$$

In equation [6.10], the terms have the following meaning:

- l_C = crossbeam span
- x = distance from considered lane to support S_l
- I_C^1 = equivalent moment of inertia of crossbeam
- A_C^1 = equivalent area of crossbeam

Table 9.4 Equivalent spring constants of crossbeams K_C^1 (N/mm²)

Crossbeam type	Lane 1	Lane 2
"AA" and "BB"	$1.38 \cdot 10^5$	$1.09 \cdot 10^5$
"CC"	$1.96 \cdot 10^5$	$1.62 \cdot 10^5$

The results of the crossbeam spring stiffnesses at Lane 1 and Lane 2 respectively, are shown in Table 9.4.

9.8 Equivalent deck spring stiffness properties

The lane deck stiffness K_D^1 is calculated with eqs. [6.7] and [6.8]:

δ_3 , at the location of the considered crossbeam (Crossbeam 3 in a deck with 5 crossbeams) due to a unit load P_{D3V} :	$\delta_3 = P_{D3V} \cdot \left\{ \frac{5}{2 \cdot K_c^1} + \frac{l_s^3}{3 \cdot E \cdot I_D} \right\} - \frac{\left\{ \frac{3}{K_c^1 \cdot l_s} + \frac{5 \cdot l_s^2}{6 \cdot E \cdot I_D} \right\}^2}{4 \cdot \left\{ \frac{1}{K_c^1 \cdot l_s^2} + \frac{2 \cdot l_s}{3 \cdot E \cdot I_D} \right\}}$	[6.7]
Spring stiffness:	$K_{D3}^1 = \frac{P_{D3V}}{\delta_3}$	[6.8]

with:

l_s = stiffener span = centre-to-centre distance of the crossbeams

The equivalent deck spring stiffness K_D^1 of the deck for the traffic lanes 1 and 2 is shown in Table 9.5.

Table 9.5 Equivalent spring constants of the deck K_D^1 (N/mm²) for traffic lanes 1 and 2

Crossbeam type	Thick wearing course		Thin wearing course		These values include the deck stiffness and the spring stiffness effects of the other supporting crossbeams (crossbeams 1, 2, 4 and 5).
	Lane 1	Lane 2	Lane 1	Lane 2	
"AA, BB"	2.95·10 ⁴	2.79·10 ⁴	1.93·10 ⁴	1.87·10 ⁴	
"CC"	3.14·10 ⁴	3.04·10 ⁴	2.01·10 ⁴	1.98·10 ⁴	

9.9 Stiffness ratios

Table 9.6 shows the stiffness ratios K_D^1/K_c^1 (deck spring stiffness divided by crossbeam spring stiffness) for Lanes 1 and 2 of crossbeams "AA", "BB" and "CC" for a thick and a thin wearing course.

Table 9.6 Stiffness ratios K_D^1/K_c^1 for traffic lanes 1 and 2

Crossbeam type	Thick wearing course		Thin wearing course		From the stiffness ratios, the relevant influence lines determined for various crossbeam depths in chapter 6
	Lane 1	Lane 2	Lane 1	Lane 2	
"AA", "BB"	0.213	0.256	0.140	0.171	
"CC"	0.160	0.187	0.103	0.122	

can be selected (see dotted lines) based on the graph of Fig. 6.12 for $W = 175$, which is shown here again as Fig. 9.7. The values of K_D^1/K_c^1 of the example crossbeams "AA", "BB" and "CC" with $H = 1200$ mm are equal to specific values of the range of "reference" crossbeams, analysed in chapters 4 and 6, with a much larger depth, so they are much more rigid.

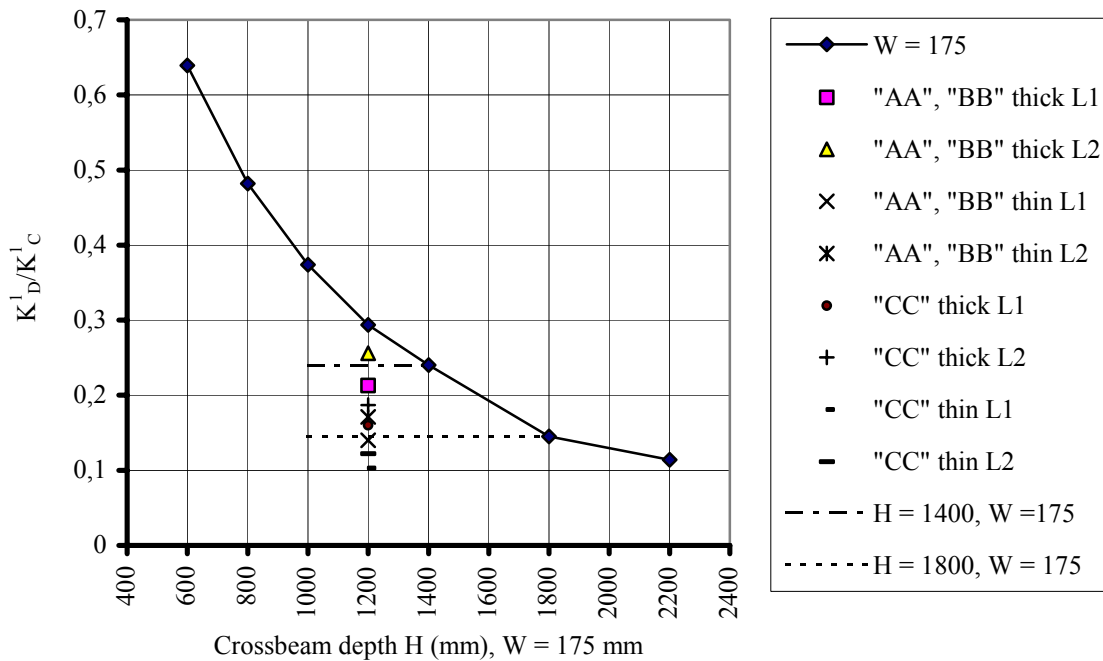


Fig. 9.7 K_D^1 divided by K_C^1 with the values for crossbeams "AA", "BB" and "CC" indicated

Explanation to Fig.9.7:

- AA, BB, CC: Example crossbeam type
- L1, L2: Traffic lane number
- Thick; thin: Wearing course thickness

Table 9.7 Selection of reference crossbeams for influence lines

Crossbeam	Wearing course	K_D^1/K_C^1		Selected reference crossbeams for influence lines
		Lane 1	Lane 2	
"AA", "BB"	Thick	0.213	0.256	Type 5, H = 1400 mm, W = 175 mm
"AA", "BB"	Thin	0.140	0.171	
"CC"	Thick	0.160	0.187	Type 7, H = 1800 mm, W = 175 mm
"CC"	Thin	0.103	0.122	

The value of K_D^1/K_C^1 and the selection of relevant influence lines for the various traffic lanes of the example crossbeams is given in Table 9.7.

This selection of reference crossbeams is appropriate,

as it is only used to determine the relevant influence lines. With these influence lines the load, rotation and deck bending moment intervals are characterised.

9.10 Influence lines and load/rotation/moment intervals

The values for the load intervals in Fig. 6.20 can be used without correction as the reactions are only related to the portion of the transferred load, which is dimensionless. For the rotations, the intervals from Fig. 6.23 must be scaled with a factor $I_D/I_{D,L}$.

The bending moment intervals in the lane as shown in Fig. 6.26 can be used without correction.

Table 9.8 gives an overview of the selection of the relevant reference crossbeam types described in chapter 6 and the load, rotation and deck bending moment intervals. For the out-of-plane rotations, the correction factors for the deck lane width are included. All (maximum) load intervals ΔR , rotation intervals $\Delta\phi$ and deck bending moment intervals ΔM_D are given with the equivalent numbers of cycles n_{eq} in relation to 100 lorries, are based on ENV 1991-3 FLM2, with the lorry distribution of FLM4.

Table 9.8 Selected reference crossbeams for influence lines with equivalent reaction, rotation and bending moment intervals for FLM2 determined with $m=3$

Crossbeam	Traffic lane number	Wearing course	Reference crossbeam type	ΔR (kN) / cycles (c) per 100 lorries	$\Delta\phi$ (mrad) / cycles (c) per 100 lorries	ΔM_D (kNm) / cycles (c) per 100 lorries
“AA”, “BB”	1, 2	Thick	Type 5, H = 1400, W = 175	259 / 64c	(1.6 · 1.13 / 39c) 1.81 / 39c	115.0 / 64c
“AA”, “BB”	1, 2	Thin	Type 7, H = 1800, W = 175	270 / 64c	(2.7 · 0.97 / 57c) 2.62 / 57c	108.0 / 109c
“CC”	1, 2	Thick	Type 7, H = 1800, W = 175	270 / 64c	(1.6 · 0.97 / 57c) 1.55 / 57c	108.0 / 109c
“CC”	1, 2	Thin	Type 7, H = 1800, W = 175	270 / 64c	(2.7 · 0.97 / 57c) 2.62 / 57c	108.0 / 109c

9.11 Crossbeam and traffic lane in-plane section force, out-of-plane rotation and deck bending moment intervals at trough 8

With the reaction, rotation and bending moment intervals given in Table 9.8, the crossbeam in-plane shear force intervals ΔS , the bending moment intervals ΔM in the cross section and the out-of-plane rotation intervals $\Delta\phi$ of the crossbeam can be calculated for the cross section of the crossbeams at Trough no. 8 (see Fig. 9.1), due to the lorries on Lane 1 and Lane 2. This also applies for the bending moment intervals ΔM_D in the traffic lane deck. The results for the load intervals on Lane 1 and Lane 2 are shown in Table 9.9. The equivalent numbers of cycles “c” are in relation to 100 lorries.

Table 9.9 Shear force and in-plane bending moment intervals in the crossbeam, rotation and deck bending moment intervals at the trough to crossbeam connection with equivalent numbers of cycles for 100 lorries at the connection of Trough no. 8.

Crossbeam	Traffic lane number	Wearing course	ΔS (kN) / cycles per 100 lorries	ΔM (kNm) / cycles per 100 lorries	$\Delta\phi$ (mrad) / cycles per 100 lorries	ΔM_D (kNm) / cycles per 100 lorries
“AA”, “BB”	1	Thick	202 / 64c	242 / 64c	1.81 / 39c	115.0 / 64c
“AA”, “BB”	1	Thin	210 / 64c	253 / 64c	2.62 / 57c	108.0 / 109c
“CC”	1	Thick	210 / 64c	253 / 64c	1.55 / 57c	108.0 / 109c
“CC”	1	Thin	210 / 64c	253 / 64c	2.62 / 57c	108.0 / 109c
“AA”, “BB”	2	Thick	111 / 64c	133 / 64c	-	-
“AA”, “BB”	2	Thin	115 / 64c	138 / 64c	-	-
“CC”	2	Thick	115 / 64c	138 / 64c	-	-
“CC”	2	Thin	115 / 64c	138 / 64c	-	-

Table 9.10 Reference loads in reference crossbeams

In-plane	Shear force (kN)	Bending moment (kNm)
	390	700
Out-of-plane	Applied rotation (mrad)	
	10	

Chapter 4 described the range of “reference” crossbeams, analysed with an in-plane uniformly distributed load of 108 N/mm¹. That resulted in the crossbeam in-plane shear forces given in Table 9.10, which also shows the unit rotation chosen for the out-of-plane rotation.

The nominal stresses determined in chapter 4, can be used for the determination of the nominal stress intervals in the crossbeams “AA” and “BB”, using scale factors between the in-plane shear forces, bending moments and the out-of-plane rotations of the stiffener supports. Due attention must be paid to the position of the neutral axis for the whole crossbeam section and the T-beam and the geometry of the cut-outs (including cope holes).

9.12 Detailed analyses for Crossbeam type "AA"

9.12.1 Stresses due to crossbeam in-plane behaviour

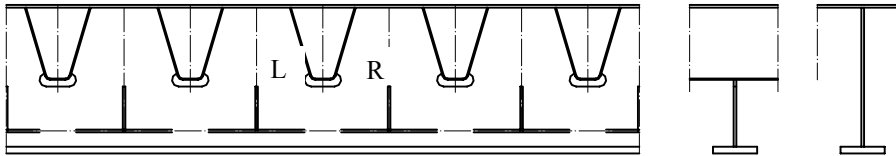


Fig. 9.8 Crossbeam type “AA” with Vierendeel system

Fig. 9.8 shows the crossbeam web with cope holes and the troughs with the locations L and R, which are susceptible to fatigue.

Fig. 9.9 shows the relative horizontal displacements of the locations S.4.2 due to crossbeam in-plane bending (Figs. 9.9a and 9.9b) and shear (Fig. 9.9c). The relative horizontal displacement is calculated for Crossbeam “AA” with the method described in 4.2.1.1 with:

$$\delta_h = \frac{M \cdot a_{cz}}{EI_{cut-out}} \cdot W \tag{4.25}$$

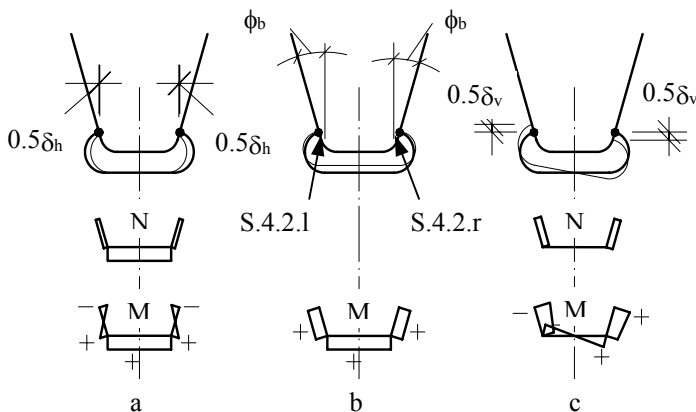


Fig. 9.9 Relative displacements of trough bottom connections

in which:

- M = bending moment in crossbeam
- W = cope hole width
- a_{cz} = distance from location S.4.2 to neutral axis
- I_{cut-out} = moment of inertia of crossbeam over cross section with cut-out

The relative displacements are shown in Table 9.11. The low values result from the position of the neutral axis and the smaller bending moment compared to the reference beam.

Table 9.11 Relative hor. displacements of S.4.2.1 and S.4.2.r

Lane	Displacement (mm)	
	Thick	Thin
1	$4.26 \cdot 10^{-8}$	$4.43 \cdot 10^{-8}$
2	$2.34 \cdot 10^{-8}$	$2.43 \cdot 10^{-8}$

Table 9.12 Nominal bending stresses in trough web at S.4.2.1 and S.4.2.r

Lane	Stress (N/mm ²)	
	Thick	Thin
1	0	0
2	0	0

Comparing these relative displacements to those, shown in Fig. 4.24, it is obvious that negligible stresses are generated here. Therefore, the stresses in the trough

web caused by horizontal displacements from crossbeam bending, shown in Table 9.12, are taken zero.

The rotations ϕ_l and ϕ_r can be calculated with equation [4.29] and are shown in Table 9.13:

$$\phi_l = -\phi_r = \frac{M \cdot W}{2E \cdot I_{cut-out}} \quad [4.29]$$

in which:

M = bending moment in crossbeam

W = width of cut-out (including cope hole)

$I_{cut-out}$ = moment of inertia of the crossbeam at the cut-out

Table 9.13 Rotations of S.4.2.1 and S.4.2.r

Lane	Rotation rad	
	Thick	Thin
1	$6.73 \cdot 10^{-6}$	$7.00 \cdot 10^{-6}$
2	$3.70 \cdot 10^{-6}$	$3.83 \cdot 10^{-6}$

Table 9.14 Nominal bending stresses in trough web at S.4.2.1 and S.4.2.r

Lane	Stress (N/mm ²)	
	Thick	Thin
1	0.4	0.4
2	0.2	0.2

The nominal stresses in Table 9.14 are derived from the relationship between the rotations and stresses shown in Figs. 4.27 and 4.28.

Due to the high stiffness of crossbeam “AA”, low values for the rotations and the stresses are found with respect to the reference crossbeams described in chapter 4. The stresses for crossbeam “AA” are negligible.

$$\delta_{vl} = -\delta_{vr} = \frac{S_v \cdot 0.5W}{G \cdot A_{T-beamweb}} + \frac{[S_h \cdot c_c \cdot l_{IV} + S_h \cdot (l_{IV} - d_c)] \cdot c \cdot (c_c \cdot l_{IV} - l_{IV} + d_c)}{2 \cdot 2 \cdot E \cdot I_{tooth}} \quad [4.33]$$

The relative vertical displacements of S.4.2.1 and S.4.2.r due to the shear forces are determined with the method described in 4.2.3.4. If the deflections due to the normal force on the tooth are ignored, only equation 4.33 has to be used:

in which:

W = width of cut-out (including cope hole)

c_c = centre-to-centre distance of troughs

l_{IV} = tooth length

c_c = correction factor for tooth length (see Table 4.2).

d_c = depth of cut-out (including cope hole)

See also Fig.9.5.

The following abbreviations also apply:

- S_v = Vertical shear force
- I_{tooth} = moment of inertia of the tooth
- $A_{(T-beamweb)}$ = area of T-beam
- δ_{vl} = vertical deformation of T-beam (left side)
- δ_{vr} = vertical deformation of T-beam (right side)

Table 9.15 Relative vertical displacements of S.4.2.1 and S.4.2.r

Lane	Displacement (mm)	
	Thick	Thin
1	0.143	0.149
2	0.078	0.081

Table 9.16 Nominal Bending stresses in trough web at S.4.2.1 and S.4.2.r

Lane	Stress (N/mm ²)	
	Thick	Thin
1	14	14
2	8	8

The displacements of S.4.2.1 and S.4.2.r are shown in Table 9.15 and the nominal bending stresses are shown in Table 9.16.

Table 9.17, Nominal stresses (N/mm²) in S.4.2.1 and S.4.2.r of stiffener 8 due to shear and bending in crossbeam

Load on	Crossbeam load transfer effect	Nominal stresses (N/mm ²)	
		Wearing course	
		Thick:	Thin:
Lane 1	Shear	14	14
	Bending	0	0
	SUM	14	14
Lane 2	Shear	8	8
	Bending	0	0
	SUM	8	8

When the nominal bending stresses at S.4.2 from crossbeam in-plane shear and bending are combined, the results shown in Table 9.17 are obtained.

The combined nominal stresses are used as a basis for the determination of the stresses perpendicular to the weld toe at other locations in the trough and in the crossbeam web locations C.4.2.1 and C.4.2.r with the stress concentration (relation) factors shown in Table 5.4.

Fig. 9.10 shows the location S.4.2 of the trough, together with the locations C.4.2 and C.4.3 where the stresses are calculated.

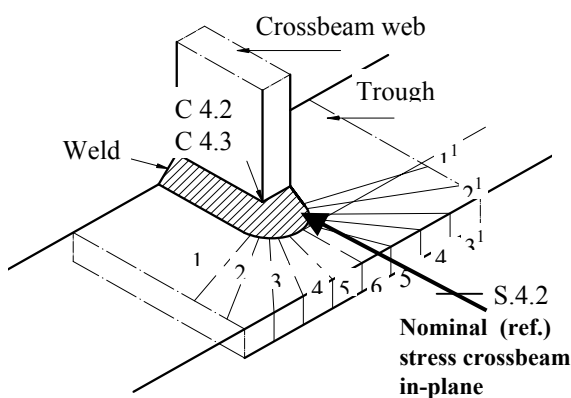


Fig. 9.10 Crossbeam in-plane stress relation factors

The calculated interval stresses for the concentrated stresses perpendicular to the weld toe are shown in Table 9.18. Here, the stresses are used without sign.

However, for the combination of the stresses from in-plane bending with those from in-plane shear, due attention must be paid to the respective signs of the stresses in relation to bending and shear deformation.

For the cope hole in the crossbeam web (location C.4.5), the nominal stresses could also be obtained by scaling the results from the crossbeam with $H = 1200$ mm, $W = 175$ mm in Fig. 4.38.

In crossbeam “AA”, a radius of 35 mm is used, which is in line with practical applications. This means that the geometrical stress concentration factor at the cope hole location C.4.5.s is 2.4 and the SCF at the cope hole location C.4.5.b is 2.7, as shown in chapter 5.

Table 9.18 Concentrated stress intervals due to traffic on Lane 1 and Lane 2 for a thick and a thin wearing course for crossbeam in-plane loading

Locations		Geometrical stress concentration (relation) factors	Concentrated stress intervals (N/mm ²)	
Edge B S.4.2 S.4.3	End of Radial Beam	σ_{nom} at trough web is nominal (reference) stress	Traffic on Lane 1	Traffic on Lane 2
	1	0.3	4	2
	2	0.4	6	3
	3	0.5	7	4
	4	0.7	10	6
	5	0.6	8	5
	6	0.6	8	5
Crossbeam web Locations C.4.2, C.4.3		0.3	4	2

When the stresses for the locations C.4.5 are calculated in accordance with the procedure in 4.2.4.1, the nominal stress intervals become as shown in Table 9.19 and the stress intervals including the stress concentration factors (SCF = 2.4 and 2.7 respectively) become as shown in Table 9.20. The stresses from the crossbeam in-plane bending are neglected as they turn out to be zero, due to the position of the neutral axis of the crossbeam.

As indicated in Tables 9.8 and 9.9, the stress intervals for crossbeams “AA” and “BB” for a deck with a thick and a thin wearing course have 64 cycles per 100 lorries.

Table 9.19 Nominal stresses at cope hole

Load on lane no..	Nominal stress (N/mm ²)	
	Thick and thin wearing course	
	Location C.4.5.s	Location C.4.5.b
1	136	7

Table 9.20 Concentrated stresses at cope hole

Load on lane no.	Concentrated stress (N/mm ²)	
	Thick and thin Wearing course	
	Location C.4.5.s	Location C.4.5.b
1	329	19
2	180	22

9.12.2 Stresses due to crossbeam out-of plane behaviour

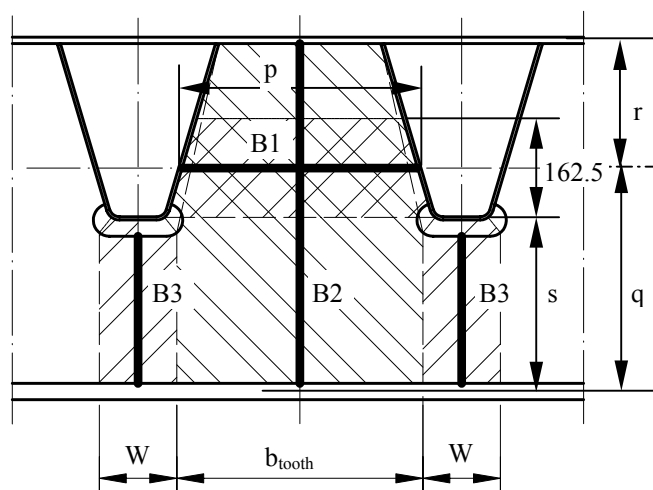


Fig. 9.11 Model for out-of-plane crossbeam behaviour

The nominal stress intervals can be calculated with the procedure described in 4.3. The model is shown in Fig. 9.11 and in more detail in Figs. 4.43 and 4.44.

The deflection of B1 due to a load P_{unity1} :	$\delta_h = \frac{r+q}{r} \cdot \frac{P_{unity1} \cdot r^3}{192 \cdot E \cdot I_{B2}}$	[4.45]
The clamping moment M_{cw} at the ends of B1:	$M_{cw} = \frac{r+q}{r} \cdot \frac{P_{unity1} \cdot p}{8}$	[4.46]
The reaction force P_t , assuming B2 temporarily clamped at the connection with B1:	$P_t = P_{unity1} \cdot \frac{q}{r}$	[4.47]
The deflection at the top δ_{ht} :	$\delta_{ht} = \frac{P_{unity1} \cdot q \cdot r^2}{3 \cdot E \cdot I_{B2}}$	[4.48]
The deflection at the bottom δ_{hb} :	$\delta_{hb} = \frac{P_{unity1} \cdot q^3}{3 \cdot E \cdot I_{B2}}$	[4.49]
The total deflection:	$\delta_{hB1B2} = \frac{q+r}{r} \cdot \delta_h + \frac{q}{r} \cdot \delta_{ht} + \delta_{hb}$	[4.50]
The spring constant K_{B1B2} :	$K_{B1B2} = \frac{P_{unity1}}{\delta_{hB1B2}}$	[4.51]
The deflection at the bottom δ_{hb3} , due to a load P_{unity2} :	$\delta_{hb3} = \frac{P_{unity2} \cdot s^3}{3 \cdot E \cdot I_{B3}}$	[4.52]
The clamping moment M_{cb} at the trough bottom is:	$M_{cb} = P_{unity2} \cdot s$	[4.53]
The spring constant K_{B3} :	$K_{B3} = \frac{P_{unity2}}{\delta_{hb3}}$	[4.54]

The dimensions of the crossbeam web are similar to the crossbeams analysed in chapter 4, thus as an alternative to the calculation above, the nominal stresses for $H = 1200$ mm, $W = 175$ mm in Figs. 4.46 and 4.48 can be used. They must be scaled with a factor 1.81/10 for a thick wearing course and with a factor 2.62/10 for a thin wearing course (for actual rotation interval/rotation interval of reference crossbeams, see Tables 9.9 and 9.10).

Table 9.21 Nominal stress intervals (N/mm^2) and cycles c per 100 lorries

Load on Lane 1	Nominal stress intervals (N/mm^2) /cycles	
	Wearing course	
	Thick	Thin
Stresses in crossbeam web Location S.4.2	4/ 39c	6/ 57c
Stresses in cut-out Location C.4.5	5/ 39c	8/ 57c

The stress intervals and the numbers of cycles per 100 lorries are shown in Table 9.21. When the geometrical stress concentration (relation) factors, given in Table 5.5 are used, the concentrated stress intervals for the locations shown in Fig. 9.12 become as shown in Table 9.22.

Trough number 8 is not directly situated under Lane 1. However, in order to analyse a most adverse situation, it is treated as if it were, so the stresses generated by the rotations of the connections due to loads on Lane 1 are used.

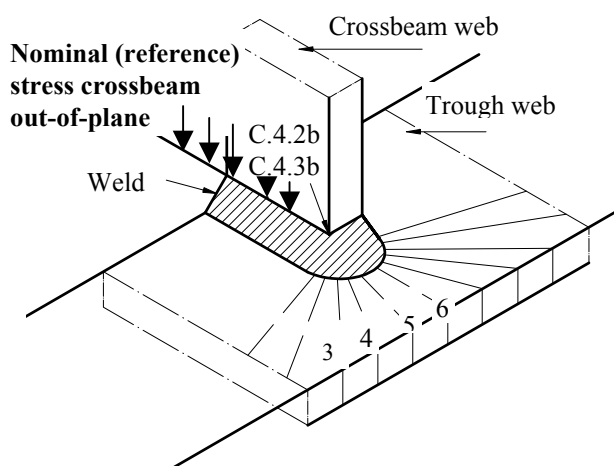


Fig. 9.12 Locations at stiffener to crossbeam connection for stress relation factors.

Table 9.22 Concentrated stress intervals (N/mm^2) from out-of-plane rotations and cycles c per 100 lorries

Load on Lane No.	Loc. (radial beam)	SCF	Wearing course	
			Thick	Thin
1	3	1.2	5/39c	7/66c
	4	0.9	4/39c	5/66c
	5	0.5	2/39c	3/66c
	6	0.	0	0
	Web C.4.2	4.7	19/39c	28 /66c
	Cut-out C.4.5.s	1.3	11/ 39c	18 /66c

9.12.3 Stresses in deck stiffeners due to deck bending

Table 9.23 Nominal stress intervals (N/mm^2) in the stiffener (Connection position = position of S.4.2)

Lane	Nominal stress intervals (N/mm^2)			
	Wearing course			
	Thick		Thin	
	Trough Bottom	Connection level	Trough Bottom	Connection level
1	37	34	57	49

The nominal stresses in the trough bottom can be calculated from the bending moment interval in the traffic lane given in Table 9.9, namely 115 kNm for a thick and 108 kNm for a thin wearing course respectively and the section properties given in 9.6.2 and 9.6.3. The stress intervals are shown in Table 9.23.

9.12.4 Combination of stresses

For each location of the connection of trough 8 to the crossbeam web, the stress intervals caused by in-plane loads are increased by half the stress intervals caused by the out-of-plane rotations (modified in-plane stress intervals) as described in 8.4.2.

The following stress intervals are used for damage calculations of crossbeam web locations:

1. (Modified) Stress interval for in-plane behaviour due to Lorries on Lane 1 only
2. (Modified) Stress interval for in plane behaviour due to lorries on Lane 1 and Lane 2
3. Stress interval for out-of-plane behaviour due to lorries on Lane 1

Table 9.24 shows a complete overview of the stresses in the crossbeam and in the stiffener near the crossbeam generated by the crossbeam behaviour.

Table 9.24 Concentrated stress intervals (N/mm²) in stiffener 8 and crossbeam

	Thick wearing course			Thin wearing course		
	Modified in-plane stress intervals		Out-of-plane stress intervals	Modified in-plane stress intervals		Out-of-plane Stress interval
Traffic on Lane no.	1	1 + 2	1	1	1 + 2	1
Stiffener location S.4.2 Edge B Radial beam end						
3	10	14	5	11	15	7
4	12	18	4	13	19	5
5	9	15	2	10	15	3
6	8	13	0	8	13	0
Web location C.4.2	14	16	19	18	20	28
Cut-out location C.4.5	335	515	11	338	518	18
Stiffener location	34			49		

9.12.5 Fatigue assessments

With the stresses shown in Table 9.24, the fatigue assessments for the locations at and in the vicinity of Trough 8 can be carried out. For each location, the fatigue detail class $\Delta\sigma_C$ and the appropriate partial factor γ_{Mf} are used; the fatigue class reduced by γ_{Mf} is indicated with $\Delta\sigma_{Cr}$, the reduced constant amplitude fatigue strength with $\Delta\sigma_{Dr}$ and the reduced cut-off limit with $\Delta\sigma_{Lr}$. Only calculations for a “thin” wearing course are made, as these stresses are near to, but somewhat higher than those for a “thick” wearing course.

Fig. 9.13 shows the relevant locations of the detail for a continuous closed stiffener to crossbeam connection in Crossbeam “AA”.

Location S4.2 (lower end of weld)

Class 100 (geometric), $\gamma_{Mf} = 1.0$: $\Delta\sigma_{Cr} = 100$, $\Delta\sigma_{Dr} = 73$ ($N = 5 \cdot 10^6$), $\Delta\sigma_{Lr} = 41$ ($N = 1 \cdot 10^8$)

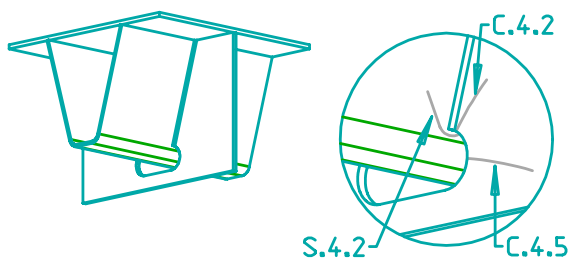


Fig. 9.13 Closed stiffener through crossbeam with oval cope hole

For location S.4.2 near the bottom of the connection, the maximum concentrated stress interval (modified in-plane and out-of-plane) in relation to FLM2 for a thin wearing course is 19 N/mm² (See Table 9.24), which is far below $\Delta\sigma_{Dr}$, being 73 N/mm². It can be concluded that no damage is to be expected.

Expectations for other crossbeam depths

The stress intervals due to in-plane behaviour were determined with influence lines for $H = 1400$ mm and $H = 1800$ mm, with $\Delta P_{C3V} = 259$ kN and 270 kN.

Ignoring the fact that shallow crossbeams with $H = 600$ mm have smaller load intervals (see chapter 6), it can be derived from Fig. 4.32 that the stresses due to in-plane behaviour are 2.1 times larger than in a crossbeam with $H = 1400$ mm, so the maximum sum of the stresses in Table 9.18 (Radial beam 4) becomes: $2.1 \times (10 + 6) = 34$ N/mm²

For shallow crossbeams with a depth of $H = 600$ mm, $\Delta\phi_3 = 2.05$ mrad (see Fig. 6.23), which is 1.6 times higher than the rotation for a crossbeam with $H = 1400$ mm. It can also be concluded from Fig. 4.46, that the stresses are approximately 2.7 times higher in the shallow crossbeam. The maximum stress interval (see Table 9.22, Radial beam 4) due to out-of-plane behaviour becomes now: $2.7 \times 1.6 \times 5 = 22$ N/mm². The maximum modified in-plane stress interval becomes 45 N/mm², which is still below $\Delta\sigma_{Dr}$ and results in an unlimited fatigue life.

For deeper crossbeam webs, smaller stresses will be found.

Location S4.2 (vertical weld)

Class 80 (nominal), $\gamma_{Mf} = 1.0$: $\Delta\sigma_{Cr} = 80$, $\Delta\sigma_{Dr} = 59$ ($N = 5 \cdot 10^6$), $\Delta\sigma_{Lr} = 32$ ($N = 1 \cdot 10^8$)

For location S.4.2 near the vertical weld of the connection, the maximum nominal stress interval due to FLM2 for a thin wearing course is 49 N/mm² (See Table 9.23), which is below $\Delta\sigma_{Dr} = 59$ N/mm². It can be concluded that no damage is to be expected.

Expectations for other crossbeam depths

The stress intervals due to the deck bending were determined with influence lines for $H = 1400$ mm and $H = 1800$, resulting from $\Delta M_{D3} = 115$ kNm and 108 kNm.

All shallower crossbeams have much higher bending moment intervals (1.3 – 1.5 times), which will result in short design lives.

Location C4.2

Class 100 (geometric), $\gamma_{Mf} = 1.0$: $\Delta\sigma_{Cr} = 100$, $\Delta\sigma_{Dr} = 73$ ($N = 5 \cdot 10^6$), $\Delta\sigma_{Lr} = 41$ ($N = 1 \cdot 10^8$)

For location C.4.2, the maximum stress intervals in relation to FLM2 for a thin wearing course is shown in Table 9.24 and is 28 N/mm² (in-plane and out-of-plane), which is far below $\Delta\sigma_{Dr}$, being 73 N/mm². No damage is to be expected.

Expectations for other crossbeam depths

The stress intervals due to in-plane behaviour were determined with influence lines for $H = 1400$ mm and $H = 1800$ mm, with $\Delta P_{C3V} = 259$ kN and 270 kN.

Ignoring the fact that shallow crossbeams with $H = 600$ mm have smaller load intervals (see chapter 6), it can be derived from Fig. 4.32 that the stresses due to in-plane behaviour are 2.1 times larger than in a crossbeam with $H = 1400$ mm, so the maximum sum of the stresses in Table 9.18 (Radial beam 4) becomes: $2.1 \times (4 + 2) = 13$ N/mm²

For shallow crossbeams with $H = 600$ mm, $\Delta\phi_3 = 2.05$ mrad (see Fig. 6.23). This is 1.6 times higher than the rotation in a crossbeam with $H = 1400$ mm. It can also be concluded from Fig. 4.46, that the stresses are approximately 2.7 times higher in the shallow crossbeam.

The maximum stress interval (see Table 9.22, Radial beam 4) for a thick wearing course due to out-of-plane behaviour becomes: $2.7 \times 1.6 \times 19 = 82$ N/mm² and $2.7 \times 1.6 \times 28 = 121$ N/mm² for a thin wearing course.

The maximum modified in-plane stress interval for a thin wearing course becomes: 74 N/mm² and the out-of-plane stress interval 121 N/mm², both above $\Delta\sigma_{Dr}$, and making a damage calculation necessary.

For shallow crossbeams with $H = 800$ mm, $\Delta\phi_3 = 1.39$ mrad (see Fig. 6.23); this is 1.2 times higher than the rotation in a crossbeam with $H = 1400$ mm. It can also be concluded from Fig. 4.46, that the stresses are approximately 1.8 times higher in the shallow crossbeam. The maximum stress intervals (see Table 9.22, Radial beam 4) for a thick wearing course due to out-of-plane behaviour become: $1.8 \times 1.2 \times 19 = 41$ N/mm² and $1.8 \times 1.2 \times 28 = 60$ N/mm² for a thin wearing course.

The maximum modified in-plane stress interval for a thick wearing course becomes: $1.4 \times (4 + 2) + 21 = 29$ N/mm² and $1.4 \times (4 + 2) + 30 = 38$ N/mm² for a thin wearing course. For a thick wearing course the out-of-plane stress interval is 41 N/mm² and for a thin wearing course the stress interval is 60 N/mm², which are both below $\Delta\sigma_{Dr}$ and result in an unlimited fatigue life.

The minimum depth for an unlimited fatigue life is 800 mm.

Location C4.5.s (at narrowest part of tooth)

Class 140 (geometric), $\gamma_{Mf} = 1.15$: $\Delta\sigma_{Cr} = 122$, $\Delta\sigma_{Dr} = 90$ (N = $5 \cdot 10^6$), $\Delta\sigma_{Lr} = 49$ (N = $1 \cdot 10^8$)

Table 9.25 Fatigue life Fatigue life calculation procedure for location C.4.5

Wearing course "thick" or "thin"							
Load on	FLM2			FLM4			n _c
	Mode	$\Delta\sigma_{max2}$	$\Delta\sigma_{max} < \Delta\sigma_{Dr}$?	$\Delta\sigma_{max4}$	$\Delta\sigma_{max} < \Delta\sigma_{Lr}$?	n	
Lane 1	In-plane	338	N	270	N	0.6 x 0.64x 8000x250x25	9.62 x n = 1.85x10 ⁸
	Out-of-plane	18	Y	14	Y	0	0
Lane 1 and Lane 2	In-plane	518	N	414	N	0.2x 0.64x8000x250x25	39.1 x n = 2.50 x 10 ⁸
Σn_c							4.35 x 10 ⁸
Fatigue life (years) L1 + L2 (L1 only)							0.11 (0.16)

The resulting fatigue life is extremely short and does not reflect practical experience

Observations:

As usual, the restraining effect of the deck stiffness is ignored for the Vierendeel model used for the in-plane load transfer and the determination of the stress intervals, .

The fatigue detail classifications used, are meant for design purposes and for damage calculations to compare fatigue damage in practice.

9.12.6 Additional analyses for the fatigue location C.4.5.s.

Appendix 1 describes additional analyses of the influences of the deck restraint (deck bending stiffness and trough torsion), fatigue detail classification and traffic loads (measured traffic vs. traffic in EN 1991-2).

Deck restraint effect on the in-plane behaviour

Additional analyses of the deck restraint on the in-plane behaviour are described Appendix 1, paragraphs A1.2.1 – A1.3.3, A1.3.6 and A1.6, a summary of the results is shown in Table 9.26.

Table 9.26 Fatigue design lives in years (y) without and with deck restraint effect (for EN 1991-2 lorries)

Oval cope hole, thin wearing course, Location C.4.5.s, $t_w = 10$ mm						
	Par. 9.12.5		Effective restraining width b_{eff} (mm)			
			4000		6000	
	L1+L 2	L1	L1 + L2	L1	L1 + L2	L1
Fatigue life (y)	0.11	0.16	0.28	0.37	0.50	0.63
Haibach cope hole, thin wearing course, Location C.4.5.s, $t_w = 10$ mm						
	Par. 9.12.5		Effective restraining width b_{eff} (mm)			
			4000		6000	
			L1 + L2	L1	L1 + L2	L1
Fatigue life (y)	No results		0.92	1.18	1.60	2.03

in which:

- L1+L2: Simultaneous lorries on Lane 1 and Lane 2
- L1: Lorries on Lane 1 only
- t_w : Crossbeam web thickness
- b_{eff} : Effective width of the deck bending restraint

Table 9.26 shows, that the deck restraint gives a fatigue life extension with a factor between 2.3 and 4.5 respectively. In addition to the details analysed before, the effect of the use of a Haibach cope hole is analysed, which gives a fatigue life extension with a factor of 3.2, when compared to the oval cope hole

Detail classification

Additional analyses of the effect of the fatigue detail classification are described Appendix 1, paragraph A1.4.

If the mean detail classification is used for the calculations, the γ_{Mf} of 1.15 is disregarded, the detail classification $\Delta\sigma_C = 210$ N/mm². The calculation allows comparison with observed damages in practice.

Table 9.27 Fatigue life in years for FLM4 and “mean” detail classification, including the deck restraint effect

“Mean” fatigue classification (N/mm ²)	b _{eff} (mm)	Oval cope hole	Haibach cope hole
210	4000	1.3	2.8
	6000	1.9	8.6

Table 9.27 shows the fatigue life in years for FLM4 on L1 + L2 with a “mean” detail classification and including the deck restraint effect.

Traffic

Additional analyses of the axle loads are described in Appendix 1, paragraphs A1.4 and A1.6..

Comparison of traffic measurements on the Moerdijk Bridge in 1998, Nieuwsma (1998), with FLM4 of EN 1991-2 showed a larger fraction of lower axle loads on the Moerdijk Bridge than given in FLM4.

Further, due to the development of the traffic volume, 30 years of service correspond with approximately 24 “traffic” years of Moerdijk 1998 for heavily trafficked bridges and 12 years for many other bridges in the Netherlands.

Table 9.28 Fatigue life in service years for Moerdijk 1998 traffic and “mean” detail classification

“Mean” fatigue classification (N/mm ²)	b _{eff} (mm)	Oval cope hole	Haibach cope hole
210	4000	15	58
	6000	28	625

Table 9.28 shows the fatigue life in service years for Moerdijk 1998 traffic on L1 + L2, including the deck restraint effect and the “mean” detail classification.

Effects not quantifiable

The fatigue lives are based on equivalent numbers of lorries determined with a S- N line with a continuous inverse log – log slope with m = 3, which overestimates the damage effect for the lower axle loads.

9.12.7 Conclusions and observations for Crossbeam type “AA”

The locations S.4.2 and C.4.2 show an infinite fatigue life, but for other crossbeam depths, restrictions apply.

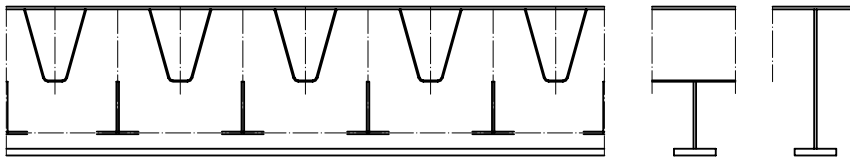
As shown in more detail in Appendix 1, location C.4.5.s shows realistic fatigue lives if:

- 1.The deck restraint is applied for the in-plane crossbeam behaviour
- 2.The “mean” detail classification is used
- 3.The lorry loads are modified in line with the Moerdijk 1998 traffic.

9.13 Detail analyses for Crossbeam type "BB"

9.13.1 Stresses due to crossbeam in-plane behaviour

The crossbeam type "BB" is part of an orthotropic deck with continuous trough stiffeners. Each trough passes through a close fitting hole in the crossbeam (see Fig. 9.14).



Analogous with chapter 4, the equilibrium of a part of the crossbeam comprising one tooth and adjacent reversed T-beams, as shown in Fig. 9.5, is calculated.

Fig.9.14 Crossbeam type "BB" with Vierendeel system

From the vertical shear force intervals ΔS in Table 9.9, the horizontal force ΔS_h at the top of the tooth can be calculated. With these forces, the secondary bending moments and the nominal stress intervals for the crossbeam in-plane behaviour are calculated with the procedures described in 4.2.4.2.

The nominal stress intervals in the trough web and bottom due to normal forces and in-plane bending are calculated with the procedures given in 4.2.1.3.

As described in 5.3.4.1, the geometrical stress concentration factors (SCF) at the tooth of the crossbeam web, can be calculated with Roark & Young (1986). For the tooth at location C.4.1.w (see Fig. 4.35), the SCF = 1.7 and for the crossbeam web at location C.4.1.b (see Fig. 4.35), the SCF = 3.1. In chapter 7, the results of this calculation procedure with these factors were compared to FE calculations and measurements and proved to be very conservative.

The stresses in the crossbeam web perpendicular to the weld at the trough web (C.4.1.w) and the trough bottom (C.4.1.b) locations are calculated with:

$$\sigma_{wr} = \frac{SCF \cdot \sigma_s \cdot t_i \cdot 1.56 \cdot \sqrt{r_i \cdot t_i}}{r_c \cdot t_{tw}} \quad [4.44]$$

The stress concentrations occur due to the curvature of the tooth and increase the stresses parallel to the weld. The stresses used for the fatigue analyses however are perpendicular to the weld and a nominal fatigue classification is used.

Table 9.29 Stress intervals (N/mm²) at C.4.1b parallel to the weld toe due to crossbeam bending

Traffic load on	Nominal stresses (N/mm ²)		Geometrical stresses (N/mm ²)	
	Thick	Thin	Thick	Thin
Lane 1	2	2	6	6
Lane 2	1	1	3	3

Table 9.29 shows the nominal and geometrical stress intervals parallel to the weld toe for a deck with a thick and a thin wearing course respectively due to crossbeam bending.

Table 9.30 Stress intervals (N/mm²) at C.4.1.b parallel to the weld toe due to secondary bending in the T-beams

Traffic load on	Nominal stresses (N/mm ²)		Geometrical stresses (N/mm ²)	
	Thick	Thin	Thick	Thin
Lane 1	5	5	9	10
Lane 2	3	3	5	6

Table 9.30 shows the stress intervals at location C.4.1.b, due to secondary bending moments in the T-beam.

Table 9.31 Stress intervals (N/mm²) at C.4.1.w, parallel to the weld toe due to secondary bending of the tooth

Traffic load on	Nominal stresses (N/mm ²)		Geometrical stresses (N/mm ²)	
	Thick	Thin	Thick	Thin
Lane 1	2	2	6	6
Lane 2	1	1	3	3

Table 9.31 shows stress intervals parallel to the weld toe, in the location C.4.1.w, due to secondary bending moments in the tooth.

Table 9.32 Geometrical stresses (N/mm²) perpendicular to the weld toe due to in-plane bending and shear

Traffic load on	Geometrical stresses (N/mm ²)			
	C.4.1.b		C.4.1.w	
	Thick	Thin	Thick	Thin
Lane 1	15	16	163	170
Lane 2	8	9	90	94

The stress intervals at C.4.1.b (see Fig. 4.35) due to crossbeam bending and secondary bending can be added, as, for a considered location, the stresses always have the same sign. From the resulting stress intervals parallel to the weld toe, the stress intervals perpendicular to the weld toe can be calculated with the procedure described in 4.2.4.2.

Table 9.32 shows the geometrical stress intervals perpendicular to the weld toe at the locations C.4.1b and C.4.1w, due to in-plane bending and shear.

9.13.2 Stresses due to crossbeam out-of plane behaviour

The nominal stress intervals can be calculated with the procedure described in 4.3.1 and 9.12.2. The model is shown in Fig. 9.11 and more in detail in Figs. 4.43 and 4.44. The nominal stresses at the locations C.4.1.b and C.4.1.w can also be derived from the stresses in Fig. 4.46 by scaling. The scaling factor takes into account the applied rotation angle, which was 10 mrad in the crossbeams analysed in chapter 4 but for the crossbeam analysed here, is 1.81 mrad for a deck with a thick and 2.62 mrad for a thin wearing course, as shown in Table 9.9

Table 9.33 Nominal stress intervals (N/mm²), perpendicular to the weld toe due to out-of-plane rotation

Deck	Ch4	Thick	Thin
Rotation angle	10 mrad	1.81 mrad	2.62 mrad
Location	Nominal stress intervals (N/mm ²)		
C.4.1.b	24	4	6
C.4.1.w	50	9	13

Table 9.34 Concentrated stress intervals (N/mm²), perpendicular to the weld toe due to out-of-plane rotation

Deck	Thick	Thin
Rotation angle	1.81 mrad	2.62 mrad
Location	Concentrated stress intervals (N/mm ²)	
C.4.1.b	6	10
C.4.1.w	9	13

Table 9.33 shows the nominal stress intervals perpendicular to the weld toe at the locations C.4.1.b and C.4.1.w, due to out-of-plane rotation of the trough to crossbeam connection for a deck with a thick and a thin wearing course respectively, together with the nominal stresses calculated in 4.3.4.1, for a rotation of 10 mrad.

The geometrical stress concentration factors described in 5.3.4.2 are used to obtain the geometric stress intervals.

Table 9.34 shows the geometrical stress intervals perpendicular to the weld toe at the locations C.4.1.b and C.4.1.w, due to out-of-plane rotation of the trough to crossbeam connection for a deck with a thick and a thin wearing course respectively.

9.13.3 Bending of the deck

Table 9.35 Nominal stress intervals (N/mm²) perpendicular to the weld toe due to the deck bending moment

Wearing course	Thick	Thin
Bending moment	115 kNm	108 kNm
Location	Nominal stress intervals (N/mm ²)	
S.4.1.b (bottom)	37	57
S.4.1w (near C.4.1.w)	34	49

The bending moment intervals are taken from Table 9.8 and are 115 kNm for a deck with a thick wearing course and 108 kNm for a deck with a thin wearing course.

Table 9.35 shows the nominal stress intervals perpendicular to the weld toe at the locations S.4.1b and S.4.1w, due to the deck bending moment at the trough to crossbeam connection for a deck with a thick and a thin wearing course respectively.

9.13.4 Combination of stresses

For the stiffener to crossbeam connection, the stress intervals caused by the in-plane behaviour shown in Table 9.32 are enlarged by half the stress intervals caused by the out-of-plane behaviour as shown in Table 9.34.

The following stress intervals are used for damage calculations of crossbeam web locations:

1. (Modified) Stress interval for in-plane behaviour due to Lorries on Lane 1 only
2. (Modified) Stress interval for in plane behaviour due to lorries on Lane 1 and Lane 2
3. Stress interval for out-of-plane behaviour due to lorries on Lane 1

Table 9.36 shows an overview of all stresses in the crossbeam and in the neighbourhood of the crossbeam generated by the crossbeam behaviour for a deck with a thick and with a thin wearing course. These stresses should be used for the fatigue assessment.

The origin of the stress is indicated with the loads on Lane 1 and Lane 2 together with the load transfer through the crossbeam, in-plane and out-of-plane.

The in-plane behaviour of the crossbeam is considered not to generate stresses in the trough web. The out-of-plane behaviour will not affect the trough web as the fillet welds together with the crossbeam web and the stiffener web prevent the local bending stresses occurring.

Table 9.36. Geometrical stress intervals (N/mm²) for specified stiffener and crossbeam locations

	Thick wearing course			Thin wearing course		
	Modified in-plane stress intervals		Out-of-plane stress intervals	Modified in-plane stress intervals		Out-of-plane stress intervals
Traffic on lane no.	1	1 + 2	1	1	1 + 2	1
Stiffener location S.4.1b	37	-	-	57	-	-
Stiffener location S.4.1w	34	-	-	49	-	-
Crossbeam location C.4.1b	18	26	6	21	31	10
Crossbeam location C.4.1.w	168	258	9	177	271	13

9.13.5 Fatigue assessment

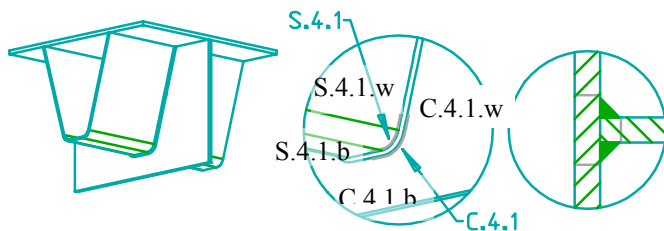


Fig. 9.15 Continuous closed stiffener through crossbeam with a close fit

Fig. 9.15 shows the locations for the fatigue assessment with a distinction between locations at the upper ends of the trough bottom curvature S.4.1.w and C.4.1.w, and locations at the lower end of the trough bottom curvature S.4.1.b and C.4.1.b.

For each location, the fatigue detail class and the appropriate partial factor γ_{Mf} are used; the reduced fatigue class is indicated with $\Delta\sigma_{Cr}$, the reduced constant amplitude fatigue strength with $\Delta\sigma_{Dr}$ and the reduced cut-off limit with $\Delta\sigma_{Lr}$.

Location S.4.1.b and S.4.1.w

Class 80 (nominal), $\gamma_{Mf} = 1.0$: $\Delta\sigma_{Cr} = 80$, $\Delta\sigma_{Dr} = 59$ (N=5.10⁶), $\Delta\sigma_{Lr} = 32$ (N=1.10⁸)

For locations S.4.1.b and S.4.1.w, the maximum stress interval in relation to FLM2 for a thin wearing course shown in Table 9.36 is 57 N/mm², which is below $\Delta\sigma_{Dr}$, being 59 N/mm². Hence, no damage is to be expected.

Expectations for other crossbeam depths

The stress intervals due to the deck bending were determined with $\Delta M_{D3} = 115$ kNm and 108 kNm for influence lines related to $H = 1400$ mm and $H = 1800$ respectively.

For shallower crossbeams with $H = 1000$ mm, $\Delta M_{D3} = 167$ kNm (see Fig. 6.26) which is approximately 1.5 times higher than 115 kNm. Based on Table 9.35, the stress interval for a deck with a thick wearing course will never be larger than 56 N/mm^2 (1.5×36), which is still below $\Delta \sigma_{Dr}$ at 59 N/mm^2 .

For a deck with a thin wearing course, however, the stress interval becomes 86 N/mm^2 , which is larger than 59 N/mm^2 . For FLM4 the maximum stress interval becomes $0.8 \cdot 86 = 68 \text{ N/mm}^2$ and the fatigue life becomes 3.9 years.

Conclusion: With a thick wearing course shallow crossbeams ($H = 600$ mm) can be used, but with a thin wearing course the fatigue life is extremely short and in this case shallow crossbeams have no practical use.

Location C.4.1

Class 80 (nominal), $\gamma_{Mf} = 1.15$: $\Delta \sigma_{Cr} = 70$, $\Delta \sigma_{Dr} = 52$ ($N=5 \cdot 10^6$), $\Delta \sigma_{Lr} = 28$ ($N=5 \cdot 10^8$)

For location C.4.1.b, the maximum stress interval in relation to FLM2 for a thin wearing course shown in Table 9.36 is 31 N/mm^2 , which is far below $\Delta \sigma_{Dr}$ at 52 N/mm^2 . Hence, no damage is to be expected.

Expectations for other crossbeam depths

The stress intervals due to the in-plane behaviour were determined with $\Delta P_{C3V} = 259$ kN and 270 kN resulting from influence lines for $H = 1400$ mm and $H = 1800$ mm respectively.

For crossbeams of infinite rigidity, $\Delta P_{C3V} = 332$ kN (see Fig. 6.20), which is 1.3 times higher than 259 kN and results in a stress interval for decks with a thin wearing course of 40 N/mm^2 for lorries simultaneously on Lane 1 and Lane 2.

For decks with a thick wearing course the stress interval becomes: 34 N/mm^2 .

The stress intervals due to out-of-plane behaviour were determined with an influence line for $H = 1400$ mm, resulting from $\Delta \phi_3 = 1.13$ mrad. For shallow crossbeams with $H = 600$ mm, $\Delta \phi_3 = 2.05$ mrad (see Fig. 6.23), which is 1.8 times higher and results in a stress interval of 11 N/mm^2 for decks with a thick wearing course and 18 N/mm^2 for decks with thin wearing course.

The modified in-plane stress interval for a deck with a thick wearing course will never be higher than 45 N/mm^2 and the out-of-plane stress interval will always be smaller than 11 N/mm^2 .

The modified in-plane stress interval for a deck with a thin wearing course will never be higher than 49 N/mm^2 and the out-of-plane stress interval will always be smaller than 11 N/mm^2 .

These stresses are below $\Delta \sigma_{Dr}$, and will result in an unlimited fatigue life.

Tables 9.37 and 9.38 show the assessment procedure for the cut-out location C.4.1.w, which is similar to the procedure described in 8.4.2.

Table 9.37 Fatigue life calculation procedure for location C.4.1.w

Wearing course "thick"							
Load on	FLM2			FLM4			n _c
	Mode	$\Delta\sigma_{\max 2}$	$\Delta\sigma_{\max} < \Delta\sigma_{Dr} ?$	$\Delta\sigma_{\max 4}$	$\Delta\sigma_{\max} < \Delta\sigma_{Lr} ?$	n	
Lane 1	In-plane	168	N	134	N	0.6x0.64x8000x250x25	7.0x n = 1.35x10 ⁸
	Out-of-plane	9	Y	7	Y	0	0
Lane 1 and Lane 2	In-plane	258	N	206	N	0.2x0.64x8000x250x25	25.6x n = 1.6x10 ⁸
Σn_c							3.0 x10 ⁸
Fatigue life (Years) L1 + L2 (L1 only)							0.17 (0.23)

Table 9.38 Fatigue life calculation procedure for location C.4.1.w

Wearing course "thin"							
Load on	FLM2			FLM4			n _c
	Mode	$\Delta\sigma_{\max 2}$	$\Delta\sigma_{\max} < \Delta\sigma_{Dr} ?$	$\Delta\sigma_{\max 4}$	$\Delta\sigma_{\max} < \Delta\sigma_{Lr} ?$	n	
Lane 1	In-plane	177	Y	142	N	0.6x0.64x8000x250x25	8.3xn = 1.60x10 ⁸
	Out-of-plane	13	N	10	Y	0	0
Lane 1 and Lane 2	In-plane	271	Y	217	N	0.2x0.64x8000x250x25	29.8xn = 1.91x10 ⁸
Σn_c							3.51x10 ⁸
Fatigue life (Years) L1 + L2 (L1 only)							0.14 (0.19)

The resulting fatigue life is extremely short and does not reflect practical experience.

Observations:

As usual, the restraining effect of the deck stiffness is ignored for the Vierendeel model used for the in-plane load transfer and the determination of the stress intervals.

The fatigue detail classifications used, are meant for design purposes and for damage calculations to compare fatigue damage in practice.

9.13.6 Additional analyses for the fatigue location C.4.1.w

Appendix 1 describes additional analyses of the influences of the deck restraint (deck bending stiffness and trough torsion), fatigue detail classification and traffic loads (measured traffic vs. traffic in EN 1991-2).

Deck restraint effect on the in-plane behaviour

Additional analyses of the deck restraint on the in-plane behaviour are described Appendix 1, paragraphs A1.2.1 – A1.3.3, A1.3.6 and A1.6, a summary of the results is shown in Table 9.39.

Table 9.39 Fatigue design lives in years (y) without and with deck restraint effect (for EN 1991-2 lorries)

Thick wearing course, Location C.4.1.w, $t_w = 10$ mm						
	Par. 9.13.5		Effective restraining width b_{eff} (mm)			
			4000		6000	
	L1+L 2	L1	L1 + L2	L1	L1 + L2	L1
Fatigue life (y)	0.17	0.23	0.43	0.57	0.78	1.01
Thin wearing course, Location C.4.1.w, $t_w = 10$ mm						
	Par. 9.13.5		Effective restraining width b_{eff} (mm)			
			4000		6000	
	L1+L 2	L1	L1 + L2	L1	L1 + L2	L1
Fatigue life (y)	0.14	0.19	0.37	0.49	0.65	0.85

in which:

- L1+ L2: Simultaneous lorries on Lane 1 and Lane 2
- L1: Lorries on Lane 1 only
- t_w : Crossbeam web thickness
- b_{eff} : Effective width of the deck bending restraint

Table 9.39 shows, that the deck restraint gives a fatigue life extension with a factor between 2.5 and 4.6

Detail classification

Additional analyses of the effect of the fatigue detail classification are described Appendix 1, paragraphs A1.4 and A1.6.

If the mean detail classification is used for the calculations, the γ_{Mf} of 1.15 is disregarded, the detail classification $\Delta\sigma_C = 210$ N/mm². The calculation allows comparison with observed damages in practice.

Considering that the stress intervals due to FLM4 have the same relationship to the stress interval of the fatigue classification as for the oval cope hole, the fatigue lives will be within the same range.

Traffic

Comparison of traffic measurements on the Moerdijk Bridge in 1998, Nieuwsma (1998), with FLM4 of EN 1991-2 shows a larger proportion of lower axle loads on the Moerdijk Bridge than given in FLM4. Also, due to the increase in the volume of traffic, 30 years of service correspond with approximately 24 “traffic” years of Moerdijk 1998 for heavily trafficked bridges and 12 years for many other bridges in the Netherlands.

Location C.4.1.w will show realistic fatigue lives if the deck restraint is applied for the in-plane crossbeam behaviour; the “mean” detail classification is used and the lorry loads are modified in line with the Moerdijk 1998 traffic, since the fatigue lives in table 9.39 are longer than those in Table 9.26 for C.4.1.s.

Effects not quantifiable

These fatigue lives are based on equivalent numbers of lorries determined with a S- N line with a continuous inverse log – log slope with $m = 3$, which overestimates the damage effect for the lower axle loads.

9.13.7 Conclusions and observations for Crossbeam type “BB”

The locations S.4.1 and C.4.1.b show an infinite fatigue life, but for other crossbeam depths, restrictions apply. Location C.4.1.w shows an extremely short fatigue life.

As shown in Appendix 1, location C.4.1.w will show realistic fatigue lives if:

- 1.The deck restraint is applied for the in-plane crossbeam behaviour
- 2.The “mean” detail classification is used
- 3.The lorry loads are modified in line with the Moerdijk 1998 traffic.

9.14 Detail analyses for Crossbeam type "CC"

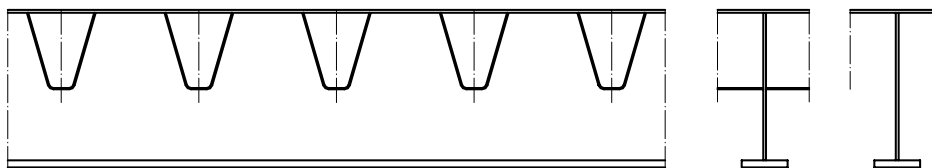


Fig. 9.16 shows the crossbeam type “CC”, with the trough stiffeners fitted between the crossbeams.

Fig. 9.16 Crossbeam type “CC” with troughs fitted between the crossbeams.

The stress intervals in the stiffeners and the crossbeam web at the locations S.3 and C.3 (see Figs. 1.11 and 8.4) can be calculated with the trough to crossbeam connection rotations and the deck bending moments given in Table 9.9.

9.14.1 Stresses due to crossbeam in-plane behaviour

Table 9.40 Nominal stress intervals (N/mm²) at C.3 due to global bending

Location	C.3.b		C.3.w	
	Thick	Thin	Thick	Thin
Wear course				
Traffic load on	Nominal stress intervals (N/mm ²)			
Lane 1	18	18	13	13
Lane 2	10	10	7	7

Table 9.40 shows the nominal stress intervals in the horizontal direction at the locations C.3.b (crossbeam at trough bottom) and C.3.w (crossbeam at upper end of the trough bottom curvature) due to the crossbeam bending moment intervals caused by the traffic loads on Lane 1 and Lane 2 for a deck with a thick and a thin wearing course respectively. These bending moment intervals 253 and 138 kNm respectively, act on the crossbeam at the location

of trough number 8.

9.14.2 Stresses due to crossbeam out-of plane behaviour

Table 9.41 Nominal stresses, perpendicular to the weld toe due to out-of-plane rotation

Deck	Ch4	Thick	Thin
Rotation angle	10 mrad	1.55 mrad	2.62 mrad
Location	Nominal stresses (N/mm ²)		
C.3.b	24	4	6
C.3.w	50	8	13

Table 9.41 shows the nominal stress intervals perpendicular to the weld toe at the locations C.3.b and C.3.w, due to an out-of-plane rotation of the trough to crossbeam connection for a deck with a thick and a thin wearing course respectively in relation to the nominal stresses shown in 4.3.4.1.

The nominal stresses at the locations C.3.b and C.3.w are derived from the stresses in Fig. 4.46 by scaling with a factor that takes into account the applied 10 mrad rotation angles in the crossbeams, analysed in chapter 4 and the rotation intervals of: 1.55 mrad for a deck with a thick and 2.62 mrad for a deck with a thin wearing course. (see also Table 9.9)

Table 9.42 Geometrical stresses perpendicular to the weld toe due to out-of-plane rotation

Wearing course	Thick	Thin
Rotation angle	155 mrad	2.62 mrad
Location	Geometrical stress intervals (N/mm ²)	
C.3.b	5	10
C.3.w	8	13

Table 9.42 shows the geometrical stress intervals perpendicular to the weld toe in the locations C.4.1b and C.4.1w, due to out-of-plane rotation of the trough to crossbeam connection for a deck with a thick and a thin wearing course respectively, based on the nominal stresses shown in 4.3.4.1

9.14.3 Bending of the deck

Table 9.43 Nominal stress intervals, perpendicular to the weld toe due to the deck bending moment

Wearing course	Thick	Thin
Deck bending moment	108 kNm	108 kNm
Location	Nominal stress intervals(N/mm ²)	
S.3b (bottom)	37	62
S.3w (near C.3w)	34	53

Table 9.43 shows the nominal stress intervals perpendicular to the weld toe at the locations S.3.b and S.3.w, due to the deck bending moment interval at the trough to crossbeam connection for a deck with a thick and a thin wearing course, respectively

9.14.4 Combination of stresses

For the stiffener to crossbeam connection, the stress intervals caused by the in-plane behaviour shown in Table 9.40 are increased by half the stress intervals caused by the out-of-plane behaviour as shown in Table 9.42.

The following stress intervals are used for damage calculations of crossbeam web locations:

1. (Modified) Stress interval for in-plane behaviour due to Lorries on Lane 1 only
2. (Modified) Stress interval for in plane behaviour due to lorries on Lane 1 and Lane 2
3. Stress interval for out-of-plane behaviour due to lorries on Lane 1

Table 9.44 gives an overview of all stresses in the crossbeam and in the stiffener, generated by the crossbeam behaviour for a deck with a thick and with a thin wearing course. These stresses are to be used for the fatigue assessment.

The origin of the stress is indicated with the loads on Lane 1 and Lane 2 together with the load transfer through the crossbeam, in-plane and out-of-plane.

The in-plane behaviour of the crossbeam is considered not to generate stresses in the trough web. The out-of-plane behaviour will not affect the trough web.

Assuming the effective weld root thickness is equal to the thickness of the trough, the stresses in Table 9.38 are used for a fatigue assessment with nominal detail classifications.

Table 9.44 Stress intervals (N/mm²) for specified stiffener and crossbeam locations

	Wearing course Thick			Wearing course Thin		
	Modified stress intervals	in-plane stress intervals	Out-of-plane stress intervals	Modified stress intervals	in-plane stress intervals	Out-of-plane stress intervals
Traffic on lane no.	1	1 + 2	1	1	1 + 2	1
Stiffener location S.3.b	37	-	-	62	-	-
Stiffener location S.3.w	34	-	-	53	-	-
Crossbeam location C.3.b	-	-	6	-	-	10
Crossbeam location C.3.w	17	24	9	17	27	13

9.14.5 Fatigue assessment

Fig.9.17 shows the relevant locations for fatigue of the stiffener to crossbeam connection when the troughs are fitted between the crossbeams.

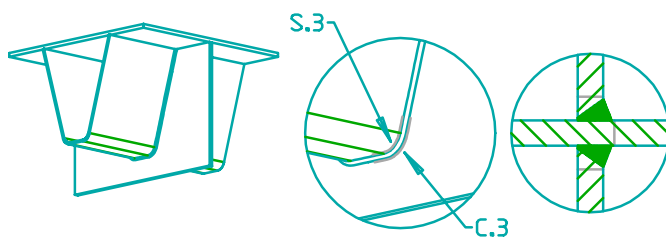


Fig. 9.17 Closed stiffener fitted between crossbeams

For each location, the detail class and the appropriate partial factor γ_{Mf} are used; the reduced class is indicated with $\Delta\sigma_{Cr}$, the reduced constant amplitude fatigue strength with $\Delta\sigma_{Dr}$ and the reduced cut-off limit with $\Delta\sigma_{Lr}$.

Location S.3, fillet welds

Class 36 (nominal), $\gamma_{Mf} = 1.0$: $\Delta\sigma_{Cr} = 36$, $\Delta\sigma_{Dr} = 27$ ($N=5 \cdot 10^6$), $\Delta\sigma_{Lr} = 15$ ($N=1 \cdot 10^6$)
 The Tables 9.45 and 9.46 give a fatigue assessment as described in 8.4.3.

Location S.3.b

Table 9.45 Fatigue life calculation procedure for location S.3.b

Wearing course "thick"								
Load on	FLM2			FLM4			n	n _c
	Mode	$\Delta\sigma_{\max 2}$	$\frac{\Delta\sigma_{\max}}{\Delta\sigma_{Dr}} < ?$	$\Delta\sigma_{\max 4}$	$\frac{\Delta\sigma_{\max}}{\Delta\sigma_{Lr}} < ?$			
Lane 1	Deck bending	37	N	30		0.8x1.09x8000x250x25	0.58 x n = 2.52x10 ⁷	
Σn_c							2.52 x 10 ⁷	
Fatigue life (Years)							1.98	

Location S.3.w

Table 9.46 Fatigue life calculation procedure for location S.3.w

Wearing course "thick"								
Load on	FLM2			FLM4			n	n _c
	Mode	$\Delta\sigma_{\max 2}$	$\frac{\Delta\sigma_{\max}}{\Delta\sigma_{Dr}} < ?$	$\Delta\sigma_{\max 4}$	$\frac{\Delta\sigma_{\max}}{\Delta\sigma_{Lr}} < ?$			
Lane 1	Deck bending	34	N	27	N	0.8x1.09x8000x250x25	0.42 x n = 1.83 x 10 ⁷	
Σn_c							1.83x10 ⁷	
Fatigue life (Years)							2.73	

Location S.3.b

Table 9.47 Fatigue life calculation procedure for location S.3.b

Wearing course "thin"								
Load on	FLM2			FLM4			n	n _c
	Mode	$\Delta\sigma_{\max 2}$	$\frac{\Delta\sigma_{\max}}{\Delta\sigma_{Dr}} < ?$	$\Delta\sigma_{\max 4}$	$\frac{\Delta\sigma_{\max}}{\Delta\sigma_{Lr}} < ?$			
Lane 1	Deck bending	62	N	50		0.8x1.09x8000x250x25	2.68 x n = 1.17x10 ⁸	
Σn_c							1.17x10 ⁸	
Fatigue life (Years)							0.43	

Location S.3.w

Table 9.48 Fatigue life calculation procedure for location S.3.w

Wearing course "thin"								
Load on	FLM2			FLM4			n	n _c
	Mode	$\Delta\sigma_{\max 2}$	$\frac{\Delta\sigma_{\max}}{\Delta\sigma_{Dr}} < ?$	$\Delta\sigma_{\max 4}$	$\frac{\Delta\sigma_{\max}}{\Delta\sigma_{Lr}} < ?$			
Lane 1	Deck bending	53	N	42	N	0.8x1.09x6400x250x25	1.59 x n = 9.95x10 ⁷	
Σn_c							6.95x10 ⁷	
Fatigue life (Years)							0.72	

The design lives found are short, which is in line with practical experience for densely trafficked motorways.

The traffic used in these calculations comprises $1.6 \cdot 10^6$ lorries per year, which is very near to traffic category 1 of EN 1991-3 Table 4.5. If traffic category 3 (low flow of lorries) is applied, the fatigue life is multiplied with a factor 16. So, for a “thick” wearing course the fatigue life for S.3.b becomes 32 years and the fatigue life for S.3.w becomes 43 years. For a “thin” wearing course, the fatigue life for S.3.b becomes 6 years and the fatigue life for S.3.w becomes 11 years

Locations C.3.b and C.3.w

Class 80 (nominal), $\gamma_{Mf} = 1.0$: $\Delta\sigma_{Cr} = 80$, $\Delta\sigma_{Dr} = 59$ ($N=5 \cdot 10^6$), $\Delta\sigma_{Lr} = 32$ ($N=1 \cdot 10^6$)

For locations C.3.b and C.3.w, the maximum modified in-plane stress interval in relation to FLM2 for a thin wearing course shown in Table 9.40 is 27 N/mm^2 , which is far below $\Delta\sigma_{Dr} = 59 \text{ N/mm}^2$. Hence, no damage is to be expected.

9.15 Summary of fatigue life results and concluding remarks

Summary of fatigue life results

Table 9.49 gives a summary of the fatigue design lives for the relevant locations of the trough to crossbeam connections (Figs. 9.18 to 9.20).

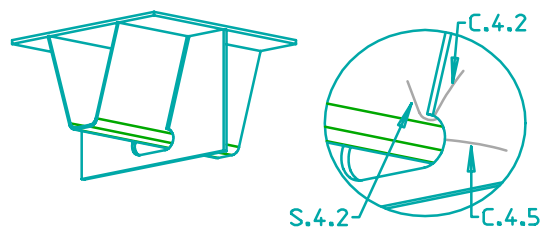


Fig. 9.18 Closed stiffener through crossbeam with oval cope hole

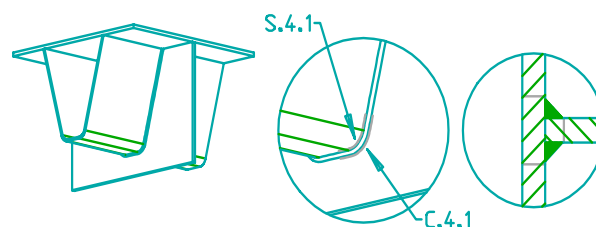


Fig. 9.19 Continuous closed stiffener through crossbeam with a close fit

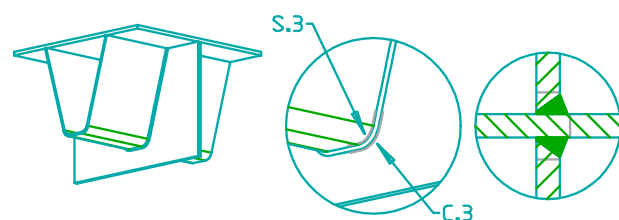


Fig. 9.20 Closed stiffener fitted between crossbeams

For the fatigue lives of these locations, the following is considered:

- 25 years
- 8000 lorries per day
- ENV 1991-3, Long distance traffic lorry distribution
- Traffic of Moerdijk 1998 measurements
- Load configuration L1+L2: 80% of lorries on slow and 20% of lorries on fast lane
- Load configuration L1: 100% of lorries on slow lane
- 250 working days per year

Table 9.49 Fatigue lives in years (y) calculated for Crossbeams “AA”, ”BB” and “CC”, with a deck plate thickness of 16 mm and a web depth of 1200 mm. (Values *in italics* apply for analyses without deck restraint effect)

Crossbeam web thickness (mm)	10		18		Lane load configuration	Note
	Fatigue life (y)		Fatigue life (y)			
Wearing course	Thick	Thin	Thick	Thin		
Location	Crossbeam “AA” Continuous troughs, Connections with cope holes					
S.4.2	∞	$\infty^{(1)}$	-	-	L1 + L2	See 9.12.5
C.4.2	∞	$\infty^{(2)}$	-	-	L1 + L2	
C.4.5.s “Oval”	-	<i>0.11</i> ⁽³⁾	-	-	L1 + L2	See 9.12.6 and A1.3.6
	-	<i>0.16</i> ⁽³⁾	-	-	L1	
	-	0.28 – 0.50 ⁽⁴⁾ 15 ⁽⁵⁾ - 28 ⁽⁵⁾	-	0.80 – 1.05 ⁽⁴⁾	L1 + L2	
	-	0.37 – 0.63 ⁽⁴⁾	-	0.99 – 1.29 ⁽⁴⁾	L1	
C.4.5.s “Haibach”	-	0.92 – 1.60 ⁽⁴⁾	-	1.85 – 3.11 ⁽⁴⁾	L1 + L2	
	-	1.18 - 2.03 ⁽⁴⁾	-	3.02 – 3.73 ⁽⁴⁾	L1	
Location	Crossbeam “BB” Continuous troughs, connections with a close fit					
S.4.1b	∞	$\infty^{(6)}$	-	-	L1 + L2	See 9.13.5
S.4.1w	∞	$\infty^{(6)}$	-	-	L1 + L2	
C.4.1.b	∞	∞	-	-	L1 + L2	
C.4.1.w	(0.17) ⁽³⁾	(0.14) ⁽³⁾	-	-	L1 + L2	See 9.13.5
	(0.23)	(0.19)			L1	
	0.43 – 0.78 ⁽⁴⁾	0.37 – 0.65 ⁽⁴⁾⁽⁵⁾	2.16 – 4.20 ⁽⁴⁾	1.61 – 2.62 ⁽⁴⁾	L1 + L2	See 9.13.6 and A1.3.6
	0.57 – 1.01 ⁽⁴⁾	0.49 – 0.85 ⁽⁴⁾⁽⁵⁾	2.75 – 5.79 ⁽⁴⁾	1.95 – 3.40 ⁽⁴⁾	L1	
Location	Crossbeam “CC” Troughs fitted between the crossbeams					
S.3b	2.0 ⁽⁷⁾ 32.0 ⁽⁸⁾	0.4 ⁽⁷⁾ 6.4 ⁽⁸⁾	-	-	L1 + L2	See 9.14.5
S.3w	2.7 ⁽⁷⁾ 43.2 ⁽⁸⁾	0.9 ⁽⁷⁾ 11.2 ⁽⁸⁾	-	-	L1 + L2	
C.3.b	∞	∞			L1 + L2	
C.3.w	∞	∞			L1 + L2	

Notes:

- Not calculated
- 1) Minimum crossbeam depth of 1200 mm allowed for infinite life due to deck bending. Further study into the detail classification may lead to the acceptance of lower crossbeam depths.
- 2) Minimum crossbeam depth of 800 mm allowed for infinite life for deck bending.
- 3) Result deviates completely from practical experience. The location has been re-analysed with an adapted model described in Appendix A1, summarized in (5).
- 4) The fatigue life depends on the effective width of the deck restraint, here taken 4000 mm and 6000 mm
- 5) If the “mean” value of the detail classification is taken, in combination with a realistic traffic history, derived from the Moerdijk 1998 traffic, 15 to 28 years fatigue life result for a crossbeam with oval cope holes for a motorway with average traffic. For a connection with a close fit the fatigue life results are equal or longer.
- 6) Minimum crossbeam depth of 1200 mm allowed for infinite life for thin wearing course.
- 7) The design lives for S.3w and S.3b are short, but this tendency is also found in practice for bridges with high traffic flows. If shallow crossbeams are needed in motorway bridges in practice, normally these connections are only used with short stiffener spans
- 8) Design lives for S.3w and S.3b for Traffic category 3 (low flow of lorries) given in ENV 1991-3 (EN 1991-2)

Concluding remarks

With the exception of the locations C.4.5.s (Cope hole) (see 9.12.5) and C.4.1.w (crossbeam web at cut-out) (see 9.13.5):

- All locations of the crossbeams “AA”, “BB” and “CC” show realistic design lives.
- Some locations of the crossbeams “AA” and “BB” with a web depth smaller than 800 mm show very short design lives.
- Crossbeams “CC” show short design lives

For the locations C.4.5.s and C.4.1.w, additional analyses were carried out, as described in Appendix A1. If these additional analyses are taken into account, the following observations can be made for the locations C.4.5.s and C.4.1.w:

- Considering a deck restraint with $b_{\text{eff}} = 4000$ mm, the fatigue life increases by a factor between 2.3 and 2.6. An increase of the deck restraint from $b_{\text{eff}} = 4000$ mm to $b_{\text{eff}} = 6000$ mm, increases the fatigue life by an additional factor between 1.3 and 2.1 and an increase of the crossbeam web thickness t_w from 10 to 18 mm, increases the fatigue life by an additional factor between 1.8 and 5.7
- The total effect of the deck restraint and crossbeam web increase can result in a fatigue life extension factor between 2.3 and 25.0.
- Including the deck stiffness effect in the geometrical stresses in the cut-out of the ECSC test crossbeam described in chapter 7, leads to stresses similar to the measured stresses and those determined with an FE shell element model.
- The stress intervals due to the lorries are mainly at the inverse log-log slope $m = 3$ to $m = 5$ transition part, which makes the fatigue life assessment very sensitive to the shape of S - N lines. This can lead to a fatigue life extension factor between 3 and 5.
- The measured axle loads on the Moerdijk Bridge show a larger percentage of axles with loads lower than FLM4.
- Combining the effects of the deck restraints, the “mean” classification and the measured loads vs. FLM4, can lead to fatigue life extension factor of 36 (= 2 x 3 x 6) to 60 (= 2.6 x 2.1 x 11) and higher with respect to the fatigue lives calculated in chapter 9 for crossbeams with web thicknesses of 10 mm.
- The fatigue design lives are conservative, because the equivalent numbers of lorries, as determined in chapter 6 are based on S-N lines with continuous slopes $m = 3$ and $m = 5$ on a log – log scale respectively and no cut-off limits, below which axle loads do not contribute to fatigue damage, are considered.

The deck restraint effect, the detail classification and the axle distribution have such a large influence on the calculated fatigue lives that further study on these subjects will be needed, in order to obtain more precise fatigue life predictions for the locations C.4.5.s (free edge of cope hole) and C.4.1.w (Crossbeam web side at the trough bottom of the fully welded connection).

10 CONCLUSIONS, REMARKS AND RECOMMENDATIONS

10.1 Introduction

This chapter gives an overview of the results and the conclusions drawn in this study in relation to the objectives described in 1.5. (repeated in 10.2 for easy reference.)

The results of the analyses in the various chapters are compared to the objectives in 10.2. Results from the various chapters are summarized in 10.4 and design recommendations based on the results are presented in 10.5. The subjects proposed for further study are given in 10.6 and the general conclusions are in 10.7.

10.2 Objectives

1. To obtain insight into the mechanical behaviour and interaction effects of closed stiffener to crossbeam connections in orthotropic steel bridge decks
2. To gain insight into past design errors
3. To derive simple methods for the fatigue design of closed stiffener to crossbeam connections in orthotropic steel bridge decks
4. To devise a basis for the improvement of the fatigue behaviour of closed stiffener to crossbeam connections in orthotropic steel deck design
5. To develop knowledge to be applied to inspection, repair and modifications of existing bridges

10.3 Comparison of the results to the objectives

Objective 1: Mechanical behaviour and interaction effects

To some extent all the chapters of this study describe these effects. The most relevant aspects are described hereafter.

Chapter 3 distinguishes between cracks that grow under direct load transfer (category A), cracks that grow due to imposed deformations (category B) or that can start as the second category (B) and change into the first (A). The effects resulting from the cracks are described and linked to the partial factors γ_{MF} for fatigue resistance. A short description of the mechanical behaviour of the deck, crossbeam and the interaction is given.

Chapter 4 describes a Vierendeel model for the in-plane behaviour, which is not only used for the analysis of the local behaviour of the continuous trough to crossbeam behaviour, but also for the derivation of equivalent crossbeam properties. The analytical model is verified and where necessary corrected, based on the results of FE-shell element models, but ignoring the deck restraint effects. The in-plane crossbeam bending and shear behaviour is analysed for a range of crossbeam depths and cut-out (cope hole) widths. The analytical model is further developed in Appendix 1 with the effects of the deck restraint, which are usually neglected in analytical models.

The out-of-plane behaviour of the trough to crossbeam connection is analysed with a beam model, comprising the tooth and the remaining crossbeam web below the troughs. This model is suitable for trough to crossbeam connections with a close fit and for connections with cope holes. The out-of-plane crossbeam behaviour is analysed for the same range of crossbeam depths and cut-out (cope hole) widths as used for the in-plane behaviour.

For in-plane and out-of plane behaviour, section forces, section moments and nominal stresses are calculated, which clearly show the influences of the various dimensions.

Chapter 5 describes the local models and calculation methods for the determination of geometrical stress concentration factors for one combination of structural dimensions. In some cases, these factors also include the relation of the stresses between two locations. The results show the relevant locations for fatigue in relation to crossbeam in-plane and crossbeam out-of-plane behaviour. The FE solid element models are more accurate than the analytical radial beam models. So, the results from the FE model results are considered more suitable for design purposes. For some locations, it is shown that the stress concentration factors could be calculated with formulas given in literature.

Chapter 6 describes the effect of the interaction between the deck stiffness and the crossbeam stiffness on the influence lines for the load, the rotation, and the deck bending moment amplitudes, intervals and the numbers of cycles. The analytical models are verified with FE beam grid models. The results, presented as load, rotation and deck bending moments with equivalent numbers of cycles in relation to ENV 1991-3, show the relationship between the fatigue loads and the structural dimensions.

Chapter 7 describes the calculation results from the ECSC 3rd Phase single trough specimens with FE shell models and with an analytical method. These specimens were directly loaded, not influenced by a crossbeam in-plane “Vierendeel” behaviour.

As a second subject, the analyses and measurements of 4th Phase full-scale specimen are described. They include both the in-plane (“Vierendeel”) and out-of-plane effects and comprise calculations with FE shell models, FE solid models and analytical models. The calculations and measurements confirm the crossbeam behaviour and local stress effects described in the chapters 4 and 5. In general, the calculation results show that both FE models, and the analytical models are a good representation of the crossbeam behaviour. At some locations, high stress gradients are found.

Chapter 8 describes the aspects and the procedure needed for carrying out fatigue analyses. A relationship between the fatigue load models FLM2 and FLM4 given in ENV 1991-3 has been derived. This chapter also deals with simultaneous loads on adjacent traffic lanes and the interaction between stress intervals resulting from in-plane crossbeam load intervals and out-of-plane rotation intervals of the trough to crossbeam connection. An overview of examples of detail classifications for the trough to crossbeam connection is given, which is based on standards and research.

Appendix 1 describes the influence of the deck restraint (local deck plate and trough bending) on the stresses in the tooth, the effect of a modified detail classification and last but not least the influence of differences between the axle loads of FLM4 lorries and the measured axle loads at a bridge. This appendix also shows the large influence of the summation of these effects on the fatigue life.

Objective 2: Insight into past design errors

Although only a few cases of damage at trough to crossbeam connections are known in the Netherlands, the observed damage can be better explained with the methods and the results presented in this study.

Objective 3: Simple methods for fatigue design

With the models presented in chapters 4, 5, and 6 and the aspects described in chapter 8, fatigue assessments can be carried out.

As examples, the fatigue strength of the trough to crossbeam connections of three types of crossbeams with “thick” and “thin” wearing courses have been analysed in chapter 9 and Appendix 1.

Objective 4: Basis for improvement

The results of this study show the nominal stress variations for a range of crossbeams (see chapter 4), which are transferred into concentrated (geometrical) stresses with the results of chapter 5. The concentrated stresses are used as a basis for the fatigue analysis of the sensitive spots of three types of connections (see chapters 8, 9 and Appendix 1).

The influence of the various geometrical parameters of the crossbeam can be used as a basis for design modifications.

Objective 5: Knowledge to be applied to inspection, repair and modifications

The analytical and numerical results of this study indicate the critical locations for several trough to crossbeam connection types. The stresses and fatigue lives of these locations can be calculated with the models described. These results can provide the basis for modifications, where necessary.

10.4 Conclusions

Crossbeam behaviour

In-plane

- For crossbeam bending (global behaviour), the effect of the cut-out with cope holes can be neglected.
- For crossbeam shear (global behaviour), the effect of the cut-out must be taken into account, which can be done by using a modified thickness for the crossbeam web.
- For the shear transfer in the crossbeam the deformation contribution due to bending of the T-beam below the cut-out can be ignored.
- The tooth length used in calculations for the bending deformation caused by crossbeam shear has to be corrected due to local deformations in the crossbeam web below the tooth.
- The stresses in the trough web caused by a crossbeam bending moment increase for larger cope hole widths
- The stresses in the trough web caused by a crossbeam bending moment depend on the position of the neutral axis of the crossbeam.
- The stresses in the trough web caused by crossbeam shear decrease for wider cope holes and deeper crossbeams.
- The effect on the stresses at the trough to crossbeam connection at the cope hole due to local loads on the troughs can be ignored.
- Wider cope holes show increasing stresses at the cope hole edge in the crossbeam.
- Deeper crossbeams show a decrease of the stresses at the cope hole edge in the crossbeam.
- For the investigated crossbeams, the largest stresses at the cope hole edge occur at the narrowest cross section of the tooth.
- The stresses perpendicular to the weld toe at the trough to crossbeam connection are lower in connections with a close fit than in connections with a cope hole.

Out-of-plane

- An increase in the width of the trough bottom results in a larger stiffness of the connection for rotation
- Subjected to the same out-of-plane rotation, deeper crossbeams give lower stresses than shallow ones.

Stress concentration (relation) factors

- As no parameter calculations have been carried out, no conclusions can be drawn for geometrical variations.

Transfer functions

Crossbeam reactions

- For the crossbeam load histories for fully loaded crossbeams, the calculation with influence lines for beams on rigid supports overestimates the crossbeam load effects for shallow crossbeams.

Trough to crossbeam connection rotations

- For the rotation histories, the calculation with influence lines for fully loaded crossbeams “beams on rigid supports” underestimates the deck to crossbeam connection rotation effect for shallow crossbeams.

Bending moments in the deck

- For the deck bending moment histories, the calculation with influence lines for “beams on rigid supports” may underestimate the deck bending moment effect for shallow crossbeams.

Comparison of analytical models with measurements and FE calculations

- FE-models with shell elements are only reliable for the determination of the geometrical peak stresses for locations not affected by the weld geometry and can give, in conjunction with fatigue tests, a contribution to the fatigue classification of the details, for other locations FE element models with solid elements should be used.
- The analytical models give a good representation of the behaviour of the structure.
- Where geometrical peak stresses have to be determined, due attention shall be paid to the use of appropriate stress concentration factors.
- In trough to crossbeam connections with a cope hole, the stresses in the trough web below the trough to crossbeam web connection are very sensitive for the location considered and small changes in the geometry.
- The stress gradients at some locations are high, which can lead to large deviations of the actual stresses in the structure from the calculated stresses
- FE solid element models in conjunction with test specimens can partly replace the strain gauge measurements needed for extrapolation to the weld toe in fatigue detail classification procedures.

Assessment procedures

The ENV 1991-3 (EN 1991-2) fatigue load model 4 (FLM4) give about the same results as fatigue load model 2 (FLM2), if the axle loads are scaled by a factor 0.8.

Conclusions based on Example calculations

Crossbeam depth \leq 800 mm

All locations

- Fatigue assessment is necessary.
- The deck restraint effect should be included.
- The classifications need more research
- The vehicle and axle load model should be improved.
- Deeper crossbeams have lower stress intervals, also at the cope hole locations (C.4.5.s), and the crossbeam web locations (C.4.1.w). These locations will show much longer fatigue lives.
- The “Haibach” cope hole has a better fatigue resistance than the oval cope hole, due to the lower stress concentration effect at the cope hole.
- For orthotropic decks with crossbeams with troughs in a close fitting hole, due attention must be paid to the out-of-plane effects.
- Connections of stiffeners fitted between the crossbeams are very susceptible to fatigue and very sensitive to the assembly tolerances because of secondary effects.

Crossbeam depth $>$ 800 mm

All locations, except C.4.5.s and C.4.1.w:

- No fatigue assessment is needed for crossbeams deeper than 800 mm of decks with continuous troughs, as fatigue assessment without the deck restraint effect results in infinite fatigue life.
- Fatigue cracks may only occur due to manufacturing deficiencies.
- Connections of stiffeners fitted between the crossbeams are always very susceptible to fatigue and very sensitive to the assembly tolerances because of secondary effects

Locations C.4.5.s and C.4.1.w

- Fatigue assessment is necessary.
- The deck restraint effect should be included.
- The classification needs more research
- The vehicle and axle load model should be improved.
- Deeper crossbeams have lower stress intervals, also at the cope hole locations (C.4.5.s), and the crossbeam web locations (C.4.1.w). These locations will show much longer fatigue lives.
- The “Haibach” cope hole has a better fatigue resistance than the oval cope hole, due to the lower stress concentration effect at the cope hole.

10.5 Recommendations

Based on the findings in this study, the following recommendations are made:

- Standards should include the restraining effect of the deck for the analysis of the in-plane behaviour of the crossbeams in order to obtain more accurate stress intervals.
- Relatively shallow crossbeams should be avoided, as they reduce the shear capacity of the crossbeams and necessitate stiffeners being fitted between the crossbeams.
- Deeper crossbeams are recommended as they allow continuous troughs.
- For orthotropic decks with deeper crossbeams, it is recommended that a cope hole with a large radius (Haibach cope hole) is used, to minimize the geometrical stress concentration effect.
- Due attention must be paid to the assembly tolerances of connections of stiffeners fitted between the crossbeams in order to avoid secondary effects.

10.6 Aspects proposed for further study

The following aspects are proposed for further study:

- More detailed study into stress concentration factors.
- More detailed analysis of the existing fatigue classifications in relation to stresses as used in engineering processes.
- If needed, additional tests, in order to establish fatigue detail classifications and in particular for those locations subjected to local out-of-plane bending.
- More study into the application of ENV 1991-3 (EN 1991-2) Fatigue Load Models (number of lorries, distribution of axle loads) and its relation with real traffic, e.g. derivation of calibration factors, which adapt the fatigue loads to more realistic values

REFERENCES

- AISC Design manual (1963), *Design Manual for Orthotropic steel plate deck bridges*, American Institute of Steel Construction Inc., New York, United States of America
- Bats, J.O., Kingma, A., (1962), *Determination of the stress distribution in an orthotropic steel deck and the influence of the wearing course*, Report 6-64-5OP-5, Stevin Laboratory, Delft University of Technology, Delft, The Netherlands. (in Dutch)
- Beales, C, (1979), *Severn/Wye Bridge Project - Tests on Crossbeam Joints*, Working paper WP/BD 44, Transport Research Laboratory, Crowthorne, Berkshire, United Kingdom. (Confidential)
- Bercum, J.Th. van, Stark, J.W.B., (1971), *Onderzoek naar de vermoeiingssterkte van verbindingen tussen langsliggers en dwarsdragers van orthotrope plaatbruggen*, TNO Report B-71-29, TNO Building and Construction Research, Rijswijk, The Netherlands (in Dutch)
- Bruls, A., Caramelli, S., Cuninghame, J.R., Jacob, B., Kolstein, M.H., Lehrke, H.P., Pautremat, E. Le, (1997), *Measurement and Interpretation of Dynamic Loads on Bridges, Phase 4, Fatigue Strength of Orthotropic Steel Decks*, Research sponsored by European Community of Steel and Coal, Report Delft University of Technology, Faculty of Civil Engineering, The Netherlands.
- BS 5400, (1980), *British Standard - Steel, Concrete and Composite Bridges*, British Standards Institute, London, United Kingdom
- DIN 1073, (1974), *Stählerne Strassenbrücken, Berechnungsgrundlagen*, Published by DIN as German standard, Berlin.
- Dijkstra, O.D., Vrouwenvelder, A.C.W.M., (2001), *Vermoeiing stalen rijdekken – Praktijk S-N lijnen voor dekplaatscheur*, TNO, Delft
- Dowling, P.J., (1971), *The Behaviour of Orthotropic Steel Deck Bridges*, Conference, University of Cardiff, United Kingdom.
- Drost, T. (1965), *Vermoeiingsonderzoek aan Verbindingen tussen Langsliggers en Dwarsdragers bij Orthotrope Plaatvloeren*, Report 6-65-8, Stevin laboratory, University of Technology, Delft, The Netherlands. (in Dutch)
- Eb, W.J.van der, (1962), *De orthotrope plaat als modern constructielement*, Polytechnisch Tijdschrift 7/9/1962; 21/9/1962, The Netherlands.
- EN 1990, (2001), *Eurocode 1 - Basis of structural design*, published as standard by CEN Technical Committee CEN/TC 250
- EN 1991-2, (2005.), *Eurocode 1 - Basis of Design and actions on structures, Part 2: Traffic loads on bridges*, published as standard by CEN Technical Committee CEN/TC 250

- ENV 1991-3, (1995), *Eurocode 1 - Basis of Design and actions on structures, Part 3: Traffic loads on bridges*, published as Prestandard by CEN Technical Committee CEN/TC 250
- EN 1993-1, (1995), *Eurocode 3 - Design of Steel Structures, Part 1: General Rules and Rules for Buildings*, published as Prestandard by CEN Technical Committee CEN/TC 250
- EN 1993-1-9, (2003), *Eurocode 3 - Design of Steel Structures, Part 1.9: Fatigue*
- EN 1993-2, (1998), *Eurocode 3 - Design of Steel Structures, Part 2: Steel bridges and Plated Structures*, published as Prestandard by CEN Technical Committee CEN/TC 250
- Falke, J., (1983), *Zum Tragverhalten und zur Berechnung vor Querträgern orthotroper Platten*, Dissertation, Technische Universität Carolo-Wilhelmina, Braunschweig, Germany.
- Fisher, J.W. (1977), *Bridge Fatigue Guide, Design and Details*, American Institute of Steel Construction Inc., New York, United States of America.
- Haibach, E., Plasil, I., (1983), *Untersuchungen zur Betriebsfestigkeit von Stahlleichtfahrbahnen mit Trapezhohlsteifen im Eisenbrückenbau*, Der Stahlbau, Wilhelm Ernst und Sohn.
- Hobbacher, A., (2003), *Recommendations for Fatigue design of welded joints and components, Document XIII-1965-03/XV-1127-03*, International Institute of Welding, doc. XIII-1965-03/XV-1127-03, Paris, France 2003
- Jong, H.de, (1981), *Vereenvoudigde Berekeningsmethode voor Orthotrope Platen*, Rapport 6-81-1, Stevin Laboratory, Delft University of Technology, Faculty of Civil Engineering and Geosciences, The Netherlands.
- Jong, F.B.P. de, (2007), *Renovation techniques for fatigue cracked orthotropic steel bridge decks*, Thesis, Delft University of Technology, Faculty of Civil Engineering and Geosciences, The Netherlands.
- Klöppel, K., Roos, E., (1960), *Statische Versuche und Dauerversuche zur Frage der Bemessung von Flachblechen in orthotropen Platten*, Der Stahlbau, Volume 29.
- Kingma, A., (1964), *Literatuuronderzoek naar de berekeningsmethoden voor stalen orthotrope platen*, Rapport 6-64-4-OP-5, Stevin Laboratory, Delft University of Technology, Faculty of Civil Engineering and Geosciences, The Netherlands.
- Kollbrunner, C.F., Basler K. (1969), *Torsion in Structures*, Springer-Verlag, Berlin, Heidelberg, New York.
- Kolstein, M.H., Back, J.de, (1989), *Measurement and Interpretation of Dynamic Loads on Bridges, Phase 3, Fatigue Strength of Orthotropic Steel Decks, Part 2, Trough to Crossbeam Connections*, Research sponsored by European Community of Steel and Coal, Delft University of Technology, Faculty of Civil Engineering, The Netherlands.

- Kolstein, M.H., Wardenier, J., Leendertz, J.S., (1995a), *Fatigue Performance of the trough to Crossbeam Connections in Orthotropic Steel Bridge Decks*, Proceedings Nordic Steel Conference Malmö, Sweden.
- Kolstein, M.H., Leendertz, J.S., Wardenier, J., (1995b), *Fatigue Design Aspects of Orthotropic Steel Bridge Decks*, Proceedings First European Conference on Steel Structures, Athens, Greece.
- Kolstein, M.H., Cuninghame, J.R., Bruls, A., (1996), *Fatigue Classification of Welded Detail in Orthotropic Steel Bridge Decks*, Proceedings International Conference on Fatigue of Welded Components and Structures, Paris, France.
- Kolstein, M.H., (1997), *Stress Reduction due to Surfacing on Orthotropic Steel Decks*, Proceedings IABSE Workshop Evaluation of Existing Steel and Composite Bridges, Lausanne, Switzerland.
- Kolstein, M.H., et al, (1998a), *Fatigue Strength of Welded Joints in Orthotropic Steel Bridge Decks*, Proceedings Conference by the International Institute of Welding, Budapest, Hungary.
- Kolstein, M.H., (1998b), *Strain gauge measurements Moerdijk Bridge*, Report 6-98-16, Stevin Laboratory, Stevin II laboratory, section SH, Delft University of Technology, Faculty of Civil Engineering and Geosciences, The Netherlands.
- Kolstein, M.H., (2007), *Detail classifications of orthotropic steel bridgedecks*, Thesis, Delft University of Technology, Faculty of Civil Engineering and Geosciences, The Netherlands.
- Leendertz, J.S., Kolstein, M.H., Wardenier, J., (1995a), *Numerical Analyses of the trough to Crossbeam Connections in Orthotropic Steel Bridge Decks*, Proceedings Nordic Steel Conference Malmö, Sweden.
- Leendertz, J.S., Kolstein, M.H., Wardenier, J., (1995b), *Fatigue design of Crossbeams for Orthotropic Steel Decks with Parametric Investigations of the Details*, Proceedings of the Pacific Steel Structures Conference, Singapore.
- Leendertz, J.S., Kolstein, M.H., (1995c), *The behaviour of Trough Stiffener to Crossbeam Connections in Orthotropic Steel Bridge Decks*, Heron Volume 40, Delft University, The Netherlands.
- Leendertz, J.S., Kolstein, M.H., (1996a), *Need for Additional Fatigue Detail Categories in Eurocode 3 and Assessment Procedure Tools*, Proceedings International Conference on Fatigue of Welded Components and Structures, Paris, France.
- Leendertz, J.S., Kolstein, M.H., (1996b), *Structural types and Endurance Aspects of Crossbeams in Steel Plate Girder Bridges*, Proceedings of the ICASS Conference, Hong Kong.

- Leendertz, J.S., Weijde, H.v.d., Kolstein, M.H., (1997), *Inspection of bridges with Orthotropic Steel decks with particular Attention for Fatigue*, Proceedings IABSE Workshop Evaluation of Existing Steel and Composite Bridges, Lausanne, Switzerland.
- Lehrke, H.P., (1990), *Fatigue Tests on Large Size Specimens of Stiffener to Crossbeam Connection*, Proceedings of the IABSE Workshop Evaluation of Existing Steel and Composite Bridges, Lausanne, Switzerland.
- Maddox, S.J., (1991), *Fatigue Strength of Welded Structures*, Abington Publishing, Cambridge, United Kingdom.
- Mang, F. Bucak, Ö, Kärcher, D., (1995), *Fatigue of Orthotropic Steel Bridge Decks*, Proceedings of the third International Conference on Steel and Aluminium Structures, Istanbul, Turkey.
- Matsuishi, M, Endo, T, (1968), *Fatigue of Metals subjected to varying Stress*, Japan Society of Mechanical Engineers, Fukuoka, Japan
- NEN 6788, (1995), *Het Ontwerpen van Stalen Bruggen - Basiseisen en eenvoudige rekenregels (VOSB 1995)*, Nederlands Normalisatie Instituut, Delft, The Netherlands.
- Nieuwsma, R (1998), *Moerdijkbrug – Eindrapportage aslastmetingen*, IB-R-98-47, Road Division, Ministry of Transport and public Works, The Netherlands.
- Pelikan, W., Eßlinger, M. (1957), *Die stahlfahrbahn - Berechnung und Konstruktion*, M.A.N.-Forschungsheft Nr. 7/1957, Germany
- Roark, R.J., Young, W.C., (1986), *Formulas for Stress and Strain*, 14 Printing, Mc. Graw hill Book Co., Singapore.
- Stroosma, D., (1982), *Richtlijn voor het Berekenen van Orthotrope Rijnvloeren*, Internal Guideline, Department for Mechanical Structures, Civil Engineering Division, Ministry of Transport and public Works, The Netherlands.
- Troitsky, M.S., (1967), *Orthotropic Bridges - Theory and Design*, Design Guide, The James Lincoln Arc Welding Foundation, Cleveland, Ohio, United States of America.
- Tromp, W.A.J., (1969), *Onderzoek van de Verbinding Langsligger - Dwarsdrager voor een Ontworpen Stalen brug over de IJssel bij Deventer*, Rapport 6-69-6, Stevin Laboratory, Delft University of Technology and Geosciences, The Netherlands.
- Tromp W.A.J., (1974), *Fatigue of a rib to Cross - girder Connection in an Orthotropic Steel Bridge Deck*, Report 6-74-16, Stevin Laboratory, Delft University of Technology and Geosciences, The Netherlands.

- Weitz, F.R., (1975), *Entwurfsgrundlagen und Entscheidungskriterien für Konstruktionssysteme im Großbrückenbau unter besonderer Berücksichtigung der Fertigung*, Dissertation Technical University of Darmstadt, Germany.
- Wolchuk, R., Ostapenko, A., (1962), *Secondary Stresses in Closed Orthotropic Deck Ribs at Floor Beams*, ASCE Journal of Structural Engineering, Volume 118, United States of America.
- Yamada, K., (1990), *Fatigue tests on Large Size Specimens of Stiffener to Crossbeam Connection*, Proceedings IABSE Workshop Remaining Fatigue life of Steel Structures, Lausanne, Switzerland.
- Yamada, K., Ojio, T., Kainuma, S., Obata, T., (1997), *Stress Measurement and Repair of a Fatigue Cracked Box Girder Bridge*, Proceedings of the IABSE Workshop Evaluation of Existing Steel and Composite Bridges, Lausanne, Switzerland.
- Ypeij, E., (1972), *New Developments in Dutch Steel Bridge Building*, IABSE Congress, Amsterdam, The Netherlands

APPENDIX 1 MORE DETAILED ANALYSES LOCATIONS C.4.5.s and C.4.1.w.

A1.1 Introduction

Calculations for three typical crossbeams are presented in chapter 9. These are based on the in-plane and out-of-plane models described in chapter 4, the geometrical stress concentration factors described in chapter 5, the maximum load intervals with equivalent numbers of cycles, described in chapter 6 and the selected detail classifications given in chapter 8.

However, the analyses presented in chapter 9 resulted in very short design lives for the locations C.4.5.s and C.4.1.w. These predicted design lives do not correspond with the fatigue lives found in practice for these locations. For the other locations, the calculated design lives are generally infinite, which corresponds with experience in practice up to now.

In this appendix, more detailed analyses are presented reconsidering one aspect of the Vierendeel model, used for the in-plane behaviour as presented in chapter 4, which may lead to a reduction in the stresses at the locations C.4.5.s (Cope hole) and C.4.1.w (crossbeam web) and thus extend the design lives predicted earlier. In addition, the effects of the fatigue detail classification and the difference between measured axle loads and those given in EN 1991 are investigated.

Modelling of the crossbeam in-plane behaviour

As already mentioned in 9.12.5 and 9.13.5, the Vierendeel model described in chapter 4 ignores the deck stiffness and has a hinged connection at the top of the tooth. Consequently, the analyses in chapter 9 do not consider the restraining effect for the tooth in-plane bending due to the local bending of the deck plate and the trough and the torsion in the trough, which could be the cause of an overestimation of the stresses in the tooth at the cope hole (C.4.5.s) or near the tooth base (C.4.1.w).

For the analysis of these effects, the following aspects are analysed in more detail:

- Rotation of the top of the tooth due to the in-plane shear in the crossbeam, if rotations are not restrained
- Rotational stiffness of the tooth due to a unit moment applied at the top
- Restraining stiffness due to local deck plate bending and trough bending
- Restraining torsional stiffness of the troughs

For the range of crossbeams analysed in chapter 4, for the locations C.4.5.s and C.4.1.w, the effect of the deck plate and trough restraints is analysed for crossbeam “AA” in A1.3.1 to A1.3.3. In A1.3.4, similar analyses are described for Crossbeam “BB”. The analysis for the location C.4.5.s of the Test Crossbeam used for the European 4th Phase fatigue research project as described in chapter 7, is given A1.3.5.

Fatigue detail classification

The effect of a variation of the fatigue detail classification is investigated with a simple method. This method uses the relationship between the stress intervals caused by the highest axle load and the stress intervals related to the detail classification.

FLM4 axle loads compared with measured axle loads

The effect on the fatigue life of the FLM4 axle load histogram of EN 1991-2 is compared with that of the axle load histogram at the Moerdijk Bridge, measured in 1998.

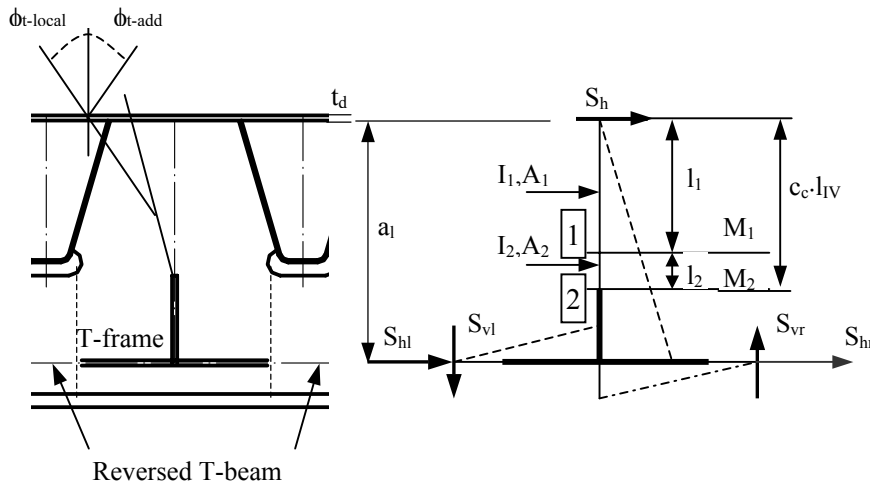
A1.2 Modelling of the crossbeam in-plane behaviour

A1.2.1 Rotation of the top of the tooth due to in-plane shear

The shear transfer in the crossbeam with cut-outs has been described in 4.2.1.3

Fig. A1.1 shows a part of the crossbeam, comprising two reversed half T-beams, the tooth and the rigid T-frame connecting the reversed T-beams with the tooth. As described in chapter 4, the moments generated by the vertical shear forces S_{vl} and S_{vr} acting on the reversed T-beams are in equilibrium with the moment caused by a horizontal shear force S_h acting at the top of the tooth. The moment diagrams are indicated with dotted lines.

The difference between the horizontal forces S_{hl} and S_{hr} , acting in the reversed T-beams, balances the horizontal force S_h .



The bending due to the horizontal force S_h in the tooth causes a rotation of the top of the tooth. In the analyses, two sets of physical properties I and A are used.

As described in 4.2.2.2, the total length of the tooth to be used for analyses equals to c_c times l_{IV} , as given Table 4.2.

Fig. A1.1 Part of crossbeam with Vierendeel model subjected to shear forces

This total length is subdivided into l_1 for the part above the cut-out and l_2 for the remaining part. I_1, A_1 is based on the dimensions of the narrowest part of the tooth (the cope hole) and is used for cross section 1. The properties I_2, A_2 are based on a larger cross section at the bottom of the cope hole, cross section 2, which is used at the bottom end of $c_c \cdot l_{IV}$. The rotation is calculated with equation A1.1.

$$\phi_{t-local} = \frac{M_1 \cdot (l_1 + 0.5t_d)}{2EI_1} + \left(\frac{M_1 \cdot l_2}{2EI_1} + \frac{M_2 \cdot l_2}{2EI_2} \right) \quad [A1.1]$$

As shown in 4.2.1.3, the reversed T-beams will deform vertically, mainly due to the shear forces S_{vl} and S_{vr} in the crossbeam web. This deflection $0.5\delta_{V-add}$ also causes an additional rotation of the tooth between two adjacent troughs, which can be calculated with equation A1.2, including the deflection $0.5\delta_{V-add}$.

$$\phi_{t-add} = 2 \cdot \frac{S_v \cdot 0.5 \cdot W}{GA_{T-beam}} \cdot \frac{1}{600} \quad [A1.2]$$

With:

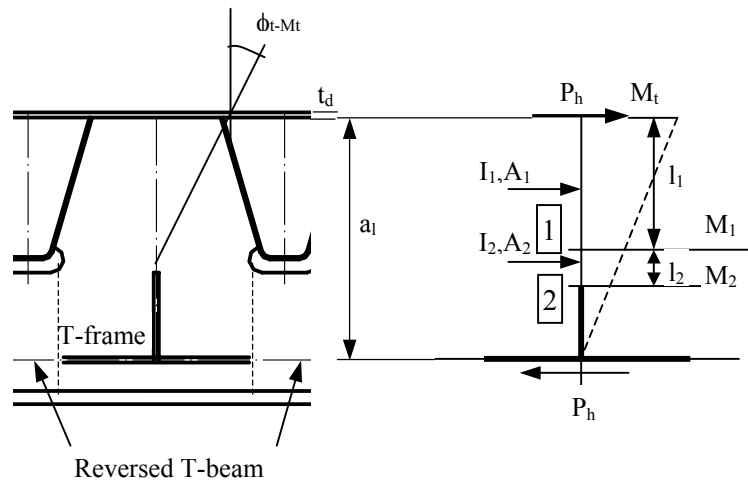
- W=the total cope hole width (mm).
- 600=the centre distance of the teeth and troughs respectively (mm)
- $M_1 = S_h \cdot l_1$
- $M_2 = S_h \cdot (l_1 + l_2)$

As a result, the total rotation of the tooth due to shear ϕ_{t-Sh} with respect to its surroundings is:

$$\phi_{t-Sh} = \phi_{t-local} + \phi_{t-add} \quad [A1.3]$$

A1.2.2 Rotational stiffness of the tooth top

Any restraint against rotation of the tooth caused by a boundary effect will impose a moment M_t on the tooth. The moment M_t is assumed to be introduced by two vertical forces of opposite sign acting at the centres of the trough web to tooth connections.



This moment will cause two reaction forces P_h in horizontal direction, one at the top of the tooth and one at the centroid of the reversed T-beams. The lever arm is a_1 . For calculation purposes the moment is assumed to act as a notional moment M_t at the top of the tooth, shown in Fig. A1.2.

Due to the transfer of M_t in the connection of the trough webs with the tooth, in combination with the stiffness I_1 , the main

contribution to the rotation will be generated over the length l_2 .

Fig. A1.2 Part of crossbeam with Vierendeel model with tooth moment deformations, due to an applied unit moment at the top

The statical values and dimensions are as given in A1.2.1. The calculation is carried out with equation [A1.4], which is identical to equation [A1.1], but in relation to a column with a notional bending moment M_t at the top of the tooth.

$$\phi_{t-M_t} = \frac{M_1 \cdot l_2}{2EI_1} + \frac{M_2 \cdot l_2}{2EI_2} \quad [A1.4]$$

In which:

$$M_1 = \frac{a_1 - l_1}{a_1 + 0.5t_d} \cdot M_t \quad [A1.5]$$

and

$$M_2 = \frac{a_t - (l_1 + l_2)}{a_t + 0.5t_d} \cdot M_t \quad [A1.6]$$

This method also applies for a connection with a trough in a close fitting hole (see 4.2.4.2).

Table A1.1, Moment rotation relationship for a tooth

Crossbeam depth H (mm)	Rotation c_t (rad/Nmm)
600	$2.484 \cdot 10^{-12}$
800	$3.281 \cdot 10^{-12}$
1000	$3.794 \cdot 10^{-12}$
1200	$4.173 \cdot 10^{-12}$
1400	$4.461 \cdot 10^{-12}$
1800	$4.881 \cdot 10^{-12}$
2200	$5.172 \cdot 10^{-12}$

The rotational stiffness of the tooth is given by:

$$\phi_{t-M_t} = c_t \cdot M_t \quad [A1.7]$$

Table A1.1 gives values of c_t for the range of crossbeams, analysed in chapter 4.

A1.2.3 Restraining stiffness due to local deck plate bending and trough bottom bending

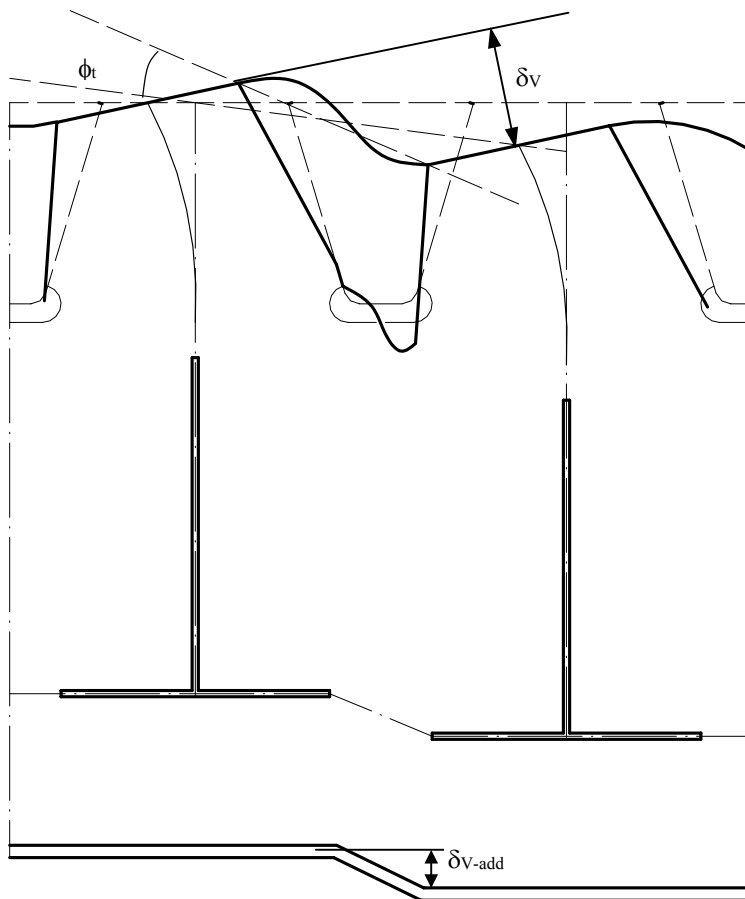


Fig. A1.3 shows the deformations of the crossbeam, the deck plate and the trough bottom, caused by the shear transfer at the trough to crossbeam connection.

Two sections with different physical mechanisms are distinguished, namely near the crossbeam and between the crossbeams.

Fig. A1.3 Deformations of crossbeam and trough in the vicinity of the crossbeam

A1.2.3.1 Restraint near the crossbeam

Near the crossbeam, the deck plate is considered to be clamped at the top of the tooth and the trough bottom is considered to be clamped in the bottom of the tooth, near the cope hole. This clamping influence is limited to a certain width of the deck plate and the trough bottom, which is assumed to be 300 mm, 150 mm either side of the crossbeam (in longitudinal direction of the trough).

The relative vertical shift between two adjacent teeth δ_v , including the effect of the shear deformation $\delta_{V\text{-add}}$ of the reversed T-beam below the cope hole, can be related to a rotation ϕ_t of a tooth, with equation [A1.8]:

$$\phi_t = \frac{\delta_v}{600} \quad \text{[A1.8]}$$

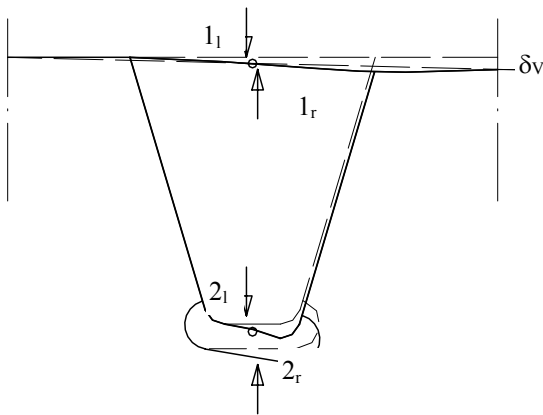


Fig. A1.4 Local deformation of deck plate and trough bottom in relation to the tooth rotation

Fig. A1.4 shows the local deformation of the deck plate and the trough bottom near the crossbeam, related to the rotation of the top of the tooth. On each part, indicated with (1_l), (1_r) for the deck plate and (2_l) and (2_r) for the trough bottom, unit forces can be applied and the related deflections due to local plate bending can be calculated. From these deflections, the vertical shift of the right hand system with respect to the left hand system can be calculated. When the deflections are divided by, the centre distance of the troughs and teeth, 600 mm, a rotation angle is found in relation to the unit forces and when these unit forces are multiplied with the respective lever arms, the applied unit moment results.

A1.2.3.2 Restraint between the crossbeams

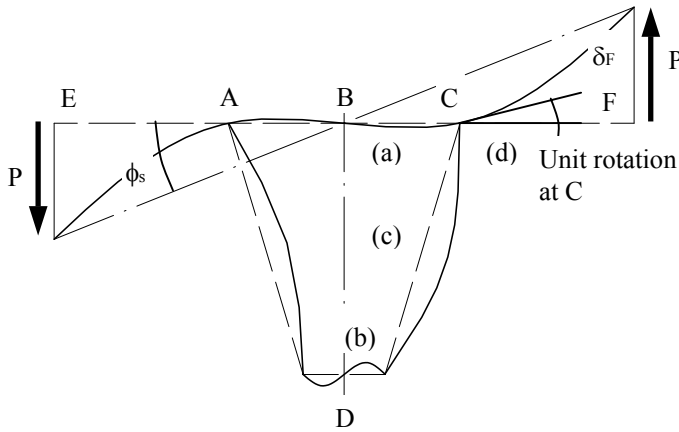


Fig. A1.5 Deformation of deck plate and trough between the crossbeams due to rotations of the teeth

Fig. A1.5 shows the deformation of the deck plate and the trough between the crossbeams.

The deck plate is deformed in a “wave” shape due to the rigid webs of the trough.

In these calculations, A, B, C and D are assumed not to displace vertically in order to simulate the asymmetric local bending behaviour of the deck on the supporting edges of the trough webs.

The rigidity of one half (right hand side) against bending of this asymmetric system with elements a (AC), b and c (DC) and d (DF) can be derived as follows:

- Rotate C with a unit rotation
- Calculate M_a at C for element (a) with length l_{A1} .
- Calculate M_{bc} , at C for elements (b, c), with lengths l_b and l_c .
- Calculate the displacement δ_F
- Determine $M_d = M_a + M_{bc}$
- Calculate P with $M/(l_d)$
- $M_d = P(l_a + l_d)$ is the related moment
- Calculate δ_F , due to M_d at C
- Calculate ϕ_s with $\delta_F/2(l_a + l_d)$
- $M_s = 2P \cdot (l_a + l_d)$

The rotation stiffness for the complete cross section (left and right) resulting from these calculations is: M_s/ϕ_s . (M_s is moment in stiffener, ϕ_s = effective rotation of stiffener due to M_s) Here, $2(l_a + l_d) = 600$ mm, the centre distance of the teeth and troughs. The sum of the bending moments caused by the deflections δ_F (the free edges shown in Fig. A1.5), divided by 600 mm gives the rotation related to the moment M_s .

As the indicated forces act over the whole span length of the stiffener, the calculation can be made for elements of 1 mm wide and can be expanded over 3700 mm (4000 mm – 300 mm). An overview of the generated moments caused by the deck plate and trough bending for an applied rotation of 1 mrad is given in table A1.2:

Table A1.2, Reaction moments of a trough with deck plate in relation to a rotation of 1mrad ($l_s = 4000$ mm)

	Reaction moments (kNm)		
	$t_{deck\ plate} = 12$ mm	$t_{deck\ plate} = 14$ mm	$t_{deck\ plate} = 16$ mm
Deck plate and trough bending between crossbeams ($b_{eff} = 3700$ mm) (M_s)	9.09	14.43	21.30
Deck plate bending at crossbeam ($b_{eff} = 300$ mm)	1.52	2.32	3.46
Trough bottom bending ($b_{eff} = 300$ mm)	$5.35 \cdot 10^{-3}$	$5.35 \cdot 10^{-3}$	$5.35 \cdot 10^{-3}$
Sum of moments M_d	10.61	16.75	24.76

Table A1.2 shows that the main contribution to the restraining moment M_d is generated by the deck-plate-with-trough mechanism between the crossbeams and that the clamped parts of the deck plate and the trough bottom near the crossbeam are of less importance. An increase in the deck plate thickness from 12 to 16 mm results in an increased in the restraining effect by a factor of 2.33, which is mainly due to the bending stiffness of the deck plate.

The reaction forces at A and C cause bending and shear in the trough, theoretically resulting in vertical deflections of this continuous support of the deck plate. However, these deflections will be limited, because of the horizontal bending stiffness of the trough bottom (including the parts of the adjacent trough webs acting as flanges). The effect of this bending stiffness is disregarded in the calculations

The following relationship can be given:

$$\phi_d = c_d \cdot M_d \quad [A1.9]$$

Table A1.3, Coefficients c_d

Deck plate thickness (mm)	c_d (rad/Nmm)
12	$9.421 \cdot 10^{-11}$
14	$5.970 \cdot 10^{-11}$
16	$4.039 \cdot 10^{-11}$

Table A1.3 gives values for deck thicknesses of 12, 14 and 16 mm. As in most decks, deck plates of 12 mm are used, a “thicker” deck plate in the calculation, can also be considered as a notional thickness due to the composite action of the wearing course.

A1.2.4 Restraint provided by torsion

The trough can be considered as a box section with a torsional stiffness for which the adjacent teeth act as diaphragms at every crossbeam.

The rotation due to a torsion moment acting over a length l_t can be calculated with Bredt’s formula, discussed in Kollbrunner et al. (1969):

$$\phi_{torsion} = \frac{M_{torsion} \cdot l_t}{G \cdot 4 \cdot F^2} \int \frac{du}{s} \quad [A1.10]$$

In which:

- du = elemental part (of the perimeter u)
- s = thickness of element with length “du”
- $M_{torsion}$ = torsion moment
- l_t = length of the structure subjected to torsion
- G = shear modulus
- F = enclosed area of the cross section

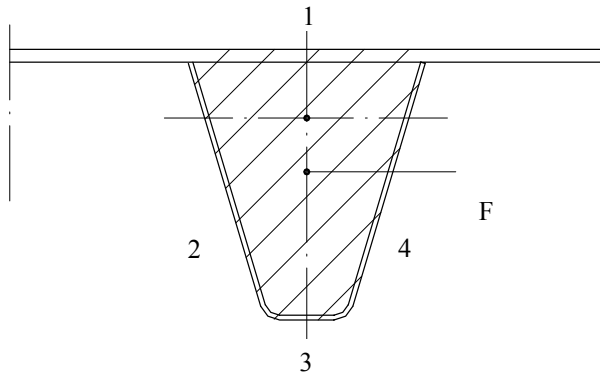


Fig. A1.6 Cross section of trough for torsion

Fig. A1.6 shows the subdivision of the cross section for calculation of the torsional rigidity of a trough with deck plate and equation [A1.11] becomes:

$$\phi_{torsion} = \frac{M_{torsion} \cdot l_t}{G \cdot 4 \cdot F^2} \sum \left(\frac{l_1}{s_1} + \frac{l_2}{s_2} + \frac{l_3}{s_3} + \frac{l_4}{s_4} \right)$$

[A1.11]

for the crossbeams A, B and C:

$$s_1 = 16 \text{ mm}$$

$$s_2, s_4 = 6 \text{ mm}$$

$$s_3 = 6 \text{ mm}$$

$$F = 6.58 \cdot 10^4 \text{ mm}^2$$

For the orthotropic steel deck, the length l_t for a stiffener relates to two cross sections with a relative rotation, here the distance between two crossbeams.

The transfer of the load of one lorry over several crossbeams cannot really be determined with an analytical procedure; consequently, the rotation in a trough between two crossbeams cannot be estimated accurately. This also applies for the generated torsion.

Concluding remark with respect to torsion

The effect of torsion is analysed separately with FE shell element models, comprising a complete deck with 5 crossbeams, described in A1.2.5. Disregarding these torsion effects leads to an overestimation of the stresses in the analytical approach, which is a conservative approach.

A1.2.5 FE model

Fig. A1.7 shows an FE shell model of a deck with five crossbeams. The troughs and the crossbeams in this model do not have the same properties as the analysed Crossbeam Type “AA”. The troughs are 300 mm deep, the crossbeam depth is 800 mm, the crossbeam spacing is 3000 mm, and the crossbeam spans are 5600 mm. The supports are modelled as strips in order to accommodate crossbeam in-plane rotations, while restraining the out-of-plane rotations.

The strips also act as rigid supports in the vertical and longitudinal horizontal directions. This means that the relevant results for the tooth can be compared with crossbeam type 2 with $H = 800 \text{ mm}$ from chapter 4.

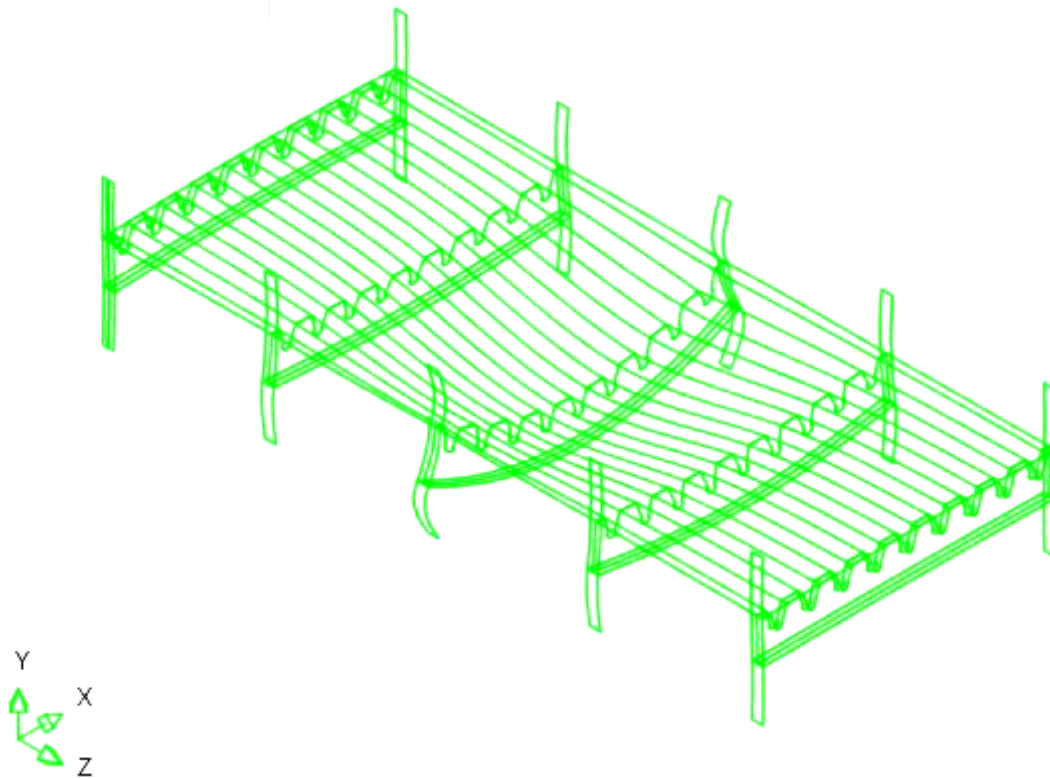


Fig. A1.7 Deformed deck with crossbeams

The middle crossbeam is loaded with a uniformly distributed load of 108 N/mm^1 . The deformations of the teeth of the middle crossbeam clearly indicate the crossbeam deformations and the deck bending.

A1.3 Analyses of crossbeam behaviour with deck restraint

The rotation of the top of the tooth is considered to be reduced only by the restraining effect of the deck plate with troughs (see A1.2.3). The restraining moment M_{res} can be calculated with the following equation:

$$\phi_{t-sh} - c_t \cdot M_t = c_d \cdot M_d \quad [\text{A1.12}]$$

In which:

- ϕ_{t-sh} = Rotation of the tooth without restraining effects (see A1.2)
- c_t = Rotation stiffness coefficient in relation to an applied moment M_t on the top of the tooth (see A1.3)
- c_d = Rotation stiffness coefficient in relation to an applied moment M_d on the deck plate with trough stiffener (see A1.4)
- M_t = Moment introduced to the top of the tooth
- M_d = Moment introduced to the deck (deck plate and troughs)
- M_{res} = Resulting moment at tooth-deck connection

For equilibrium: $M_t = M_d = M_{res}$

A1.3.1 Crossbeams analysed in chapter 4

The nominal stresses at the cope hole location C.4.5.s for the analysed crossbeams in chapter 4 are shown in Fig. 4.34. These crossbeams with a span length of 7200 mm are loaded with a uniformly distributed load of 108 N/mm^1 , resulting in a vertical shear force at the end of the crossbeams $S_v = 390 \text{ kN}$. Table A1.4 shows the rotations ϕ_{t-S_h} of the top of the tooth due to S_h , the factor c_t , representing the stiffness of the tooth against rotation by an applied moment M_t , the factor c_d , representing the stiffness of the deck against a rotation by an applied moment M_d . The effective width $b_{eff,b}$ for the restraining effects is 4000 mm. This includes 300 mm of the trough behaviour described in A1.2.3.1 and 3700 mm of the trough behaviour described in A1.2.3.2.

Table A1.4. Rotations and restraining moments

Beam type	Web depth H (mm)	ϕ_{t-S_h} (mrad)	c_t ($\times 10^{-11}$ rad/Nmm)	c_d ($\times 10^{-11}$ rad/Nmm) $t_d = 12 \text{ mm}$	M_{res} (kNm)	c_d ($\times 10^{-11}$ rad/Nmm) $t_d = 14 \text{ mm}$	M_{res} (kNm)	c_d ($\times 10^{-11}$ rad/Nmm) $t_d = 16 \text{ mm}$	M_{res} (kNm)
1	600	3.080	0.248	9.421	31.85	5.970	49.53	4.039	71.84
2	800	2.362	0.328		24.23		37.50		54.09
3	1000	1.975	0.379		20.15		31.11		44.70
4	1200	1.716	0.417		17.44		26.87		38.51
5	1400	1.517	0.446		15.37		23.64		33.82
7	1800	1.282	0.488		12.94		19.85		28.32
9	2200	1.084	0.517		11.01		16.71		23.79

The resulting nominal stress $\sigma_{nom,sum}$ due to M_{sum} (the bending moment due to shear minus the effect of the restraining moment at the top) at the cope hole location C.4.5.s can be calculated by subtracting the nominal stress due to the portion of the restraining moment M_{res} from the stress caused by the moment due to the horizontal shear force at location C.4.5.s:

$$\sigma_{nom,sum} = \frac{S_h \cdot (l_{IV} + 0.5t_d - 0.5d_c)}{W_{tooth}} - \frac{(a_l - l_1)M_{res}}{(a_l + 0.5t_d) \cdot W_{tooth}} \quad [A1.14]$$

In which:

- $\sigma_{nom,sum}$ = Resulting nominal stresses
- S_h = Horizontal shear force at the top of the tooth due to the in-plane load transfer
- a_l = Lever arm
- l_1 = See A1.3 and Fig. A1.2
- d_c = Depth of cope hole (see 4.2.4.1 and Fig. 4.30)
- t_d = Deck plate thickness
- W_{tooth} = Section modulus of tooth

Table A1.5 and Fig. A1.8 show again the nominal stresses at the cope hole location C.4.5.s due to S_h only (for crossbeams with $W = 175 \text{ mm}$); the stresses due to the reduction effect of the restraining moment M_{res} and due to the resulting moment M_{sum} at the level of the cut-out, for deck plate thicknesses of 12, 14 and 16 mm.

Table A1.5. Resulting nominal stresses at cut-out location C.4.5.s

Crossbeam type	H crossbeam web (mm)	Nominal bending stresses (N/mm ²)						
		Stress resulting from S_h	$t_d = 12$ mm		$t_d = 14$ mm		$t_d = 16$ mm	
			M_{res}	M_{sum}	M_{res}	M_{sum}	M_{res}	M_{sum}
1	600	-463	+43	-420	+67	-396	+97	-366
2	800	-380	+41	-339	+64	-316	+92	-288
3	1000	-326	+39	-287	+60	-266	+86	-240
4	1200	-286	+37	-249	+56	-230	+81	-205
5	1400	-256	+34	-222	+53	-203	+75	-181
7	1800	-212	+31	-185	+48	-164	+68	-144
9	2200	-181	+28	-153	+43	-138	+61	-120

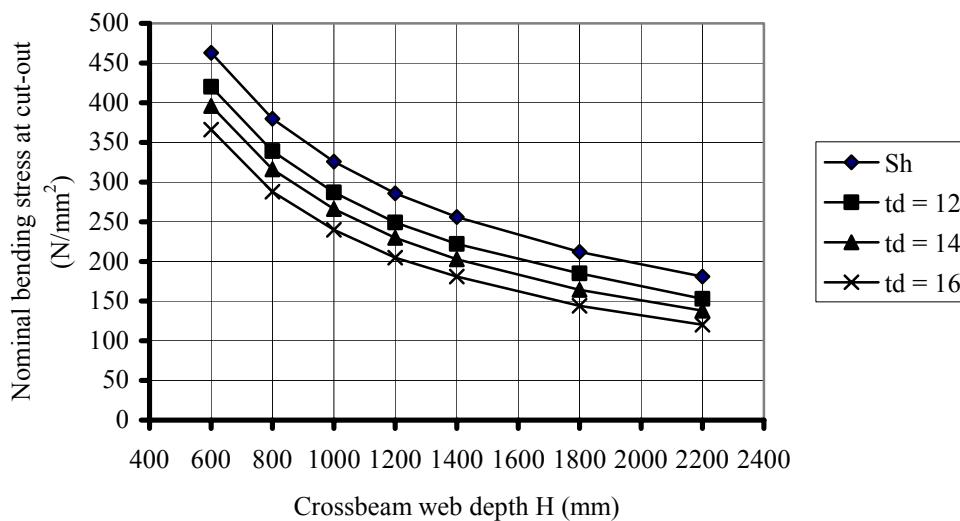


Fig. A1.8 Nominal stresses at C.4.5.s for reference crossbeams in chapter 4

Explanation to Fig A1.8:

Sh: Nominal stresses due to Vierendeel behaviour only (no influence of deck plate thickness)

$t_d = 12$: Reduced nominal stresses due to Vierendeel behaviour and restraint by deck plate $t = 12$ mm

$t_d = 14$: Reduced nominal stresses due to Vierendeel behaviour and restraint by deck plate $t = 14$ mm

$t_d = 16$: Reduced nominal stresses due to Vierendeel behaviour and restraint by deck plate $t = 16$ mm

The analytical results of crossbeam type 2 with $H = 800$ mm can be compared with the results of the FE calculation as the web depths are equal.

For $t_d = 12$ mm, the reduced bending moment in the tooth due to the deck plate restraint is 89% with the analytical approach and 81% with the FE model, compared to the bending moment due to S_h only. For $t_d = 16$ mm, the reduced bending moment found with the analytical approach is 76% and with the FE model is 78%.

The FE model, shown in Fig. A1.7, confirms the effect of the restraints caused by the deck bending stiffness and no substantial torsion was observed in the troughs.

Considering that these results have been obtained for a deck with one loaded crossbeam, this is a conservative approach, as only one loaded crossbeam generates the maximum torsion in the troughs to the adjacent unloaded crossbeams.

A1.3.2 Crossbeam “AA”

The nominal stresses for the cope hole location C.4.5.s of Crossbeam “AA” are given in Table 9.19 for an in-plane shear load interval of 313 kN, which is generated by simultaneous lorries on Lane 1 and Lane 2.

Table A1.6 shows the rotations ϕ_{t-S_h} of the top of the tooth due to S_h ; the factor c_t , representing the stiffness of the tooth against rotation by an applied moment M_t ; the factor c_d , representing the stiffness of the deck against a rotation by an applied moment M_d . All values relate to crossbeam web thicknesses t_w of 10, 12, 14 and 16 mm in combination with an effective width $b_{eff,b} = 4000$ mm and 6000 mm. The crossbeam distance of 4000 mm justifies a $b_{eff,b} = 4000$ mm if all crossbeams are equally loaded. In a case where the considered crossbeam carries substantially more load than the adjacent ones, the deformed shape of the deck will generate a larger b_{eff} , which makes it appropriate to investigate an additional $b_{eff} = 6000$ mm

Table A1.6. Rotations and restraining moments for Crossbeam “AA”

Crossbeam web thickness t_w (mm)	ϕ_{t-S_h} (mrad)	c_t ($\times 10^{-11}$)	c_d ($\times 10^{-11}$)		M_{res} (kNm)	M_{res} (kNm)
			$b_{eff} = 4000$ mm	$b_{eff} = 6000$ mm		
10	1.316	50.22	4.039	2.693	28.98	41.19
12	1.117	41.33			25.09	35.96
14	0.971	35.09			22.12	31.90
16	0.861	30.46			19.82	28.72
18	0.742	25.23			17.29	25.19

Table A1.7 shows the nominal stress intervals due to S_h and the resulting nominal stress interval due to M_{sum} for various crossbeam web thicknesses calculated with equation [A1.14]. The stress interval for a crossbeam web thickness of 10 mm is taken from Table 9.19 and is shown in bold.

Table A1.7. Resulting nominal stress intervals at cut-out location C.4.5.s

	Crossbeam web thickness t_w (mm)	Stress resulting from S_h	Stress resulting from M_{sum}		Stress resulting from M_{sum}	
			$b_{eff,b} = 4000$ mm	$b_{eff,b} = 6000$ mm	$b_{eff,b} = 4000$ mm	$b_{eff,b} = 6000$ mm
		L1 + L2	L1 + L2	L1	L1 + L2	L1
Stress interval due to S_h (see Table 9.19: Lane 1: 136 + Lane 2: 75 N/mm²)	10	211	152	99	125	82
	12	184	138	90	119	78
	14	160	126	82	111	72
	16	142	115	75	104	68
	18	122	102	67	93	61

The resulting nominal stress interval is 0.72 times (= 152/211) the original nominal stress interval for $b_{eff,b} = 4000$ mm and 0.59 times (= 125/211) for $b_{eff} = 6000$ mm.

If the nominal stresses are multiplied with an SCF = 2.4 for an oval and 1.6 for a “Haibach” cope hole the stresses become as shown in Table A1.8.

Table A1.8. Resulting concentrated stresses at cut-out location C.4.5.s

Crossbeam web thickness t_w (mm)	Oval cope hole				Haibach cope hole			
	$b_{eff,b} = 4000$ mm		$b_{eff,b} = 6000$ mm		$b_{eff,b} = 4000$ mm		$b_{eff,b} = 6000$ mm	
	L1 + L2	L1	L1 + L2	L1	L1 + L2	L1	L1 + L2	L1
10	365	238	300	197	243	158	200	131
12	331	216	286	187	221	144	286	125
14	302	196	266	173	202	197	266	115
16	276	180	250	163	184	180	166	109
18	245	161	223	146	163	161	149	98

Further analyses are carried out for the crossbeams “AA” with crossbeam web thicknesses of 10 and 18 mm and an effective width $b_{eff,b}$ of 4000 and 6000 mm respectively. (See Table A1.8 figures in bold) For the out-of plane behaviour the stress intervals shown in Table A1.9 should be used (see also Table 9.22).

Table A1.9, concentrated stress intervals (N/mm²) from Out of plane rotations (c=cycles per 100 lorries) for a Crossbeam web thickness of 10 mm

Load on Lane No.	Location	Wearing course	
		Thick	Thin
		Concentrated stress (N/mm ²)	
1	C.4.5.s	11/ 39c	18 /66c

The modified stress intervals for the fatigue assessment given in Table 9.24 can be replaced by the values shown in Table A1.10. As the difference between the stress intervals for a “thick” and a “thin” wearing course is small, only the (higher) stress intervals (for a “thin” wearing course) for the crossbeams are calculated.

Table A1.10, Modified in-plane concentrated stress intervals (N/mm²) in crossbeam at cut-out location C.4.5.s for a “thin” wearing course

Crossbeam web thickness t_w (mm)	Oval cope hole					Haibach cope hole				
	$b_{eff,b} = 4000$ mm		$b_{eff,b} = 6000$ mm		O.P.	$b_{eff,b} = 4000$ mm		$b_{eff,b} = 6000$ mm		O.P.
	L1 + L2	L1	L1 + L2	L1	L1	L1 + L2	L1	L1 + L2	L1	L1
10	374	247	309	206	18	252	167	209	140	18
18	261	177	239	162	32	211	123	165	114	32

Hereafter, the fatigue assessments are carried out using a procedure similar to that, used in chapter 9. Three categories of stress intervals are distinguished in relation to FLM2: Modified stress intervals due to in-plane behaviour for Lorries on Lane 1 only, modified stress intervals due to lorries on Lane 1 and Lane 2 simultaneously and stress intervals caused by the out-of-plane rotations due to Lorries on Lane 1. When at least one of these categories is above $\Delta\sigma_D$, unlimited fatigue life is excluded and a damage calculation must be carried out with FLM4. In this case, the stress intervals below $\Delta\sigma_L$ do not contribute to fatigue damage.

Tables A1.11 to A1.14 give the fatigue calculations for the location C.4.5.s for Lane 1 and Lane 2 simultaneously loaded by lorries assuming a cope hole with an oval shape.

Tables A1.15 to A1.18 give the fatigue calculations for the location C.4.5.s for Lane 1 and Lane 2 simultaneously loaded by lorries, assuming a cope hole with a “Haibach” shape.

The fatigue lives between brackets refer to fatigue calculations for lorries on Lane 1 only.

Fatigue assessment for location C4.5.s (with oval cope hole)

Class 140 (geometric), $\gamma_{Mf} = 1.15$: $\Delta\sigma_{Cr} = 122$, $\Delta\sigma_{Dr} = 90$ ($N = 5 \cdot 10^6$), $\Delta\sigma_{Lr} = 49$ ($N = 1 \cdot 10^8$)

Table A1.11 Fatigue life at cope hole location

Thin wearing course (Crossbeam web $t_w = 10$ mm, $b_{eff,b} = 4000$ mm)							
Load on	FLM2			FLM4			n _c
	Mode	$\Delta\sigma_{max}$	$\Delta\sigma_{max} < \Delta\sigma_{Dr}?$	$\Delta\sigma_{max}$	$\Delta\sigma_{max} < \Delta\sigma_{Lr}?$	n	
Lane 1	In-plane	247	N	198	N	$1.92 \cdot 10^7$ ($3.20 \cdot 10^7$)	$4.28 \cdot x_n = 8.21 \cdot 10^7$ ($1.37 \cdot 10^8$)
	Out-of-plane	18	Y	14	Y	0	0
Lane 1 and Lane 2	In-plane	374	N	299	N	$6.40 \cdot 10^6$ (0)	$14.72 \cdot x_n = 9.42 \cdot 10^7$
Σn_c							$1.76 \cdot 10^8$ ($1.37 \cdot 10^8$)
Fatigue life (y) L1 + L2 (L1 only)							0.28 (0.37)

Table A1.12 Fatigue life of cope hole location

Thin wearing course (Crossbeam web $t_w = 18$ mm, $b_{eff,b} = 4000$ mm)							
Load on	FLM2			FLM4			n _c
	Mode	$\Delta\sigma_{max}$	$\Delta\sigma_{max} < \Delta\sigma_{Dr}?$	$\Delta\sigma_{max}$	$\Delta\sigma_{max} < \Delta\sigma_{Lr}?$	n	
Lane 1	In-plane	177	N	142	N	$1.92 \cdot 10^7$ ($3.20 \cdot 10^7$)	$1.58 \cdot x_n = 3.03 \cdot 10^7$ ($5.05 \cdot 10^7$)
	Out-of-plane	32	Y	26	Y	0	0
Lane 1 and Lane 2	In-plane	261	N	209	N	$6.4 \cdot 10^6$ (0)	$5.03 \cdot x_n = 3.22 \cdot 10^7$
Σn_c							$6.25 \cdot 10^7$ ($5.05 \cdot 10^7$)
Fatigue life (y) L1 + L2 (L1 only)							0.80 (0.99)

Table A1.13 Fatigue life at cope hole location

Thin wearing course (Crossbeam web $t_w = 10$ mm, $b_{eff,b} = 6000$ mm)							
Load on	FLM2			FLM4			n _c
	Mode	$\Delta\sigma_{max}$	$\Delta\sigma_{max} < \Delta\sigma_{Dr}?$	$\Delta\sigma_{max}$	$\Delta\sigma_{max} < \Delta\sigma_{Lr}?$	n	
Lane 1	In-plane	206	N	165	N	$1.92 \cdot 10^7$ ($3.20 \cdot 10^7$)	$2.47 \cdot x_n = 4.75 \cdot 10^7$ ($7.92 \cdot 10^7$)
	Out-of-plane	18	Y	14	Y	0	0
Lane 1 and Lane 2	In-plane	306	N	245	N	$6.40 \cdot 10^6$ (0)	$8.10 \cdot x_n = 5.18 \cdot 10^7$
Σn_c							$1.31 \cdot 10^8$ ($7.92 \cdot 10^7$)
Fatigue life (y) L1 + L2 (L1 only)							0.50 (0.63)

Table A1.14 Fatigue life of cope hole location

Thin wearing course (Crossbeam web $t_w = 18$ mm, $b_{effb} = 6000$ mm)							
Load on	FLM2			FLM4			n _c
	Mode	$\Delta\sigma_{max}$	$\Delta\sigma_{max} < \Delta\sigma_{Dr}?$	$\Delta\sigma_{max}$	$\Delta\sigma_{max} < \Delta\sigma_{Lr}?$	n	
Lane 1	In-plane	162	N	130	N	$1.92 \cdot 10^7$ (3.20×10^7)	$1.21 \times n = 2.32 \cdot 10^7$ (3.87×10^7)
	Out-of-plane	32	Y	26	Y	0	0
Lane 1 and Lane 2	In-plane	239	N	191	N	$6.4 \cdot 10^6$ (0)	$3.84 \times n = 2.46 \cdot 10^7$
Σn_c							$4.78 \cdot 10^7$ (3.87×10^7)
Fatigue life (y) L1 + L2 (L1 only)							1.05 (1.29)

A1.3.3 Fatigue assessment for location C4.5.s (with “Haibach” cope hole)

Class 140 (geometric), $\gamma_{Mf} = 1.15$: $\Delta\sigma_{Cr} = 122$, $\Delta\sigma_{Dr} = 90$ ($N = 5 \cdot 10^6$), $\Delta\sigma_{Lr} = 49$ ($N = 1.10^8$)

Table A1.15 Fatigue life at cope hole location

Thin wearing course (Crossbeam web $t_w = 10$ mm, $b_{effb} = 4000$ mm)							
Load on	FLM2			FLM4			n _c
	Mode	$\Delta\sigma_{max}$	$\Delta\sigma_{max} < \Delta\sigma_{Dr}?$	$\Delta\sigma_{max}$	$\Delta\sigma_{max} < \Delta\sigma_{Lr}?$	n	
Lane 1	In-plane	167	N	134	N	1.92×10^7 (3.20×10^7)	$1.33 \times n = 2.54 \times 10^7$ (4.24×10^7)
	Out-of-plane	18	Y	14	Y	0	0
Lane 1 and Lane 2	In-plane	252	N	201	N	$6.40 \cdot 10^6$ (0)	$4.47 \times n = 2.86 \cdot 10^7$
Σn_c							$5.41 \cdot 10^7$ (4.24×10^7)
Fatigue life (y) L1 + L2 (L1 only)							0.92 (1.18)

Table A1.16 Fatigue life of cope hole location

Thin wearing course (Crossbeam web $t_w = 18$ mm, $b_{eff} = 4000$ mm)							
Load on	FLM2			FLM4			n _c
	Mode	$\Delta\sigma_{max}$	$\Delta\sigma_{max} < \Delta\sigma_{Dr}?$	$\Delta\sigma_{max}$	$\Delta\sigma_{max} < \Delta\sigma_{Lr}?$	n	
Lane 1	In-plane	123	Y	98	N	$1.92 \cdot 10^7$ (3.20×10^7)	$0.52 \times n = 9.95 \cdot 10^6$ (1.66×10^7)
	Out-of-plane	32	Y	20	Y	0	0
Lane 1 and Lane 2	In-plane	211	N	169	N	$6.4 \cdot 10^6$ (0)	$2.66 \times n = 1.70 \cdot 10^7$
Σn_c							$2.70 \cdot 10^7$ (1.66×10^7)
Fatigue life (y) L1 + L2 (L1 only)							1.85 (3.02)

Table A1.17 Fatigue life at cope hole location

Thin wearing course (Crossbeam web $t_w = 10$ mm, $b_{eff,b} = 6000$ mm)							
Load on	FLM2			FLM4			n_c
	Mode	$\Delta\sigma_{max}$	$\Delta\sigma_{max} < \Delta\sigma_{Dr}?$	$\Delta\sigma_{max}$	$\Delta\sigma_{max} < \Delta\sigma_{Dr}?$	n	
Lane 1	In-plane	140	N	112	N	1.92×10^7 (3.20×10^7)	$0.77 \times n = 1.49 \times 10^7$ (2.46×10^7)
	Out-of-plane	18	Y	14	Y	0	0
Lane 1 and Lane 2	In-plane	209	N	167	N	$6.40 \cdot 10^6$ (0)	$2.57 \times n = 1.65 \cdot 10^6$
Σn_c							$3.14 \cdot 10^7$ (2.46×10^7)
Fatigue life (y) L1 + L2 (L1 only)							1.60 (2.03)

Table A1.18 Fatigue life of cope hole location

Thin wearing course (Crossbeam web $t_w = 18$ mm, $b_{eff,b} = 6000$ mm)							
Load on	FLM2			FLM4			n_c
	Mode	$\Delta\sigma_{max}$	$\Delta\sigma_{max} < \Delta\sigma_{Dr}?$	$\Delta\sigma_{max}$	$\Delta\sigma_{max} < \Delta\sigma_{Dr}?$	n	
Lane 1	In-plane	114	Y	91	N	$1.92 \cdot 10^7$ (3.20×10^7)	$0.42 \times n = 7.97 \cdot 10^6$ (1.34×10^7)
	Out-of-plane	32	Y	26	Y	0	0
Lane 1 and Lane 2	In-plane	165	N	132	N	$6.4 \cdot 10^6$ (0)	$1.27 \times n = 8.11 \cdot 10^6$
Σn_c							$1.61 \cdot 10^7$ (1.34×10^7)
Fatigue life (y) L1 + L2 (L1 only)							3.11 (3.73)

A1.3.4 Crossbeam “BB”

The load transfer in Crossbeam “BB” acts in a similar way to that in Crossbeam “AA”, and the reduction factor due to the deck plate restraint for the stress intervals, as found for Crossbeam “AA”, being 0.72 for $b_{eff,b} = 4000$ mm and 0.59 for $b_{eff,b} = 6000$ mm, (see results of Table A1.7), can also be applied for the stress intervals of Crossbeam “BB”.

Table A1.19 Resulting concentrated stress intervals at C.4.1.w, perpendicular to the weld toe, due to in-plane bending and shear (N/mm^2)

Crossbeam web thickness t_w (mm)	Thick wearing course				Thin wearing course			
	$b_{eff,b} = 4000$ mm		$b_{eff,b} = 6000$ mm		$b_{eff,b} = 4000$ mm		$b_{eff,b} = 6000$ mm	
	L1 + L2	L1	L1 + L2	L1	L1 + L2	L1	L1 + L2	L1
10	(0.72 x 253=) 182	(0.72 x 163=) 117	(0.59 x 253=) 149	(0.59 x 163=) 96	(0.72 x 264=) 190	(0.72 x 170=) 122	(0.59 x 264=) 156	(0.59 x 170=) 100
18	101	65	83	53	106	68	87	55

Table A1.19 shows the concentrated stress intervals perpendicular to the weld toe at location C.4.1.w, due to in-plane bending and shear for a deck with a thick and a thin wearing course respectively, derived from Tables 9.29 and 9.31.

Table A1.20 Concentrated stress intervals at C.4.1.w, perpendicular to the weld toe due to out-of-plane rotation (N/mm²)

For location C.4.1w		
Wearing course	Thick	Thin
Rotation angle	1.81 mrad	2.62 mrad
Concentrated stress (N/mm ²)	9	13

Table A1.20 shows the stress intervals perpendicular to the weld toe at location C.4.1.w due to out-of-plane rotation for a crossbeam web thickness of 10 mm. Table A1.21 shows the stresses to be used for the fatigue assessment.

Table A1.21 Modified in-plane and out-of-plane concentrated stress intervals (N/mm²) in crossbeam at cut-out location C.4.5.w for a “thick” and a “thin” wearing course

Crossbeam web thickness t _w (mm)	Thick wearing course					Thin wearing course				
	b _{eff} = 4000 mm		b _{eff} = 6000 mm		O.P.	b _{eff} = 4000 mm		b _{eff} = 6000 mm		O.P.
	L1 + L2	L1	L1 + L2	L1	L1	L1 + L2	L1	L1 + L2	L1	L1
10	187	122	154	101	9	197	129	163	107	13
18	109	73	90	60	16	118	81	103	68	23

Fatigue assessment for Location C.4.1.w

Tables A1.22 to A1.29 give the fatigue calculations for the location C.4.5.w for Lane 1 and Lane 2 simultaneously loaded by lorries, in the case where the cope hole has a “Haibach” shape. The fatigue lives between brackets refer to fatigue calculations for lorries on Lane 1 only.

Class 80 (nominal), $\gamma_{Mf} = 1.15$: $\Delta\sigma_{Cr} = 70$, $\Delta\sigma_{Dr} = 52$ (N=5·10⁶), $\Delta\sigma_{Lr} = 28$ (N=1·10⁸)

Table A1.22 Fatigue life of cut-out location C.4.1.w

Thick wearing course (t = crossbeam web = 10 mm, b _{eff,b} = 4000 mm)							
Load on	FLM2			FLM4			n _c
	Mode	$\Delta\sigma_{max}$	$\Delta\sigma_{max} < \Delta\sigma_{Dr}?$	$\Delta\sigma_{max}$	$\Delta\sigma_{max} < \Delta\sigma_{Lr}?$	n	
Lane 1	In-plane	122	N	98	N	1.92x 10 ⁷ (3.2x10 ⁷)	2.74xn = 5.27 x 10 ⁷ (8.78x10 ⁷)
	Out-of-plane	9	Y	7	Y	0	0
Lane 1 and Lane 2	In-plane	187	N	150	N	6.40 x 10 ⁶ (0)	9.84xn = 6.30 x 10 ⁷ (0)
Σn_c							1.16·10 ⁸ (8.78 x 10 ⁷)
Fatigue life (y) L1 + L2 (L1 only)							0.43 (0.57)

Table A1.23 Fatigue life of cut-out location C.4.1.w

Thick wearing course (t = crossbeam web = 10 mm, b _{eff,b} = 6000 mm)							
Load on	FLM2			FLM4			n _c
	Mode	$\Delta\sigma_{max}$	$\Delta\sigma_{max} < \Delta\sigma_{Dr}?$	$\Delta\sigma_{max}$	$\Delta\sigma_{max} < \Delta\sigma_{Lr}?$	n	
Lae 1	In-plane	101	N	81	N	1.92x 10 ⁷ (3.2x10 ⁷)	1.55xn = 2.98 x 10 ⁷ (4.96x10 ⁷)
	Out-of-plane	9	Y	7	Y	0	0
Lane 1 and Lane 2	In-plane	154	N	123	N	6.40 x 10 ⁶ (0)	5.43xn = 3.47 x 10 ⁷ (0)
Σn_c							6.45 x 10 ⁷ (4.96 x 10 ⁷)
Fatigue life (y) L1 + L2 (L1 only)							0.78 (1.01)

Table A1.24 Fatigue life of cut-out location C.4.1.w

Thick wearing course (t=crossbeam web = 18mm, b _{effb} = 4000 mm)							
Load on	FLM2			FLM4			
	Mode	$\Delta\sigma_{max}$	$\Delta\sigma_{max} < \Delta\sigma_{Dr}?$	$\Delta\sigma_{max}$	$\Delta\sigma_{max} < \Delta\sigma_{Lr}?$	n	n _c
Lane 1	In-plane	73	N	58	N	1.92x 10 ⁷ (3.2x10 ⁷)	0.57xn = 1.09 x 10 ⁷ (1.82 x 10 ⁶)
	Out-of-plane	16	Y	10	Y	0	0
Lane 1 and Lane 2	In-plane	109	N	87	N	6.40 x 10 ⁶ (0)	1.92xn = 1.23 x 10 ⁷ (0)
Σn_c							2.32x10 ⁷ (1.82 x 10 ⁷)
Fatigue life (y) L1 + L2 (L1 only)							2.16 (2.75)

Table A1.25 Fatigue life of cut-out location C.4.1.w

Thick wearing course (t=crossbeam web = 18 mm, b _{effb} = 6000 mm)							
Load on	FLM2			FLM4			
	Mode	$\Delta\sigma_{max}$	$\Delta\sigma_{max} < \Delta\sigma_{Dr}?$	$\Delta\sigma_{max}$	$\Delta\sigma_{max} < \Delta\sigma_{Lr}?$	N	n _c
Lane 1	In-plane	60	N	48	N	1.92x 10 ⁷ (3.2x10 ⁷)	0.27xn = 5.18 x 10 ⁶ (8.64 x 10 ⁶)
	Out-of-plane	16	Y	10	Y	0	0
Lane 1 and Lane 2	In-plane	90	N	72	N	6.40 x 10 ⁶ (0)	1.09xn = 6.69 x 10 ⁶ (0)
Σn_c							1.19 x 10 ⁷ (8.64 x 10 ⁶)
Fatigue life (y) L1 + L2 (L1 only)							4.20 (5.79)

Table A1.26 Fatigue life of cut-out location C.4.1.w

Thin wearing course (t=crossbeam web = 10 mm, b _{effb} = 4000 mm)							
Load on	FLM2			FLM4			
	Mode	$\Delta\sigma_{max}$	$\Delta\sigma_{max} < \Delta\sigma_{Dr}?$	$\Delta\sigma_{max}$	$\Delta\sigma_{max} < \Delta\sigma_{Lr}?$	n	n _c
Lane 1	In-plane	129	N	103	N	1.92x 10 ⁷ (3.2x10 ⁷)	3.19xn = 6.13 x 10 ⁷ (1.02 x 10 ⁸)
	Out-of-plane	13	Y	10	Y	0	0
Lane 1 and Lane 2	In-plane	197	N	158	N	6.40 x 10 ⁶ (0)	11.15xn = 7.36 x 10 ⁷ (0)
Σn_c							1.35 x 10 ⁸ (1.02 x 10 ⁸)
Fatigue life (y) L1 + L2 (L1 only)							0.37 (0.49)

Table A1.27 Fatigue life of cut-out location C.4.1.w

Thin wearing course (t=crossbeam web = 10 mm, b _{effb} = 6000 mm)							
Load on	FLM2			FLM4			
	Mode	$\Delta\sigma_{max}$ _x	$\Delta\sigma_{max} < \Delta\sigma_{Dr}?$	$\Delta\sigma_{max}$	$\Delta\sigma_{max} < \Delta\sigma_{Lr}?$	N	n _c
Lane 1	In-plane	107	N	86	N	1.92x 10 ⁷ (3.2x10 ⁷)	1.85xn = 3.56 x 10 ⁷ (5.92 x 10 ⁷)
	Out-of-plane	13	Y	10	Y	0	0
Lane 1 and Lane 2	In-plane	163	N	130	N	6.40 x 10 ⁶ (0)	6.41xn = 4.10 x 10 ⁷ (0)
Σn_c							7.66 x 10 ⁷ (5.92 x 10 ⁷)
Fatigue life (y) L1 + L2 (L1 only)							0.65 (0.85)

Table A1.28 Fatigue life of cut-out location C.4.1.w

Thin wearing course (t=crossbeam web = 18 mm, b _{effb} = 4000 mm)							
Load on	FLM2			FLM4			
	Mode	$\Delta\sigma_{max}$	$\Delta\sigma_{max} < \Delta\sigma_{Dr}?$	$\Delta\sigma_{max}$	$\Delta\sigma_{max} < \Delta\sigma_{Lr}?$	N	n _c
Lane 1	In-plane	81	N	65	N	1.92x 10 ⁷ (3.2x10 ⁷)	0.80xn = 1.54 x 10 ⁷ (2.56 x 10 ⁷)
	Out-of-plane	23	Y	14	Y	0	0
Lane 1 and Lane 2	In-plane	118	N	94	N	6.40 x 10 ⁶ (0)	2.42xn = 1.55 x 10 ⁷ (0)
Σn_c							3.09 x 10 ⁷ (2.56 x 10 ⁷)
Fatigue life (y) L1 + L2 (L1 only)							1.61 (1.95)

Table A1.29 Fatigue life of cut-out location C.4.1.w

Thin wearing course (t=crossbeam web = 18 mm, b _{effb} = 6000 mm)							
Load on	FLM2			FLM4			
	Mode	$\Delta\sigma_{max}$	$\Delta\sigma_{max} < \Delta\sigma_{Dr}?$	$\Delta\sigma_{max}$	$\Delta\sigma_{max} < \Delta\sigma_{Lr}?$	N	n _c
Lane 1	In-plane	68	Y	54	N	1.92x 10 ⁷ (3.2x10 ⁷)	0.46xn = 8.81 x 10 ⁶ (1.47 x 10 ⁷)
	Out-of-plane	23	Y	18	Y	0	0
Lane 1 and Lane 2	In-plane	103	N	82	N	6.40 x 10 ⁶ (0)	1.61xn = 1.03 x 10 ⁷
Σn_c							1.91 10 ⁷ (1.47 x 10 ⁶)
Fatigue life (y) L1 + L2 (L1 only)							2.62 (3.40)

A1.3.5 Test crossbeam European 4th Phase fatigue research project

The results of the analyses of the test crossbeam of the European 4th Phase fatigue research project were presented in chapter 7, where the conclusion was drawn that the results from the analytical model, the FE shell model and the measurements corresponded fairly well.

In the following, the influence of the deck bending stiffness is also investigated for the ECSC crossbeam.

The contribution of the deck with trough restraint is related to an effective width $b_{\text{eff},b}$ of 1.7 m (2.0 – 0.3 m), as the test specimen has a deck plate with a width of 2.0 m and the width of the clamped part near the crossbeam is assumed to be unchanged, (i.e. 300 mm).

Due to the smaller width of the deck plate than in the crossbeams analysed in chapter 4, c_d becomes: $1.754 \cdot 10^{-10}$ and the lack of support at the ends of the trough could even lead to a smaller value.

Table A1.30 shows the stresses at the cope hole location C.4.5.w.

Table A1.30 Additional analyses for ECSC crossbeam

	Stress (N/mm ²)	Type
Stress interval due to S_h for test loads	146	Nominal
Reducing stress interval due to restraining moment M_{res} caused by the deck (reduction)	(-) 9	Nominal
Resulting stress interval	137	Nominal
Resulting stress interval analytical model	329	Concentrated
Resulting stress interval FE shell model	356	-
Resulting stress interval measurement	341	-

A very good agreement is found between the stresses obtained with the analytical model, the FE analyses and the measurements.

A1.3.6 Concluding remarks for the deck restraint effect on the crossbeam in-plane behaviour

Crossbeams analysed in chapter 4

As shown in Table A.1.5, the restraining effect of the deck reduces the bending moment in the tooth by 10% for an effective deck plate thickness of 12 mm, by 20% for an effective deck plate thickness of 14 mm and by 30% for an effective deck plate thickness of 16 mm. For a fatigue life this may lead to an increase by factors of 1.4, 2.0 and 2.9 for $m = 3$ and 1.7, 3.1 and 6.0 for $m = 5$ respectively. These fatigue life extension factors apply to a crossbeam web $t_w = 10$ mm and a $b_{eff} = 4000$ mm for the deck restraining effect.

Crossbeam “AA” and Crossbeam “BB”

Table A1.31 gives an overview of the design lives for the locations C.4.5.s of Crossbeam “AA” and C.4.5.w of Crossbeam “BB” as found in 9.12.5, 9.13.5 and A1.7, where the restraining effect of the deck plate is included.

Table A1.31 Design lives in years (y)

Crossbeam “AA” Oval cope hole, thin wearing course, Location C.4.5.s						
t_w (mm)	Par. 9.12.5		Effective restraining width $b_{eff,b}$ (mm)			
			4000		6000	
	L1+L2	L1	L1 + L2	L1	L1 + L2	L1
10	0.11 y	0.16 y	0.28 y	0.37 y	0.50 y	0.63 y
18	-	-	0.80 y	0.99 y	1.05 y	1.29 y
Crossbeam “AA” Haibach cope hole, thin wearing course, Location C.4.5.s						
t_w (mm)	Par. 9.12.5		Effective restraining width $b_{eff,b}$ (mm)			
			4000		6000	
	L1+L2	L1	L1 + L2	L1	L1 + L2	L1
10	-	-	0.92 y	1.18 y	1.60 y	2.03 y
18	-	-	1.85 y	3.02 y	3.11 y	3.73 y
Crossbeam “BB” Close fit, thick wearing course, Location C.4.1.w						
t_w (mm)	Par. 9.13.5		Effective restraining width $b_{eff,b}$ (mm)			
			4000		6000	
	L1+L2	L1	L1 + L2	L1	L1 + L2	L1
10	0.17	0.23	0.43 y	0.57 y	0.78 y	1.01 y
18	-	-	2.16 y	2.75 y	4.20 y	5.79 y
Crossbeam “BB” Close fit, thin wearing course, Location C.4.1.w						
t_w (mm)	Par. 9.13.5		Effective restraining width $b_{eff,b}$ (mm)			
			4000		6000	
	L1+L2	L1	L1 + L2	L1	L1 + L2	L1
10	0.14	0.19	0.37 y	0.49 y	0.65 y	0.85 y
18	-	-	1.61 y	1.95 y	2.62 y	3.40 y

in which:

L1+L2: Simultaneous lorries on Lane 1 and Lane 2

L1: Lorries on Lane 1 only

From Table A1.31 the following conclusions can be drawn:

- Considering a deck restraint with $b_{\text{eff},b} = 4000$ mm increases the fatigue life by a factor between 2.3 and 2.6
- Considering an increase of the deck restraint from $b_{\text{eff},b} = 4000$ mm to $b_{\text{eff},b} = 6000$ mm increases the fatigue life by an additional factor between 1.3 and 2.1
- An increase of the crossbeam web thickness t_w from 10 to 18 mm increases the fatigue life by an additional factor between 1.8 and 5.7
- The total effect of the restraints and crossbeam web increase can be expressed as a fatigue life extension factor between 2.3 and 25.0.

All design lives however, remain very short and do not compare with experience in practice, therefore further analyses are carried out as described in A1.4.

Test crossbeam European 4th Phase fatigue research project

The analyses of the test crossbeam of the European 4th Phase fatigue research project showed a small influence of the deck restraint due to the small width of the deck (flange).

A1.4 Effect of fatigue detail classification

The effect of the detail classification can be investigated through the “Stress Quotient” SQ_i , the maximum stress interval due to each type “i” of FLM4 lorry passage divided by the stress interval related to the classification for 2 million cycles:

$$SQ_i = \left(\frac{\Delta\sigma_{\text{max},i}}{\Delta\sigma_C} \right) \quad [\text{A1.15}]$$

in which:

$\Delta\sigma_{\text{max},i}$ = maximum stress interval caused by a lorry “i”

$\Delta\sigma_C$ = stress interval related to a fatigue strength of 2 million cycles

The fatigue endurance expressed as numbers of cycles can be calculated for a given load distribution.

Considering that the endurance limit $\Delta\sigma_D$ ($N = 5 \times 10^6$) is 0.737 times $\Delta\sigma_C$ and the cut-off limit $\Delta\sigma_L$ ($N = 1 \times 10^8$) is 0.404 times $\Delta\sigma_C$, the calculation of the equivalent numbers of cycles for the long distance lorry distribution of FLM4 is as follows:

1. Stress cycles larger than $\Delta\sigma_D$

If $\Delta\sigma_{\text{max},i} / \Delta\sigma_C \geq 0.737$:

$$n_{\text{eq},i} = \left(\frac{\Delta\sigma_{\text{max},i}}{\Delta\sigma_C} \right)^3 \cdot f_i \quad [\text{A1.16}]$$

In which:

f_i = fraction of lorry type “i” (percentage divided by 100, here: EN 1991-2, FLM4, “Long distance”)

2. Stress cycles smaller than $\Delta\sigma_D$

If $0.737 > \Delta\sigma_{\max,i}/\Delta\sigma_C \geq 0.404$:

$$n_{eq,i} = \left(\frac{\Delta\sigma_{\max,i}}{\Delta\sigma_C}\right)^5 \cdot \left(\frac{1}{0.737}\right)^3 \cdot f_i \quad [A1.17]$$

3. Stress cycles smaller than $\Delta\sigma_L$

If $0.404 > \Delta\sigma_{\max,i} / \Delta\sigma_C$: $n_{eq,i} = 0$

4. Summation for five lorry types

For the five lorry types of FLM4 the sum of the equivalent number of lorries is:

$$\sum n_{eq} = n_{eq,1} + n_{eq,2} + n_{eq,3} + n_{eq,4} + n_{eq,5} \quad [A1.18]$$

For each stress quotient SQ_1 , the design capacity of number of lorries N is found as:

$$N = \frac{1}{\sum n_{eq}} \cdot 2 \cdot 10^6 \quad [A1.19]$$

Fig. A1.9 shows the design lives N_1 (lorries) for the long distance lorry distribution of FLM4 of EN 1991-2 in relation to the stress interval quotient $\Delta\sigma_{\max}/\Delta\sigma_C$. Here, the equivalent number of lorries n_{eq} summarizes the lorry distribution similar to chapter 6, into the relationship between the maximum stress interval based on the lorry load and an equivalent number of lorries with respect to one lorry.

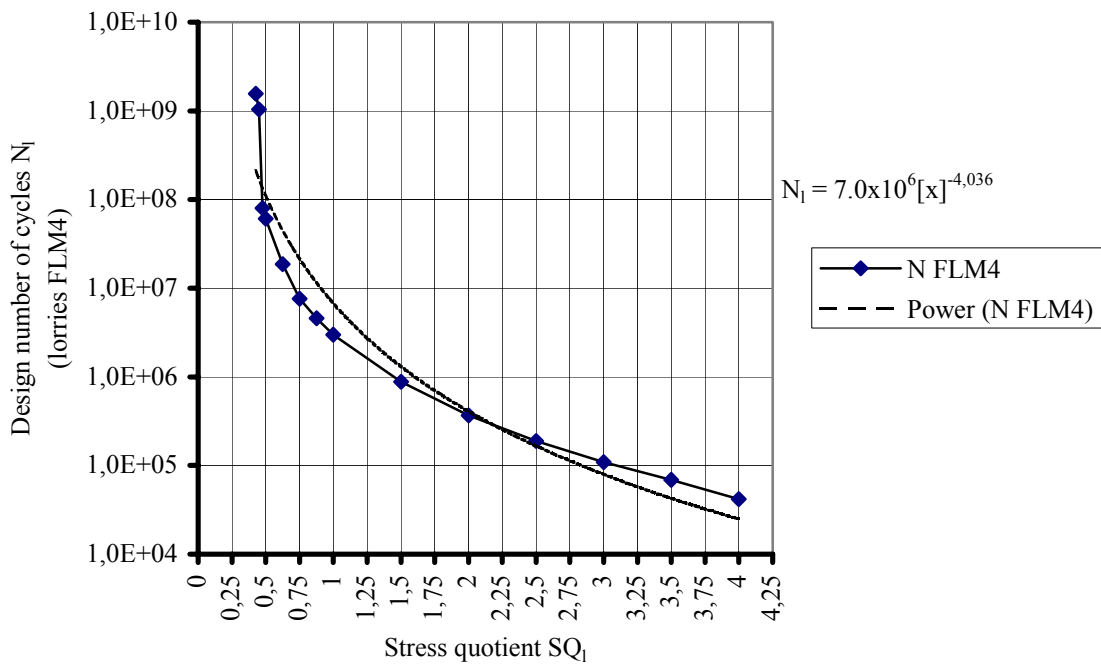


Fig. A1.9, Design lives (lorries) N_1 for lorries FLM4

Each stress quotient SQ_i has a design number of lorries N_i .

With equation [A1.20], obtained from curve fitting on the graph shown in Fig. A1.8, the design numbers of cycles N_i (lorries) can be calculated, for a given stress quotient SQ_i .

$$N = 7.0 \times 10^6 \cdot [x]^{-4.3036} \quad [A1.20]$$

in which:

$$[x] = \text{Stress quotient } SQ_i$$

In chapter 8, the free edge details of the cope hole, C.4.5.s have been classified as $\Delta\sigma_{Cr} = 140/1.15 = 122 \text{ N/mm}^2$ and the welded location with a close fit C.4.1.w the classification of $80/1.15 = 70 \text{ N/mm}^2$ has been used.

For comparison of fatigue calculation results with experience from real bridges, tentatively a “mean” classification can be used. This classification should be based on test results, which in many cases are insufficient. Dijkstra et al. (2001) mention a factor of 1.552 for a design classification with a $\beta = 3.6$, based on statistical methods. In the following analyses a factor of 1.5 is adopted between the “mean” and the design classification $\Delta\sigma_C$. As the design classifications $\Delta\sigma_{Cr}$ for C.4.5.s and C.4.1.w used in chapter 9 also include the effect of the partial factor $\gamma_{Mf} = 1.15$, the “mean” classification is 1.7 (1.5 x 1.15) times higher. A summary of the following calculations was already described in chapter 9.

Table A1.32 shows the stress quotients for the maximum stress intervals caused by complete FLM4 lorries $\Delta\sigma_{max}$, divided by the classification stress interval as $\Delta\sigma_{Cr}$.

Table A1.32 Stress Quotients $SQ_i \Delta\sigma_{max}/\Delta\sigma_C$

Connection		Crossbeam “AA” Oval cope hole Loc. C.4.1.s		Crossbeam “AA” Haibach cope hole Loc.		Crossbeam “BB” Close fit Loc. C.4.1.w	
$\Delta\sigma_{Cr}$ (N/mm ²)	$b_{eff,b}$ (mm)	L1+L2	L1	L1+L2	L1	L1+L 2	L1
C.4.5.s: 122	4000	2.5	1.6	1.6	1.1	2.1	1.4
C.4.1.w: 70	6000	2.0	1.4	1.4	0.9	1.8	1.2
C.4.5.s: 210	4000	1.4	0.9	1.0	0.7	1.2	0.8
C.4.1.w: 120	6000	1.2	0.8	0.8	0.5	1.1	0.7

The cycle capacity N (lorries) can be calculated for the increased (“mean”) detail classifications of FLM4 lorries as calculated before.

Tables A1.33 and A1.34 show the numbers of cycles (FLM4 lorries), the design capacities N , which include the reduction caused by the restraining effect of the deck, the damages D_{L1+L2} , D_{L1} (for the remaining lorries on L1), accumulated damage ΣD and the expected average fatigue life y of the locations.

Table A1.33 Expected “mean” fatigue life of oval cope hole

$b_{eff,b}$ (mm)	Stress quotient SQ_i		L1 + L2	D_{L1} +L2	Stress quotient SQ_i		L1	D_{L1}	ΣD_{L1+L2}	y
4000	1.4	n	6.4×10^6	8.3	0.9	n	1.9×10^7	10.	18.7	1.3
		N	7.8×10^5			N	1.8×10^6			
6000	1.2	n	6.4×10^6	6.8	0.8	n	1.9×10^7	6.3	13.1	1.9
		N	9.5×10^5			N	1.8×10^6			

Table A1.34, Expected “mean” fatigue life of Haibach cope hole

$b_{\text{eff},b}$ (mm)	Stress quotient SQ_I		L1 + L2	D_{L1+L2}	Stress quotien t SQ_I		L1	D_{L1}	ΣD_{L1+L2}	y
4000	1.0	n	6.4×10^6	5.5	0.7	n	1.9×10^7	3.5	8.8	2.8
		N	1.2×10^6			N	5.4×10^6			
6000	0.8	n	6.4×10^6	2.1	0.5	n	1.9×10^7	0.8	2.9	8.6
		N	3.1×10^6			N	2.3×10^7			

If, for the oval cope hole location of crossbeam “AA”, at C.4.5.s the stress quotient for L1+L2 with $b_{\text{eff}} = 4000$ mm changes from 2.5 to 1.4 (1.7), this extends the fatigue life from 0.28 (see Table A1.31) to 1.3, which is a factor 4.6.

If the stress quotient for L1+L2 with $b_{\text{eff}} = 4000$ mm changes from 2.0 to 1.2 (1.7), this extends the fatigue life from 0.50 (see Table A1.31) to 1.9 Moerdijk 1998 traffic years, which is a factor 3.8.

If for the Haibach cope hole location of crossbeam “AA”, at C.4.1.s the stress quotient for L1+L2 with $b_{\text{eff}} = 4000$ mm changes from 1.6 to 1.0, this extends the fatigue life from 0.92 (see Table A1.31) to 2.8, which is a factor 3.0.

If the stress quotient for L1+L2 with $b_{\text{eff}} = 4000$ mm changes from 1.4 to 0.8, this extends the fatigue life from 1.6 (see Table A1.31) to 8.6 Moerdijk 1998 traffic years, which is a factor 5.4.

For the close fit connection of crossbeam “BB”, at C.4.1.w the stress quotient for L1+L2 with $b_{\text{eff}} = 4000$ mm changes from 2.1 to 1.2; the extension of the fatigue life will be as for the oval cope holes with $b_{\text{eff}} = 4000$ mm.

It can be concluded that, for FLM4, due to the assumed 1.7 times higher “mean” fatigue classification, depending on the effective width of the deck plate restraint and the simultaneity of lorries on lane L1 and lane L2, an extension of the fatigue life can be found, varying from 3 to 5 times the values given in Table A1.31.

The design lives however, remain very short and do not yet correspond with experience in practice.

Observations

The equivalent number of cycles in chapter 6 for crossbeam loads, trough to crossbeam connection rotations and deck bending moments have been determined for lorries first and then for the maximum values in relation to FLM4. For these equivalent numbers of cycles continuous S – N lines have been used with an inverse slope $m = 3$ and $m = 5$ on a log – log scale.

Another aspect, not yet addressed here, is the geometry of the S-N line. If the inverse slopes (m) and the associated numbers of cycles deviate from the assumed $m = 3$ and $m = 5$ as laid down in EN 1993-1-9, large differences in fatigue life can be found.

A further investigation into the effect of variable stress intervals instead of constant stress intervals could also lead to modified fatigue lives.

A1.5 Effect of axle load distribution

The deck restraint effect discussed in A1.3 and the “average” classification described do not yet result in fatigue lives observed in practice. Therefore, in this paragraph, in situ traffic measurements at the Moerdijk Bridge 1998, reported in Nieuwsma (1998), are compared with EN 1991-2 Fatigue Load Model 4 with a “long distance” lorry distribution.

Fatigue assessments for limited fatigue life are to be carried out with the EN 1991-2 Fatigue Load Model FLM4 “Equivalent loads”, also described in NAD NVN-ENV 1991-3, which is related to EN 1991-3, the predecessor of EN 1991-2 “Traffic Loads on Road Bridges”.

Table A 1.35 Axle load distribution (kN)

Moerdijk 1998		EN 1991-2 FLM4	
Axle load	percentage	Axle load	percentage
210	0	-	-
190	0,01	-	-
170	0,02	-	-
150	0,2	150	12,1
-	-	140	3,6
130	1,6	130	7,2
-	-	120	2,4
110	6,7	-	-
90	13,6	90	45,8
-	-	80	4,8
70	33,9	70	24,1
50	37,9	-	-
30	27,2	-	-
10	5,9	-	-

As a first comparison, the axle load distributions of the measurement at the Moerdijk Bridge 1998, and the axle histogram of FLM4 of EN 1991-2 are shown in Table A1.35. It is shown that the axle loads of 30 and 50 kN have a higher proportion on the Moerdijk bridge and the axle loads of 150 and 90 kN have a substantial proportion for FLM4.

A1.5.1. Analysis of cumulative axle load per year

Table A1.36 shows the cumulative axle load per year (kN/y) caused by the Moerdijk Bridge loads of 1998 and those of EN 1991-2 FLM4.

Table A1.36 Cumulative axle load per year

Traffic type	Weighed average axle load (kN)	Axles per week	Axles per lorry	Lorries per week	Lorries per year	Cumulative axle load per year kN/y
Moerdijk 1998	73.5	151100	4	3778	1.964×10^6	5.775×10^8
FLM4	97.4	-	4.15	-	2.0×10^6	8.084×10^8

Based on the cumulative axle load, the load of FLM4 is 1.4 times the Moerdijk 1998 load.

From various observations and counting at the Moerdijk Bridge, Nieuwsma (1998), the weighed average number of axles proved to be approximately 4, which leads to the conclusion that the Moerdijk 1998 and FLM4 have about the same number of lorries per year.

The traffic volume of Moerdijk 1998 can be used as a reference to investigate the traffic history of bridges.

Three scenarios are shown in Table A1.36. Scenario I assumes that the traffic volume in 1978, the year when the bridge was put into service, was 20% of the traffic of 1998 and the estimated traffic volume in 2008 will be 140% of that of 1998. Scenario II assumes 10% in 1978 and 150% in 2008. Scenario III assumes 60% in 1978 and 120% in 2008.

Table A1.36 Effective “Traffic years” expressed as Moerdijk 1998 in relation to 30 service years

Year	Scenario of traffic volume in relation to Moerdijk 1998		
	I	II	III
1978	0.2	0.1	0.6
1998	1.0	1.0	1.0
2008	1.4	1.5	1.2
Cumulative traffic years for Moerdijk 1998	24	24	27
Cumulative traffic years average location	12	12	13

It is shown that the three scenarios result in approximately 24 “Moerdijk 1998” traffic years for a time period of 30 years and that more accurate descriptions of the traffic growth are not necessary.

As most other locations in the Netherlands have a number of lorries, about 50% of that of the Moerdijk Bridge, an effective number of 12 years “Moerdijk 1998 traffic” could be used for the calculation of fatigue damage accumulated up to now for most of the locations in the country.

If the relationship between axle loads of FLM4 and the “Moerdijk 1998” axle loads also applies for the lorry loads, the relationship can be used to relate the fatigue lives determined with FLM4 to those with the real traffic (Moerdijk 1998).

With the “Stress quotient” SQ_a , the fatigue numbers of cycles N_a (axles) can be calculated for the axle loads of FLM4 and those of “Moerdijk 1998” with the method described in A1.4 but here related to axles.

A1.5.2 Comparison of axle load effects

Fig. A1.10 shows the fatigue lives N_a (axle loads) for the Moerdijk 1998 traffic, the FLM4 lorries and a factor which indicates the extension of the fatigue life if the “Moerdijk 1998” traffic is used instead of FLM4. The SQ_{aM} related to the maximum measured axle load of the Moerdijk Bridge can be found multiplying SQ_a with a factor $150/210=0.71$.

The ordinates $[x]$ show the values of stress quotients SQ_a , with respect tot the maximum axle loads of FLM4.

The fatigue life (axles) for the Moerdijk 1998 traffic can be represented by equation [A1.21], obtained with curve fitting:

$$N_a = 8 \cdot 10^7 [x]^{-5.1754} \quad [A1.21]$$

in which:

$$[x] = \text{Stress Quotient } SQ_a$$

The fatigue life (axles) for FLM4 can be represented by equation [A1.22], obtained with curve fitting:

$$N_a = 10^7 [x]^{-3.9859} \quad [A1.22]$$

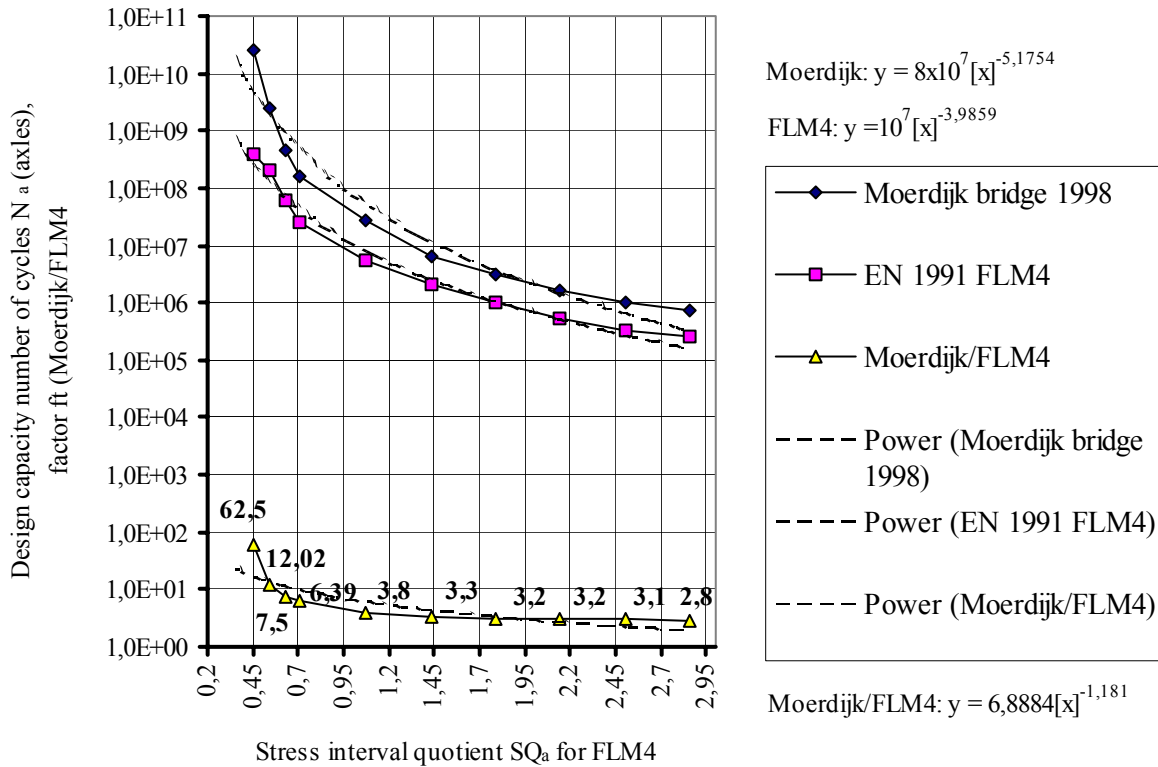


Fig. A.10, Design lives (axles) N_a and factor f_t between Moerdijk and FLM 4 traffic

From Fig. A1.10, it follows that the Moerdijk 1998 loads results in a longer expected fatigue life than that with FLM4. The increase is a factor varying from 62.5 for a S_{Q_a} of 0.45 to 2.8 for a S_{Q_a} of 2.86 with S_{Q_a} for FLM4.

The fatigue lives calculated in chapter 9 and this appendix however, are based on stress intervals caused by lorries. Assuming that the fatigue damage relationship for Moerdijk 1998 and FLM4 axles is also valid for lorries, fatigue lives calculated for FLM4 can be transferred into fatigue lives for the Moerdijk 1998 traffic with factor f_t calculated with equation [A1.23] also obtained from curve fitting,:

$$f_t = 6.8884 \cdot [x]^{-1.181} \quad [A1.23]$$

in which:

$$[x] = \text{Stress Quotient } S_{Q_a}$$

Tables A1.38 and A1.39 show the expected fatigue lives y in years when the FLM4 is substituted by the Moerdijk 1998 traffic. Here, D is the fatigue damage caused by 25 years of traffic.

Table A1.38 Expected “mean” fatigue life of oval cope hole

$b_{\text{eff},b}$ (mm)	Stress quotient	Reductio n factor for $D_{L1} +$ $L2$	D	Stress quotien t	Reductio n factor for D_{L1}	D	ΣD	y
4000	1.4	0.303	2.5	0.9	0.161	1.7	4.2	6
6000	1.2	0.204	1.4	0.8	0.149	0.9	2.3	11

Table A1.39. Expected “mean” fatigue life of Haibach cope hole

$b_{\text{eff},b}$ (mm)	Stress quotient	Reductio n factor for $D_{L1} +$ $L2$	D	Stress quotien t	Reductio n factor for D_{L1}	D	ΣD	y
4000	1.0	0.139	0.8	0.7	0.074	0.3	1.1	23
6000	0.8	0.121	0.3	0.5	0.046	0	0.1	250

Table A1.36 shows that the Moerdijk Bridge, which has been in service for almost 30 years has been submitted to 24 years of the Moerdijk 1998 traffic, which means that the fatigue lives can be multiplied with 1.25 (= 30/24) to obtain a period in service years.

In addition, a factor 2 could be taken into account for bridges at other locations due to the lower traffic density.

The fatigue analyses carried out here are for typical crossbeams used in a fictitious bridge subjected to FLM4 lorries.

The expected fatigue life for the crossbeam “AA”, taking into account the deck restraint, the mean fatigue detail classification, the lower axle loads in practice and the lower traffic density for an average location will be between 15 (= 1.25 x 2 x 6) and 28 (= 1.25 x 2 x 11) years for connections with oval cope holes. For Haibach cope holes the expected fatigue lives would have been between 58 and 625 years.

The equivalent numbers of cycles in relation to the number of lorries has been determined in chapter 6, assuming continuous S-N lines, with an inverse log -log slope of $m = 3$ or $m = 5$. The equivalent numbers of cycles for $m = 3$ have been used for further analyses in chapter 9 and in this Appendix, which is a conservative approach. Based on the values for n_{eq} determined in chapter 7 an approximate fatigue life extension factor of 1.4 can be expected, if all stress intervals are in the $m = 5$ part.

A1.6 Concluding remarks

- Considering a deck restraint with $b_{\text{eff}} = 4000$ mm, increases the fatigue life by a factor between 2.3 and 2.6. An increase in the deck restraint from $b_{\text{eff}} = 4000$ mm to $b_{\text{eff}} = 6000$ mm, increases the fatigue life by an additional factor between 1.3 and 2.1 and an increase of the crossbeam web thickness t_w from 10 to 18 mm, increases the fatigue life by an additional factor between 1.8 and 5.7
- The total effect of the deck restraint and crossbeam web increase can result in a fatigue life extension factor between 2.3 and 25.0
- Including the deck stiffness effect in the geometrical stresses in the cut-out of the ECSC test crossbeam described in chapter 7, leads to stresses similar to the measured stresses and those determined with an FE shell element model.
- The stress intervals due to the lorries are mainly at the inverse log-log slope $m = 3 - m = 5$ transition part, which makes the fatigue life assessment very sensitive to the classification level.
- The measured axle loads on the Moerdijk Bridge show a larger percentage of axle loads lower than FLM4, which can lead to a fatigue life extension with a factor between 6 and 11.
- Combining the effects of the deck restraints, the “mean” classification and the measured loads vs. FLM4, can lead to fatigue life extension factor of 36 ($= 2 \times 3 \times 6$) to 60 ($= 2.6 \times 2.1 \times 11$) and higher with respect to the fatigue lives calculated in chapter 9 for crossbeams with web thicknesses of 10 mm.

APPENDIX 2 LOAD AND ROTATION INTERVALS FROM FE CALCULATIONS

Table A2.1, Crossbeam in-plane load intervals ΔP_{3CV}

Crossbeam						Unit load and FLM2 with the distribution of FLM4					
H	Nr. (A)	K_{1c} (A)	Nr. (FE-G)	K_{1c} (FE-G)	K_{1D}^1 / K_{1c}^1	Unit Load 100kN	Lorry 1	Lorry 2	Lorry 3	Lorry 4	Lorry 5
600	1	3.4	1	3.4	0.3333	r. 57 s. 61 (61) t. 65	r. 123 s. 137 (134) t. 148	r. 165 s. 181 (181) t. 194	r. 192 s. 215 (212) t. 235	r. 150 s. 169 (164) t. 187	r. 144 s. 162 (170) t. 179
800	2	5.9	2	5.9	0.1923	r. 63 s. 68 (68) t. 76	r. 131 s. 142 (144) t. 158	r. 177 s. 194 (196) t. 210	r. 204 s. 227 (224) t. 246	r. 164 s. 177 (175) t. 194	r. 150 s. 165 (175) t. 179
1000	3	8.8	3	8.8	0.1282	r. 68 s. 73 (73) t. 81	r. 139 s. 150 (153) t. 165	r. 187 s. 204 (217) t. 219	r. 215 s. 237 (234) t. 256	r. 175 s. 187 (185) t. 200	r. 154 s. 169 (185) t. 181
1200	4	12.6	4	12.6	0.0901	r. 76 s. 81 (81) t. 87	r. 144 s. 166 (159) t. 179	r. 196 s. 220 (221) t. 243	r. 225 s. 254 (249) t. 279	r. 183 s. 200 (195) t. 218	r. 158 s. 179 (185) t. 195
1400	5	16.5	5	16.5	0.0685	r. 80 s. 86 (86) t. 92	r. 156 s. 172 (171) t. 189	r. 212 s. 233 (229) t. 254	r. 243 s. 264 (259) t. 286	r. 200 s. 212 (204) t. 223	r. 166 s. 183 (186) t. 201
1800	7	30.5	6	27.6	0.0410	r. 88 s. 94 (98) t. 99	r. 168 s. 174 (174) t. 200	r. 218 s. 250 (228) t. 271	r. 262 s. 283 (270) t. 304	r. 218 s. 227 (225) t. 237	r. 177 s. 204 (194) t. 208
2200	9	40.2	7	40.2	0.2817	r. 94 s. 100 (100) t. 103	r. 175 s. 190 (187) t. 206	r. 242 s. 260 (256) t. 279	r. 273 s. 294 (294) t. 312	r. 230 s. 236 (233) t. 246	r. 184 s. 202 (200) t. 212
-	-	-	8	402.	0.0028	r. 103 s. 114 t. 115	r. 204 s. 214 t. 225	r. 283 s. 293 t. 306	r. 325 s. 328 t. 336	r. 273 s. 270 t. 266	r. 214 s. 223 t. 223
-	-	-	9	803.	0.0014	r. 115 s. 115 t. 115	r. 208 s. 216 t. 227	r. 285 s. 294 t. 307	r. 329 s. 329 t. 340	r. 273 s. 272 t. 278	r. 216 s. 223 t. 229
-	-	-	10	2008.	0.0006	r. 116 s. 116 t. 116	r. 208 s. 216 t. 227	r. 287 s. 296 t. 307	r. 329 s. 334 t. 338	r. 275 s. 272 t. 270	r. 216 s. 225 t. 227
∞	-	∞	11	∞	∞	r. 116 s. 117 (116) t. 117	r. 208 s. 216 (198) t. 227	r. 287 s. 298 (294) t. 307	r. 327 s. 334 (332) t. 340	r. 281 s. 274 (266) t. 268	r. 216 s. 225 (224) t. 227

Note: (...) Analytical values

Table A2.2a, Rotation intervals $\Delta\varphi_3$

CROSSBEAM						$\Delta\varphi_3 \cdot 10^{-4}$ due to FLM2 with the distribution of FLM4	
H	Nr	K _C	Nr	K _C	K _D ¹ /K _C ¹	Unit Load 100kN	Lorry 1 (kN)
600	1	3.4	1	3.4	0.3333	r. 3.6/7.4/3.6 s. ----- (7.8) t. 4.1/8.2/4.1	r. 5.8/13.4/7.6 s. 6.8/15.4/8.6 (10.9) t. 7.4/16.9/9.5
800	2	5.9	2	5.9	0.1923	r. 2.9/5.8/2.9 s. 3.2/6.4/3.2 (6.8) t. 3.5/7.0/3.5	r. 4.0/9.8/5.8 s. 4.5/11.3/6.8 (8.8) t. 5.1/12.7/7.6
1000	3	8.8	3	8.8	0.1282	r. 2.4/4.8/2.4 s. 2.7/5.4/2.7 (5.2) t. 3.1/6.2/3.2	r. 3.0/7.8/4.8 s. 3.4/9.1/5.7 (7.4) t. 3.9/10.1/6.2
1200	4	12.6	4	12.6	0.0901	r. 2.1/4.2/2.1 s. 2.4/4.8/2.8 (4.8) t. 2.8/5.9/2.8	r. 2.5/6.6/4.1 s. 2.8/7.6/4.8 (6.8) t. 2.9/8.4/5.5
1400	5	16.5	5	16.5	0.0685	r. 1.9/3.8/1.9 s. 2.3/4.6/2.3 (4.4) t. 0.2/2.8/5.2/2.8/0.2	r. 2.3/6.0/3.7 s. 2.1/6.9/4.4 (6.3) t. 2.8/7.9/5.4/0.3
1800	7	30.5	6	27.6	0.0410	r. 1.7/3.4/1.7 s. 0.2/2.2/4.4/2.2/0.2 (3.8) t. 0.3/2.7/4.8/2.7/0.3	r. 1.4/1.4/2.3/5.3/3.0 s. 1.5/1.2/2.2/6.4/4.2/0.3 (3.9) t. 1.9/1.1/2.0/7.2/5.0/0.6
2200	9	40.2	7	40.2	0.2817	r. 0.1/1.7/3.4/1.7/0.1 s. 0.3/2.2/3.8/2.2/0.3 (3.8) t. 0.4/2.7/4.6/2.7/0.4	r. 1.1/1.5/2.7/5.1/3.1/0.3 s. 1.2/1.2/2.5/6.0/4.1/0.6 (4.0) t. 0.8/1.4/2.2/6.8/4.8/0.8
-	-	-	8	402.	0.0028	r. 0.4/1.7/2.6/1.7/0.4 s. 0.5/2.2/3.4/2.2/0.5 t. 0.6/2.9/4.6/2.9/0.6	r. 0.8/1.9/3.3/4.4/2.9/0.7 s. 0.4/1.0/1.4/3.3/5.3/3.8 /1.0 t. 1.4/0.8/2.6/6.0/4.6/1.2
-	-	-	9	803.	0.0014	r. 0.4/1.7/2.6/1.7/0.4 s. 0.5/2.2/3.4/2.2/0.5 t. 0.7/2.8/4.2/2.8/0.7	r. 1.2/2.0/3.4/4.5/3.0/0.8 s. 0.8/1.2/3.3/5.3/3.9/1.1 t. 1.8/0.7/2.8/6.3/4.7/1.2
-	-	-	10	2008.	0.0006	r. 0.4/1.7/2.6/1.7/0.4 s. 0.5/2.3/3.4/2.2/0.5 t. 0.7/2.8/4.2/2.8/0.7	r. 1.1/1.9/3.4/4.4/3.0/0.8 s. 1.0/1.4/3.3/5.3/3.9/1.1 t. 1.2/0.6/2.8/6.2/4.6/1.2
ω	-	Ω	11	ω	Ω	r. 0.4/1.7/2.6/1.7/0.4 s. 0.5/2.3/3.4/2.3/0.5 (3.0) t. 0.7/2.8/4.2/2.8/0.7	r. 1.0/1.9/3.4/4.4/3.0/0.8 s. 1.0/1.4/3.3/5.3/3.9/1.1 (3.6) t. 1.3/0.8/2.9/6.2/4.8/1.4

Note: (...) Analytical values

Table A2.2b. Rotation intervals $\Delta\phi_3$

CROSSBEAM						$\Delta\phi_3 \cdot 10^{-4}$ due to FLM2 with the distribution of FLM4	
H	Nr	K _C	Nr	K _C	K _D ¹ /K _C ¹	Lorry 2	Lorry 3
600	1	3.4	1	3.4	0.3333	r. 6.8/16.7/9.9 s. 7.9/19.1/11.2 (18.1) t. 8.4/20.8/12.4	r. 7.5/8.7/7.3/16.3/9.2 s. 8.3/10.9/7.0/14.6/10.2 (20.5) t. 9.1/11.4/6.4/15.3/11.2
800	2	5.9	2	5.9	0.1923	r. 5.2/12.8/7.6 s. 5.8/14.5/8.7 (13.7) t. 6.5/16.3/9.8	r. 5.4/8.8/7.5/11.4/7.3 s. 5.9/9.2/7.7/12.4/8.0 (13.9) t. 6.6/9.9/8.0/13.5/8.8
1000	3	8.8	3	8.8	0.1282	r. 4.6/10.9/6.3 s. 5.1/12.4/7.3 (11.1) t. 5.7/14.0/8.3	r. 4.0/7.4/7.4/9.9/5.9 s. 4.6/8.2/8.0/11.0/6.6 (13.3) t. 5.2/9.1/8.9/12.6/7.6
1200	4	12.6	4	12.6	0.0901	r. 4.1/9.5/5.4 s. 4.6/10.9/6.3 (10.2) t. 5.2/12.5/7.3	r. 3.2/6.5/7.2/8.9/5.0 s. 3.6/7.3/8.1/10.2/5.8 (12.1) t. 4.4/8.4/9.1/11.7/6.8/0.3
1400	5	16.5	5	16.5	0.0685	r. 3.9/8.7/4.8 s. 4.4/10.2/5.8 (9.2) t. 5.0/11.8/7.2/0.8	r. 2.8/6.1/7.2/8.3/4.4 s. 3.0/6.9/8.3/9.6/5.2 (11.3) t. 3.9/8.0/9.3/11.7/6.8/0.3
1800	7	30.5	6	27.6	0.0410	r. 1.2/1.2/3.4/7.5/4.1 s. 1.4/0.8/3.4/9.0/5.4/0.4 (9.0) t. 4.6/10.5/6.7/0.7	r. 1.9/5.1/6.9/7.6/3.9 s. 2.2/6.1/8.3/9.8/4.9/ 0.3 (9.0) t. 3.2/7.6/9.8/11.1/6.4/ 0.7
2200	9	40.2	7	40.2	0.2817	r. 1.1/1.4/3.6/7.0/4.0/0.3 s. 1.0/1.0/3.9/8.5/5.2/0.6 (8.9) t. 4.6/10.3/6.8/1.1	r. 1.7/4.7/6.6/6.9/3.6/0.3 s. 2.2/5.5/8.1/9.9/5.7/ 0.6 (8.2) t. 3.0/7.0/10.1/12.3/ 3/1.1
-	-	-	8	402.	0.0028	r. 0.6/1.8/4.2/5.9/3.7/0.8 s. 1.0/1.6/4.6/7.5/5.1/1.2 t. 5.0/9.2/6.4/1.6	r. 1.1/3.9/6.3/6.1/3.6/0.8 s. 1.8/5.3/8.5/8.7/5.8/1.2 t. 3/7.1/10.8/11.7/7.2/1.8
-	-	-	9	803.	0.0014	r. 0.9/2.0/4.4/5.8/3.8/1.0 s. 0.8/1.5/4.7/7.5/5.3/1.5 t. 0.6/0.6/10.3/4.6/9.1/6.5/1.7	r. 1.1/3.9/6.4/6.4/3.6/0.8 s. 1.8/5.3/8.6/8.7/5.4/1.4 t. 3.0/6.8/10.7/11.5/7.2/1.8
-	-	-	10	2008.	0.0006	r. 0.9/2.0/4.4/5.8/3.8/1.0 s. 0.8/1.5/4.7/7.5/5.3/1.4 t. 0.6/0.6/0.4/4.7/9.1/6.5/1.7	r. 1.4/3.9/6.2/6.2/3.6/0.8 s. 1.8/5.3/8.7/8.7/6.4/1.4 t. 3.1/6.9/10.7/11.5/7.3/1.9
ω	-	Ω	11	ω	Ω	r. 0.9/2.0/4.4/5.8/3.9/1.1 s. 0.8/1.5/4.7/7.3/5.1/1.4 (6.0) t. 0.6/0.6/0.4/4.5/8.8/6.4/1.7	r. 1.4/4.0/6.2/6.1/3.6/0.8 s. 2.0/5.3/8.6/8.7/5.4/1.4 (7.7) t. 3.1/6.9/10.7/11.5/ 7.3/ 1.9

Note: (...) Analytical values

Table A2.2c Rotation intervals $\Delta\phi_3$ Note: (...) Analytical values

CROSSBEAM						$\Delta\phi_3 \cdot 10^{-4}$ due to FLM2 with the distribution of FLM4	
H	Nr	Kc	Nr	Kc	K_D^1/K_C^1	Lorry 4	Lorry 5
600	1	3.4	1	3.4	0.3333	r. 7.4/10.0/10.7/16.3/9.2 s. 8.3/10.9/7.0/14.6/10.2 ((11.7)) t. 9.1/11.4/6.4/15.3/11.2	r. 5.2/6.7/4.1/10.5/7.9 s. 5.9/7.3/2.5/10.2/9.1 (13.8) t. 6.9/8.3/1.8/10.7/10.3
800	2	5.9	2	5.9	0.1923	r. 5.4/8.8/7.5/11.4/7.3 s. 5.9/9.2/7.7/12.4/8.0 (11.0) t. 6.6/9.9/8.0/13.5/8.8	r. 4.1/5.5/4.0/8.5/5.9 s. 4.5/5.9/3.3/8.9/7.0 (7.1) t. 5.0/6.4/3.1/9.7/8.0
1000	3	8.8	3	8.8	0.1282	r. 4.0/7.4/7.4/9.9/5.9 s. 4.6/8.2/8.0/11.0/6.6 (14.4) t. 5.2/9.1/8.9/12.6/7.6	r. 3.6/5.0/4.2/7.6/4.8 s. 3.9/5.3/3.9/8.3/5.8 (5.7) t. 4.1/5.6/3.8/8.9/6.6
1200	4	12.6	4	12.6	0.0901	r. 3.2/6.5/7.2/8.9/5.0 s. 3.6/7.3/8.1/10.2/5.8 9 (9.1) t. 4.4/8.4/9.1/11.9/6.8	r. 3.3/4.7/4.0/6.7/4.1 s. 3.4/4.8/4.0/7.6/5.0 (5.1) t. 3.7/5.4/4.3/8.6/5.8
1400	5	16.5	5	16.5	0.0685	r. 2.8/6.1/7.2/8.3/4.4 s. 3.0/6.9/8.3/9.6/5.2 (9.0) t. 3.9/8.0/9.3/11.7/6.8/0.3	r. 2.8/4.0/4.0/6.7/3.9 s. 3.0/4.4/4.2/7.2/4.4 (5.0) t. 3.4/5.1/4.7/8.2/5.5/0.3
1800	7	30.5	6	27.6	0.0410	r. 1.9/5.1/6.9/7.6/3.9 s. 2.2/6.1/8.3/9.0/4.9/0.3 (8.7) t. 3.2/7.6/9.8/11.1/6.4/0.7	r. 1.4/1.8/2.9/3.9/3.9/ 5.8/3.3 s. 1.4/1.8/3.2/4.2/4.4/ 6.9/ 4.2/0.3 (6.0) t. 1.7/1.7/3.0/4.7/3.1/8.0/5.2/0.6
2200	9	40.2	7	40.2	0.2817	r. 1.7/4.7/6.6/6.9/3.6/0.3 s. 1.9/5.8/8.3/8.7/4.9/0.6 (9.3) t. 2.8/7.4/10.0/10.8/6.2/0.8	r. 1.2/1.9/3.0/3.5/3.7/ 5.3/3.1/0.3 s. 1.2/1.8/3.1/4.0/4.5/6.6/4.0/0.4 (5.9) t. 1.4/1.8/3.3/4.8/5.6/7.8/4.4/0.3
-	-	-	8	402.	0.0028	r. 0.6/0.6/1.7/4.6/6.2/5.8/3.2/0.7 s. 1.9/5.4/8.3/8.1/4.8/1.1 t. 2.9/7.0/10.5/10.5/5.9/1.5	r. 0.8/2.2/3.3/3.0/3.6/ 4.7/2.9/0.7 s. 1.2/2.2/3.6/3.7/4.7/ 6.1/2.9 t. 1.4/2.2/3.7/4.5/5.9/7.4/4.8/1.4
-	-	-	9	803.	0.0014	r. 0.9/0.6/1.5/3.4/6.2/5.5/3.3/0.8 s. 1.9/5.4/8.3/8.0/3.6/1.1 t. 2.9/7.0/10.5/10.4/6.2/1.5	r. 1.1/1.2/3.3/3.3/1.3/1.1/3.7/4.7/ 3.0/0.8 s. 1.2/2.2/3.6/3.7/4.8/6.1/3.8/1.0 t. 1.4/2.0/3.7/4.4/5.9/7.4/4.8/1.4
-	-	-	10	200 8.	0.0006	r. 1.4/1.8/0.4/1.5/4.3/ 6.1/5.8/3.3 s. 1.8/5.3/8.3/8.0/4.7/1.1 t. 2.0/6.9/10.2/6.4/1.7	r. 1.1/2.2/3.3/3.0/3.8/4.8/3.0/0.8 s. 1.2/2.2/3.6/3.7/6.1/3.9/1.1 t. 1.3/1.9/3.7/4.4/5.9/7.4/4.8/1.4
ω	-	Ω	11	ω	Ω	r. 0.7/0.4/1.7/4.5/6.1/5.8/3.3/0.8 s. 2.1/5.4/8.3/8.0/4.7/1.1 (7.8) t. 2.8/6.9/10.5/10.4/6.2/1.5	r. 1.1/2.2/3.3/3.0/3.6/4.7/3.0/0.8 s. 1.4/2.2/3.6/3.7/4.8/6.1/3.9/1.1 (5.1) t. 1.3/1.9/3.7/4.4/5.9/7.3/4.7/1.4

CURRICULUM VITAE

Leendertz, Johan Sebastiaan (Han)

M

Born: 7 January 1948, Amersfoort, The Netherlands

Education:

Rijks Hogere Burgerschool, Schiedam 1967

Hogere Technische Avondschoon, Rotterdam 1972

Courses:

Basics of finite elements,

Introduction into metallurgy,

Dynamics with finite elements,

Fatigue of structures,

Probabilistic design,

Methodic design,

User course ABAQUS finite element program for geometrical and physical non-linear analysis

Han Leendertz joined Rijkswaterstaat of the Ministry of Transport in the Netherlands in 1967 and since 1969 he has worked in the steel department, as a design engineer, a structural engineer and finally as a specialist consultant. His main tasks were in the field of steel structures for bridges and hydraulic steel structures and more specifically on aspects of dynamic and non-linear behaviour, stability and fatigue. He has also specialised on the specification and application of bridge bearings and expansion joints.

He contributed to the design of several steel bridges and was particularly involved in the design of the Eastern Scheldt Storm Surge Barrier as a structural engineer, for which he carried out fatigue analyses, geometrical and physical non-linear and stability analyses, in addition to the static analyses.

In the swivel gates project for the Maeslant Storm Surge Barrier near Rotterdam he acted as a verification engineer. For the modification of the ball joint of this Storm Surge Barrier, he coordinated and contributed to the design activities and to the associated friction, wear and durability tests in Germany and Belgium.

For the Hartel Storm Surge Barrier near Rotterdam he contributed to the conceptual design and analysed the dynamic behaviour due to wave and water current excitations.

For several projects he acted as a consultant for bridge bearings and expansion joints and carried out friction, wear and fatigue tests in Germany and Great Britain.

In 1990, he joined the CEN/TC 167 for bridge bearings. He is the chairman of the Dutch mirror committee for bridge bearings and is convenor of CEN/TC 167 WG1 "Revisions".

In 2000, he joined the EOTA working group for Expansion joints, and he is the convenor of the task group for modular joints and further dealt with the drafting of detailed load models for expansion joints in accordance with the EN 1991-2, Traffic loads on bridges. He also is the chairman of the Dutch mirror committee for expansion joints.

He is a member of CEN/TC 226 WG1 TG3 "Pedestrian parapets".